Numerical and Experimental Investigation of a New Load-Sharing Implant for Early-Onset Knee Osteoarthritis

Mehdi Saeidi

A thesis submitted to Auckland University of Technology

in fulfilment of the requirements for the degree of

Doctor of Philosophy (Ph.D.)

2019

School of Engineering, Computer, and Mathematical Science

I hereby declare that this submission is my own work and that, to the best of my knowledge and belief, it contains no material previously published or written by another person (except where explicitly defined in the acknowledgements), nor material which to a substantial extent has been submitted for award of any other degree or diploma of a university or other institution of higher learning.

Signed: Mehdi Saeidi   Date: 8 March 2019

Acknowledgments

To me, this Ph.D. has been such a journey and when I look backwards, it reminds me of a peom from a well knowns Persian poet, Hafez:

Ho! O Saki, pass around and offer the bowl:
For love at first appeared easy, but difficulties have occurred.

During this journey, countless people have assisted me, and I cannot put into words how grateful I am. So, first of all, I would like to thank Auckland University of Technology (AUT) for granting me a Ph.D. position as well as their financial support. I would like to thank my supervisors at AUT, Dr Maziar Ramezani and Prof. Thomas Neitzert, and my supervisor at the University of Auckland, Assoc. Prof. Piaras Kelly, for giving me an opportunity to work on this project and supporting me in carrying out the project successfully.

Special thanks to different faculties and departments at The University of Auckland for providing cadaver specimens, facilities, funding, and amazing support without which doing the experiments was not possible. I would like to thank Mr Christian Netzel from the Centre for Advanced Composite Materials, Assoc. Prof. Maurice Curtis, Assoc. Prof. Miriam Scadeng, Dr Deborah Prendergast, Mr Peter Riordan, Mr Nick Duggan, Ms Robyn Tattley, and Mr David Mahuika from the Department of Anatomy and Medical Imaging, Ms Yuting Zhu from the Department of Engineering Science, and Dr Pranesh Kumar from the Whanganui Hospital for their assistance during the experiments. Special thanks to Ms Anna Lydon and Ms Rachel Heron from the Centre for Advanced MRI, and Ms Leigh Anderson and Ms Alice Walsh from the Auckland City Hospital for their help regarding MRI and X-ray of the specimens. I appreciate the AUT workshop for manufacturing the implant prototype, Orthoplastics Ltd for providing polyethylene samples, and Tekscan Inc. for their technical support.

I would also like to express my heartfelt appreciation to people who generously donate their bodies to the Human Body Bequest Programme, and allow many researchers to carry out invaluable studies, which would not be possible without such generosity.

I would like to thank Dr Mousa Kazemi and Assoc. Prof. Thor Besier from the Auckland Bioengineering Institute for their help regarding finite element knee modelling. Special thanks to Mr José Eduardo Gubaua, Dr Gabriela Wessling Oening Dicati, and Prof. Jucélio Tomás Pereira from the Federal University of Paraná, and Dr Frank Richter for their help regarding finite element analysis and the principles of computational subroutines for bone remodelling purposes.

Finally, I would like to express my deepest gratitude to my family for their incredible support and encouragement at every single moment of my project, although they are thousands of miles away.

What I have learned during this journey made me realise that the world is full of amazing people who are ready to support and help you, and that you just need to look for them. Now, I am a different and much more experienced person who is looking forward to taking on another challenge.

Abstract

Knee osteoarthritis (OA) is one of the major causes of musculoskeletal impairment in adults. This disease is mainly characterised by progressive degeneration of the articular cartilage and, to date, there is no known cure for it. Initiation and progression of the OA pathology is associated with knee loading conditions. For younger, active patients with knee OA, common treatments include non-invasive options in order to manage symptoms before considering, as a last resort, the surgical options, in particular the gold standard treatment: knee replacement. Recently developed load-sharing implants could be considered as suitable options lying between the symptom management and invasive treatments. One such implant is comprised of femoral and tibial components, and removes excessive load through the knee joint by attachment to the medial side. This patient-specific implant would be suitable for early-onset knee osteoarthritis and can be used for younger active patients, as no major modification in the knee joint is required. This research aimed to study the influence of the implant on tibiofemoral joint contact mechanics and bone remodelling using numerical and experimental methods. To do so, Finite Element (FE) knee models and cadaver knee specimens were used. Initially, a FE model was used for conducting stress analysis in the cartilage, then to implement an adaptive bone remodelling method. Periprosthetic Bone Mineral Density (BMD) changes induced by this new implant were investigated in the femur and tibia for the first time. The surgical procedure as well as the effects of the implant on the joint space and contact pressure were also studied using cadaver specimens and accurate real-time pressure measurement sensors. A prototype of the implant was made based on a 3D model of the specimen reconstructed using MR images. Through numerical and experimental investigations, it was deduced that this new implant can increase the joint space and effectively reduce the load going through the medial compartment, without affecting greatly the periprosthetic bone density. Specifically, after attachment of the implant, the maximum von Mises stress and contact pressure experienced by the femoral cartilage were reduced by 40% and 35%, respectively. Also, in the medial compartments of the femur and tibia, bone mineral density increased by approximately 3.4% and 4.1%, respectively, and the density for the fixation holes of both bones increased by around 2.2%. Moreover, according to the experimental contact pressure measurements, the implant reduced the load on the medial side by approximately 18% under all loading conditions. The implant was attached to the bone with a smaller incision than that used for total knee replacement, and without any bone resection or damage to soft tissue. During flexion and extension of the knee specimen, the implant did not cause any hindrance. According to the above points, this implant can be considered to be a minimally invasive treatment, which might slow down progression of knee OA without any significant adverse events and/or any detrimental influence on future surgical procedures.

Publications Arising from This Research

Honours & Awards

- 3rd Place, Falling Walls Lab Australia, September 2017, Australian Academy of Science, Canberra, Australia.
- Runner-up, IET Auckland Local Network Present Around The World (PATW), March 2017, University of Auckland, Auckland, New Zealand.
- Winner, Speak Out for Engineering (North Island), November 2016, Callaghan Innovation, Auckland, New Zealand.

Published

- **Saeidi M.**, Gubaua J.E., Kelly P., Kazemi M., Besier T., Dicati G.W.O., Pereira J.T., Neitzert T., Ramezani M., The influence of an extra-articular implant on bone remodelling of the knee joint, Biomechanics and Modeling in Mechanobiology. 2019; In Press.
- **Saeidi M.**, Ramezani M., Kelly P., Neitzert T., Kumar P., Preliminary study on a novel minimally invasive extra-articular implant for unicompartmental knee osteoarthritis, Medical Engineering & Physics. 2019; 67: 96-101.
- **Saeidi M.**, Ramezani M., Kelly P., Hussin MS, Neitzert T., Biomechanics of a novel extra-articular implant for younger patients with knee osteoarthritis, Current Directions in Biomedical Engineering. 2018; 4: 203-205.

Under Review

- **Saeidi M.**, Kelly P., Netzel C., Scadeng M., Kumar P., Prendergast D., Neitzert T., Ramezani M., Investigation of a load-sharing implant on contact mechanics of the knee joint: A cadaver study, The Knee.

Oral Presentations

- **Saeidi M.**, Ramezani M., Kelly P., Neitzert T., October 2018, Development of a novel extra-articular implant for knee osteoarthritis, Invited Speaker, Friedrich-Alexander University Erlangen, Nuremberg, Germany.

- **Saeidi M.**, Ramezani M., Kelly P., Hussin M.S., Neitzert T., September 2018, Biomechanics of a novel extra-articular implant for younger patients with knee osteoarthritis, 52nd DGBMT Annual Conference (BMT 2018), RWTH Aachen University, Aachen, Germany.

- **Saeidi M.**, Ramezani M., Kelly P., Neitzert T., September 2017, Breaking the wall of knee replacement, Falling Walls Lab Australia, Australian Academy of Science, Canberra, Australia.

- **Saeidi M.**, Ramezani M., Kelly P., Neitzert T., September 2017, Breaking the wall of knee replacement, Falling Walls Lab (FWL 2017), New Zealand Royal Society, Wellington, New Zealand.

- **Saeidi M.**, Ramezani M., Kelly P., Neitzert T., March 2017, Development of a novel engineering solution for knee osteoarthritis, IET Auckland Local Network Present Around The World (PATW), University of Auckland, Auckland, New Zealand.

- **Saeidi M.**, Ramezani M., Kelly P., Neitzert T., December 2016, Development of a novel engineering solution for knee osteoarthritis, Speak Out for Engineering (Oceania), University of Canterbury, Christchurch, New Zealand.

- **Saeidi M.**, Ramezani M., Kelly P., Neitzert T., November 2016, Development of a novel engineering solution for knee osteoarthritis, Speak Out for Engineering (North Island), Callaghan Innovation, Auckland, New Zealand.

Table of Contents

List of Figures

List of Tables

Nomenclatures

c_r	Bone resorption rate
c_f	Bone formation rate
E	Young's modulus
m	Empirical constant
n	Number of cycles
$\dot{r}$	Remodelling rate
S_v	Specific bone surface area
U	Strain energy density
w	Half of the dead zone

Δt	Bone remodelling time increment
ν	Poisson's ratio
ρ	Apparent density
$\dot{\rho}$	Density change rate
ρ_t	Maximum density
$\bar{\sigma}$	Apparent stress
σ_{ij}	Components of the Cauchy stress
$\bar{\sigma}_t$	Effective stress
ψ_t	Daily stress stimulus
ψ_t^*	Reference stimulus

List of Abbreviations

ACL	Anterior Cruciate Ligament
AUTEC	Auckland University of Technology Ethics Committee
BMD	Bone Mineral Density
CoCr	Cobalt-Chrome
CT	Computed Tomography
EBM	Electron Beam Melting
FE	Finite Element
FEA	Finite Element Analysis
FF	Fujifilm
HTO	High Tibial Osteotomy
KJD	Knee Joint Distraction
LCL	Lateral Collateral Ligament
LMPRA	Lateral Meniscus Posterior Root Avulsions
MAP	Musculoskeletal Atlas Project
MCL	Medial Collateral Ligament
MFL	Meniscofemoral Ligament
MRI	Magnetic Resonance Imaging
OA	Osteoarthritis
PCA	Principal Component Analysis
PCL	Posterior Cruciate Ligament
PE	Polyethylene
ROI	Region of Interest

SLM	Selective Laser Melting
TKA	Total Knee Arthroplasty
TKR	Total Knee Replacement
UHMWPE	Ultra-High Molecular Weight Polyethylene
UKA	Unicompartmental Knee Arthroplasty
WHO	World Health Organization

Chapter 1

Introduction

1.1 Background

Osteoarthritis (OA) is the main musculoskeletal cause of physical disability in older adults [1]. In osteoarthritis, the cartilage in the knee joint slowly wears at the tibiofemoral surface contact [2]. Degeneration of articular cartilage leads to bone-on-bone rubbing, which makes it difficult for a person with OA to carry out daily activities and can also lead to a sedentary lifestyle. Osteoarthritis appears mostly in the knee and hip joints [3-5].

There is no known cure for knee osteoarthritis; however, there are various ways to control its symptoms. The most common treatments are conservative or non-invasive treatments, such as weight loss, exercise, physical therapy, and medications. Another type of therapy is surgery, which is very invasive. In the most common type of knee surgery, Total Knee Replacement (TKR) or Total Knee Arthroplasty (TKA), parts of the knee joint are replaced with artificial ones [6]. Mostly, TKA is recommended for end-stage knee OA and patients 65 years or older and the replaced joints last on average for about 15 years; after that implants should be revised in a revision operation [7]. TKR is very expensive (between $20,600 - $29,100 in New Zealand) and the occurrence of the osteoarthritis is responsible for most of the joint replacements performed in New Zealand [8]. It should be noted that the revision operation is even more expensive, more difficult, and more complicated than the primary one [9, 10].

In 2014/15, osteoarthritis affected 11% of adults in New Zealand [11]. In New Zealand, it is estimated that 25% of the population will be over 65 by the end of the 2030s [12]. In New Zealand, by 2026 the number of total knee replacements is predicted to increase by 183% according to some statistics which were published in 2014 [12]. Excess weight is one of the main contributors to many health issues, such as osteoarthritis. According to a health survey conducted in New Zealand in 2014/15, Pacific adults had the highest obesity rate (66.2%), followed by Māori adults where 46.5% were obese and this may lead to the prevalence of TKR for Māori in the future [11]. Research has shown that Māori are younger at the time of surgical procedure and have lower improvements after procedure when their pre-and postoperative scores were compared [13].

Among all patients who undergo knee replacement, the risk of implant failure is much higher in younger patients. For instance, a study showed that when patients under 50 years underwent knee arthroplasty, risk of two-year revision due to aseptic loosening or infection was almost four times more than for those who were over 65 at the time of the surgery [14, 15]. Also, according to some studies, dissatisfaction rates after arthroplasty is higher in younger patients [16]. The question is, apart from dealing with the symptoms or undergoing invasive surgeries, is there anything that can be done for patients? In other words, are the available treatments enough for different patients with different conditions?

1.2 Treatment gap

Most patients with knee osteoarthritis undergo TKA eventually, and the main reason for use of other treatments is to postpone this last resort (an invasive TKA) [17]. Accordingly, some physicians and patients have perceived the lack of suitable treatments between non-invasive and invasive treatments, particularly in the case of early-onset knee OA and younger patients [17, 18]. According to some surveys, not only do many health care professionals recognise the treatment gap for early-onset knee osteoarthritis, but also patients would prefer to postpone the invasive surgical options, such as knee arthroplasty, until their symptoms worsen, given the longevity of the implant and possible complications and limitations after surgery [19]. Even for patients, and particularly younger ones who are willing to undergo surgery, preference is for a method in which no bone resection is required [14, 20]. Apart from natural and probably inevitable factors, such as age and hereditable predisposition, it is believed that damage to the cartilage induced by repetitive loading, as well as an altered joint condition due to injuries, contribute to knee OA, particularly in younger individuals. For instance, one out of two individuals with a previous knee injury, such as meniscal damage or an Anterior Cruciate Ligament (ACL) rupture, develops knee osteoarthritis 10 to 20 years following the injury. Accordingly, the occurrence of those injuries in younger adults may lead to osteoarthritis when they are in their 30s or 40s [21]. These injuries could arise in an accident or sport. For example, according to a study conducted by Roos [22], in women, 51% (mean age 31) developed knee OA after 12 years and in men, 41% (mean age 36) developed knee OA 14 years after an ACL injury in sport. So, with the loading condition in the knee joint as an influential factor for the development of knee osteoarthritis, there is cause to address this issue and examine ways of controlling the load distributions in the knee joint.

Considering the above points regarding the treatment gap, some load-sharing implants [14, 23] have been developed recently in order to slow down the progression of the knee OA and postpone the invasive surgical options, by partially unloading the knee and redistributing the load in the joint. These treatments allow patients with knee osteoarthritis, in particular younger ones, to have their normal lifestyle for a longer period of time before going through invasive surgeries and facing postoperative limitations. One of them is an extra-articular implant, which may fill the aforementioned gap between the conservative and invasive treatments [23].

1.3 Aim of the research

After the invention and during the development process of any new implant, several studies should be conducted in order to investigate efficacy and influence of that implant on the knee joint. As a matter of fact, there are many different features to study for each new implant and all of them cannot be covered comprehensively in one research project. Therefore, this project aimed to investigate some critical aspects of a recently invented extra-articular knee implant for knee osteoarthritis. In other words, in this thesis, the effect of the implant on the contact mechanics of the tibiofemoral joint was numerically and experimentally investigated. Also, a cadaver study was carried out to study the influence of the implant on the joint space, and density changes in the tissues around the implant were investigated using a theoretical method.

This patient-specific implant was recently invented by Kumar [23] and is still at the early stages of the development process, so the outcome of this research is fundamental for the future development of this implant and similar devices.

1.4 Thesis structure

The structure of the thesis is as follows:

In this first chapter a brief introduction to the problem is provided. In the next chapter a literature review is conducted, which includes a wide range of information regarding knee anatomy and knee implants as well as background of the research objectives. In Chapter 3, the concept of a recently invented knee implant, the design process and Finite Element Analysis (FEA) of a knee model without and with the implant is described. Chapter 4 is about investigating the influence of the implant on the bone density numerically, including studying periprosthetic Bone Mineral Density (BMD) changes as well as density variations at the fixation holes in the femur and tibia, and to determine whether any such BMD changes are likely to be damaging to the health of the knee. Chapter 5 aims to study the surgical procedure of the implant attachment and investigate the influence of this implant on the contact pressure in a cadaver knee joint under different loading scenarios. Conclusions and future work recommendations are contained in Chapter 6 (final chapter) of the thesis.

Chapter 2

Literature Review

To study an implant for osteoarthritic knees, detailed knowledge of bone and knee biomechanics and their medical principles are required. Hence, in this section, the anatomy and kinematics of the knee and bone, as well as other topics concerning knee implant design, including materials, manufacturing, Finite Element Analysis (FEA), and bone remodelling are discussed in detail. Recent and relevant literature are also reviewed in this chapter.

2.1 Background

2.1.1 Knee anatomy

The knee joint comprises bone, ligaments, cartilage, and meniscus. These parts are shown in Figure 2-1. The knee joint connects the thighbone (femur) and bones of the lower leg (tibia and fibula). The two ligaments on the outer surfaces are the Lateral Collateral Ligament (LCL) and Medial Collateral Ligament (MCL). The two ligaments inside the knee are the Posterior Cruciate Ligament (PCL) and Anterior Cruciate Ligament (ACL). The articular cartilage in the knee covers the end of the femur (distal femur), top of the tibia (proximal tibia), and back of the patella (kneecap) and allows smooth gliding of bones. Also, there are menisci (collagenous cushions) between the bones, which act as shock absorbers [24].

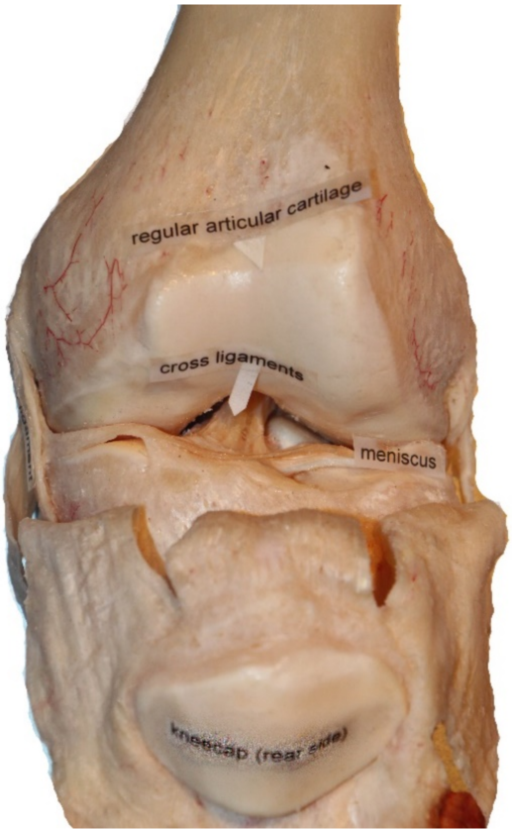

Figure 2-1. Anatomy of the knee joint.

The knee joint mainly moves in one plane (sagittal plane) similar to a hinge. Therefore, ligaments play a crucial role as bone constraints and in keeping the knee healthy. Generally, collateral ligaments limit side-to-side movements and cruciate ligaments limit front-to-back movements. Correct performance of the ligaments leads to the correct and stable motion of bones on each other. Accordingly, in the case of any laxity in, or damage to, ligaments, painful arthritis can occur due to excessive and inaccurate movement of bones [24].

In the study of human movement (kinesiology), there are three cardinal planes: sagittal, coronal or frontal, and transverse, as demonstrated in Figure 2-2. All movements happen in these planes or a combination of them [25].

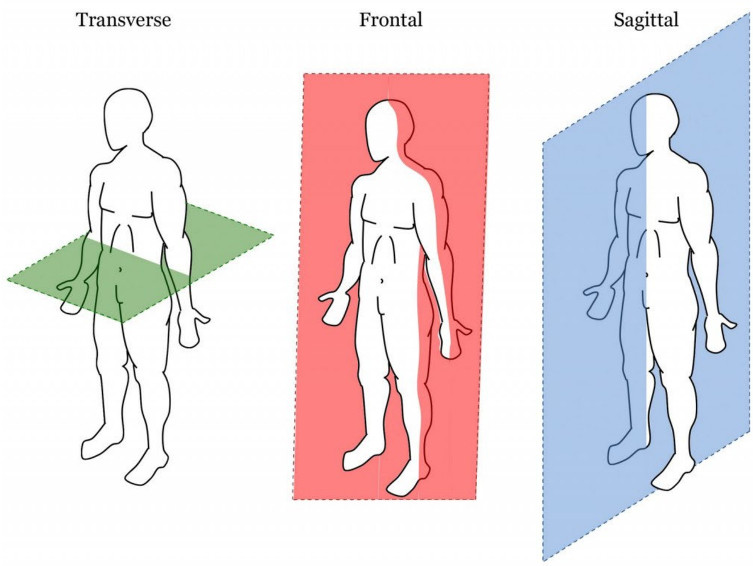

Figure 2-2. Cardinal planes of movement [26].

2.1.1.1 Femur, tibia, fibula, and patella

Of the four bones at the knee, the femur, tibia, patella and fibula, the former three are the main functional bones. The distal end of the femur creates two condyles, which articulate with the patella and tibia. The tibia and condyles form the tibiofemoral joint; the patella and trochlear groove form the patellofemoral joint, as illustrated in Figure 2-3 [27, 28].

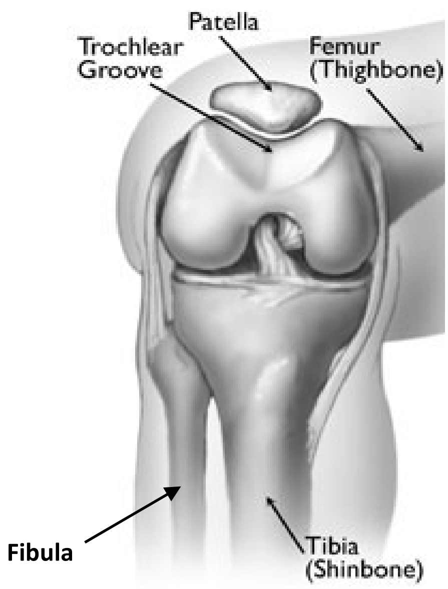

Figure 2-3. Schematic view of tibiofemoral and patellofemoral joints [28].

Similarly, the proximal head of the tibia includes the medial and lateral condyles and intercondylar area that form a joint with the condyles of the femur. The fibula, which is next to the tibia, does not articulate with the femur and patella, and it does not play a direct role in load transmission [27]. The patella, the largest sesamoid (bony nodule developed in a tendon) in the human body, might have different shapes, but is commonly proximally curved and distally tapered. It is fully encompassed by the quadriceps femoris tendon and the posterior side of it, together with the femur (trochlear groove), forms the patellofemoral joint [27].

As shown in Figure 2-4, a long bone includes two main sections: diaphysis and epiphysis. The diaphysis is a cylindrical shell, which connects the distal and proximal ends of the bone, and the epiphysis is the area at both ends of the bone, which is filled by spongy bone (cancellous bone). The inner layer of the diaphysis is covered by the endosteum, in which bone growth, repair, and remodelling happen. The outer layer of the bone is covered by the periosteum, which contains blood vessels, nerves, and lymphatic vessels. This layer covers all parts of the bone, except areas that are covered by articular cartilage [29]. Bone remodelling, i.e. the dynamic change and adaptation made by bone due to changes in its environment, is explained briefly at the end of this chapter and extensively in Chapter 4.

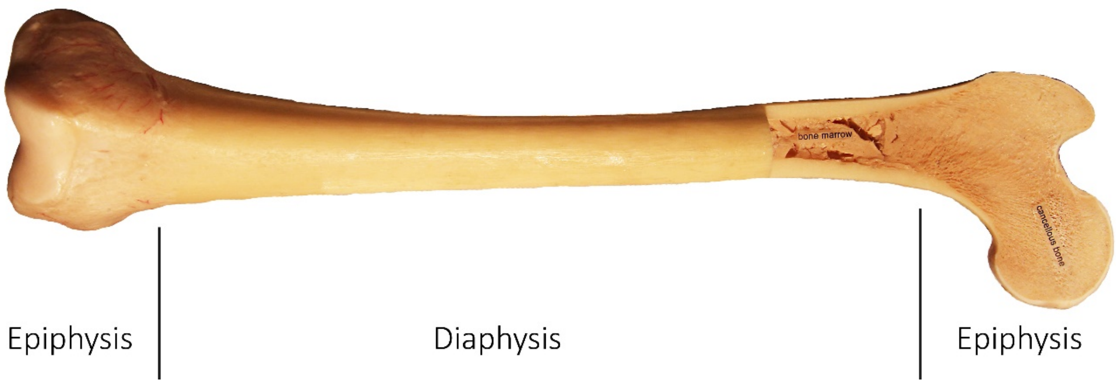

Figure 2-4. Bone structure.

There are four types of cells within bone tissue that are very important for bone function. These cells are osteocyte, osteoblast, osteogenic, and osteoclast [29]. Osteoblasts are found in the periosteum and endosteum and are responsible for developing new bone. The matrix surrounding the osteoblast calcifies, then it becomes the principle and most common cell of the bone (osteocyte). Osteocytes can communicate with each other through channels inside the bone matrix and receive nutrients. Osteogenic cells are found in the layers of the marrow and the periosteum. Based on their high mitotic activity, they differentiate and develop into osteoblasts. As mentioned earlier, bone has a dynamic nature and new tissue is continuously formed. The damaged or old bone is dissolved for repair or calcium release. Osteoclasts are responsible for bone breakdown or resorption. Old bone is constantly broken down by osteoclasts, whereas new bone is constantly formed by osteoblasts. In this way, there is a balance between bone formation and resorption processes [29]. The mentioned cells are shown in Figure 2-5.

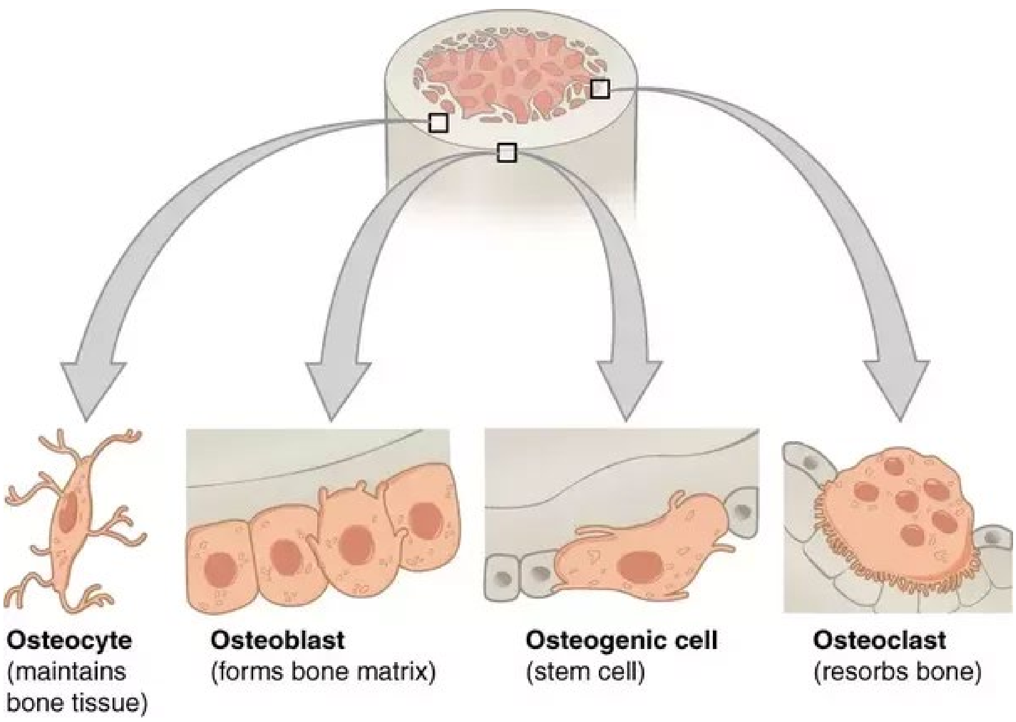

Figure 2-5. Four kinds of cell which are existed within the bone tissue [30].

2.1.1.2 Articular cartilage

Cartilage is avascular, i.e. all nutrients should diffuse through the cartilage matrix to reach the cartilage cells (chondrocytes). Therefore, the healing process of cartilaginous tissue is very slow. There are many types of cartilage tissue in the human body, but the type of cartilage found in the knee is fibrocartilage, which is tough because its matrix includes thick bundles of collagen fibers [29]. An intact femoral cartilage is shown in Figure 2-9a.

According to clinical and experimental observations, cartilage does have a limited ability to heal, hence minor damage to articular cartilage could self-repair [31]. Moreover, lesions, which extend to the subchondral bone marrow may also heal clinically. Thus, to repair or regenerate cartilage, cells should arise from the adjacent synovial tissue, underlying subchondral bone or an endogenous source [31].

2.1.1.3 Menisci

As shown in Figure 2-6, the menisci include two fibrocartilaginous c-shape pads that connect to the tibial plateau [32]. They are located between the condyles and tibia, and act as shock absorbers and load distributors. Their inner borders are concave and thin, whereas the outer borders are thick and convex. A very important point to note is: the peripheral regions are vascularized, while the inner regions are avascular. Accordingly, damage or tears to the outer meniscus normally heals, unlike tears at the inner areas [24, 27].

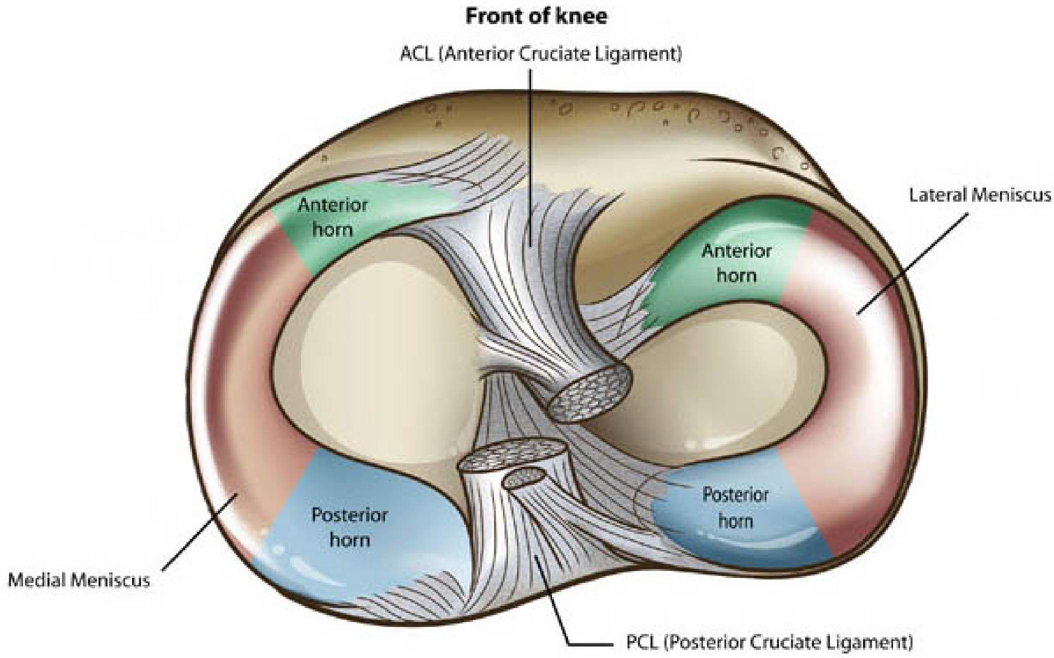

Figure 2-6. Schematic view of the menisci [32].

2.1.1.4 Ligaments

There are two types of ligament in the knee joint: extra-capsular and intra-capsular. The main extra-capsular ligaments are the Medial Collateral Ligament (MCL) and Lateral Collateral Ligament (LCL) (Figure 2-7). The main intra-articular ligaments are the Anterior Cruciate Ligament (ACL) and Posterior Cruciate Ligament (PCL) (Figure 2-6) [33]. The MCL starts from the medial epicondyle of the femur and extends to the medial condyle of the tibia. This ligament is attached to the meniscus, thus it generally damages in sports injuries. The LCL starts from the lateral epicondyle of the femur and extends to the lateral surface of the fibula, and the PCL connects the lateral surface of the medial condyle of the femur (intercondylar notch of the femur) to the posterior intercondylar area of the tibia [27]. The ACL connects the anterior intercondylar area of the tibia to the posterior section of the medial side of the lateral condyle of the femur [34].

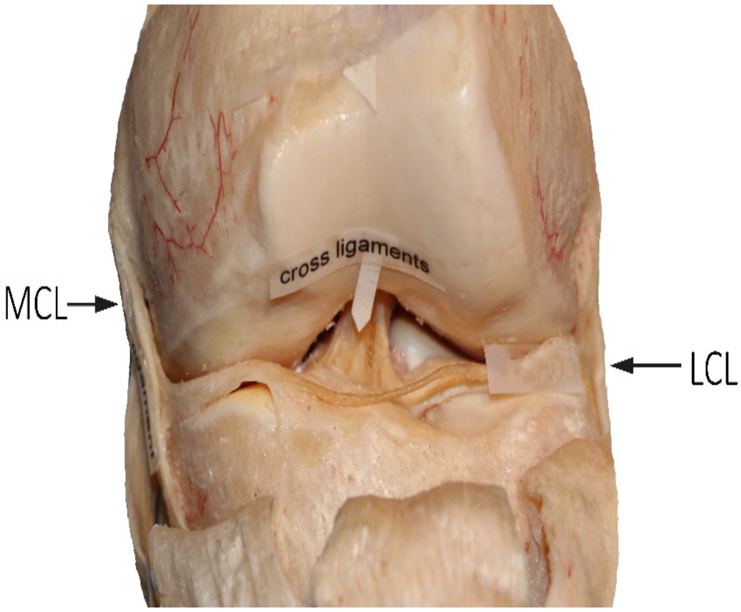

Figure 2-7. Ligaments in the knee joint.

2.1.1.5 Joint capsule

As shown in Figure 2-8, the joint capsule comprises the outer fibrous layer and inner synovial membrane. The capsule surrounds the condyles and intercondylar cavity on the posterior side. At the lower part, it joins with the margin of the tibia's articular surface [27]. All surfaces of the articular cavity which are not covered by cartilage are lined by the synovial membrane. It attaches to the cartilage's periphery and covers the femoral condyles, back surfaces of the patella and the tibia [27].

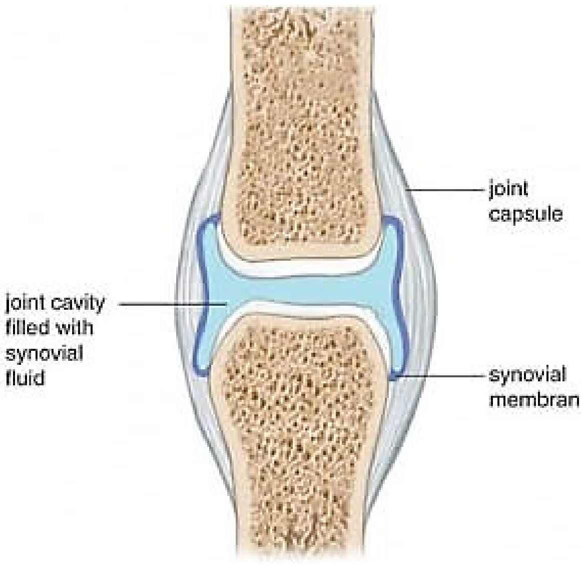

Figure 2-8. Schematic view of the knee joint capsule [35].

2.1.1.6 Synovial fluid and membrane

One of the most important functions of synovial fluid, which is found in all movable joints of the body, is lubricating the joint [27]. The synovial membrane is the main biologically active tissue of the knee joint. In some surgeries, such as total knee replacement, this membrane is damaged, although it regenerates and covers the whole joint again. This tissue has the important task of transferring any wear debris to the outside of the joint. Indeed, it filters these particles from the synovial fluid and drains them into the lymphatic vessels [36]. Synovial fluid and membrane are shown in a schematic view of the knee joint capsule in Figure 2-8.

2.1.2 Knee osteoarthritis; causes and treatments

As mentioned in the previous chapter, osteoarthritis (OA) is the most common type of arthritis and one of the main causes of musculoskeletal impairments in elderly people [1, 37]. The World Health Organization (WHO) reported that OA will be the fourth reason for disability by 2020 and that 33.6% of the population will be affected by this disease after the age of 65 [5]. Clinically, OA is defined as cartilage degeneration with inflammation, pain, and loss of joint function. An intact and degenerated femoral cartilage is shown in Figure 2-9a and b, respectively.

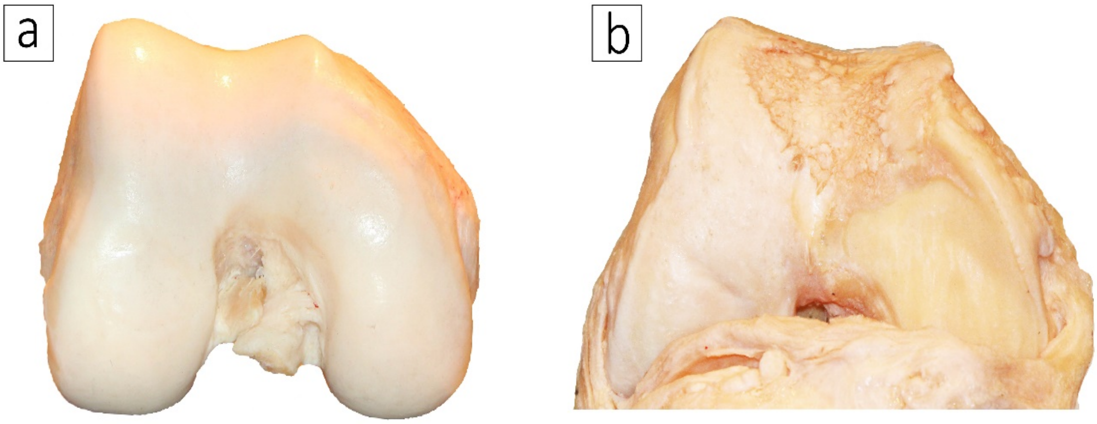

Figure 2-9. Femoral cartilage: a) intact, b) degenerated.

There are different ways to classify OA, such as from radiographic or advanced imaging, symptoms (stiffness, swelling, and range of motion), and a combination of these. Based on the joint space narrowing, knee osteoarthritis is categorised into four grades [15]:

1. Grade 0: Normal
2. Grade 1: Mild (1–33% narrowed)
3. Grade 2: Moderate (34–66% narrowed)
4. Grade 3: Severe (67–100% narrowed)

X-rays of normal (grade 0) and severe (grade 3) osteoarthritic knees are shown in Figure 2-10a and b, respectively [38]. Decrease in the joint space due to OA is clearly shown in Figure 2-10b.

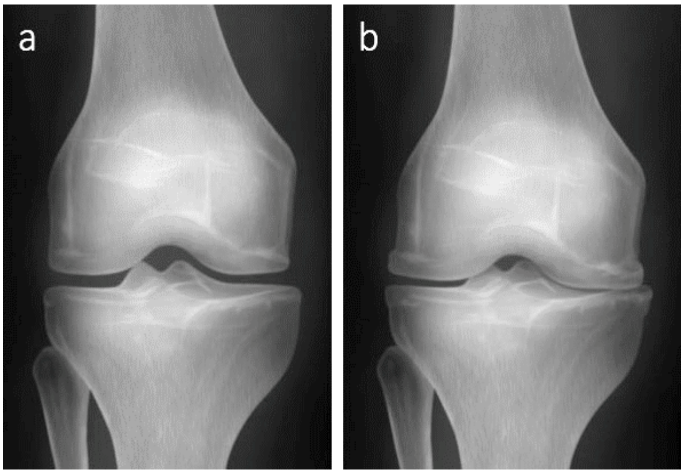

Figure 2-10. X-ray of a) normal knee, b) severe osteoarthritic knee [38].

There are many risk factors for knee OA, such as altered mechanics of the knee joint, muscle impairments, injury, obesity, and physical activities. Although there is no known cure for knee OA, there are many therapies, which are mostly used to alleviate symptoms and restore function. The main non-invasive treatments include exercise, weight loss, self-management and education programmes, injections, medications, and physical therapy [15].

For treating OA, many efforts have been made to repair focal lesions in cartilage and the menisci, without addressing the underlying etiology. Therefore, it seems that those studies have not been successful in halting the progression of OA because of the existence of an aberrant environment or biomechanical heterogeneity [2, 3, 39]. In fact, there is no nonsurgical treatment which has been shown to successfully attenuate the disease's progression [39]. Most of the time, excessive load results in stress concentrations in certain areas, which lead to cartilage degeneration. Hence, before any attempt to repair or regenerate tissue, a first-line therapy would be to address the deleterious loading condition of the knee joint. In other words, abnormal loading and an uneven stress distribution can be considered to be one of the major reasons for osteoarthritis progression [5, 39-41]. There are many biomechanical interventions, which are designed to adjust lower limb and knee joint loading during the knee movement. For example, implementing valgus knee braces, shoe inserts or foot orthoses lead to improved physical function, reduced analgesic dosage, pain reduction, and possibly slowing down disease progression [15].

Besides the above-mentioned conservative treatments, there are many kinds of invasive therapies, such as Total Knee Arthroplasty (TKA), High Tibial Osteotomy (HTO), and Knee Joint Distraction (KJD) [15]. As shown in Figure 2-11, in a TKA procedure, surfaces of the distal femoral head, proximal tibial head, and internal side of the patella are resected and replaced with metallic and polymeric parts [42]. The fact is that almost all patients with knee osteoarthritis undergo TKA eventually, and the main reason for use of other methods, specifically in younger patients, is to postpone this last resort (an invasive TKA operation) [17]. It should be noted that TKA is largely recommended for elderly people (>65 years old); however, research shows that more than 40% of TKAs have been performed before this age [6, 15].

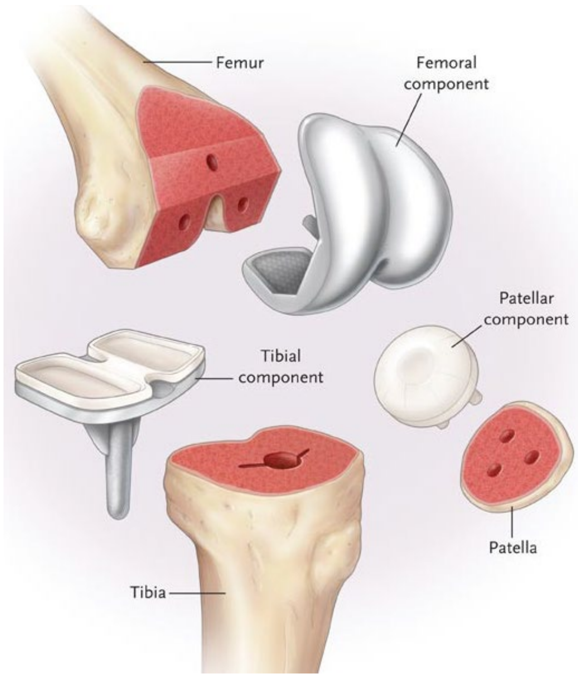

Figure 2-11. Schematic view of TKA components and procedure [43].

Based on the condition of the patient, Unicompartmental Knee Arthroplasty (UKA), which is less invasive than TKA, may be recommended. As shown in Figure 2-12, in UKA only the damaged compartment of the joint is replaced, which leads to the preservation of natural knee kinematics. Other advantages of this option compared to TKA include faster recovery and rehabilitation, lower morbidity, and less blood loss during surgery. However, higher risk of revision surgery and less longevity of the implant compared with primary TKA, as well as higher revision rates after TKA for patients who have previously had UKA, are some disadvantages of such partial knee replacement [15].

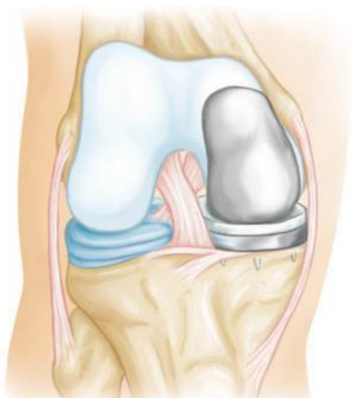

Figure 2-12. Schematic view of the UKA [44].

In an osteotomy operation, a wedge of the femur or tibia is removed in order to balance the pressure distributions on the knee joint, correct joint malalignment and slow down OA progression [45]. A schematic view of the tibial osteotomy operation is shown in Figure 2-13. Depending on the particular issue with the knee, after removing the wedge, the gap could be closed (closing wedge osteotomy) or left opened and filled with some bone graft to help the healing process [45]. Osteotomy could be considered for patients with unicompartmental knee OA and joint malalignment; however, other factors, such as age, life style, and knee condition of the patient should also be taken into account [46].

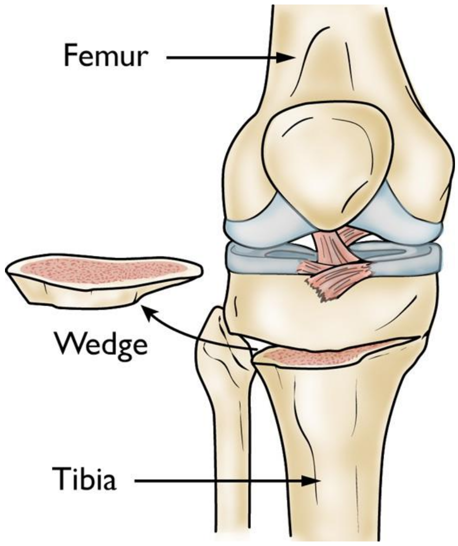

Figure 2-13. Schematic view of the tibial osteotomy operation [47].

Like any other surgical procedure, osteotomy has some advantages and disadvantages. On the one hand, with this operation the knee anatomy is preserved, TKA might be postponed for many years, and younger patients can have an active lifestyle post-operation. On the other hand, a longer, more painful, and more difficult recovery would be expected after the operation compared to the standard joint replacement recovery period [46].

Another surgical procedure to treat joint diseases including arthropathies, such as osteoarthritis is knee joint distraction, in which an external fixation (Figure 2-14) is used to increase the joint space for 6-8 weeks [48]. By distracting the knee joint about 5 mm, cartilage degeneration is halted and intrinsic cartilaginous tissue repair may occur due to intermittent intra-articular fluid pressures inside the joint capsule [48, 49].

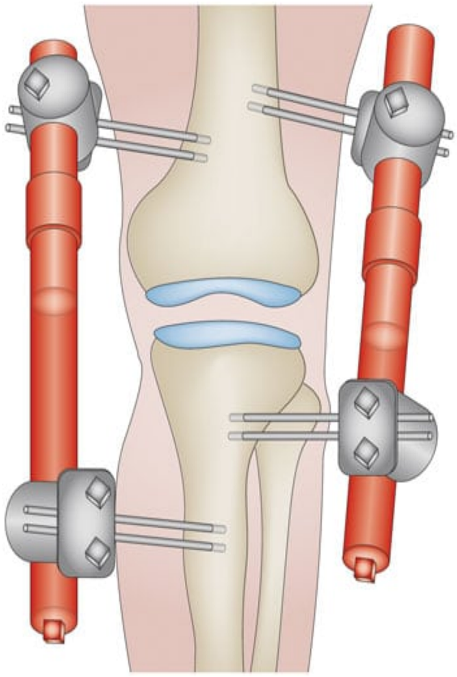

Figure 2-14. Schematic view of knee joint distraction [50].

This surgical procedure is a suitable option for young and middle-aged people and could delay a need for arthroplasty for several years. Also, similar to osteotomy, the natural anatomy of the knee joint is saved and there would be no restrictions in terms of activity after the frame removal. However, infections at the location of pins might develop due to the presence of an external fixator. The holes remaining in the bones would act as stress raisers during the healing process and might lead to bone fracture, although this is not a common issue [48, 49].

As mentioned in Chapter 1 (section 1.2) and according to the above-mentioned points, there is a gap between conservative and invasive therapies, particularly in the case of younger patients and those with early-onset knee OA; despite the many conservative treatments, many young patients suffer years of pain until they undergo a TKR operation [9, 10, 51].

A number of efforts have been made with the aim of introducing new techniques to fill the aforementioned gap between conservative and invasive therapies, such as a recently invented knee prosthesis by Kumar [23]. This patient-specific implant targets early-to-moderate grades of knee OA and might specifically be appropriate for younger patients [23]. The implant operates as a partially unloading device in order to slow down progression of OA, creating a suitable environment in which osteoarthritic lesions might be repaired and has been designed in such a way so as not to affect the natural anatomy of the knee. Moreover, it might be applied as an adjuvant treatment with other therapies. A schematic view of this implant is shown in Figure 2-15. Further details about this implant are explained in Chapter 3.

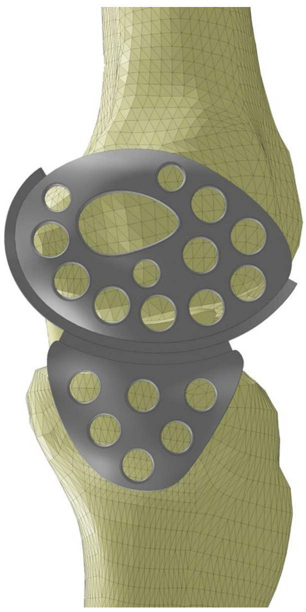

Figure 2-15. Schematic view of the new load-sharing knee implant.

Another recently developed device is the KineSpring® (Moximed) implant, which acts as a joint-unloader for unicompartmental knee osteoarthritis [19, 52, 53]. The KineSpring (Figure 2-16) implant connects to the femur and tibia and utilises a mechanism similar to a shock absorber, and is capable of unloading 13 kg of the knee load [54].

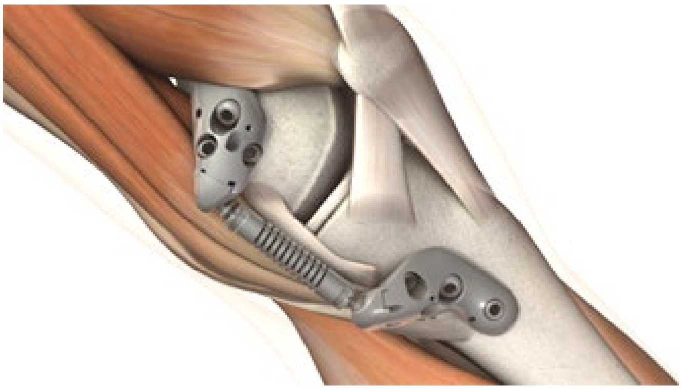

Figure 2-16. Schematic view of the KineSpring [55].

An in vitro study reported that all tested samples survived 10 million cycles of fatigue loading without any sign of plastic deformation or cracking [56]. The initial clinical studies for the KineSpring appeared promising. For instance, Miller et al. [37], after a 2-year pilot study, reported that according to the preliminary evidence, KineSpring could positively affect knee OA progression by increasing the joint space, thus reducing pain and improving joint performance. However, some treated patients with this implant have been facing serious adverse events after treatment, such as metallosis (deposition of metal debris into tissue around the implant), synovitis (inflammation of synovial membrane), implant-failure (fracture of implant components), leading to implant-removal and necessitating further therapies to solve the created issues [15, 17, 57, 58]. Furthermore, a case has been reported in which a patient mentioned the pain due to the device was far more than that experienced previously due to OA [58]. Further studies need to be done to elucidate the influences of this implant on the natural motion of the knee joint.

2.1.3 Implant materials

A wide range of biocompatible materials has been used for hip and knee implants, such as ceramics, metals, and polymers. Various combinations of these have been used to achieve the optimum articulation with minimum wear [59, 60]. The most common implant materials are as follows:

2.1.3.1 Cobalt-chrome alloy (CoCr)

Cobalt-chrome alloy is biocompatible, corrosion resistant, hard, and tough. Cobalt-chrome is one of the most popular alloys in the manufacturing of knee implants. However, it is not suitable for a small percentage of patients who have an allergy to specific metals, such as nickel. Tiny metal ions could be released into the human body from implants due to joint movement and the process of mechanical wear, and lead to an allergic reaction [59]. A cobalt-chrome knee implant is shown in Figure 2-17.

Figure 2-17. A cobalt-chrome femoral knee implant [61].

2.1.3.2 Titanium and its alloys

Titanium and its alloys are also biocompatible. Pure titanium can be implemented in implants where high strength is not important. For instance, a layer of porous (lattice structure) titanium can be bonded to the inner surface of an implant and the bone can grow into it for stronger fixation. The lattice structure around the stem of the tibial component of knee implant is shown in Figure 2-18. The most common titanium alloy, which is used to produce knee implants is Ti-6Al-4V, which includes vanadium and aluminum in addition to titanium. Titanium alloys have excellent corrosion resistance and lower density in comparison with other metals used in knee implants. Also, the elastic moduli of these alloys are lower than for other implant metals; therefore the risk of bone resorption is lower [59]. A tibial tray knee implant is shown in Figure 2-18.

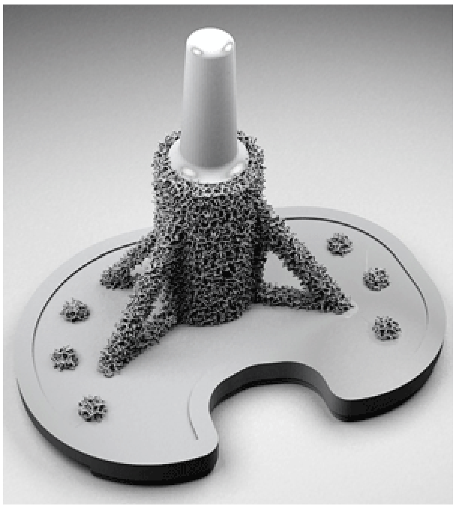

Figure 2-18. A titanium tibial tray knee implant [62].

2.1.3.3 Polyethylene (PE) and ceramics

Generally, a specific grade of polyethylene, namely Ultra-High Molecular Weight Polyethylene (UHMWPE), which is biocompatible and has significant wear resistance, is used in knee implants. This material allows the metal component to glide smoothly with minimum wear and friction, which leads to more longevity of the implant [59]. Another category of implant materials used are ceramic materials, which are not as common as metallic ones. Although they are very strong and specifically designed for implant applications, they can be vulnerable to fracture and breakage, due to their low fracture toughness. A common combination of the mentioned materials for knee implants is metal on polyethylene [63-65]. A ceramic on polyethylene knee implant is shown in Figure 2-19.

Figure 2-19. BIOLOX® ceramic knee implant components [66].

2.1.4 Manufacturing techniques for implants

There are many techniques used to produce knee implants, such as machining, forging, and casting. However, with the recent trend in producing patient-specific implants, these manufacturing techniques are not the best available options. Producing patient-specific implants could considerably improve the longevity and performance of the implant. In recent years, one of the most popular methods to produce knee implants has been additive manufacturing, which is also known as 3D-printing, particularly to produce patient-specific implants with complex geometries [67-69].

In 3D-printing, different materials, such as plastics or metals, are deposited in layers to manufacture an object [70]. Initially, this technique was used to create prototypes. However, recent developments and advancements have enabled 3D-printers to produce products that are comparable or even better than traditionally manufactured components. By using 3D-printing techniques, a wide range of materials can be used, and very complex designs can be produced in one step, without requiring extra major modifications [71]. A batch of hip stems produced in a single additive manufacturing process is depicted in Figure 2-20. Not only many individual components, but also of various sizes, can be observed in Figure 2-20 [72].

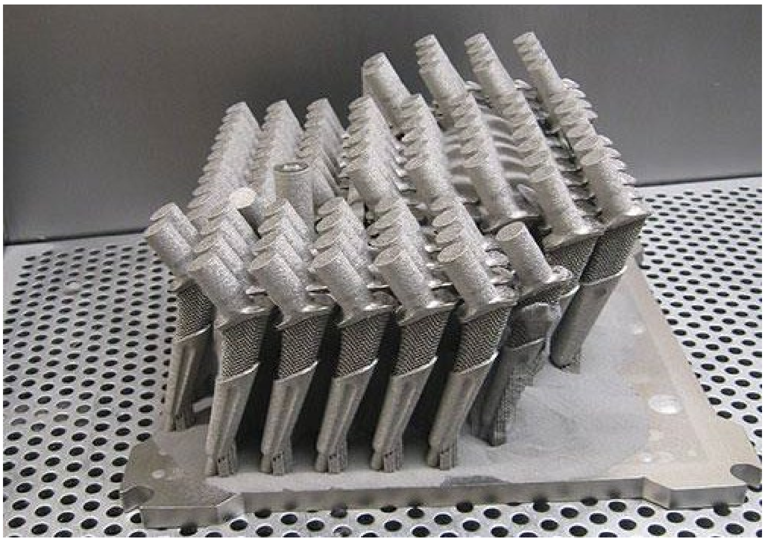

Figure 2-20. Hip implant stems produced by additive manufacturing [72].

Common types of metal additive manufacturing, which are normally used in the manufacture of implants are Selective Laser Melting (SLM) and Electron Beam Melting (EBM) processes. Both of these are based on powder bed fusion. In SLM, thin powder layers melt by laser and each layer fuses to the previous one, whereas in EBM, an electron beam is used for selectively melting the powder [73].

Almost all the common implant materials, such as stainless steel, titanium, and cobalt-chrome alloys can be utilised in these methods. The main difference between EBM and SLM is the way that they melt the powder. As mentioned, a laser beam in SLM and electron beam in EBM are used to melt powders. Another difference is, in SLM inert gas is used inside the fabricating chamber whereas, in EBM, fabrication takes place inside a vacuum chamber [73].

2.1.5 Finite Element Analysis

After initial design of any implant, and before prototyping, one of the major steps towards final design is the use of computer simulations. To do a precise Finite Element Analysis (FEA), the implant should be designed based on an anatomically accurate knee model. Such a model of the knee could be reconstructed from MRI or CT images, which can be time consuming and challenging; alternatively, it could be a model developed and validated by someone else, which are generally difficult to obtain as these models are mostly not publicly available. Then, the components of the knee model, material properties, loading and boundary conditions all depend on the type of the analysis being performed and the intended application. For example, a study into the kinematics or alternatively a stress analysis in a specific component of the joint may require two different models. In other words, the assumptions and simplifications made can play a major role and they are specified based on the aim of the project and nature of the computational model [74]. For example, Wang et al. [75] compared stress on knee cartilage during kneeling and standing using an FE knee model. In order to simulate the kneeling position, they used a model which included the patella and patellar tendon, which play a crucial role in that position. Their FE model in the kneeling position is shown in Figure 2-21 [75].

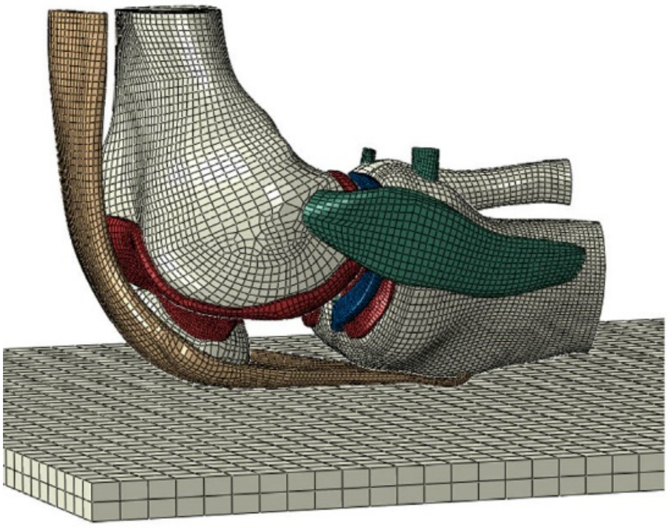

Figure 2-21. FE knee model in the kneeling position [75].

They reported that the peak contact pressure and von Mises stress were higher in the kneeling position. Kubicek and Florian [76], on the other hand, studied stress-strain analysis of the knee joint in the fully extended knee position. Therefore, their model did not include the patella and patellar tendon, since they play only a minor role in this position. Their FE model in the standing position is shown in Figure 2-22 [76].

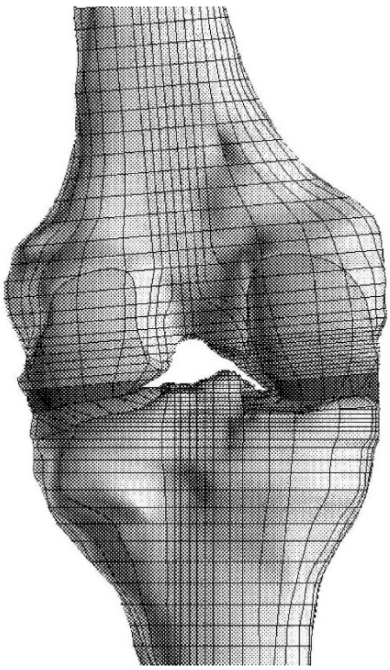

Figure 2-22. FE model in the standing position [76].

They reported that the load was higher in the medial condyle and that the maximum contact pressure between femoral and tibial cartilage and meniscus was 2.25 MPa. A further important point to be made here is that, after any FE modelling, the results should be validated either with data acquired from the literature or from experimental results [74].

FEA can be used to simulate loading conditions of the knee and the implant in order to find strengths and weaknesses of the designed model, instead of through expensive trial-and-error experimentation. By using the results of FEA, an initial design can be modified and optimised before prototyping. FEA can also be used to investigate the state of the knee in the absence of any implant in order to validate a computational model with experiments. For example, Li et al. [77] studied the stress arising in a knee model reconstructed using MR images under various tibial axial loads (up to 1400 N) in order to investigate influence of different parameters on the stress in the cartilage. Peak von Mises stresses in different loading conditions are shown in Figure 2-23 [77].

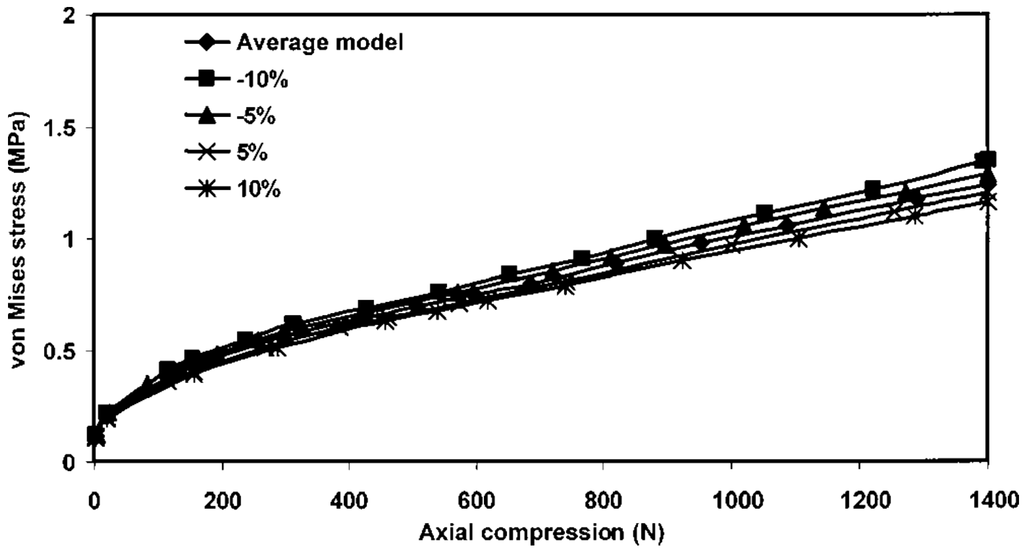

Figure 2-23. Peak von Mises stresses estimated by various finite element models [77].

They reported that variation of reconstructed cartilage thickness may lead to an approximately 10% difference in peak von Mises stress in the cartilage. Apart from cartilage thickness, there are other parameters, such as Poisson's ratio and Young's modulus, which can directly affect the stress and contact pressure in the cartilage. For example, Li et al. [77] reported that, by increasing the Poisson's ratio from 0.05 to 0.49, the peak von Mises stress in the cartilage was reduced approximately by 50%. Wang et al. [75] conducted research on a standing knee model under different compressive loads using various elastic moduli and Poisson's ratios. They reported that contact pressures in the cartilage for 300, 600, and 1000 N loads, were 1.87, 2.49, and 3.25 MPa, respectively. They also reported that a larger elastic modulus led to greater von Mises stress and contact pressure; however, increasing the Poisson's ratio resulted in greater contact pressure, but a smaller von Mises stress. A validated FE model can also be used to study the influence of an implant on stress or contact pressure distributions in the tibiofemoral joint. To do so, FEA should be conducted without and with the implant and results for both cases can be compared [78].

Many research have been conducted on the biomechanics of the total knee replacement theoretically and experimentally. Carr and Goswami [79] published a comprehensive review article on models and biomechanics of knee implants. Different areas, such as stress analysis, contact mechanics, wear, and loosening of various TKA implants were covered in their review article. As an example of the types of study which are possible, in one of the studies considered in their article, the effect of various Young's moduli of polyethylene on the contact area in metal on polyethylene TKA implants was investigated. As shown in Figure 2-24, increasing the elastic modulus led to a smaller contact area, and increasing the load led to a larger contact area [79].

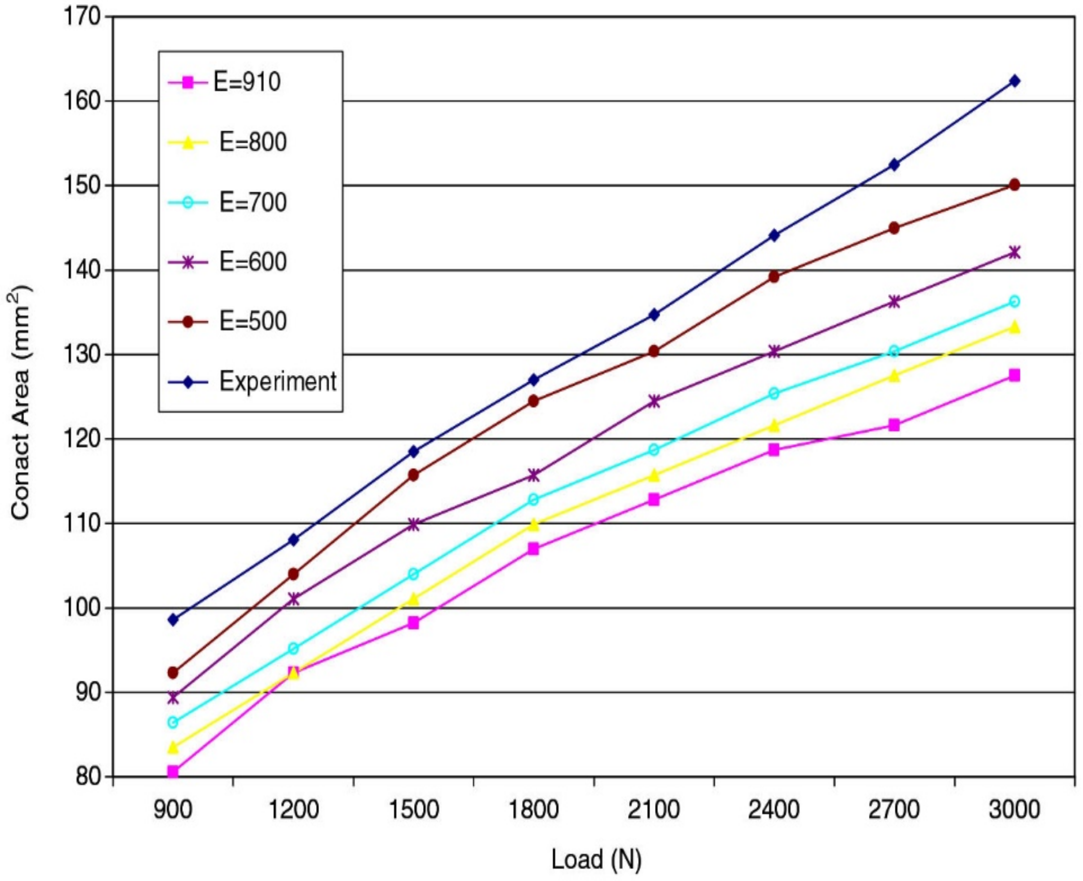

Figure 2-24. Influence of polyethylene Young's modulus (E, MPa) on contact area in metal on polyethylene TKA implants [79].

In this thesis, FEA is extensively discussed in Chapter 3.

2.1.6 Bone remodelling

In the bone remodelling process, old bone matrix is resorbed, and the new bone is formed. Although this process generally happens during bone growth, in adult life bone remodelling involves resorption of old or damaged bone and replacing it with new bone. The bone remodelling process is schematically shown in Figure 2-25.

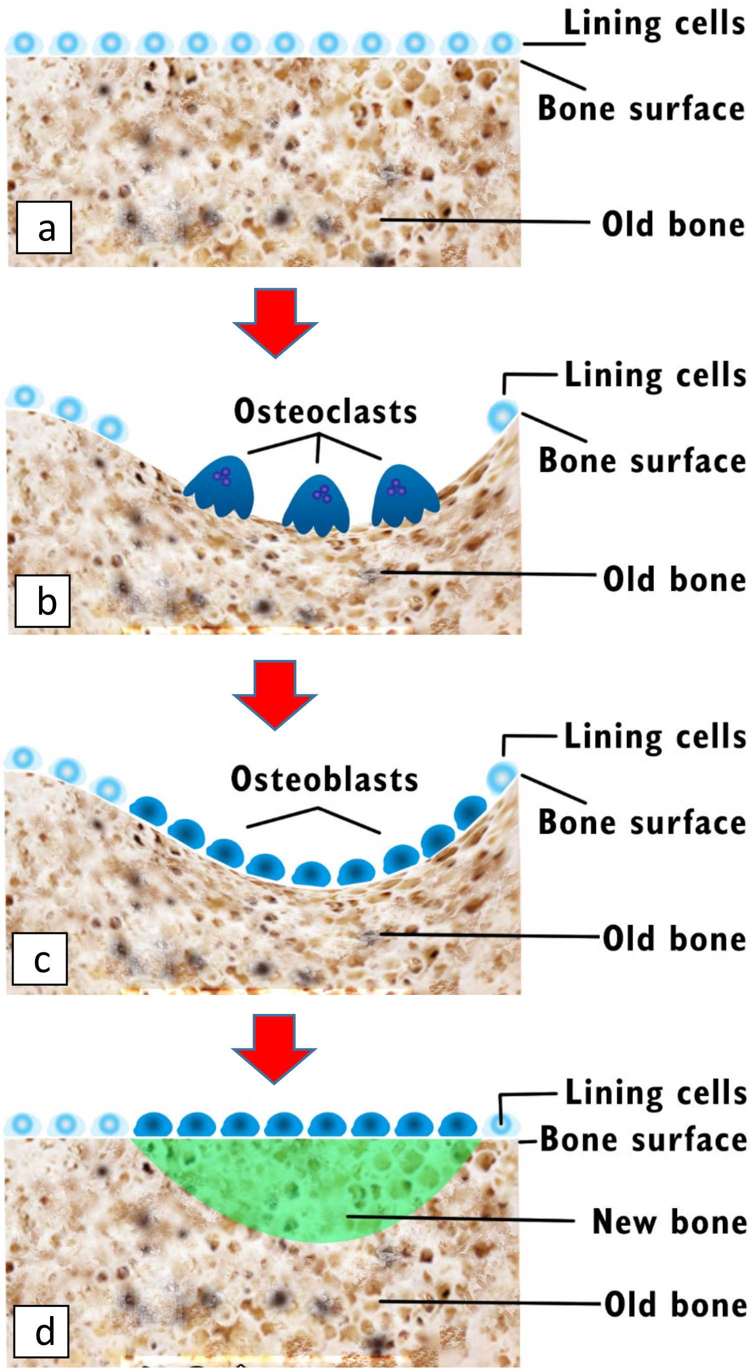

Figure 2-25. Bone remodelling process: a) old bone, b) bone resorption, c) bone formation, d) new bone [80].

Many causes, such as injury, exercise, and other heavy activities stimulate the bone remodelling process. However, even without any particular cause and only based on destroying and creating new bone, around five to ten percent of the whole skeleton is remodelled annually [29].

Regarding the crucial role of loading condition on bone remodelling, long missions in space can be used as tangible examples. In such missions, astronauts may lose about one to two percent of their bone mass per month. Seemingly, the cause is the lack of mechanical stress on the bones due to low gravitational forces. Lack of stress results in loss of mineral salt and collagen fibers and consequently decreases the bone strength. Indeed, the internal and external structures of a bone and accordingly the size and weight change based on the applied stress on the bone [29].

The use of implants in the body leads to remodelling of the adjacent bone and a consequent change in the loading condition, a phenomenon known as stress shielding. This is mainly due to the higher stiffness of the implant, which decreases the level of load applied to the bone leading to possible resorption. The type of design, shape, and fixation of the implant may also result in bone density variations. The main material property that plays a very important role here is the elastic modulus of the implant. In other words, the difference between elastic modulus of implant material and surrounding bone can be influential on the amount of bone resorption. Other factors affecting stress shielding are patient-related parameters, such as gender, age, activity level, and bone quality [36]. A schematic view of the stress shielding around a hip implant is shown in Figure 2-26 [81].

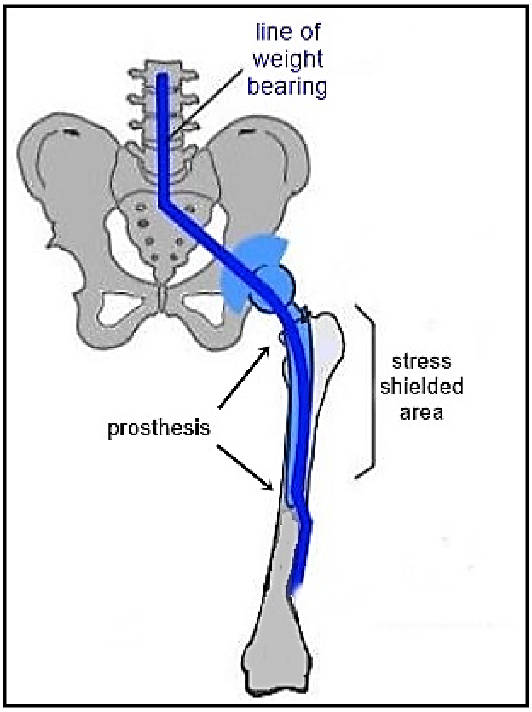

Figure 2-26. Schematic view of the stress shield area around a hip implant [81].

Apart from radiographs, mathematical methods as well as computer simulations can also be used to evaluate and predict the influence of implants on bone remodelling. This can be particularly useful for evaluating the effect of implants, as a bone remodelling computer simulation could reduce the risk of adverse effects by optimising the design before using the implant in the human body. Adaptive bone remodelling, which is based on the calculation of changes in strain energy density, has been used successfully for many years to simulate the influence of implants on bone density [82, 83]. There are other numerical bone remodelling methods [84-88]. For example, the Komarova method [88] is one of those which is based on the interaction of osteoclast and osteoblast cells. Hambli [89] studied bone remodelling of the hip joint using 2D FEA in conjunction with the Komarova method. He simulated bone density of the proximal femur up to five years (Figure 2-27), starting with isotropic homogeneous material properties [89].

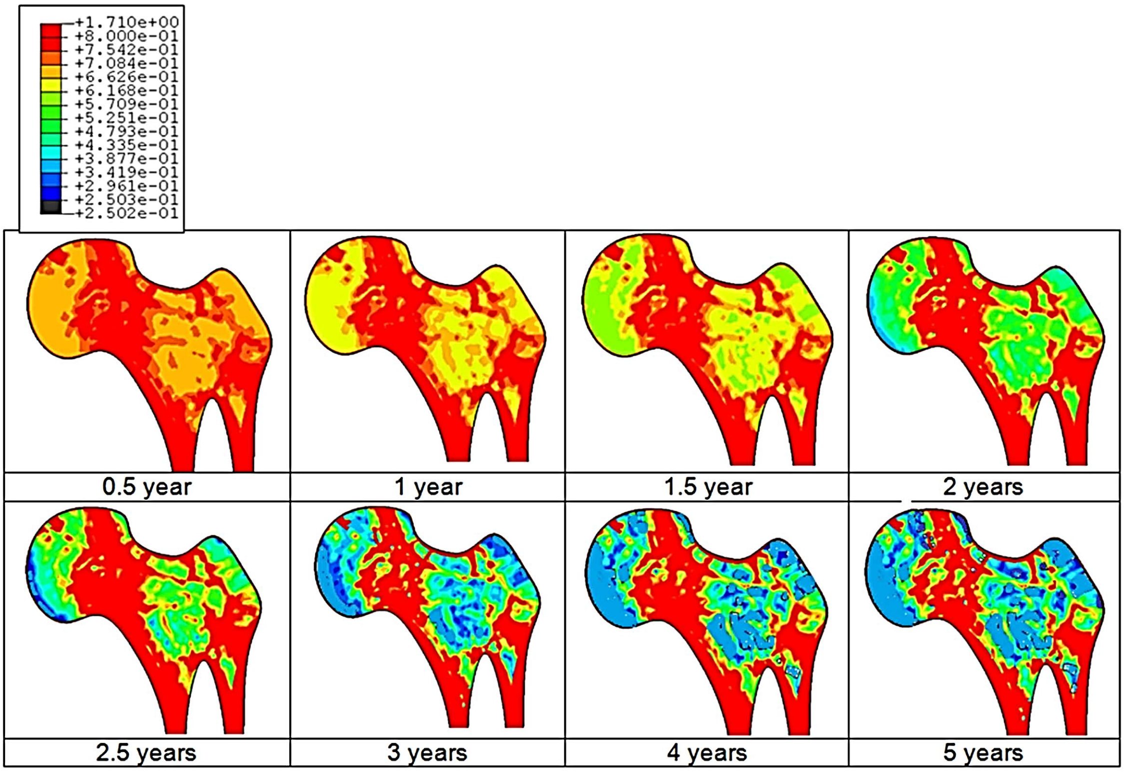

Figure 2-27. Predicted apparent bone density (g/cm^3) variation in a 5-year simulation [89].

Although he did not validate the results with the experimental data, he reported that the achieved density distributions represent many architectural features of the human femoral head. Many studies have been performed on the bone remodelling of the hip joint [90-93]. For example, Levadnyi et al. [83] investigated bone remodelling of different hip implant designs using an adaptive bone remodelling method and reported that the short stem implants provide a better load transmission to the proximal region of the femur compared to those with long stems. They also reported that, in the case of hip resurfacing, bone density was very close to an intact femur. However, only a limited number of studies have been conducted on bone remodelling of the knee joint. For example, Quilez et al. [94] and Jia et al. [95] examined and reported the influence of different TKA implants on bone density of the tibia using adaptive bone remodelling methods. Quilez et al. [94] reported that for all designs, the bone mineral density increased in the diaphysis (Figure 2-28a), while it decreased in the medullary channels and proximal epiphysis (Figure 2-28b).

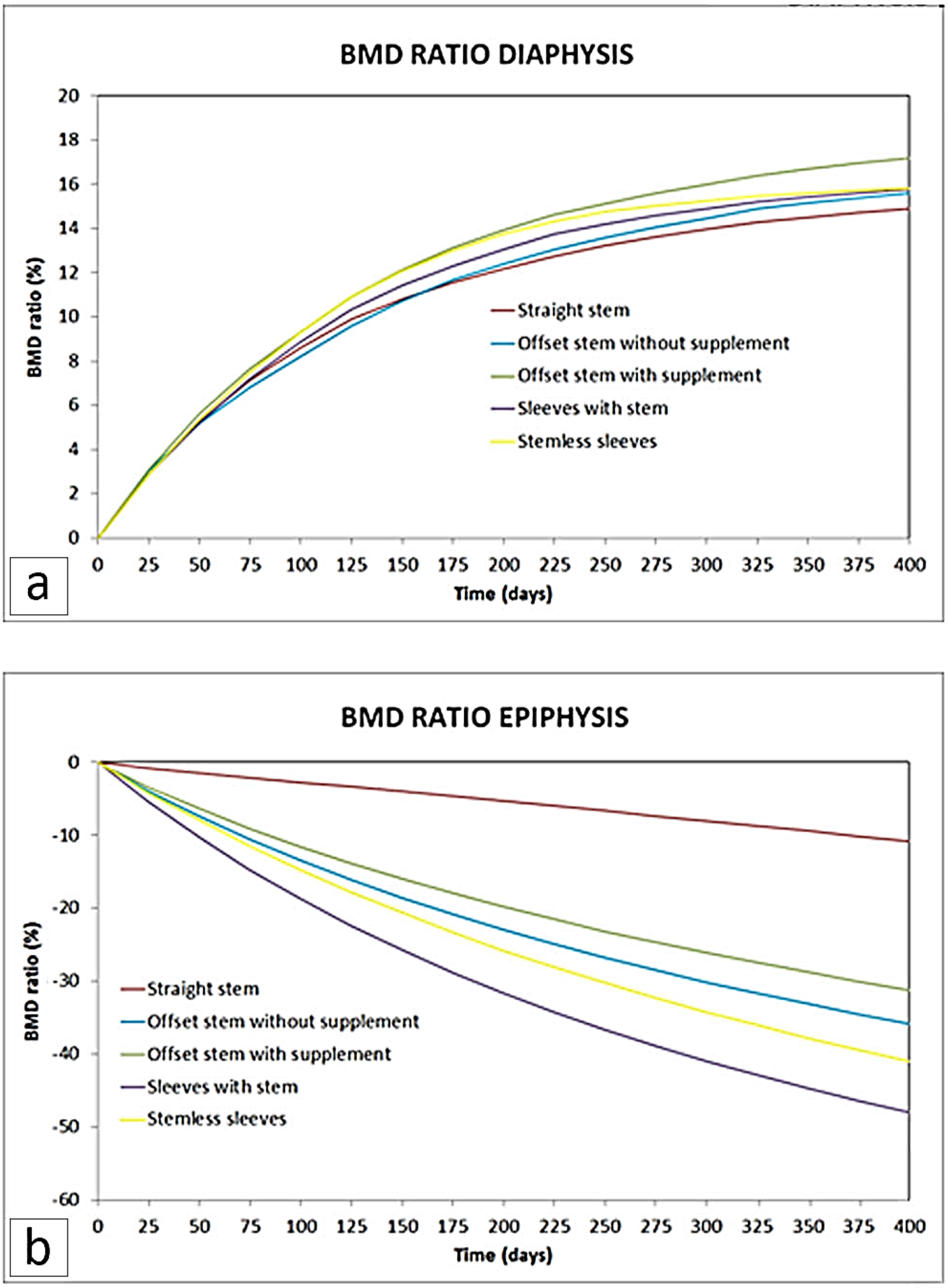

Figure 2-28. Bone mineral density variation in tibia: a) diaphysis, b) epiphysis [94].

Jia et al. [95] reported that short stem knee implants performed better, in terms of influence on bone remodelling, whereas long stems provided better stability in the bone. Other studies have also been conducted on bone remodelling in the tibia after knee replacement [96, 97]. For example, Robalo [96] developed a 3D model of the tibia from CT images and modelled it as a porous material. He then used a bone remodelling technique based on topology optimisation and reported that using long stem implants (cemented and non-cemented) led to stress shielding in proximal tibia and as a consequence, a significant periprosthetic bone density reduction. He also reported bone hypertrophy around the stem's tip due to stress concentration. Bone remodelling is discussed in detail in Chapter 4 in this thesis.

2.1.7 Cadaveric experiments

After design and analysis stages, and before animal or human trials, experiments and particularly cadaveric ones can be the next step in an evaluation process to study the influence of an implant on the joint [98]. Cadaveric knee joints without and with a TKR implant are shown in Figure 2-29a and b, respectively. For extra-articular implants in particular, the purpose of cadaveric experiments is to study the influence of the implant on the contact mechanics of the tibiofemoral joint as well as surgical considerations.

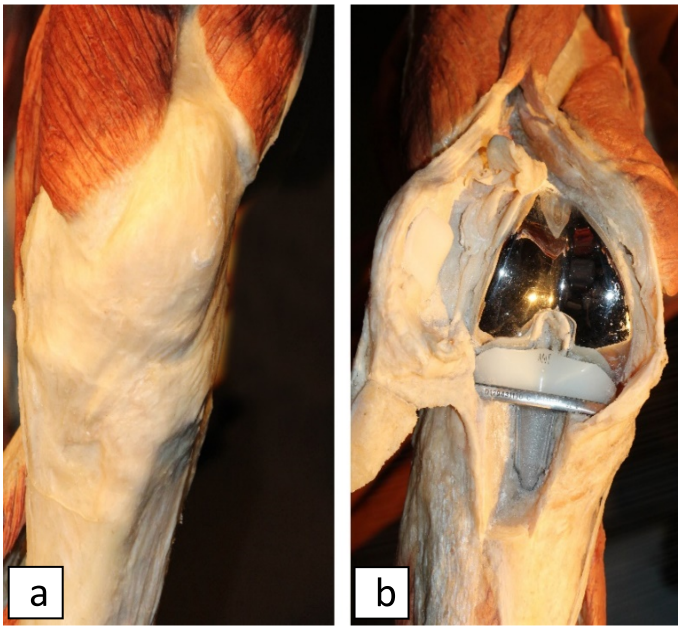

Figure 2-29. A cadaveric knee joint: a) without implant, b) with implant.

Cheong [99] carried out some preliminary experiments on cadaver knees in order to study the overall performances of an extra-articular implant, such as range of motion, attachment method, and simplicity of implant insertion. After attachment of the implant by a knee surgeon, he reported that the implant did not appear to affect the soft tissue around the implant and the articular cartilage was not damaged [99]. In terms of motion, it was observed that the plates were able to slide over one another without any hindrance and that the implant does not affect the range of motion during flexion and extension. It was also reported that the articulating surfaces remained in contact even during complete flexion. Importantly, the articulating surfaces did not dislocate and they remained in contact during the knee movement [99].

One of the methods used in order to perceive the biomechanics and specifically contact pressure at the knee joint, is pressure-mapping sensing, such as with the use of a Tekscan® sensor (Tekscan, Inc., Boston, MA) [100, 101]. This is a very thin film pressure sensor which can be used for different applications including cadaveric specimens, and provides real-time measurements under quasi-static and dynamic loading conditions [98]. Tekscan sensors can be found in different sizes and shapes as well as encompassing different pressure ranges. One type of this sensor is specifically designed for knee joint experiments, Tekscan sensor model 4000 (Figure 2-30), which is used in this research and discussed in more detail in Chapter 5.

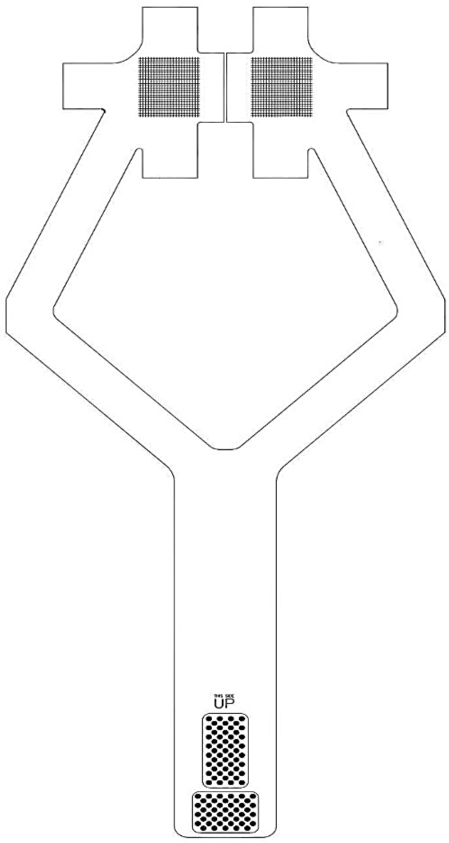

Figure 2-30. Schematic view of the Tekscan sensor model 4000 [102].

Thambyah [103] used a Tekscan sensor to compare the contact pressure in both compartments of the cadaver knee joint when larger forces are applied to one compartment. He reported that, although the applied force to both compartments was different, the average measured stresses were similar in both, due to different contact areas between condyle and tibial plateau in the medial and lateral compartments.

In a study conducted by Wang et al. [104], a Tekscan sensor was used to compare the contact area of healthy, injured and repaired joints. It was observed that an intact knee, injured knee i.e. meniscectomy, and a repaired knee with a bone plug meniscal replacement can have maximum contact areas of 546 ± 132 mm^2, 192 ± 122 mm^2, and 398 ± 148 mm^2, respectively. A schematic view of their experimental setup is shown in Figure 2-31.

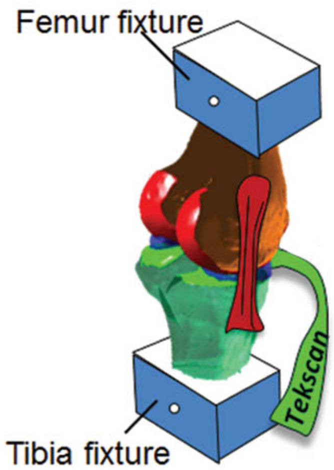

Figure 2-31. Schematic view of experimental setup used by Wang et al. [104].

Tekscan sensors can also be used to compare different TKA implants, in terms of maximum stress and its location as well as the contact area. Such information would be very useful in order to optimise implant design. For instance, in TKA implants, the range of contact stress and contact area for the tibiofemoral joint measured by Tekscan sensors are 5–50 MPa and 200–800 mm^2, respectively, and for the patellofemoral joint they are 5–25 MPa and 5–250 mm^2, respectively [105, 106]. Luyckx et al. [106] used an experimental setup as shown in Figure 2-32 in order to measure contact area and contact pressure in the patellofemoral joint using a Tekscan sensor.

Figure 2-32. Experimental setup used to measure contact area and contact stress in the patellofemoral joint [106].

Another type of sensor, which can be used to measure interfacial stress and contact area is Fujifilm (FF) pressure-sensitive film. Unlike the Tekscan sensor, it is a single-use and inexpensive film which has been used to investigate in vitro contact mechanics under static loading and does not provide real-time measurements [98].

Cadaveric experiments and contact pressure measurements are discussed in Chapter 5 of this thesis.

2.2 Research gap

As mentioned in Chapter 1 (section 1.2), there is a treatment gap between non-invasive and invasive treatments for knee OA and one of the recently invented implants to bridge this gap is a load-sharing implant, which attaches to the medial side of the knee in order to partially unload the joint [23].

According to the literature and to the best of the author's knowledge, no FEA on this implant has been conducted using an anatomically accurate FE model. Also, no cadaver study has been carried out on this implant using an accurate contact pressure measurement on a specimen with all ligaments intact. Therefore, this study aimed to numerically and experimentally investigate the influence of the implant on the contact mechanics of the knee joint. In addition, FEA in conjunction with adaptive bone remodelling was conducted to study the effect of the implant on the BMD of the femur and tibia. Also, the attachment procedure as well as surgical considerations were investigated using cadaver specimen. According to these points, objectives of the research were defined.

2.3 Objectives of the research

The following are the main objectives to be addressed in this research:

1. To investigate how an extra-articular load-sharing implant would affect the load distributions in the tibiofemoral joint using an anatomically accurate finite element knee model.

2. To study the influence of this implant on the bone mineral density of the femoral and tibial heads.

3. To perform cadaveric experiments in order to perceive surgical considerations as well as the influence of the implant on the contact pressure of the tibiofemoral joint.

These objectives are addressed in Chapter 3, Chapter 4, and Chapter 5, respectively.

Chapter 3

Stress Analysis of the Tibiofemoral Joint and Implant

3.1 Introduction

In this chapter, the concept of a recently invented knee implant [23], design procedure, and FEA of the implant are explained. As mentioned in Chapter 1 (section 1.3), the aim of this research was to evaluate a few aspects of this novel extra-articular load-sharing knee implant. The implant was developed to attach to bone in such a way such that there is no need to resect either the distal femur or the proximal tibia. In other words, the implant is supposed to support the articulation of the joint and keep the original joint anatomy intact, including the ligaments. As mentioned before, in other treatments, such as TKA, surgeons remove the tibiofemoral joint and cap the ends of the bones with metallic parts, which leads to an unnatural replication of the anatomy of the natural knee. As a matter of fact, arthroplasty leads to an elimination of any chance of cartilage healing, because the cartilage is removed during the surgery [99]. However, the novel implant was designed in order to off-load the knee joint and provide a conducive environment in order to slow down OA progression and even promote cartilage repair.

A Finite Element Analysis (FEA) was used to investigate stress distributions in the cartilage and implant, due to the fact that joint stress is one of the known risk factors contributing to the development and progression of knee OA [40]. As mentioned, reducing the stress in the osteoarthritic region could slow down progression of the disease. Therefore, in this chapter, efficacy of the implant, in terms of stress and contact pressure reduction in the femoral cartilage, particularly in the medial compartment is studied.

3.2 Methodology

3.2.1 Implant design and the knee model

The extra-articular implant discussed in this study was designed based on the inventor's concept to remove the excessive load in the medial compartment, because that side bears 60-80% of the load applied on the knee during gait [23, 107]. As shown in Figure 3-1, the main components of the implant are: a femoral plate which attaches to the medial side of the femur, and a tibial plate which attaches to the medial side of the tibia. These plates act as a load transmission medium between the distal femur and proximal tibia. The transmitted load distributes over the articulating surfaces between the plates, where the plate surfaces slide over each other.

Design was not a primary focus of this thesis. The implant was designed based on the initial invented concept design [23]. This is a patient-specific implant, so the design can be modified to fit the geometry of the patient's bone. According to the initial concept design, the suggested thickness for the implant is 4-6 mm, and for this thesis 4 mm was selected in order to avoid any soft tissue irritation caused by the thickness of the implant [23].

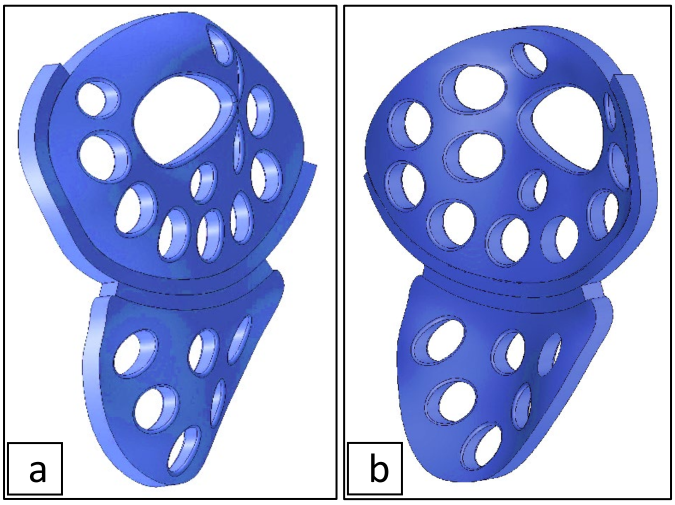

Figure 3-1. 3D model of the implant: a) external side, b) internal side.

As shown in Figure 3-1, several holes were also incorporated into both parts of the implant to reduce overall weight and to help prevent the possibility of bone or tissue necrosis around the implant [108]. These holes can be used to attach the implant to the joint using screws. A larger hole in the femoral plate was also incorporated in order to accommodate the Medial Collateral Ligament (MCL).

Finding an anatomically accurate knee model was challenging, as most of them are not publicly available. Therefore, the first model used for FEA was just a simple model (Figure 3-2a) including femur and tibia provided by the Auckland Bioengineering Institute at the University of Auckland. Soft tissues were generated by SolidWorks® (Dassault Systemes) in both compartments to act as cartilage and menisci and load transmitting medium (Figure 3-2b). The implant was then attached to the medial side of the model (Figure 3-2c) and a simplified FEA was conducted using the Abaqus®/standard (Simulia) FEA software suite. For this model, material properties for all components were defined as isotropic linear elastic material [76]. Also, instead of having cortical and trabecular bone, hard tissue was considered as cortical bone only in this simplified analysis [109].

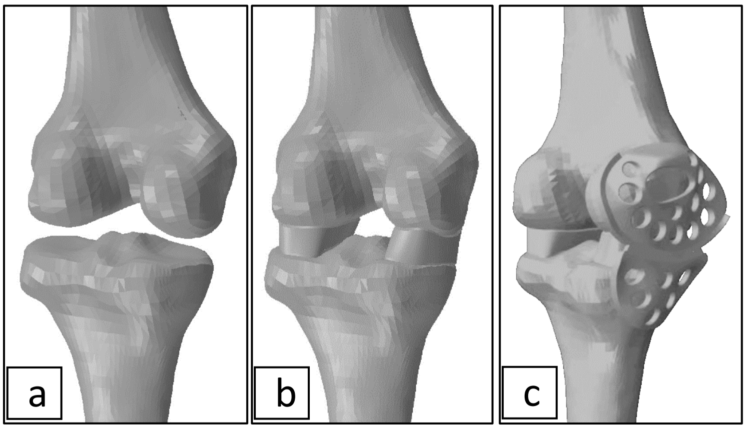

Figure 3-2. The first knee model used in this research: a) bones, b) bones and soft tissue, c) bones, soft tissue and implant.

A proper knee model is an anatomically accurate model including femur, tibia, cartilage and ligaments, and should be modifiable using a CAD package, which was not the case for the first model (Figure 3-2a). The final knee model that was used for this study was developed by Wangerin [110], and is publicly available in the biomedical repository at Simtk.org as shown in Figure 3-3.

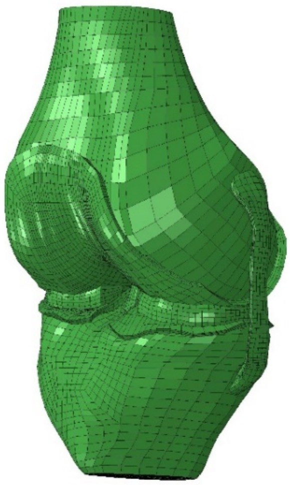

Figure 3-3. Wangerin model imported into Abaqus.

The Wangerin model is a modified version of one of the anatomically accurate publicly available knee models, from the Open Knee project [111]. The original CAD model of the Open Knee project is shown in Figure 3-4.

Figure 3-4. The original CAD model of the Open Knee project.

The main problem with the Wangerin model is the fact that it is available as an input file and, after importing to Abaqus, it is converted to an orphan mesh model; a mesh with no associated geometry (Figure 3-3), which cannot be modified in Abaqus, in terms of mesh type and size. Also, the whole model is recognized as one part and none of the components can be edited. Therefore, in order to create a modifiable model, the Wangerin model was first exported as a STL file and converted to an IGES file using SolidWorks. Thereafter, components were separated using SolidWorks and the model was rebuilt in Abaqus by importing IGES files.

Appendix A includes the input file for the new FEA model without the implant. The new knee model was imported into SolidWorks in order to design the implant. The curvature and contact surface profiles of the implant were designed to closely follow the curvature of the bone surfaces and edges as shown in Figure 3-1a and b. In order to build a 3D model of the implant, initially a plane was generated on the surface of the bone based on a 3D sketch, then a copy of that plane was created in parallel with the first one and the implant was then created using the loft command in SolidWorks.

As mentioned in Chapter 2 (section 2.1.3), one of the most widely used materials for knee and hip implants is titanium alloy (Ti-6Al-4V), which was also selected for finite element analysis of this implant [51, 112]. Other types of materials are also used for implants, such as cobalt-chrome alloy. However, for this study, titanium was selected, as its Young's modulus is lower than that of cobalt-chrome, which reduces the possibility of bone resorption [113]. The optimum material selection for the implant is not part of the scope of this research.

As mentioned previously, this implant can easily be designed fitting the surfaces of MRI-scanned or CT-scanned reconstructed models, thus it can be considered to be a patient-specific implant. A prototype of the implant was produced by additive manufacturing (selective laser sintering), which may well be the best method of manufacture for this implant. Other manufacturing techniques, which could be used to produce this implant include machining, investment casting, and forging [68, 69]. The assembled implant attached to the 3D-printed bones is illustrated in Figure 3-5.

Figure 3-5. A prototype of the implant at the medial side of the knee.

3.2.2 Finite element analysis of the knee model

A static FEA was conducted in Abaqus for the extended knee position, before and after attaching the implant, in order to study the influence of the implant on the stress distribution at the tibiofemoral joint. In other words, model results were compared with those for the case of no-implant, in order to study the efficacy of the implant: stress and contact pressure distributions of femoral cartilage were investigated in the model without and with the implant. Given that the analysis was conducted in standing position and the applied load is 400 N, cartilage deformation was assumed insignificant, so it was not investigated in the study reported in this chapter.

3.2.2.1 Material properties

A homogeneous linear elastic material model was developed for cortical bone with a Poisson's ratio of 0.33 and a Young's modulus of 17 GPa as well as for cancellous bone with a Young's modulus of 0.4 GPa and a Poisson's ratio of 0.33 [114]. The cartilage was assumed to be an isotropic elastic material with a Poisson's ratio of 0.45 and a Young's modulus of 10 MPa, as per the studies reported in [75, 114, 115]. The meniscus was modeled as a transversely isotropic, linear elastic material based on the collagen fiber directions of menisci [116]. Material orientations were assigned to the menisci as shown in Figure 3-6. Axis 1 represents circumferential fibers, axis 2 represents axial fibers and axis 3 represents radial fibers.

For the menisci, the Young's moduli in the circumferential ($\mathrm{E_\theta}$), radial ($\mathrm{E_R}$), and axial ($\mathrm{E_Z}$) directions were 125, 27.5, and 27.5 MPa, respectively [114]. The Poisson's ratios for menisci were 0.1 ($\nu_{\theta\mathrm{R}}$), 0.1 ($\nu_{\theta\mathrm{Z}}$), and 0.33 (ν_{RZ}), and the shear moduli ($\mathrm{G_{\theta R}}$ and $\mathrm{G_{\theta Z}}$) were 2.0 MPa [114]. All ligaments were assumed to be hyperelastic and their stress-strain relationship were obtained from Mesfar and Shirazi-Adl [117]. Mooney-Rivlin hyperelastic model constants were automatically calculated by Abaqus using input uniaxial tensile test data [75, 118]. For the implant material, a linear elastic model was developed for titanium with a Poisson's ratio of 0.3 and a Young's modulus of 110 GPa [112, 113].

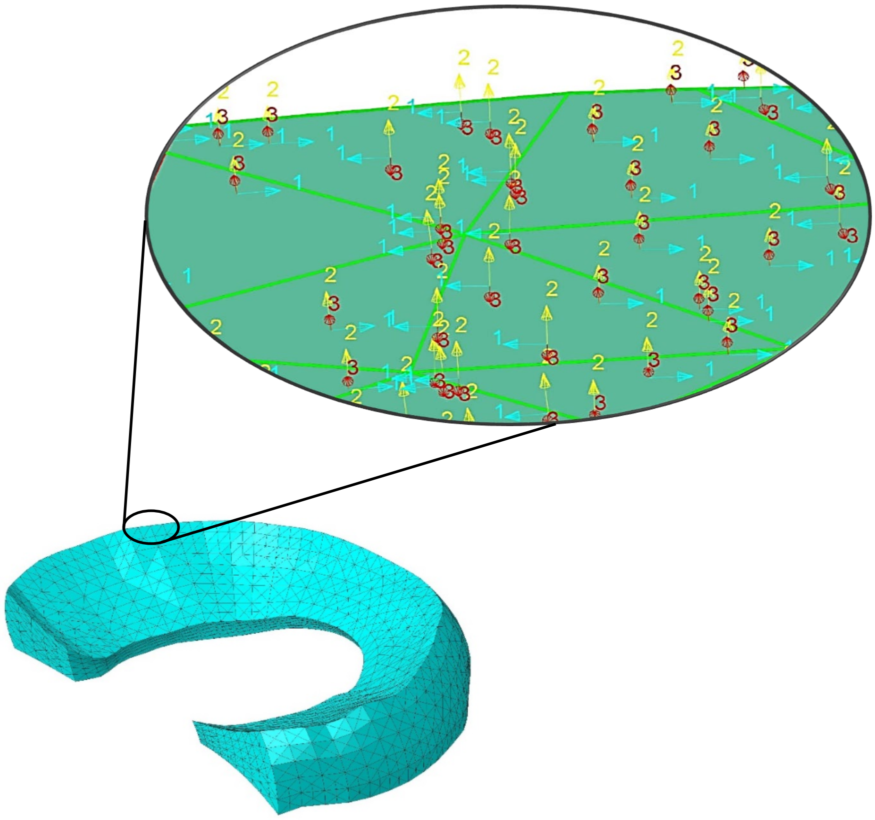

Figure 3-6. Menisci material orientation.

3.2.2.2 Mesh

According to a study by Wan et al. [119], use of the 10-node quadratic tetrahedral element (i.e. C3D10 element type) is a proper element choice for the calculation of mechanical response and stress in this model. The finite element knee model used in this study is shown in Figure 3-7. The implant is attached to the medial side between the MCL and bone. Most of the soft tissues including MCL, ACL, PCL, femoral and tibial cartilages, and menisci can clearly be seen in Figure 3-7.

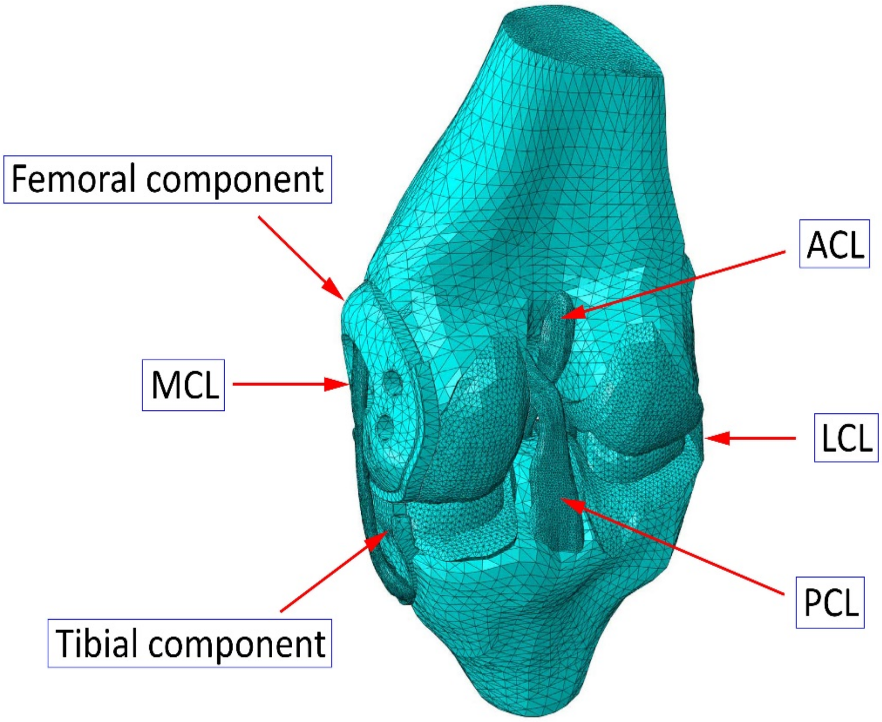

Figure 3-7. Posterior view of the finite element knee model including the implant.

The number of elements for each part of the model is listed in Table 3-1. A mesh sensitivity analysis with different mesh densities was also conducted; this showed that finer meshes with more elements than that listed in Table 3-1 increases the computation time significantly without improving the accuracy of the results.

Table 3-1. Number of elements for the knee model

Component	Number of elements
Femur	63604
Tibia	54584
Femoral cartilage	132345
Tibial cartilage	44034
Menisci	30328
ACL	38604
PCL	48794
MCL	72908
LCL	21094

3.2.2.3 Loading and boundary conditions

As shown in Figure 3-8, the cross-sectional area of the femur was measured in SolidWorks and, based on that, a distributed force of 400 N (half of the body weight) was applied on top of the femur [120].

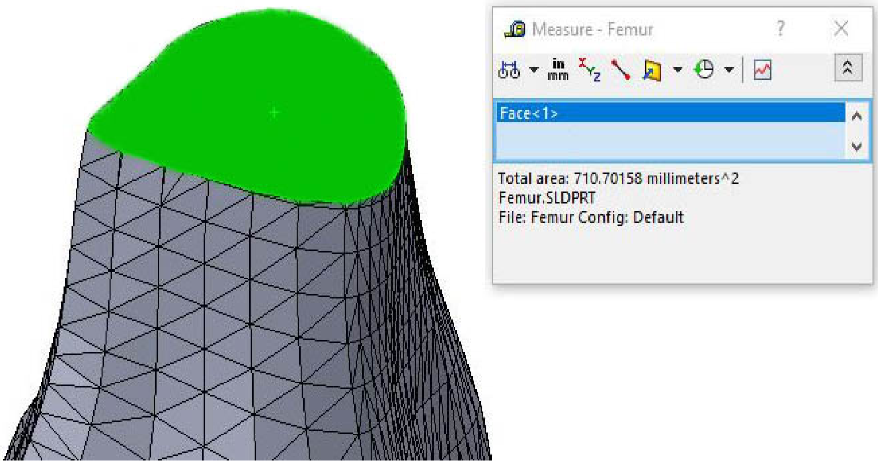

Figure 3-8. Cross-sectional area measurement of the femur in SolidWorks.

As shown in Figure 3-9, all degrees of freedom at the base of the tibia were constrained and, for the femur, transverse movements along the Y and Z axes were constrained.

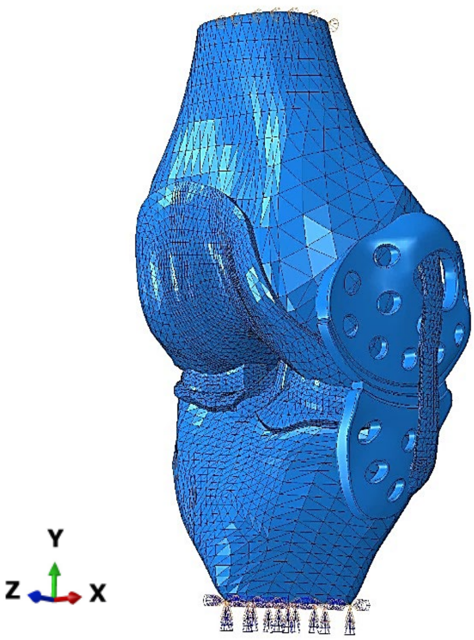

Figure 3-9. Boundary conditions of the FE knee model.

The detailed mechanism by which the implant is fixed to the bone, e.g. with pins, screws, etc., is not a primary focus of the present study. (As this is a novel implant, appropriate optimal fixation techniques will be developed for it at a later stage.) In order to keep the present model simple, both plates were tied to the bones (when surfaces or elements tie to each other, they connect together firmly to avoid any separation or sliding, and move together during deformation). The tie constraint mimics a firm attachment due to bone ingrowth into a lattice structure of the implant; however, screws would also be required, but these are not considered in this chapter, as here the focus is on a comparison study between the models without and with the implant. Such a lattice structure is shown in Figure 3-10, for the femoral part of a TKR implant [121].

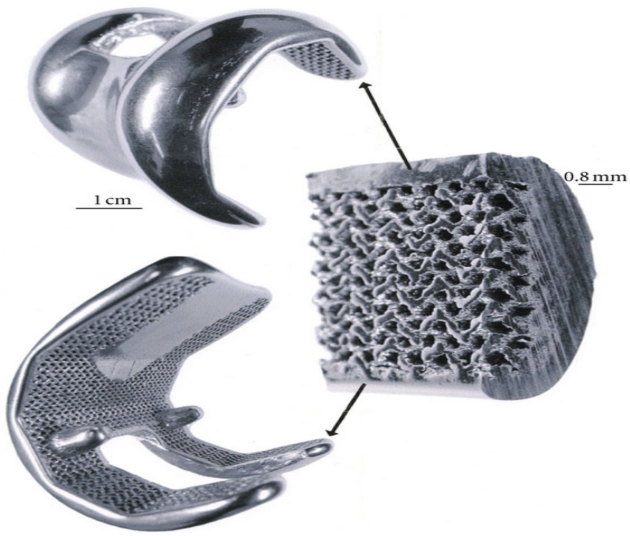

Figure 3-10. Femoral component of a knee implant [121].

3.3 Results

Results for von Mises stress distributions on the cartilage (both the medial and lateral compartments) are illustrated in Figure 3-11a (without implant) and Figure 3-11b (with implant). As observed in Figure 3-11a, the maximum von Mises stresses in the medial and lateral compartments, in the absence of the implant, were 1.44e+00 MPa and 9.88e-

01 MPa, respectively. After unloading the knee with the implant, the maximum stresses at the medial side decreased to 8.58e-01 MPa and at the lateral side increased to 1.02e+00 MPa as shown in Figure 3-11b. (See [77, 122], for example, for more on the extensive use of the von Mises stress as a metric in FE knee models involving articular cartilage.)

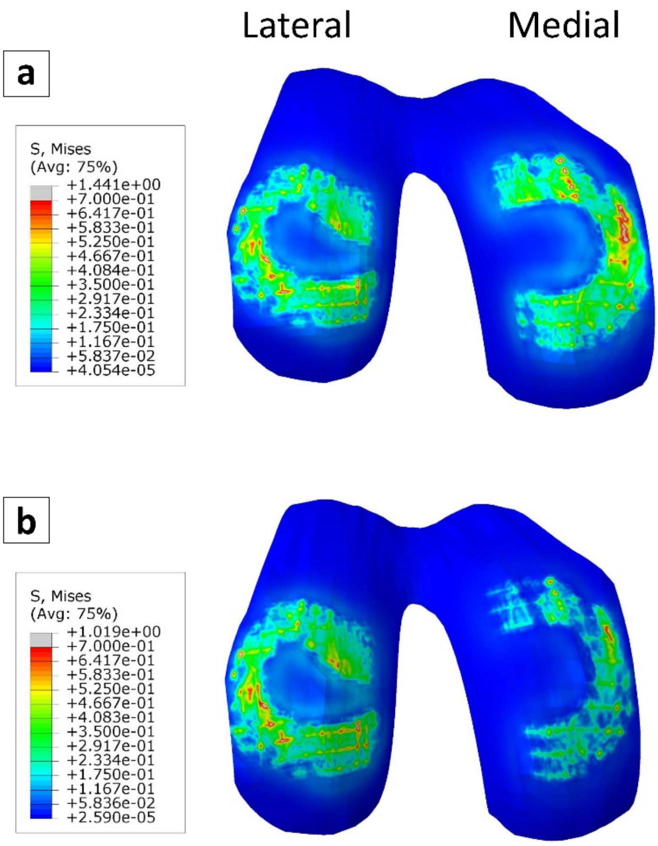

Figure 3-11. Stress distributions within femoral cartilage, a) without implant, b) with implant.

Contact pressure distributions on the surfaces of the femoral cartilage before and after attachment of the implant are depicted in Figure 3-12a and b, respectively. According to these pressure contours, the peak pressures without the implant at the medial and lateral sides were 2.36e+00 MPa and 2.48e+00 MPa, respectively. The peak pressures in the knee with implant at the medial and lateral compartments were 1.60e+00 MPa and 2.72e+00 MPa, respectively.

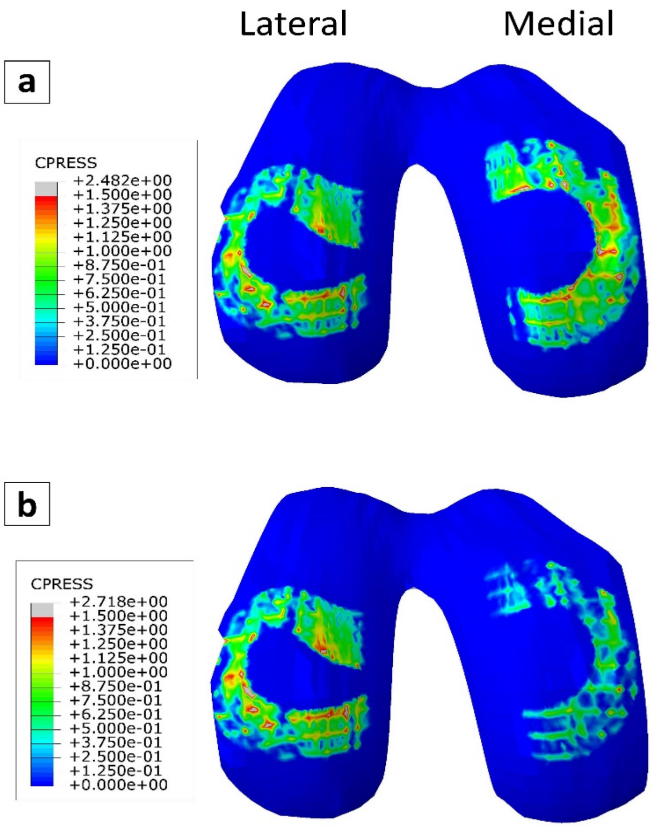

Figure 3-12. Distributions of contact pressure on the surface of the femoral cartilage, a) without implant, b) with implant.

From an osteoarthritis point of view, studying stress and contact pressure in the cartilage and particularly the femoral cartilage is of prime importance, however, it is also instructive to examine the stress and contact pressure in other soft tissues, such as menisci.

Von Mises stress distributions on the menisci without and with the implant are shown in Figure 3-13a and b, respectively. The maximum von Mises stresses at the medial and lateral meniscus, in the model without the implant, were 4.82e+00 MPa and 8.97e+00 MPa, respectively. However, after attaching the implant, the maximum stresses at the medial meniscus decreased to 2.32e+00 MPa and at the lateral meniscus increased to 1.02e+01 MPa. Before and after introducing the implant, peak stress was observed in the lateral meniscus near the intercondylar eminence.

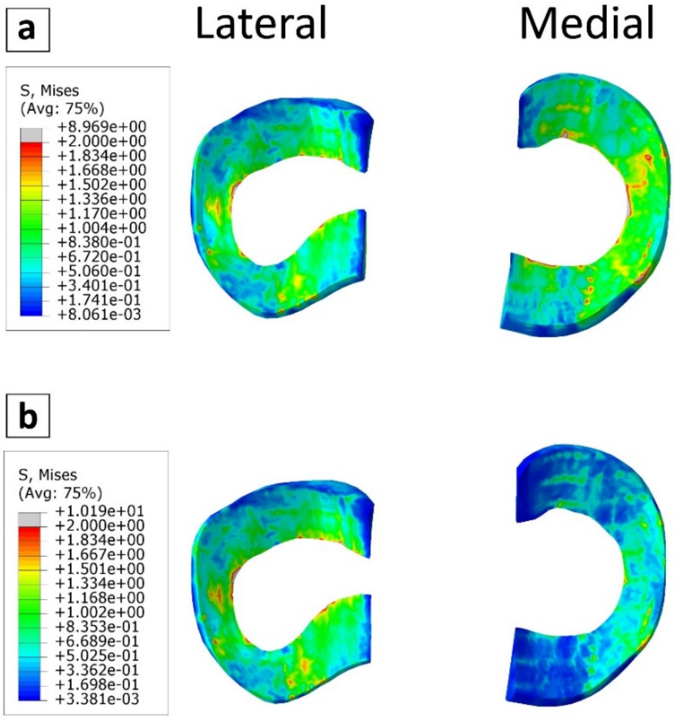

Figure 3-13. Stress distributions within menisci, a) without implant, b) with implant.

Contact pressure distributions on the top surfaces of the menisci before and after attachment of the implant are shown in Figure 3-14a and b, respectively.

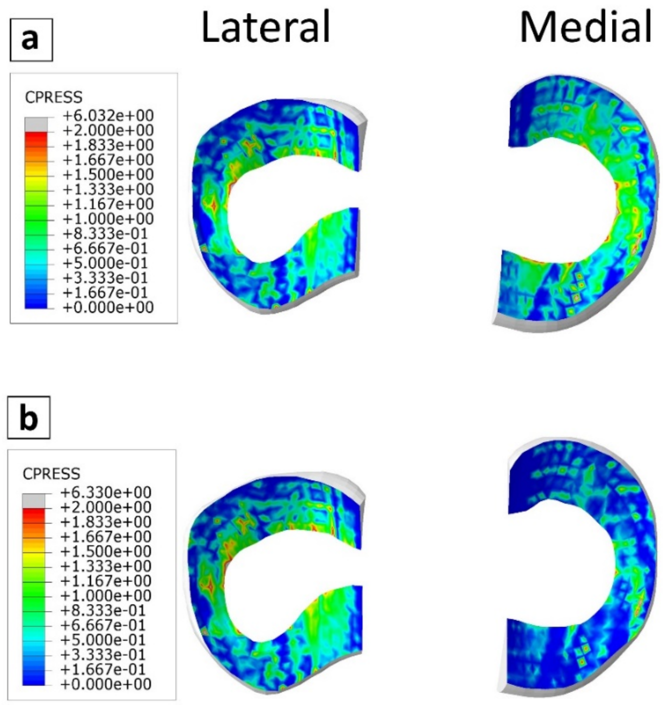

Figure 3-14. Distributions of contact pressure on the surface of the menisci, a) without implant, b) with implant.

As shown in Figure 3-14, the peak pressures without the implant at the medial and lateral meniscus were 3.50e+00 MPa and 6.03e+00 MPa, respectively. The peak pressures in the knee with implant at the medial and lateral meniscus were 3.02e+00 MPa and 6.33e+00 MPa, respectively.

Von Mises stress distributions in the femoral and tibial components of the implant are shown in Figure 3-15. The maximum stress observed was approximately 9.58e+01 MPa at the contact surfaces between the two plates on the anterior side.

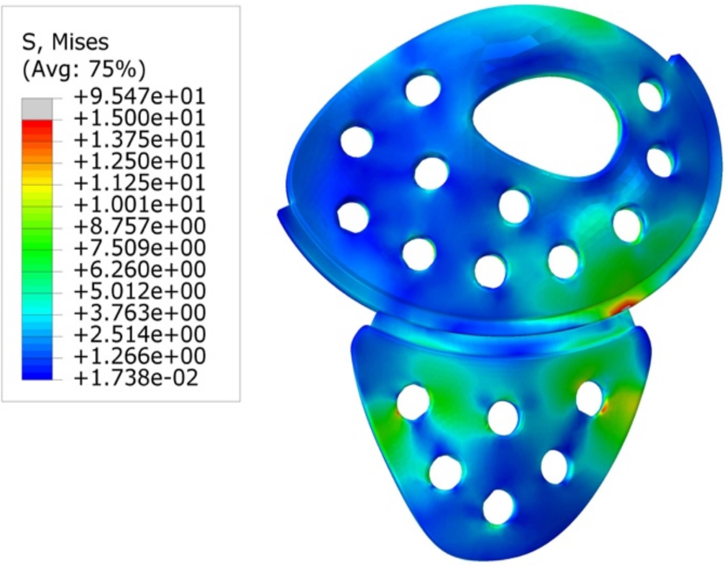

Figure 3-15. Von Mises stress distributions of femoral and tibial implant-plates.

Results of this study were compared to the results of research conducted by Wang et al. [75] and Thambyah [103] for validation, and are discussed in the next section.

3.4 Discussion

The primary aim in any OA therapy, apart from reducing present pain, is preventing the progression of OA. Studies have confirmed the influence of mechanical unloading on prevention of osteoarthritis advancement [5]. Moreover, unloading osteoarthritic knee joints alleviates pain and provides a proper condition for tissue repair. The clinical benefits of cartilage repair were seen to remain in most patients even after a five-year follow-up [2]. Steadman et al. [3] studied the influence of unloading braces on knee OA, and reported that these braces were effective for treatment of unicompartmental knee OA.

By comparing the results of the extended knee position model of the current study, before and after attaching the implant, the von Mises stresses in the femoral cartilage were clearly seen to decline in the medial compartment. Indeed, the maximum stress was reduced by 40% in the medial side, while stress in the lateral side increased slightly. Further, the maximum contact pressures on the distal femoral surface declined by 35% at the medial side, while contact pressure in the lateral side was slightly increased. Clearly, because of attaching the implant to the medial side, unloading the joint was observed in this compartment, for both von Mises stress and contact pressure. Accordingly, this implant could be considered as a potential useful treatment for unicompartmental knee OA.

Similar to the cartilage, the von Mises stress and contact pressure were seen to decrease in the medial meniscus after introducing the implant, while they increased slightly in the lateral meniscus. The von Mises stress and contact pressure in the medial meniscus declined by around 52% and 14%, respectively.

As mentioned, the peak stress was observed in the lateral meniscus and near the intercondylar eminence. The reason for this is that the 3D model of menisci was not reconstructed precisely, particularly near the eminence, as the soft tissue reconstruction from the MR images is challenging. In fact, in a real human knee joint, menisci are thicker at the edge of the tibial plateau and they get thinner towards the intercondylar eminence as shown in Figure 2-6 in Chapter 2, however, in the Wangerin model, they were thicker around the eminence and this led to higher stress.

As mentioned, after implementing the implant the maximum stress and contact pressure in the lateral compartment were slightly higher compared to the model without implant. It appears that after attaching the implant to the medial side, the femur was slightly abducted towards the lateral compartment. In other words, the whole unloading process involves removing any excessive load from the medial side, by attaching the implant on that side, leading to a slight femur abduction. Further experimentation is required to study the effect of this abduction on the other compartment and on the knee kinematics.

Wang et al. [75] conducted research on a standing knee model under different compressive loads using various Poisson's ratios. The maximum von Mises stress was reported to be just under 1.5e+00 MPa, for a 400 N applied load and a Poisson ratio of 0.45 for cartilage. This stress is very close to the observed maximum stress (1.44e+00 MPa) at the femoral cartilage in the current model without implant, intimating the reliability of the results obtained in the current study.

To further check the accuracy of the results, model contact pressures were compared with findings in the research conducted by Thambyah [103] on a cadaver knee joint. In that research, the experimental setup was designed in such a way that a major part of the load was applied to the medial compartment, similar to the current study. Although the stress on the medial side was higher, the contact pressures in the medial and lateral compartments showed no significant differences, as was observed in this study, again pointing to the reliability of the current results.

It is worth mentioning that the design of the implant was not optimised in this research, and stress concentrations occurred at the interface between the femoral and tibial plates as shown in Figure 3-15. Although this issue might be eliminated by modifying the design, at this stage the existing stress is not of any real concern, as it is a localised concentrated stress and far less than the yield strength of titanium (~900 MPa) [123]. In fact, there could be other sources of failure due to the tribological properties of the implant, which need more experimental investigation; these should be studied on the produced parts after finalising development of the implant's design.

3.5 Conclusion

In this chapter, the effect of a novel extra-articular implant on stress and contact pressure distributions in femoral cartilage and menisci was investigated using FEA. The main results are as follows:

- After attaching the implant to the medial side of the knee, the peak von Mises stress within femoral cartilage and peak contact pressures over the femoral cartilage surface were reduced by 40% and 35%, respectively.

- After attachment of the implant, the peak von Mises stress in menisci declined by around 52% and peak contact pressure over the menisci surface decreased by around 14%.

- After introducing the implant to the medial side of the knee joint, the maximum stress and contact pressure were slightly increased at the lateral compartment due to the slight abduction of the femur.

- A static FEA of the extended knee position of the model showed that the maximum observed stress in both implant plates (femoral and tibial) was about 96 MPa, which is far below the yield strength of titanium (~900 MPa). Thus, no failure of the implant is expected due to plastic yielding; however, there is a possibility of failure due to other mechanisms, such as wear.

According to the above findings, this new implant could effectively reduce the load in the medial compartment of the knee joint, which means that it may lead to slowing down progression of knee OA.

A question which arises then is: would unloading the knee joint lead to any unwanted issues, for example influencing bone remodelling which could cause harmful changes in bone density? This question is discussed extensively in the next chapter.

Chapter 4

Bone Remodelling

4.1 Introduction

In the previous chapter, a Finite Element (FE) model of the knee was developed, without and with the implant, and it was shown that the implant could decrease the contact pressure and stress in the medial cartilage considerably. On one hand, load reduction in the cartilage may lead to a slowing down of OA progression in the knee; on the other hand, bone is a mechanosensitive tissue, and changing the loading condition in the joint will affect the bone density.

In fact, joint unloading due to the attachment of this implant will affect bone remodelling in the tibiofemoral joint. Accordingly, in this chapter, the influence of this novel implant on bone remodelling of the knee joint is investigated. The aim of the chapter is to study periprosthetic Bone Mineral Density (BMD) changes as well as density variations at the fixation holes in the femur and tibia, and to determine whether any such BMD changes are likely to be damaging to the health of the knee.

Bone is a dynamic tissue and as a supporting frame and regulator of mineral homeostasis, needs to remodel continuously. During a balanced bone remodelling in cortical and trabecular bone, formation and resorption of bone occur equally [124]. One of the main purposes of bone remodelling is to provide the capability for the skeleton to conform to its mechanical conditions. This capability decreases the risk of damage, such as fracture caused by cyclic mechanical loading [125].

Bone undergoes considerable structural and compositional changes induced by physiological and mechanical conditions over a lifetime [125]. Bone remodelling caused by mechanotransduction comprises four major phases: (i) perception of the applied load to bone by sensor cells (osteocytes); (ii) conversion of the mechanical signals into biochemical signals; (iii) receiving the signals by bone forming (osteoblast) and resorbing (osteoclast) cells; (iv) response from the aforementioned cells and a consequent bone adaptation process [125]. These steps are illustrated schematically in Figure 4-1.

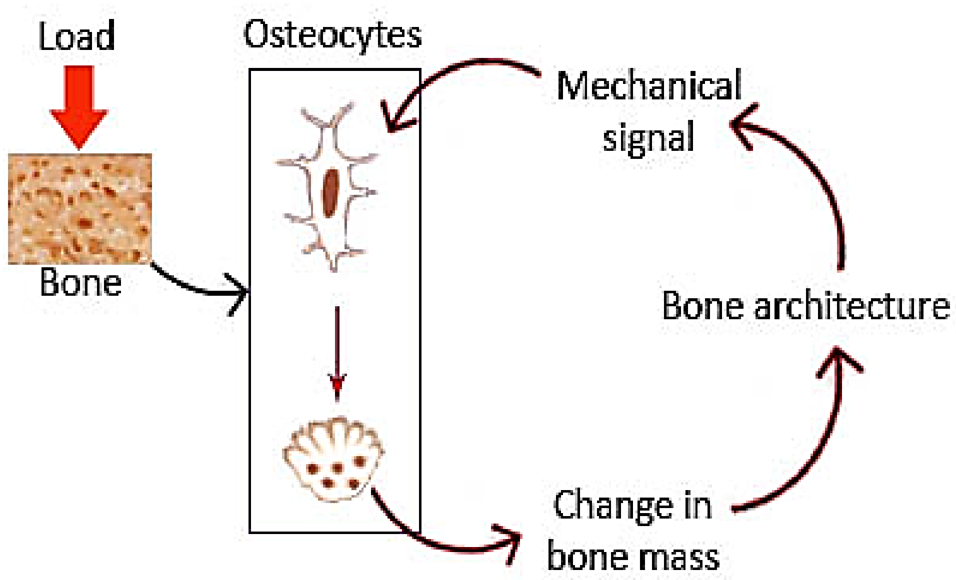

Figure 4-1. The process of cellular response to a mechanical stimulus.

According to the mechanostat theory, one of the important factors that should be taken into account in bone remodelling is the range of strain induced by the magnitude and distribution of the load [126]. Based on this theory, there is an equilibrium range of strain (homeostasis or dead zone) in which no bone remodelling occurs. As indicated in Figure 4-2, strains above this range result in an adaptive bone forming response, whereas strains below this range result in bone resorption [125, 127].

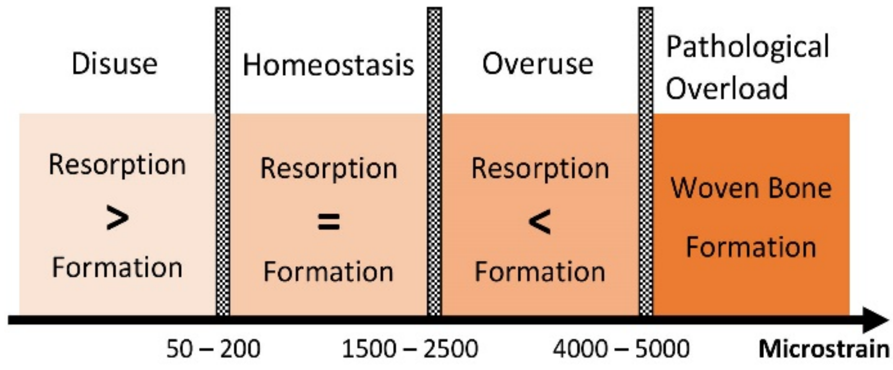

Figure 4-2. Bone dynamics at different strain ranges based on the mechanostat theory.

As mentioned, bone remodelling is affected by the mechanical environment and, in the case of considerable changes to this environment, bone structure can change significantly as well [127]. For instance, stress shielding caused by different implants, such as knee and hip implants, leads to a localised bone resorption around the implant and possible consequent aseptic loosening and other issues [128]. The stress shielding phenomenon could be even more critical in the case of unloading implants such as KineSpring and intra-capsular knee prostheses [23, 53]. Because of this and associated issues, a considerable number of studies have been conducted in order to experimentally and numerically study the effect of various types of implant, such as hip, knee, and shoulder on bone remodelling and bone density distributions [92, 129-131]. Some of the relevant studies on bone remodelling are explained in Chapter 2 (2.1.6) as well as in the discussion section of this chapter.

4.2 Materials and methods

4.2.1 Finite element model of the knee

The knee model used in this chapter was based on a model developed by the Auckland Bioengineering Institute in FEBio®. The knee joint of a 29 year old male, whose height and weight was 176 cm and 76 kg, respectively, was scanned in a previous study in the supine position using non-weight bearing MRI [132]. The participant was physically active with no knee pain, no sign of tibiofemoral and patellofemoral cartilage lesions, and no history of knee surgery. MRI was conducted at Stanford University Hospital using a GE Signal 0.5T SP/i MR scanner (GE Medical Systems, Milwaukee, WI) [132]. Bone reconstruction was conducted using the Musculoskeletal Atlas Project (MAP)-Client workflow at the Auckland Bioengineering Institute [133, 134]. This workflow uses statistical shape models of hard and soft tissues in order to combine segmented MR images of several subjects and generate subject specific bone and cartilage models [134]. A simplified flowchart of the MAP-Client workflow is shown in Figure 4-3.

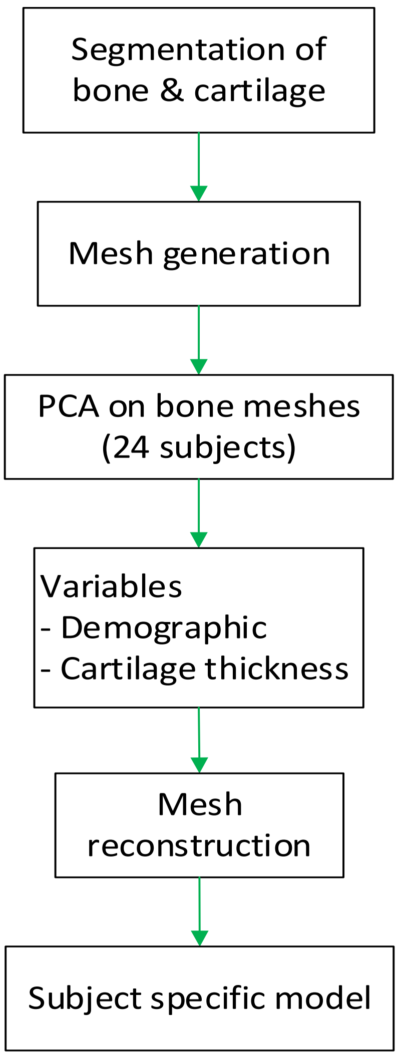

Figure 4-3. Flowchart of the MAP-Client workflow from segmented MR images to FE model. (PCA: Principal Component Analysis.)

One of the remarkable advantages of the MAP-Client workflow is that, by using this method, full-length femur, tibia and even fibula can be reconstructed by only segmenting the distal femoral and proximal tibial heads (see white areas in Figure 4-4), instead of scanning and segmenting the whole leg, which can be a very costly, time consuming and tedious procedure.

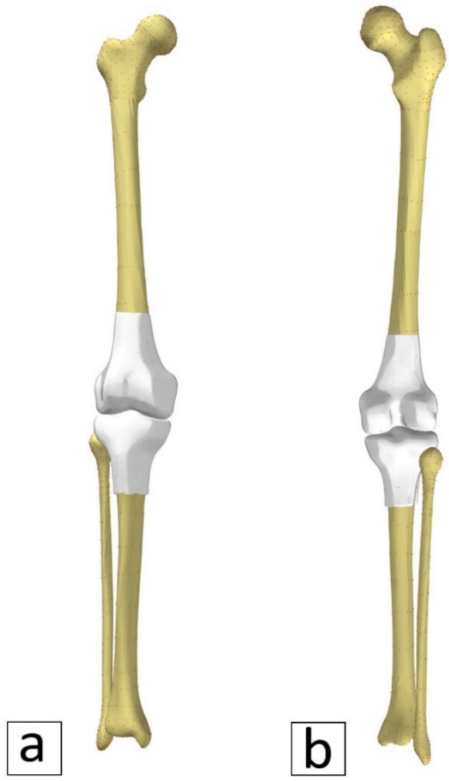

Figure 4-4. Reconstructed bones using the MAP-Client workflow, a) anterior view, b) posterior view.

Articular cartilage was reconstructed by calculating the cartilage thickness: this is the Euclidean distance between the closest points on the cartilage surface and subchondral layers on the high-resolution MRI images. Polynomial curve-fitting was implemented to fit the bone and cartilage meshes based on the segmented images [134, 135]. Ultimately, the full knee model was generated in the FEBio finite element software. In order to carry out the bone remodelling, STL files of all components of the knee model were generated using Meshmixer® and imported into the Abaqus FE software.

Loading conditions were applied to the bone to replicate the conditions that exist in the hip joint during gait. For this purpose, three sets of loadings representing three different stages of walking were implemented, as shown in Figure 4-5. According to the literature, implementing these loading conditions leads to a realistic bone density distribution [82, 136].

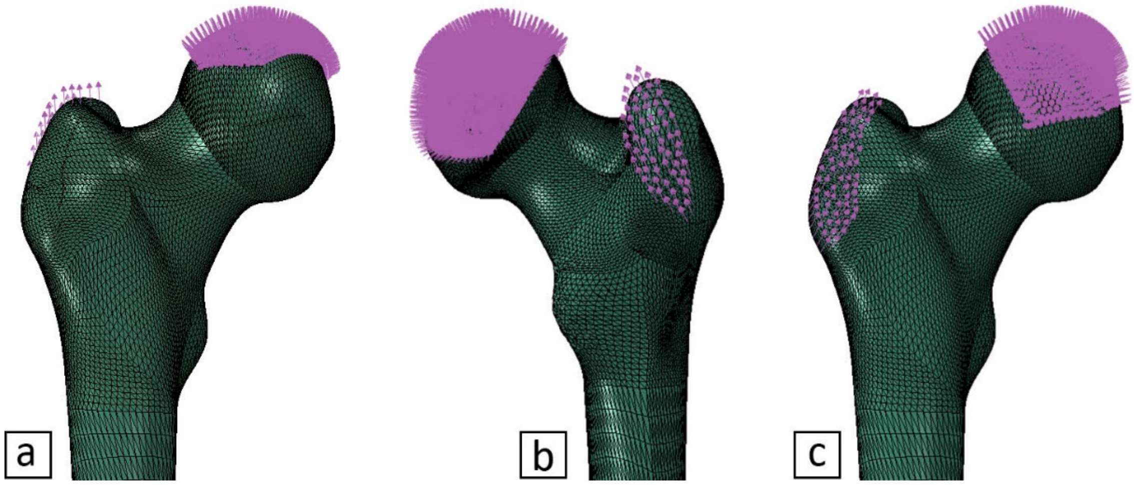

Figure 4-5. The Loading condition applied at the femoral head and greater trochanters, representing conditions at different phases of the gait cycle: a) mid-stance (compression 1 and tension 1), b) heel-off (compression 2 and tension 2), and c) heel strike (compression 3 and tension 3).

Loading conditions for the hip joint in the mid-stance are shown in Figure 4-5a and the loading conditions at the hip joint during heel-off and heel strike are shown in Figure 4-5b and c, respectively. The compression loads applied on the proximal femoral head are characterising the contact between the femur and acetabulum and the tension loads on the greater trochanter are representing the muscle forces. The intensity of the applied loads on the greater trochanter and femoral head was taken from a study conducted by Jacobs et al. [82].

Specific regions were selected on the proximal femur based on the experimental and numerical studies conducted by Greenwald and Haynes [137], and Gubaua et al. [136], respectively; the distributed loads were then applied to these regions. The directions of the loads applied on the greater trochanter were defined based on Bagge's research [138]. The loading conditions are detailed in Table 4-1. The magnitudes quoted are the resultant forces applied and distributed along the regions on the femoral head and greater trochanters.

Table 4-1. Detail of the applied loading conditions at the hip joint.

Type of force	Magnitude (N)	Direction
Compression 1	1158 [82]	Pressure (normal to the surface)
Compression 2	2317 [82]	Pressure (normal to the surface)
Compression 3	1548 [82]	Pressure (normal to the surface)
Tension 1	351 [82, 138]	27.53 ; 29.30 ; 59.65 [138]
Tension 2	703 [82, 138]	-5.93 ; 2.85 ; 39.29 [138]
Tension 3	468 [82, 138]	23.28 ; -27.93 ; 62.17 [138]

A Dirichlet boundary condition was applied to the distal side of the tibial diaphysis in order to constrain any movement of the whole model as shown in Figure 4-6. For the greater trochanter, the coordinate system is orientated such that the X-axis is in the lateral-medial direction, Y-axis in the anterior-posterior direction and the Z-axis in the distal-proximal direction.

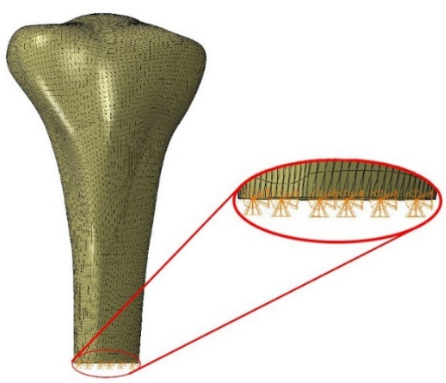

Figure 4-6. A Dirichlet boundary condition at the base of the tibia component.

In numerical bone remodelling, the checkerboard issue is often seen, which is where a discontinuity of density distribution in elements near the regions of load applications is seen [139]. This phenomenon is illustrated in Figure 4-7 [82].

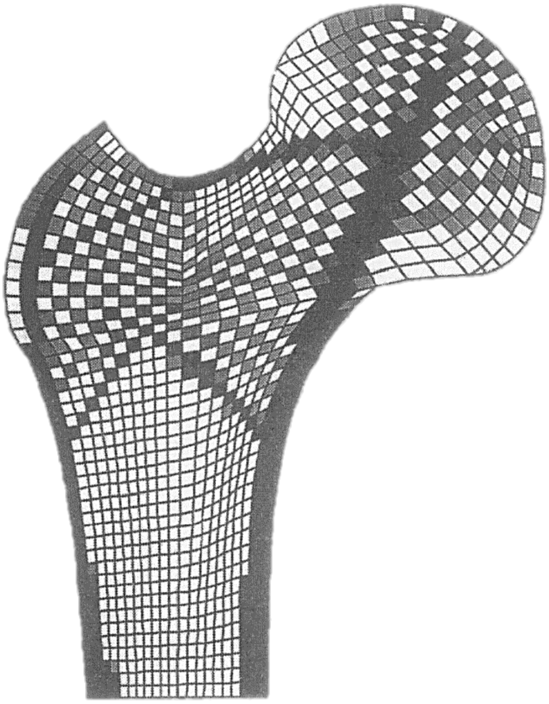

Figure 4-7. Checkerboard pattern in a bone remodelling simulation of the proximal femur [82].

In this research, the quadratic C3D10 element was used to address the checkerboard phenomenon [140-142]. There are other methods which can be used to address this issue, such as smoothing [143] and node-based approaches instead of element-based ones [144]. However, they have some limitations; for example, the node-based approach generally requires much more computational time compared to the element-based one, and the smoothing technique cannot be applied for every single step [143, 144]. The number of elements used for each part is listed in Table 4-2. Due to factors such as geometry, different element sizes were used for different parts of the model.

Table 4-2. Number of elements for components of the FE model.

Part	Number of elements
Femur	322396
Tibia	182447
Femoral cartilage	386588
Tibial cartilage	149639
Menisci	57916
Ligaments	248843
Implant	443290
Screws	142352

The FE knee model is partially shown in Figure 4-10 and the full model is shown in Figure 4-14. As mentioned previously, the load was applied to the proximal femur, which is the main difference between the models used in this chapter and the previous chapter. The design procedure of the implant is similar to that in Chapter 3, the only difference being the consideration of an additional component, the simplified screws (Figure 4-8), in order to attach the implant to the bone. Based on the hole size of the implant, the diameter and length of the screws were taken to be 5 and 25 mm, respectively.

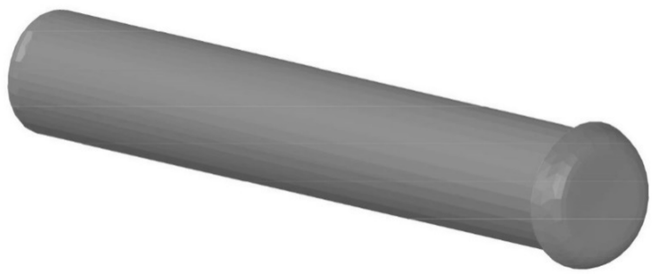

Figure 4-8. Schematic view of the screw.

The implant was attached to the knee model using screws (black colour shown in Figure 4-10) and tie constraint. All screws were also tied to the holes in the femur and tibia. As mentioned in the previous chapter, the tie constraint mimics a firm fixation induced by bone ingrowth into a porous structure. So, in this case, the basis is a porous screw, an example of which is shown in Figure 4-9, and it is assumed that the function of its thread is to keep the screw firmly in place until the bone ingrowth occurs [145]. Accordingly, a simplified screw without a thread is used here, and in conjunction with the tie constraint represents fixation with bone ingrowth, which was applied from the beginning of the simulation.

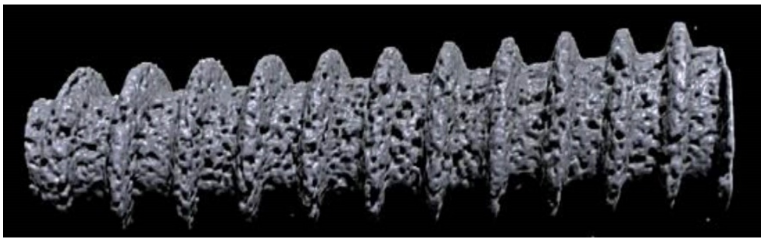

Figure 4-9. Titanium porous screw [145].

As shown in Figure 4-10, to attach the implant to the knee joint, three screws were considered for each bone similar to the Atlas knee system [14]. For both femoral and tibial components, one screw was used on the anterior side, one on the posterior side, and one in the middle, as shown in Figure 4-10.

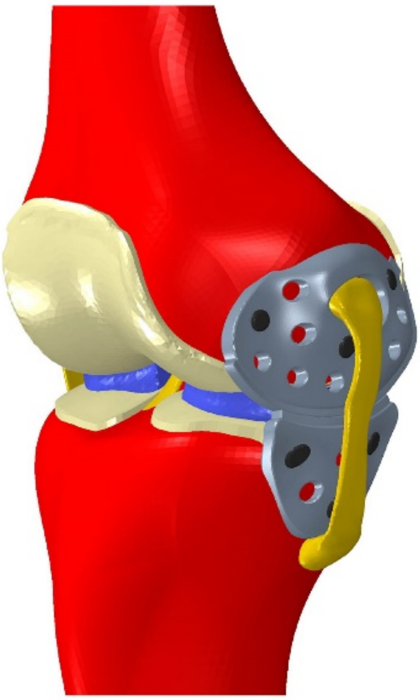

Figure 4-10. FE model of the knee joint with implant.

The cartilage was defined as an isotropic elastic material with Poisson's ratio 0.45 and Young's modulus 10 MPa [75]. The ligaments were assumed to be linear elastic isotropic materials with Young's modulus 400 MPa and Poisson's ratio 0.45 [76]. According to the fiber directions in the menisci, they were considered to be transversely isotropic linear elastic, with Poisson's ratios of 0.1 ($\nu_{\theta R}$), 0.1 ($\nu_{\theta Z}$), and 0.33 (ν_{RZ}), Young's moduli in the circumferential (E_{θ}), radial (E_R), and axial (E_Z) directions of 125, 27.5, and 27.5 MPa, respectively, and shear moduli ($G_{\theta R}$ and $G_{\theta Z}$) of 2 MPa [114, 115, 146]. A schematic view of collagen fiber directions in menisci is shown in Figure 4-11. The implant and screws were made of Ti-6Al-4V with a Young's modulus and Poisson's ratio of 110 GPa and 0.3, respectively [112, 113].

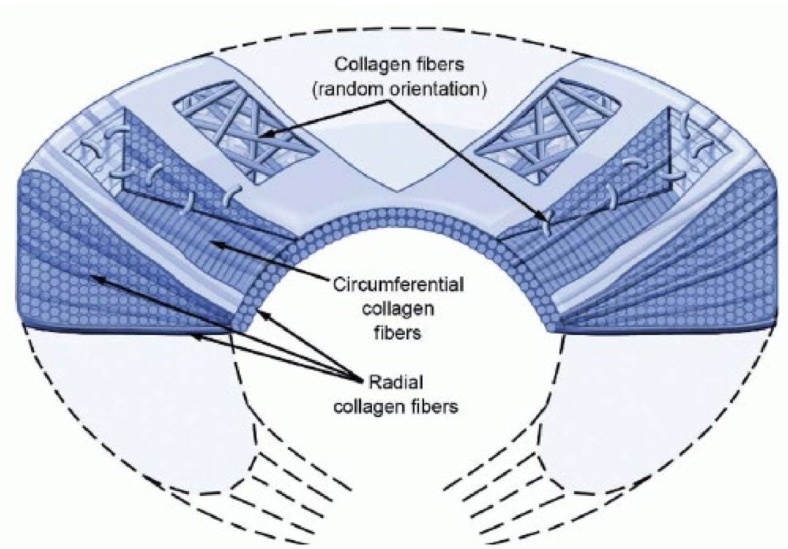

Figure 4-11. Schematic view of meniscus [116].

Bone remodelling simulations were run on an x64 operating system cluster with 24 cores Intel Xeon 2.60 GHz CPU and 128 GB RAM. The total CPU time using 22 processors required for the simulation of bone remodelling for five years postoperatively was around 90 days.

4.2.2 Bone remodelling

The method used in this chapter was based on a subroutine developed at the Federal University of Paraná for the hip joint. According to Jacobs et al. [82] and based on the Stanford method which was briefly explained in Chapter 2 (section 2.1.6), bone remodelling can be calculated as a function of the mechanical stimulus, so-called the daily stress stimulus (ψ_t) based on the Strain Energy Density (SED) caused by transmitted load through the bone. Continuum level mechanical stimulus can be formulated as:

$$\psi_t = \left(\sum_i^N n_i \bar{\sigma}_{t_i}^m\right)^{\frac{1}{m}} \tag{1}$$

where m is an empirical constant, n_i is the number of cycles of load i per day, and $\bar{\sigma}_t$ is the effective stress defined as [83]:

$$\bar{\sigma}_t = \frac{\bar{\sigma}(\rho)}{\left(\frac{\rho}{\rho_t}\right)^2} \tag{2}$$

where ρ is the apparent density, ρ_t is the maximum density of cortical bone, and $\bar{\sigma}(\rho)$ is the apparent stress [82]:

$$\bar{\sigma}(\rho) = \sqrt{2E(\rho)U(\rho)} \tag{3}$$

where $E(\rho)$ is the Young's modulus and $U(\rho)$ represents the strain energy density. Both Young's modulus and Poisson's ratio are dependent on the apparent density: $E = D\rho^n$ [94], where *D* and *n* are constants defined as follows [94]:

$$\begin{cases} \text{If } \rho <= 1.2\ \text{g/cm}^3 \Rightarrow E(\rho) = 2014\ \rho^{2.5}\ \text{(MPa)},\ \nu_1 = 0.25 \\ \text{If } \rho > 1.2\ \text{g/cm}^3 \Rightarrow E(\rho) = 1763\ \rho^{3.2}\ \text{(MPa)},\ \nu_1 = 0.3 \end{cases} \tag{4}$$

Using Hooke's law, the shear stress, and the stress-strain relations [147], the SED can be formulated as:

$$U(\rho) = \frac{1+\nu}{2E}\left[\left(\sigma_{xx}^2 + \sigma_{yy}^2 + \sigma_{zz}^2\right) + 2\left(\sigma_{xy}^2 + \sigma_{yz}^2 + \sigma_{zx}^2\right) - \frac{\nu}{1+\nu}\left(\sigma_{xx} + \sigma_{yy} + \sigma_{zz}\right)^2\right] \quad (5)$$

where ν is the Poisson's ratio and σ_{ij} are the components of the Cauchy stress. The remodelling rate is associated with the bone resorption and formation rate, $\dot{r}$. The bone remodelling process discussed earlier in connection with Figure 4-2 can be broken down into different zones as shown in Figure 4-12. ψ_t^* represents the reference stimulus and, within the range of $2w$ about this, no net bone mass change occurs. For this reason, the $\psi_t^* \pm w$ area is called a dead zone or lazy zone [148], mentioned earlier in the introduction to this chapter.

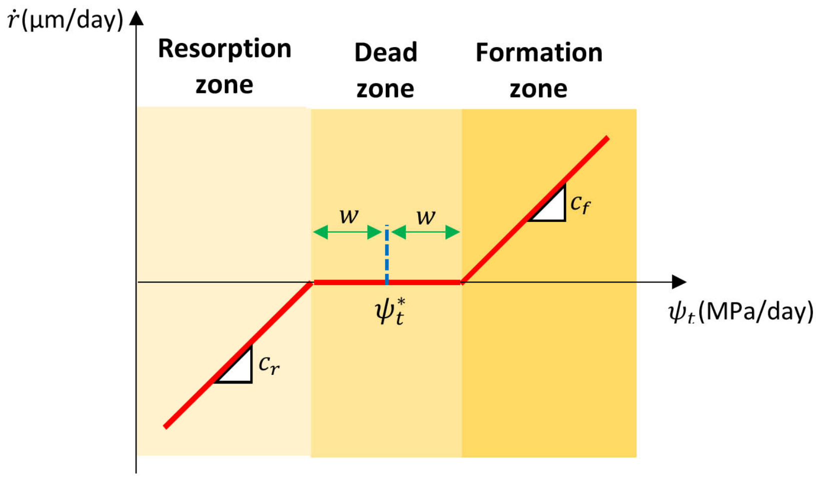

Figure 4-12. The dead zone in the process of the bone remodelling.

As shown in Figure 4-12, when the mechanical stimulus is smaller than $\psi_t^* - w$, bone is resorbing and when the mechanical stimulus is greater than $\psi_t^* + w$, bone is forming. According to the above points, the formation rate can be defined as [148]:

$$\dot{r} = \begin{cases} c_f(\psi_t - \psi_t^* - w) & if\ \psi_t > \psi_t^* + w \\ 0 & if\ \psi_t^* - w < \psi_t < \psi_t^* + w \\ -c_r(\psi_t^* - w - \psi_t) & if\ \psi_t < \psi_t^* - w \end{cases} \quad (6)$$

where c_f and c_r are rate parameters (see Figure 4-12).

The density change rate ($\dot{\rho}$) can be calculated through [83]:

$$\dot{\rho} = S_v \dot{r} \rho_t \tag{7}$$

where S_v is the specific bone surface area, which can be correlated with the bone density [149]. Values for the various parameters mentioned above as used in this study are listed in Table 4-3.

Table 4-3. Parameter values used for the numerical bone remodelling [83].

Parameter	Value
ρ_t	2e-6 kg/mm^3
n	3000
ψ_t^*	50 MPa
c_f	2.0e-5 mm/day
c_r	2.0e-5 mm/day
Δt	7 days [150]
m	4

Using a user-defined subroutine in Abaqus, the above algorithm was initially implemented for the knee model without the implant in order to achieve a heterogeneous density of the bone after 300 days, because according to the literature, a realistic bone density distribution can be achieved after 300 days [93]. For the model without the implant, the remodelling process was started with a density value of 1e-06 kg/mm^3 in order to achieve a density distribution which qualitatively represents the bone morphology [82, 90, 92, 93, 151]. Bone density was then extracted from this model (using Matlab® routines) and assigned to the model with the implant in which the geometry of the bones are slightly different due to the implant fixation holes. The bone remodelling algorithm was then implemented again for five years in order to simulate the postoperative bone density [152]. The complete process is illustrated in Figure 4-13.

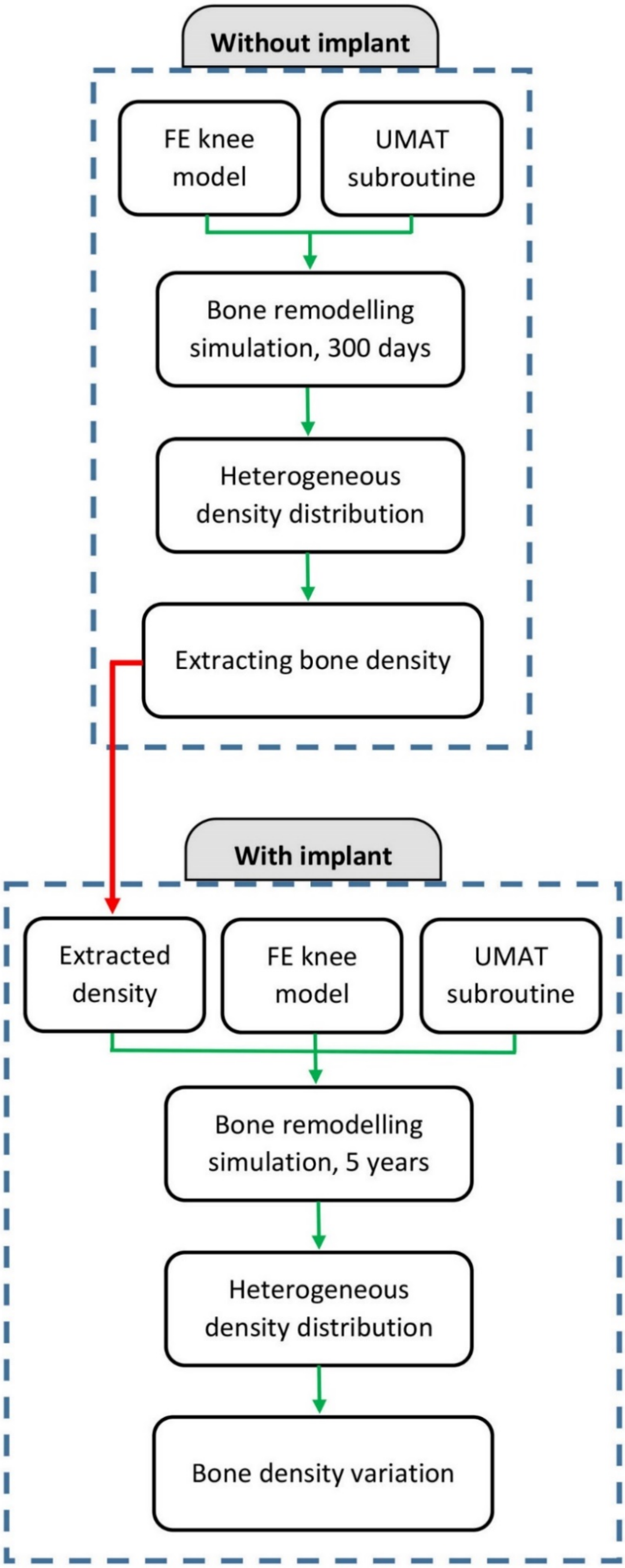

Figure 4-13. Flowchart of the bone remodelling process.

The steps involved in the bone remodelling simulation as used in this study and as discussed above are illustrated graphically in Figure 4-14.

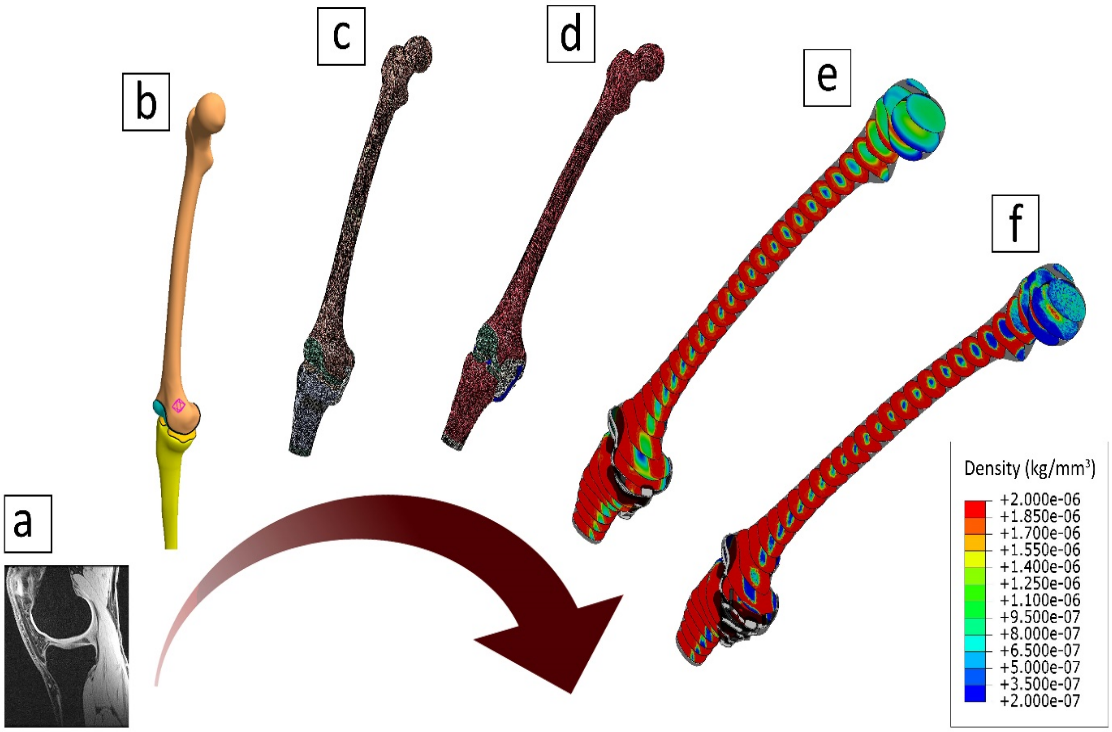

Figure 4-14. The steps involved in the bone remodelling process: a) MRI scanning [132], b) knee model in FEBio, c) knee model without implant in Abaqus, d) knee model with implant in Abaqus, e) heterogeneous density distribution after bone remodelling simulation, f) bone mineral density five years postoperative.

4.3 Results

Computer simulations were conducted in order to determine the influence of the extra-articular implant on bone remodelling of the distal femur and proximal tibia. A Region of Interest (ROI) must be chosen as the focus of study of BMD changes, mainly because attachment of an implant will not affect the density distribution in the whole model, but only in specific regions, mostly around the implant. Also, the complete affected area around the implant can be divided into smaller ROIs to help perceive which regions are affected more. For example, Gruen zones were considered as ROIs around the hip implant shown in Figure 4-15 [153].

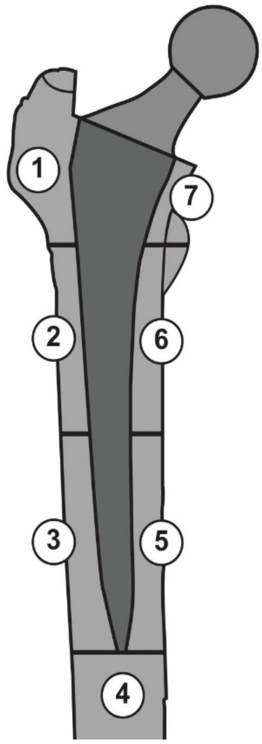

Figure 4-15. Gruen zones used to evaluate hip periprosthetic bone remodelling [153].

Regarding ROI selection for the knee joint, Tuncer et al. [154] studied bone mineral density of the knee joint post-unicompartmental knee arthroplasty and selected for ROIs the femoral parts in the medial condyle as well as underneath the tibial part in the medial compartment. Here, with periprosthetic bone resorption the primary source of concern, the ROI was chosen to be the tissue surrounding the implant [155], i.e. in the medial compartments as shown in Figure 4-16.

According to the above points, four different element sets were considered and defined in the medial compartment of the femur and tibia (ROI 1 and ROI 3) as well as holes (ROI 2 and ROI 4), which were considered for the elements surrounding the holes. ROI 2 and ROI 4 include separate non-connecting regions for the femur and tibia, respectively. ROI

1 and ROI 3 include elements inside the black bounded rectangle (see Figure 4-16), from the anterior to the posterior side of femur and tibia, respectively, because three screws for each implant were located on the anterior, middle, and posterior sides of the femur and tibia.

As mentioned before, a different FE knee model was used in this chapter to that used in the previous chapter, so before studying the influence of the implant on BMD, the effect of the implant on stress of the femoral cartilage was investigated in order to perceive how similar/different the results are compared to what was achieved in the previous chapter. Also, the loading condition in the knee is directly correlated with BMD, so if the unloading percentage were not considerable, there would be little motivation in studying bone density after attachment of the implant. To this end, average von Mises stresses on the surface of the femoral cartilage for the medial condyle were calculated before and after attaching the implant. It was observed that the average von Mises stress on the medial femoral cartilage was reduced by 36.5% due to the implant, which is relatively close to what was achieved using a different model in the previous chapter.

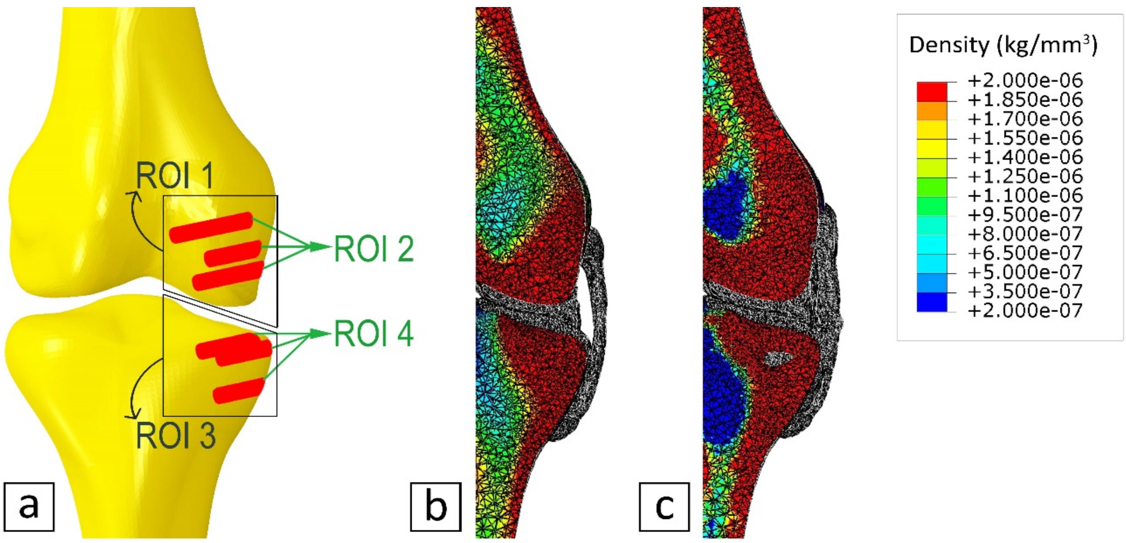

Figure 4-16. a) ROI for the study of bone remodelling in the implanted model, b) BMD of the joint without the implant, c) BMD of the joint five years postoperative.

A cross-sectional view for illustration of BMD of the model without implant is shown in Figure 4-16b and the density distributions of the knee model five years postoperative are shown in Figure 4-16c. The density distributions depicted in Figure 4-16b and c only show the final step of the simulation, while annual density changes five years postoperative are shown in Figure 4-17. It should be noted that Figure 4-16b and c, and Figure 4-17 show only one cross section of each model, whereas BMD changes were calculated for the complete 3D regions of interest.

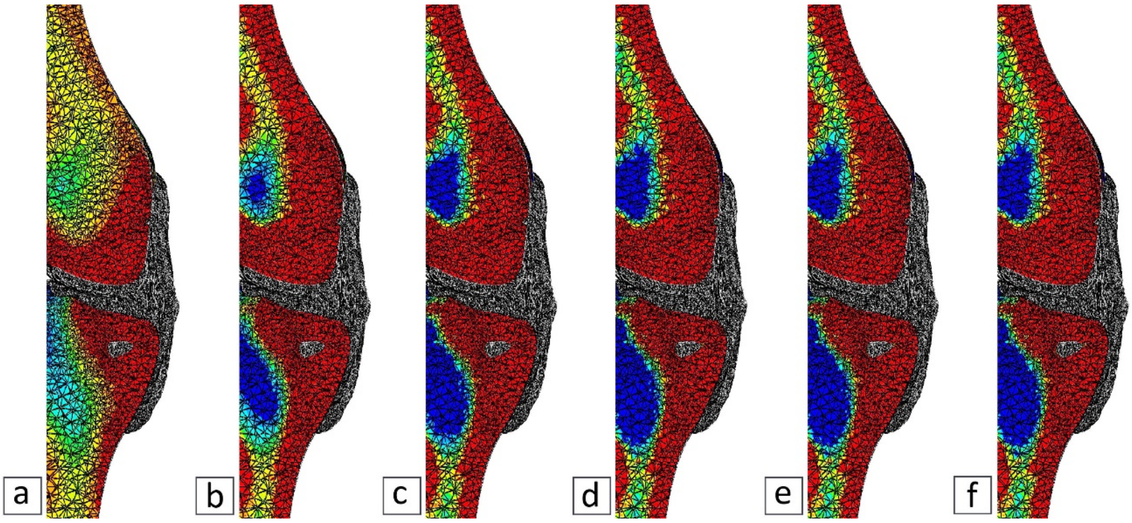

Figure 4-17. Graphical bone density changes five years postoperative, a) initial density, b) 1st year, c) 2nd year, d) 3rd year, e) 4th year, f) 5th year.

The BMD changes during the process for the ROIs are plotted in Figure 4-18a and b. This relative variation determines the difference between the initial and postoperative density values and 0% means density changes right after attachment of the implant. During the five year postoperative period, BMD for the ROI 1 and 2 increased by around 3.4% and 2.3%, respectively, and BMD for the ROI 3 and 4 increased by approximately 4.1% and 2.2%, respectively. For all regions, bone mineral density stabilised during the five years postoperative period.

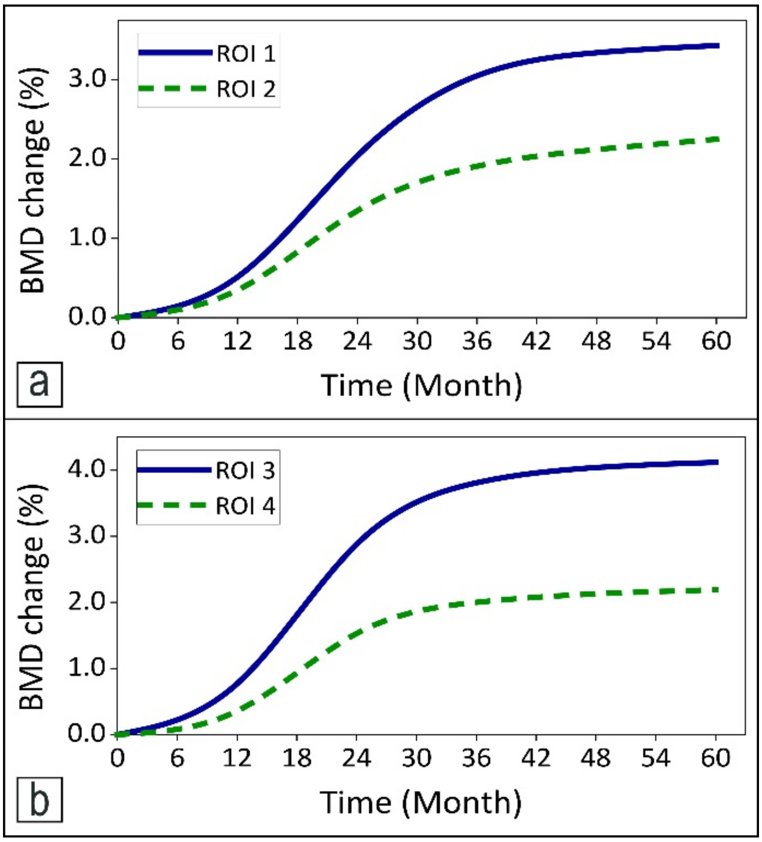

Figure 4-18. BMD variation vs. time five years postoperative: a) femur, b) tibia.

4.4 Discussion

Doblaré and Garcia [93] conducted bone remodelling simulations of the proximal femur based on the Stanford model for different time intervals and reported that a realistic distribution was achieved after 300 days. Therefore, to provide the baseline bone mineral density to be used as the initial density for the model with implant (Figure 4-14e and Figure 4-16b), the simulation was also performed for 300 days in this study.

An average BMD of the femoral head (denoted ROI 5) and the tibial head (denoted ROI 6) of the model without the implant were compared with the experimental results of a study conducted by Sievänen et al. [156], in order to examine the difference between numerical and experimental results. The regions of interest in the current study and the experimental study are shown in Figure 4-19a and b, respectively.

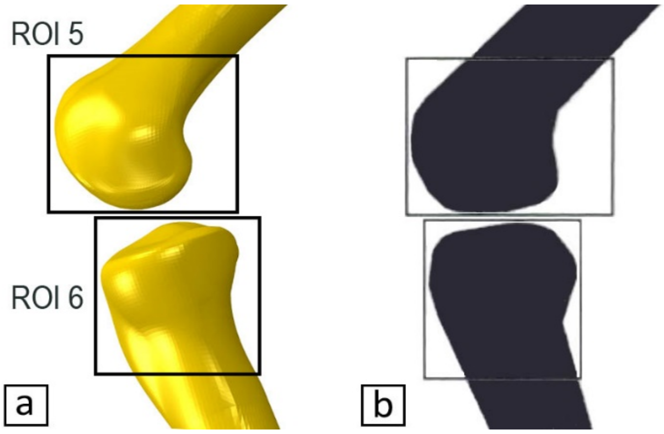

Figure 4-19. a) ROIs to study BMD in the model without implant, b) an experimental study on BMD of the knee joint [156].

In the current study, the average BMD for ROI 5 and ROI 6 were 1.73 and 1.71 g/cm^3, respectively. Sievänen et al. [156] measured the BMD of similar ROI for 15 participants and their reported mean values for the femur and tibia were 1.29 and 1.13 g/cm^3, respectively. However, there was a spread of data in the latter study with standard deviations of 0.20 and 0.19, and maximum values of 1.64 and 1.46 g/cm^3, for femur and tibia respectively, reasonably close to the computational results of the current study. It was observed that the difference between the average BMD for ROI 6 and the experimental value was higher than that for ROI 5, and development of the FE model in terms of loading and boundary conditions would be expected to lead to more accurate results.

The BMD of the medial condyle (ROI 1) is lower than that of the medial compartment of the tibia (ROI 3) due to there being relatively more trabecular bone in the condyle than in the tibia, whereas the densities around the fixation holes (ROI 2 and ROI 4) are similar, because the holes are mainly surrounded by cortical bone in both femur and tibia. As mentioned, the BMD variation stabilised in all regions three years after operation, which can also be observed in Figure 4-17. Petersen et al. [157] measured the BMD changes in the distal femur after knee arthroplasty and reported that changes were stabilised two years after operation, while Van Lenthe et al. [130] numerically investigated the density changes in the distal femur after knee replacement and reported that there is a difference between numerical results and postoperative radiographs, in terms of reaching BMD equilibrium. As mentioned in Chapter 2, there are more advanced and complex bone remodelling methods based on cell interactions, which would be expected to improve the accuracy of the results [84-88].

Petersen et al. [157] reported 36% variations in BMD behind the anterior flange of the femoral implant and 22% variations proximal to the fixation pegs, after total knee replacement. The current study shows that attachment of the current implant led to variations in BMD in all ROIs of less than 5%, suggesting that this implant will not result in significantly adverse BMD changes in the knee joint.

It was observed that, regardless of the greater than 30% stress reduction in the cartilage, BMD in the ROIs was not changed significantly after attaching the implant. It should be noted that each ROI includes both trabecular and compact bone and, as shown in Figure 4-16b and c, the density in some regions decreased while in other regions increased.

4.5 Conclusions

In this chapter, Bone Mineral Density (BMD) of the knee joint was investigated after attaching the extra-articular implant. BMD of the knee joint was simulated by applying a gait loading condition in the hip joint. The heterogeneous density distributions of the knee joint without implant were assigned as an initial density to the model with implant and BMD was simulated five years after attaching the implant. The von Mises stress in the medial femoral cartilage was seen to reduce by 36.5%; however, BMD in the medial condyle and medial compartment of the tibia increased by approximately 3.4% and 4.1%, respectively, and the density in bone surrounding fixation holes of both femur and tibia increased by around 2.2%. Also, the density changes in all regions of interest stabilised three years postoperatively. Accordingly, BMD was not changed significantly after attaching the implant to the femur and tibia.

In Chapters 3 and 4, FEA was implemented in order to understand how this new implant would change the loading conditions in the tibiofemoral joint, and how that change would influence periprosthetic bone density. After these numerical and theoretical investigations, in the next chapter, the performance of this implant will be evaluated experimentally through a cadaver study.

Chapter 5

Cadaver Study

A cadaver study was conducted under Ethics Application 17/52 approved by the Auckland University of Technology Ethics Committee (AUTEC).

5.1 Introduction

In Chapters 3 and 4, numerical and theoretical methods were used in order to perceive the effects of the novel implant on the biomechanics of the tibiofemoral joint; however, a crucial part of assessing any new product is to make use of prototypes and carry out physical experiments. In other words, although computer simulations can considerably reduce the cost of the evaluation process of orthopaedic devices, even a well-developed computer simulation can only estimate the contact pressure at the knee joint after implantation of a new prosthesis. Further, surgical considerations and questions cannot be adequately addressed using computational models.

According to the above points, this chapter aims to study the surgical procedure of the implant attachment and investigate the influence of this implant on the contact pressure in a cadaver knee joint under different loading scenarios. The latter is particularly important in order to perceive if this implant can effectively reduce the load going through the medial side in a realistic situation, considering that this is a patient-specific implant and was designed for a specific knee joint.

5.2 Materials and methods

5.2.1 Implant design and manufacturing

Knee joint specimens for this study were dissected from the left legs of two donated bodies from the Faculty of Medical and Health Sciences of the University of Auckland under the Human Tissue Act 2008. Donors had no recorded history of knee pain or surgery. Specifications of donated bodies are listed in Table 5-1.

Table 5-1. Specifications of donated bodies.

Specimen No.	**1**	**2**
Gender	Male	Male
Age	64	92
Height (cm)	155	183
Weight (kg)	88	80

Before making any incisions and whilst the knee specimen was intact, MR images were acquired with a Siemens® 3T MAGNETOM® Skyra (Siemens Medical Systems, Erlangen, Germany) scanner located in the Centre for Advanced Magnetic Resonance Imaging at the University of Auckland. The knee specimen was imaged using a 15 channel transmit/receive knee coil as shown in Figure 5-1. The imaging was carried out in order to develop a 3D model of the knee joint and to design the implant using that model.

Figure 5-1. Embalmed leg in a knee coil.

Data acquisition included regions at least 10 cm above and below the tibial plateau. Different sequences of imaging were acquired in order to facilitate accurate segmentation of tissue. Imaging of each sequence took approximately 5 minutes and imaging parameters of the sequences are as follows:

- T1 3D vibe Gradient echo sequence: Matrix 320 x 320, Field of view 200 x 200 mm, Slice thickness 0.6 mm, TE 3.79, TR 10.8, Flip angle 10, 1 average.
- T1 3D vibe Gradient echo sequence with fat sat: Matrix 320 x 320, Field of view 200 x 200 mm, Slice thickness 0.6 mm, TE 5.39, TR 10.8, Flip angle 10, 1 average.
- T2 3D Gradient echo sequence: Matrix 320 x 320, Field of view 200 x 200, Slice thickness 0.6 mm, TE 5, TR 14.1, Flip angle 25, 1 average.

The 3D T1, T1 with fat saturation, and T2- weighted images sequences were acquired using identical matrix and resolution as this facilitated segmentation by allowing superimposition of the datasets. The 0.6 mm almost-isotropic resolution facilitated accurate segmentation of the complex structures, essential for 3D modelling of the knee and precise manufacture of the implant to attach to the cadaver. The anatomy was manually segmented using Amira® software (FEI Visualization Sciences Group, Burlington, MA, USA). Segmentation was based on the image grayscale intensity of the three imaging datasets (Figure 5-2), and a priori knowledge of knee structure.

Figure 5-2. Acquired MRI sequences: a) T1 3D, b) T1 3D with fat saturation, c) T2 3D.

Segmentation of one scanned slice in Amira is shown in Figure 5-3a, and a 3D model of the segmented femur and tibia in Amira, comprised of segmentation of all slices, is shown in Figure 5-3b.

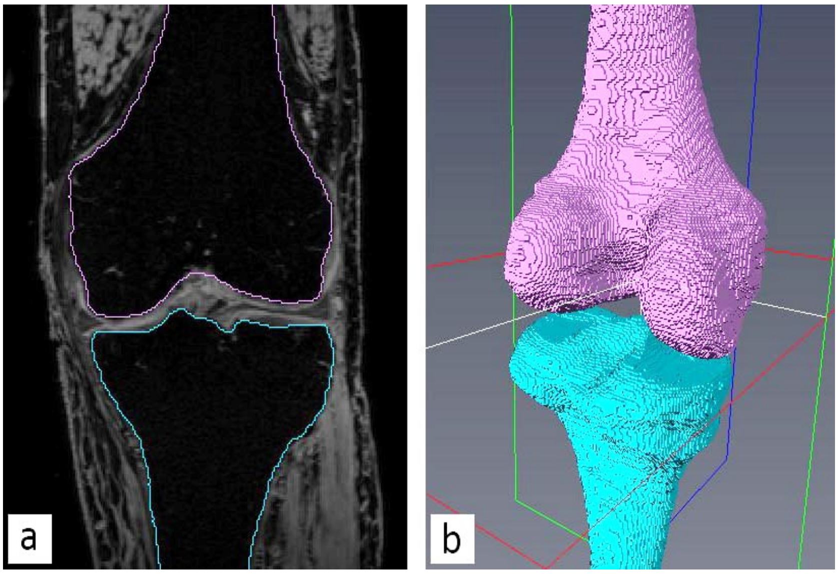

Figure 5-3. a) Segmented femur and tibia on one scanned slice in Amira, b) 3D representation of segmented femur and tibia in Amira.

Taking advantage of the aforementioned MRI sequences, and switching between them during the segmentation process, the bones were segmented precisely. A semi-transparent surface rendering of the tibia and fibula using Amira is shown in Figure 5-4a.

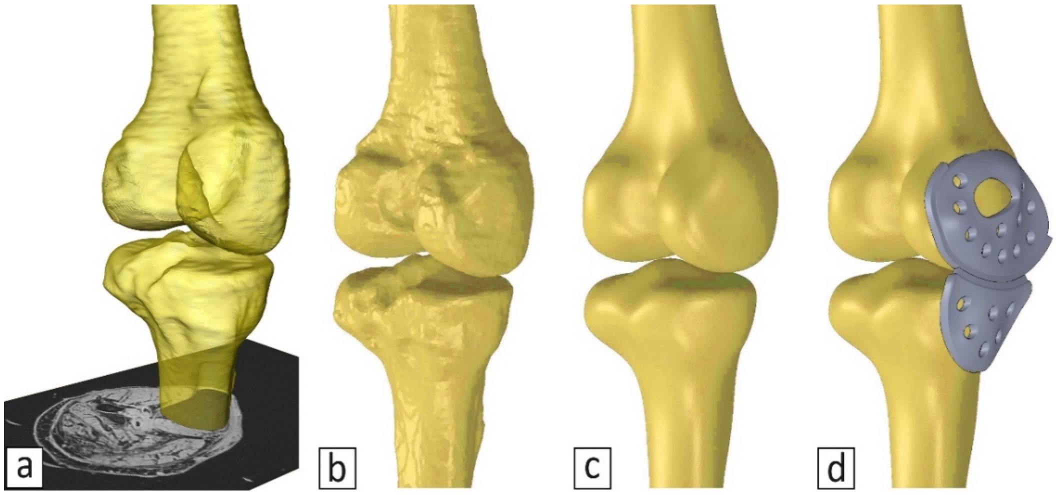

Figure 5-4. a) 3D surface rendered model (Amira software), b) bones before smoothing, c) smoothed bones using Meshmixer, d) knee bones with the implant.

After segmentation, STL files of the model were exported (Figure 5-4b) and smoothed using Meshmixer software (Figure 5-4c). The smoothing grade can be adjusted in software; however, for this model the default grade of the shape preserving smoothing type was used. The smoothed model was then imported to SolidWorks in order to design the implant to precisely fit the medial side of the model (Figure 5-4d). This allowed for compatibility between the implant and joint in terms of conformity and curvature of the femoral and tibial heads on the medial side. This is particularly helpful for accurate placement and fit of the implant on the patient’s femur and tibia.

This implant is a patient-specific implant, so the best available manufacturing technique for this purpose would be additive manufacturing, in particular Electron Beam Melting (EBM) [121]. In the Selective Laser Melting (SLM) parts, pores can be observed which decrease ductility considerably, limiting SLM use in medical applications [158]. Also, additional heat treatment is necessary for the SLM parts [158]. For this study, CNC machining was used, due to the lack of access to an EBM machine. Manufacturing the implant using CNC machining was challenging due to the complexity of the implant geometry and the availability of only a 3-axes machine. Therefore, the process planning was time consuming and, ultimately, a tale form piece (as shown in Figure 5-5) was added to the design in order to be used as a reference surface, which is crucial, because both sides of the implant should be machined. This extra tale was also used to clamp the work-piece firmly during the machining process.

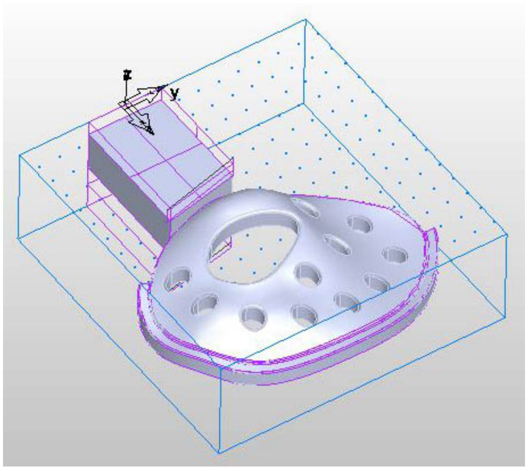

Figure 5-5. CAD file of the femoral implant in FeatureCAM® software.

After the process planning, a CAD file of the implant was imported into FeatureCAM® software (Autodesk, Inc.) as shown in Figure 5-5 in order to generate the G-code for CNC machining. The work-piece was cut from a bulk stainless steel part (Figure 5-6a) using wire-cutting; the femoral work-piece is shown in Figure 5-6b.

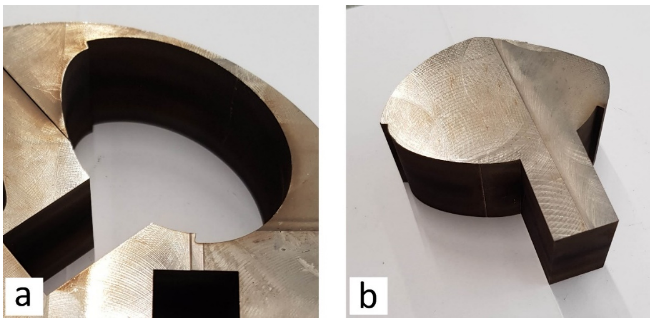

Figure 5-6. a) Bulk stainless steel part after wire-cut, b) wire-cut femoral work-piece.

After clamping the work-piece, the G-code was sent to the CNC machine controller as shown in Figure 5-7.

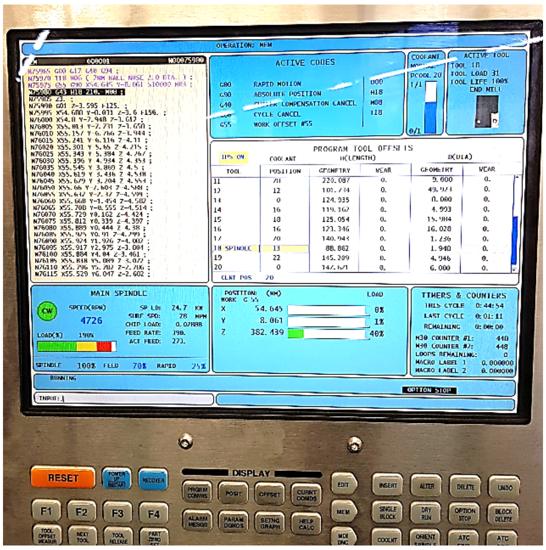

Figure 5-7. Controller of the CNC machine during the femoral part machining.

The external side of the implant was machined first (Figure 5-8a). The internal side of the implant before and during the machining process are shown in Figure 5-8b and c, respectively. Machining times for the femoral and tibial components were approximately 17 and 13 hours, respectively.

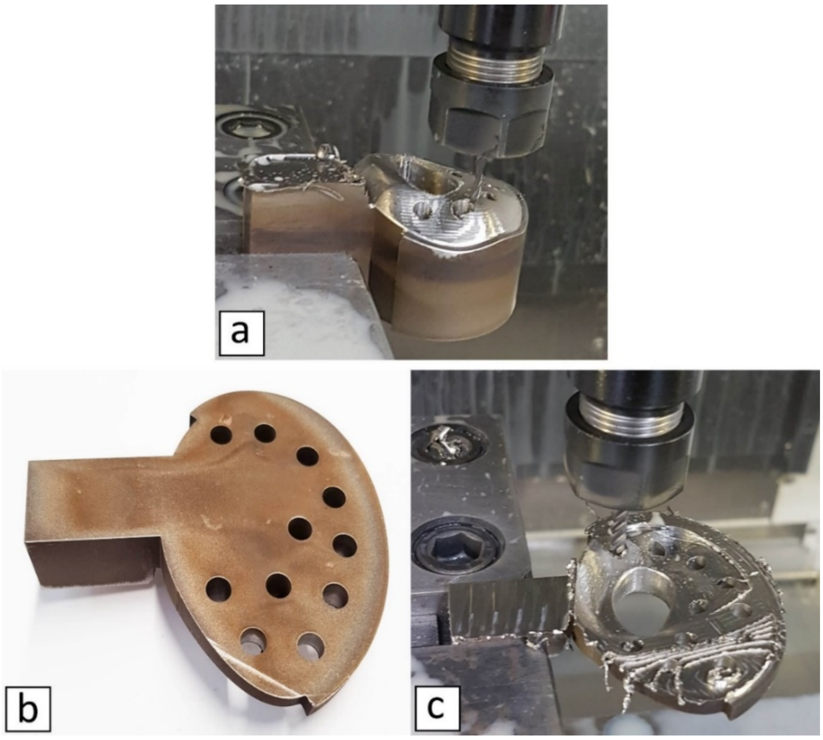

Figure 5-8. Machining process for the femoral part: a) machining of the external side, b) internal side before machining, c) machining of the internal side.

After machining each part (Figure 5-9), the wire-cutting machine was used to cut off the surplus piece of the implant.

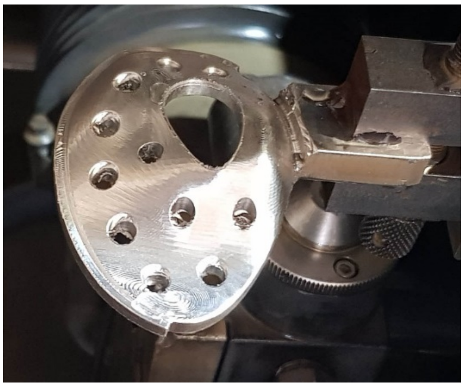

Figure 5-9. Clamped femoral part in the wire-cutting machine.

A final prototype of the implant is shown in Figure 5-10.

Figure 5-10. A prototype of the implant manufactured by CNC machining. (Upper part is the femoral component of the implant, and lower one is the tibial component.)

5.2.2 Cadaver experiments

The complete leg was embalmed before specimen preparation. For the embalming process, 7 L Dodge® (Dodge Co., Cambridge, MA) anatomical arterial fluid along with 1 L Plasdopake, a tracer dye, which allows the embalmer to see evidence of distribution, were used. Hot water (3 L) was added to drive the embalming fluid to the tissue [159, 160]. The knee joint was then isolated from near the middle of the femur to the middle of the tibia as shown in Figure 5-11.

Figure 5-11. Embalmed specimen No. 1.

Cadaver experiments in this study were divided into two parts: (i) investigating the implant attachment procedure from a surgical point of view (without using any special tools), contact of the femoral and tibial parts at different flexion angles, and the effect of the implant on the joint space in the medial side using X-ray imaging, (ii) comparing the contact pressure in the tibiofemoral joint before and after attaching the implant in the fully extended knee position. The researcher performed the experiments with the help of a knee surgeon to make sure that the surgical considerations were taken into account.

5.2.2.1 Surgical procedure

Specimen No. 1 had small joint osteophytes which were irrelevant for this part of the study. Surgery was performed by a knee surgeon in order to determine the limitations, requirements and any specific surgical considerations for the future development of the implant or related tools. Initially, AP and lateral X-ray of the specimen was taken, an incision was made on the medial side of the knee joint to expose the Medial Collateral Ligament (MCL). After exposure of the ligament, the implant was attached to the femur and tibia using screws without damaging the MCL. After attaching the implant, X-rays were taken again in order to determine the difference in the joint space induced by the implant. A surgeon then examined the contact of the femoral and tibial components at different flexion angles.

5.2.2.2 Contact pressure measurement

For this section, specimen No. 2 was used. Initially, the experiments were conducted on the specimen without dissecting the soft tissue. Loading scenarios were applied using an Instron machine with a 10 kN load cell in the fully extended knee position. Assuming 80 kg as average body weight, three loading forces from one to two times body weight were used for the experiments. Depending on the activity and joint angle, the knee joint can undergo much higher pressures but, for this study, only the mentioned loads were applied to the joint; experiments were conducted using a specific setup only to compare the contact pressure in the knee joint before and after attaching the implant and not necessarily to exactly mimic the large range of real-life loading conditions, as this needs a more advanced test rig and could be done at the later stages of implant development.

Each load was applied three times and the average was reported for each test condition. The knee joint was mounted on the machine using fixtures (Figure 5-12). These fixtures were designed and manufactured specifically for this study. The contact pressure in the tibiofemoral joint was measured using a Tekscan® pressure mapping sensor model 4000-1500 (Tekscan, Inc., Boston, MA), which can measure up to 10 MPa pressure. As mentioned in Chapter 2 (section 2.1.7), this is a standard sensor, which was specifically designed by Tekscan for studying contact mechanics in the knee joint. A photo of the sensor used in this study and its specifications are shown in Figure 5-13 and Table 5-2, respectively.

Figure 5-12. Fixture for the femur (left) and tibia (right).

As shown in Figure 5-13, intersections of conductive paths, which are covered by a pressure-sensitive ink, form a sensing matrix. This sensor is very thin (0.1 mm) and flexible, and so can be used in the narrow joint space, in which the bone surface is not flat. Specifications of the sensor are listed in Table 5-2.

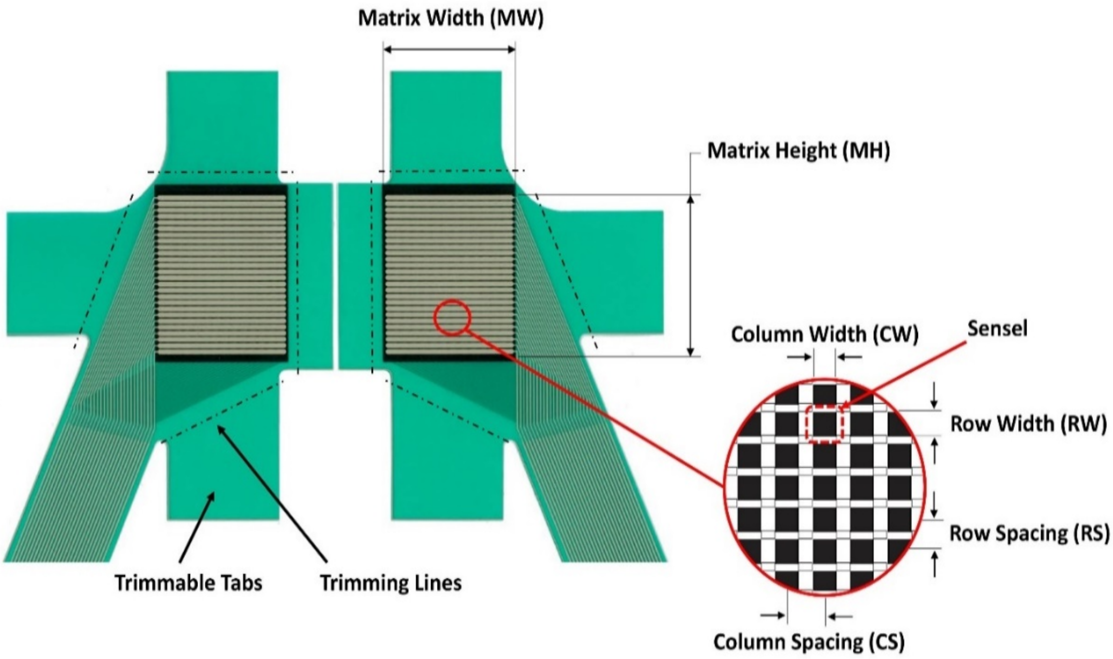

Figure 5-13. Tekscan pressure mapping sensor 4000 and a magnified sensing matrix, used for the experiments.

Table 5-2. Tekscan pressure mapping sensor 4000 specifications [102].

MW (mm)	MH (mm)	Columns			Rows			Total No. of Sensels	Sensel Spatial Resolution
		CW (mm)	CS (mm)	Qty.	RW (mm)	RS (mm)	Qty.		[sensel/cm^2]
27.9	33.0	0.8	1.3	22	1.0	1.3	26	572	62.0

Care was taken during placement of the sensor in the joint to avoid damaging or wrinkling the sensor, and to ensure a correct fitting of the sensor on the soft tissue. In order to fit the sensor properly, most of the tabs around the sensing area need to be trimmed before insertion. Positioning and fixing the sensor in the joint is crucial to accurately record and compare the pressures obtained from experiments without and with the implant. The experimental setup is shown in Figure 5-14.

Figure 5-14. An experiment conducted on the specimen before dissection.

Although the soft tissue surrounding the joint was beneficial in terms of keeping the joint moist in between the experiments, it led to some difficulties due to lack of enough space for proper insertion of the sensor and consequently the damaging of several sensors during insertion, as shown in Figure 5-15a-c. Sometimes, damage was not visually detectable during an experiment, as this damage arose inside the joint, usually when the sensor area was pinched or subjected to a very concentrated pressure over a small area (Figure 5-15d). Damage also took the form of wrinkles. As a result, some pressure data would be missing from the damaged area (which might be a critical area for determination of the contact pressure through the knee).

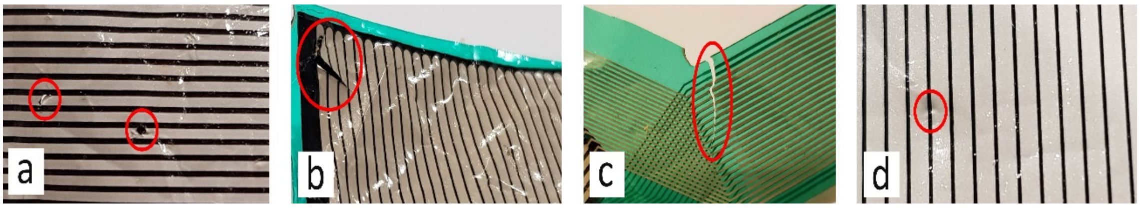

Figure 5-15. Damaged sensors during insertion into the joint space, a) small holes on the sensor area, b) torn sensor area, c) torn printed circuit, d) internal damage to the sensor area.

According to the above issues, ultimately all of the soft tissues except for the menisci, and cruciate and collateral ligaments were removed as shown in Figure 5-21b (the complete dissection process, from the embalmed leg all the way to the final specimen, is summarised in Appendix B). In order to have an accurate understanding of how the implant influences the contact pressure in both compartments, the applied load should be fully transmitted through the sensor. After inserting the sensor into the joint space, it was observed that the sensor could not cover the whole contact area of the cartilage and menisci, so the menisci were removed. The sensor was connected to the handle (as shown in Figure 5-18a) to begin measurements once all preparations were complete. Experiments were performed with two different set-ups: without and with the implant. Prior to the experiments, the sensor was preconditioned in order to improve repeatability, by loading and unloading five cycles up to 110 % of the maximum load.

Because the knee joint was a cadaver specimen, instead of using specific surgical grade screws, ordinary wood screws (length 25 mm, diameter 5 mm) were used to attach the implant to bone. As mentioned, no ligament is sacrificed in this method and the attachment point of the MCL to the femur was considered during the design procedure of the implant.

During the experiments, raw data was collected and the calibration process was conducted based on the collected data after the experiments. Generally, the calibration process can also be performed before the experiments, but because the sensors are fragile and a number were damaged, calibration was conducted after doing the experiments without damaging the sensor. It should be noted that, one calibration file cannot be used for multiple sensors and it has to be generated for each sensor separately even if they are of the same type. The sensitivity level should be the same for the calibration process and the experiments. To adjust the sensitivity, the sensor was placed in the experimental setup and loaded up to 90% of the maximal intended experimental load. The saturation level was then adjusted in such a way as not to see oversaturation (purple colour). Three different sensitivity levels are demonstrated in Figure 5-16a-c with S19 (sensitivity level adjusted in the I-Scan™ software) being an optimum sensitivity based on the maximum load.

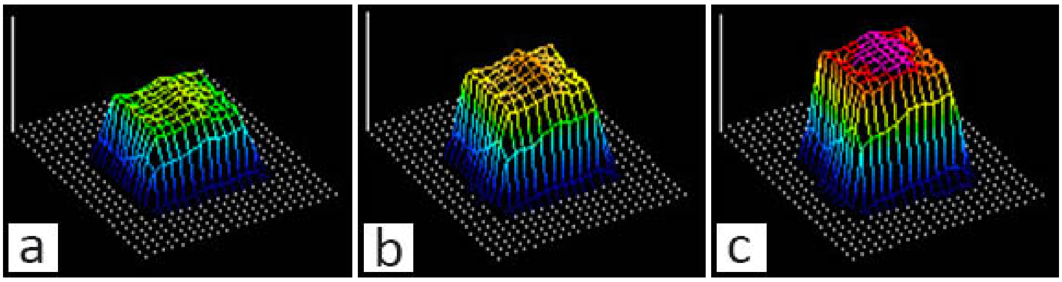

Figure 5-16. Examples of the pressure contours at different sensitivity levels: a) low sensitivity (S17), b) optimal sensitivity (S19), c) oversaturation (S21)

To calibrate the sensor, initially the average raw pressure of the collected data during experiments was measured for all loading conditions. To ensure an accurate calibration over the whole loading range, a multipoint calibration was performed due to the non-linear correlation between the applied load and the measured raw data from the sensor. Therefore, a 3-point calibration was conducted using three average raw values previously collected during the experiments [98]. I-Scan^{TM} software was then used to create a calibration curve as shown in Figure 5-17.

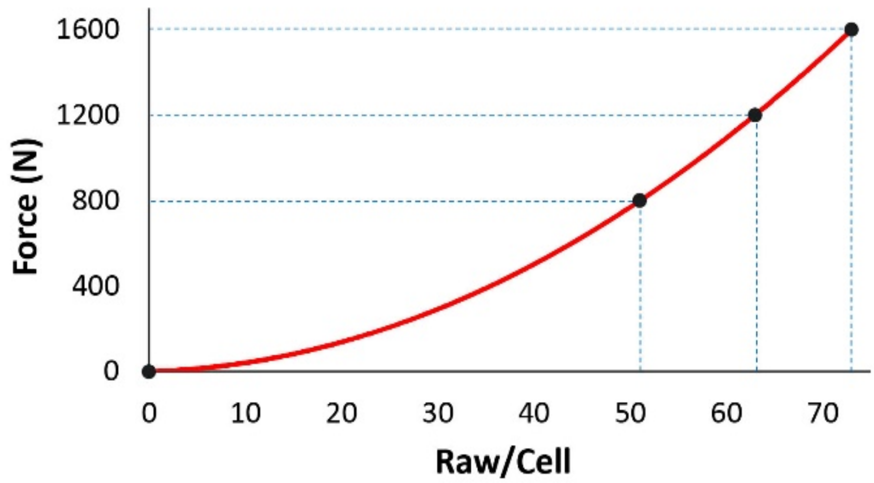

Figure 5-17. Calibration curve generated by the I-Scan software.

The calibration was performed using the setup shown in Figure 5-18a, in which polyethylene simulates the cartilage surface and a rubber layer ensures uniform pressure distributions on the sensor [98]. An alignment tool at the bottom of the experimental setup was introduced in order to balance the axial load at both sides of the sensor. Pressure distributions under a 1600 N load during the calibration process are shown in Figure 5-18b.

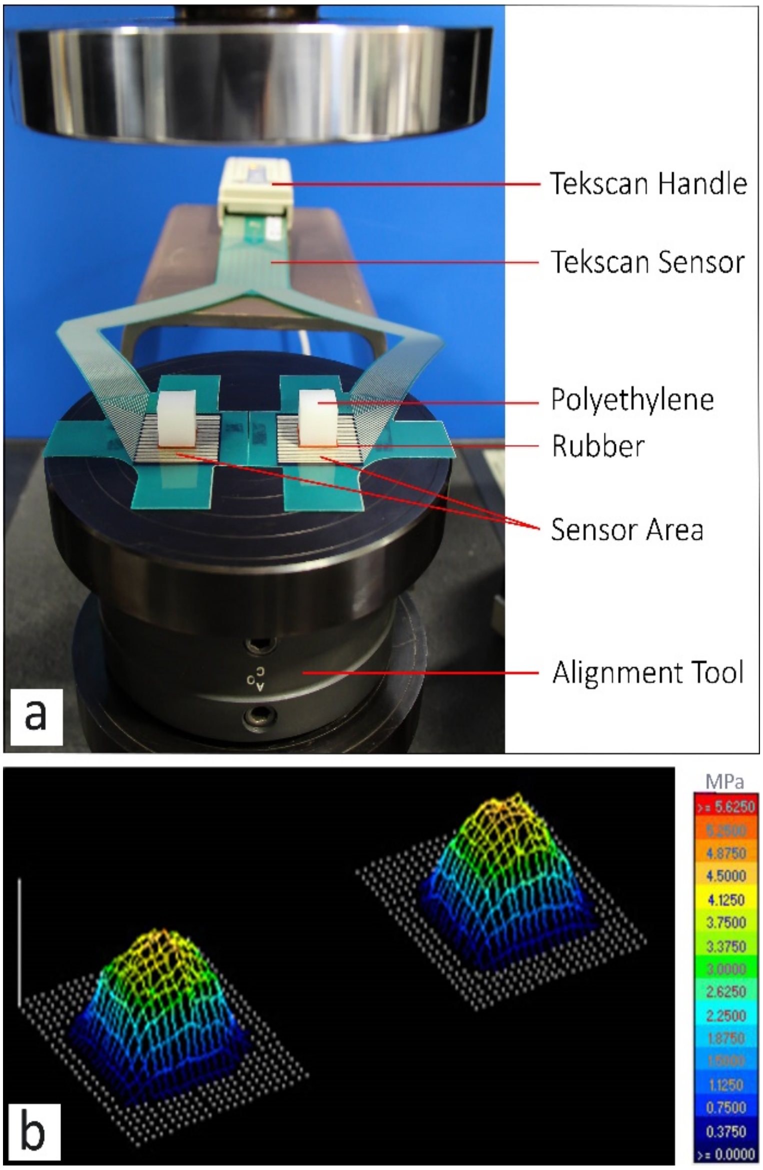

Figure 5-18. a) Sensor calibration setup, b) graphic representation of pressure distributions during the calibration process.

5.3 Results

5.3.1 Surgical procedure

After making an incision (Figure 5-19a), exposing the MCL (Figure 5-19b) and attachment of the implant, the knee joint was examined at different flexion angles as shown in Figure 5-19c – e. Finally, the incision was closed as shown in Figure 5-19f.

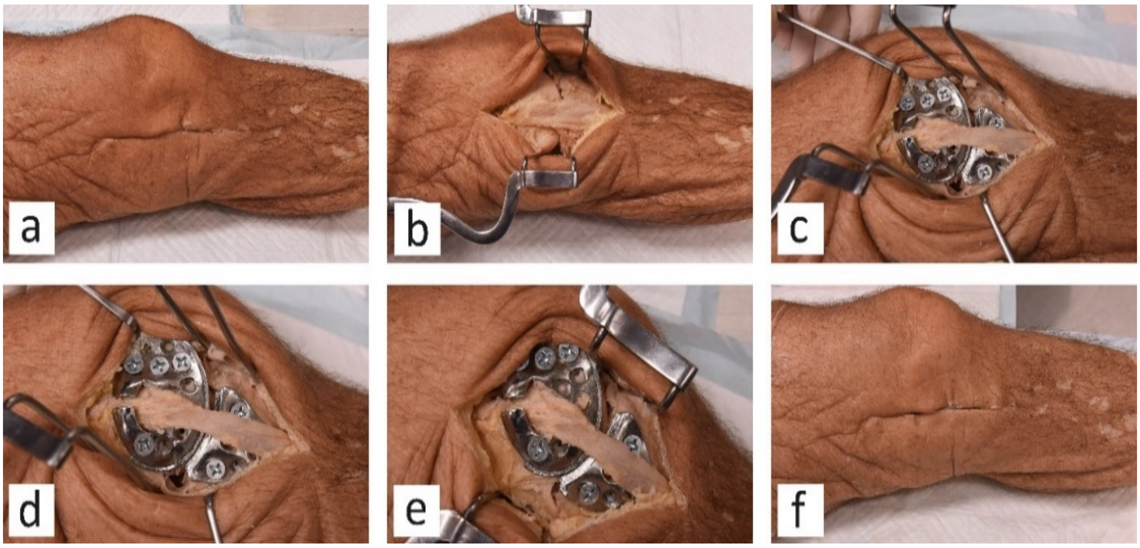

Figure 5-19. a) Incision made in the medial side of the specimen, b) exposed MCL, c) joint at 0°, d) joint at ~30°, e) joint at ~60°, f) closed incision after attachment of the implant.

An AP X-ray of the knee joint conducted when the specimen was intact is shown in Figure 5-20a. AP and lateral X-rays of the joint after introducing the implant are shown in Figure 5-20b and c, respectively.

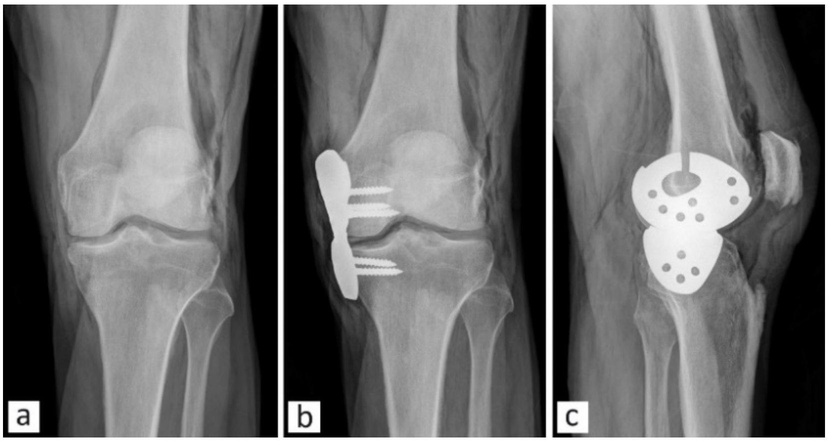

Figure 5-20. X-ray of the knee joint: a) AP without implant, b) AP with implant, c) lateral with implant.

5.3.2 Contact pressure

As previously described, cadaver experiments were performed under different loading scenarios and results were recorded using a pressure mapping sensor. As shown in

Figure 5-21a, the top and bottom of the pressure map show the anterior and posterior sides of the joint, respectively. After conducting the initial experiments, the implant was introduced to the joint. Joint space should be increased before attachment of the implant in order for the implant to perform properly, i.e. remove through the implant some of the load that would otherwise pass through the knee joint. To do so, the knee joint would be subjected to valgus strain during a real surgery; however, doing so during the experiment could lead to a different experimental setup and consequent error. Therefore, the implant was attached to the specimen, while the joint was still mounted on the Instron machine.

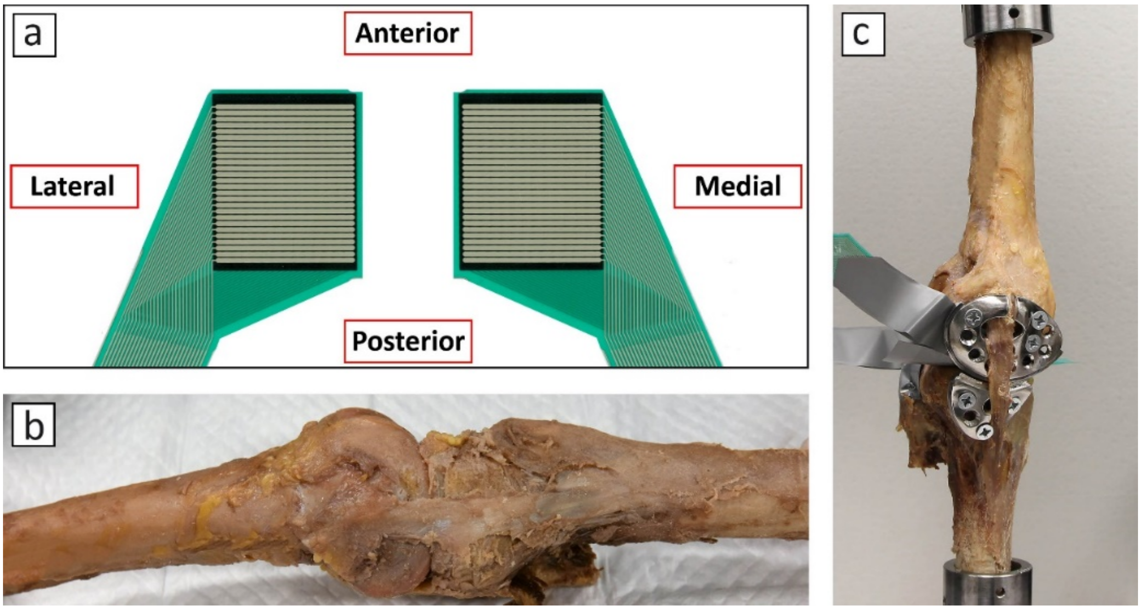

Figure 5-21. a) Direction of the sensor in the joint during experiments, b) medial view of the specimen without implant, c) experimental setup with implant.

Pressure distributions under each loading condition for the experiments without and with the implant are shown in Figure 5-22a-f. The orientation of the sensor in the joint is shown in Figure 5-21a, i.e. the right and left sides of each image in Figure 5-22 show the pressure distributions in the medial and lateral compartment, respectively.

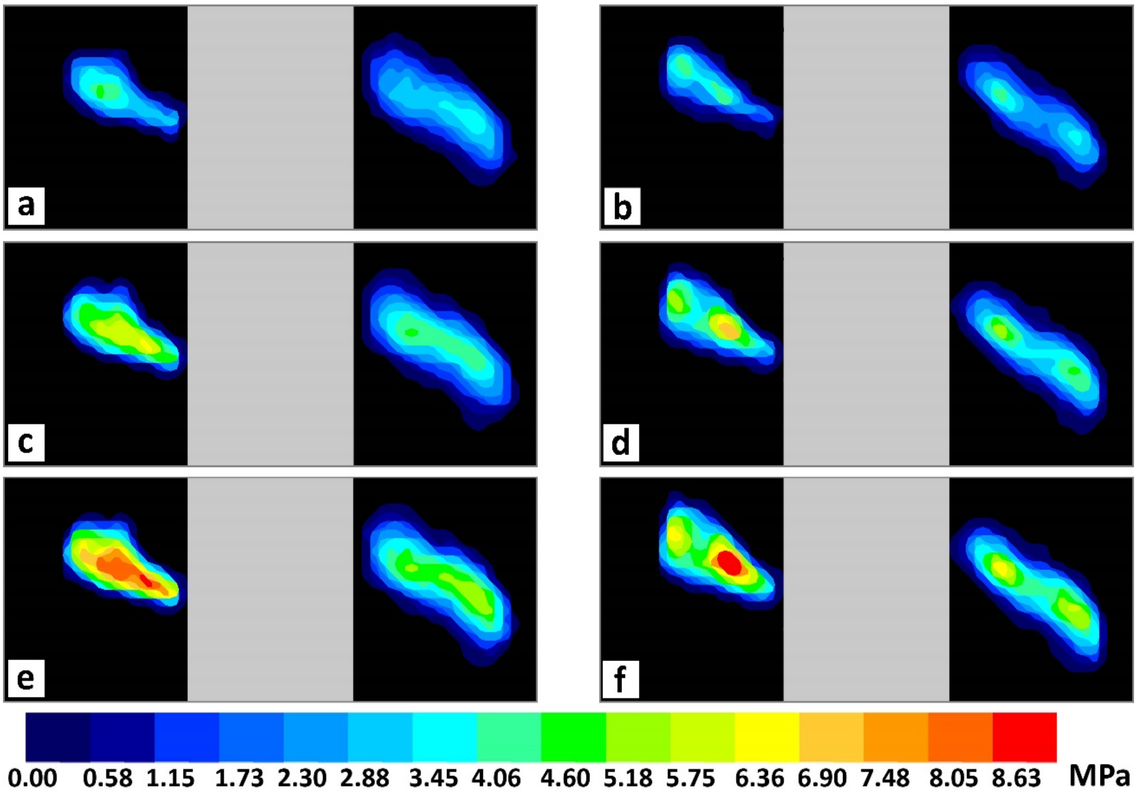

Figure 5-22. Contact pressure distributions in the knee joint under different loads, a) 800 N without implant, b) 800 N with implant, c) 1200 N without implant, d) 1200 N with implant, e) 1600 N without implant, f) 1600 N with implant.

Dodge restorative was applied to the specimen in between the experiments to keep the tissue moist.

5.4 Discussion

5.4.1 Surgical procedure

As shown in Figure 5-19a, the incision made to attach the implant is smaller than the typical incision required for a standard joint replacement. It should be considered that the actual incision during surgery could well be smaller than what was made during the experiments, as a good exposure of the implant was required in this study in order to take photographs during the experiments. As mentioned previously, one of the advantages of this implant is that the anatomy of the joint is not disrupted during the procedure. Indeed, as shown in Figure 5-19, the MCL was not sacrificed or damaged, nor were the bones modified, thus the implant can be easily removed if required. This is a patient-specific implant and its thickness would be different for each patient. In the case where there is an insufficient gap between the MCL and bones, a thin layer of the bone surface would be removed in order to prevent stretching of the MCL. However, further studies need to be performed to investigate the possibility of knee laxity upon removal of the implant.

The joint moved smoothly during flexion and extension without any resistance due to the implant. In the fully extended position of the knee joint, a distributed load was observed between the articulating surface of the femoral and tibial components (Figure 5-19c), while at other angles a more concentrated load was observed (Figure 5-19d and e). Given the fact that point loads at metal-on-metal contacts could lead to wear, and metal debris and complications such as metallosis, it should be emphasised here that this implant is a prototype; optimal material selection for this implant is being investigated in a separate project. The contact points between components for the final design is likely to be a metal (Ti-6Al-4V or CoCr) on polymer (Ultra High Molecular Weight Polyethylene), similar to that in common TKA implants.

X-ray of the knee joint was conducted to determine the impact of the implant on the joint space. As shown in Figure 5-20, the gap between femur and tibia increased after introducing the implant. For this experiment, a slight valgus deflection was manually created and the implant was then attached to the joint; a tool or specialised equipment will be developed for actual surgery, to create a measurable deflection based on preoperative radiographs. The X-rays also clearly showed the position of the femoral and tibial implant components on the bone and on each other (Figure 5-20b and c). Both parts of the implant were positioned on each other as expected and no gap was observed between them in either the AP view or lateral view.

This method has some benefits compared to other surgical treatments. For instance, a HTO is not suitable if there is unicompartmental knee OA without deformity, and compared to the proposed implant in this study, HTO is a relatively invasive option [161]. In comparison with TKA, the surgery required for the implant introduced here can be categorised as a minimally invasive operation. In other words, unlike in the case of TKA, such surgery does not require to resect bone from the surfaces of the distal femur and proximal tibia [162]. Accordingly, the patient's recovery should be quicker and less painful. It should also be noted that this implant is not considered to be a permanent implant such as TKR. Thus, the risk of implant surgery is minimised, and younger patients should be more willing to undergo the surgery as soon as osteoarthritis is detected. In other words, a surgical option for early-onset knee osteoarthritis might well be suggested more often by surgeons, if the operation was reversible and the patient could recover relatively quickly [39]. Indeed, instead of using various types of conservative methods to postpone invasive surgical therapies, the implant considered here partially unloads the knee, before degeneration worsens, and allows for the possibility for cartilaginous tissue to be repaired [2, 17].

The reason for the above suggestion from most orthopaedic surgeons for patients with early-onset OA is that they believe this kind of implant, or any other viable treatment for the mentioned gap, might be suitable for patients who are young or not yet willing to undergo invasive surgical therapy [163]. It would also help the patient to avoid sedentary lifestyle morbidity and encourage them back to a normal life and exercise, which would lead to a decrease in the possibility of obesity and depression [163].

Moreover, by reducing the post-operation expenses and limiting the related costs of invasive surgeries and revisions, this novel implant could help produce savings for the healthcare system [56, 163].

5.4.2 Contact pressure

Measured forces in the medial and lateral compartments of the knee joint are shown in Figure 5-23a and b, respectively. The implant was attached to the medial side, so it had a greater effect on this side, in terms of reducing the force. As mentioned, the implant was attached to the specimen while it was mounted on the machine without creating a valgus deflection; otherwise more load reduction would have been observed.

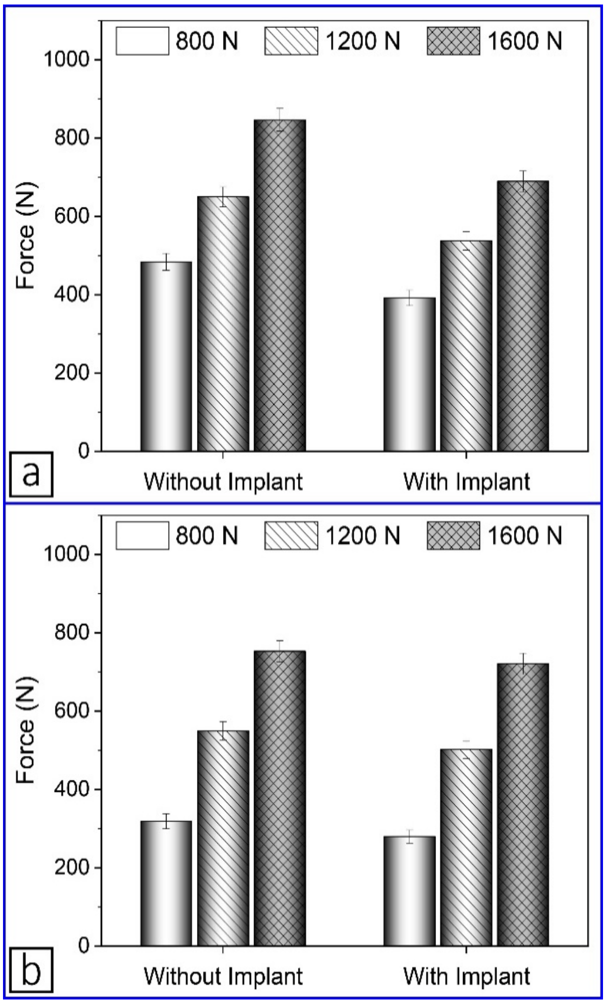

Figure 5-23. Force in the knee compartment without and with implant: a) medial, b) lateral.

The percentage load reductions in the medial and lateral compartments after attachment of the implant are shown in Figure 5-24. It was observed that under different loading conditions, the implant reduced the load going through the medial side by approximately 18%, which is relatively close to the unloading amount of the KineSpring implant [54]. Increasing the applied load on the specimen from 800 N to 1600 N caused the percentage of load reduction in the lateral side to decrease approximately from 12% to 4%. This implies that increasing the load led to abduction of the joint and the transmission of a higher percentage of the applied load through the lateral side. According to the mentioned results, the implant was effectively reducing the load going through the medial side.

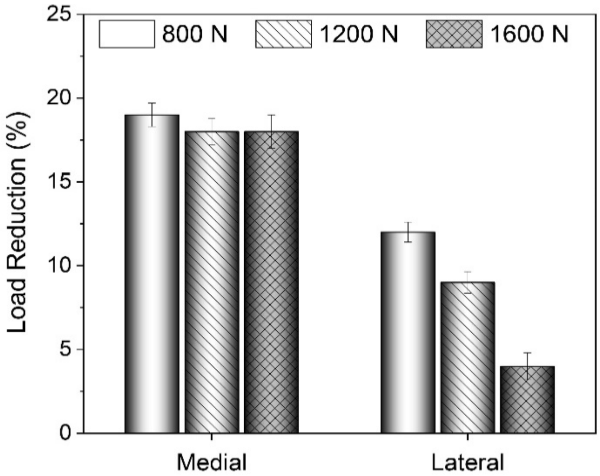

Figure 5-24. Load reductions in both compartments after attachment of the implant.

The experimental results were compared with similar studies: Pressure distributions were compared with cadaver research conducted by Fojtik [164] on the influence of Lateral Meniscus Posterior Root Avulsions (LMPRA) and Meniscofemoral Ligament (MFL) deficiency on contact mechanics of the tibiofemoral joint. She compared pressure contours of an intact knee joint, a joint with LMPRA, and a knee joint with LMPRA and deficient MFL. Pressure contour patterns were similar for the two aforementioned conditions. Pressure contour patterns in experiments performed by Fojtik [164] (Figure 5-25) are similar to what was observed in the present study (Figure 5-22). Similarly, higher peak contact pressure in the lateral compartment was observed in both studies, due to a smaller contact area on this side as compared to the medial side.

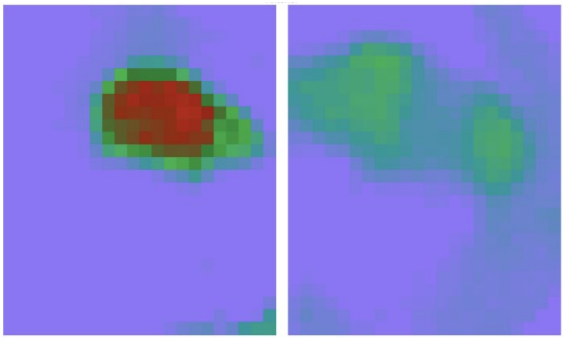

Figure 5-25. Measured contact pressure in the knee joint under 1000 N by Tekscan sensor [164].

Peak contact pressure on the medial side was also compared with what was reported in a cadaver study conducted by Wang et al. [104]. They used a dynamic knee simulator in order to simulate the gait cycle and measure the contact pressure in the knee joint for different conditions, i.e. intact knee joint and meniscectomy. Due to the menisci removal in the present study, the meniscectomy condition was selected for comparing results. The input of the dynamic knee simulator and peak contact pressure reported by Wang et al. [104] are shown in Figure 5-26a and b, respectively.

Applied loads for the present study were 800, 1200, and 1600 N, and they were applied at zero degree flexion. In the research conducted by Wang et al. [104], these loads were applied on the joint at different angles during the gait cycle. For instance, 1200 N (green dash-line in Figure 5-26a) was applied on the knee joint six times during one gait cycle (red points). The percentage of the gait cycle was read from the input graph for all six times and the equivalent peak pressure for each percentage was read from Figure 5-26b (green points). The mean value and standard deviation for the six peak pressure values were around 4.3 (black dash-line in Figure 5-26b) and 0.25 MPa, respectively. It should be noted that the peak pressure does not significantly differ for any given load at various percentages of the gait cycle, and the X-axis of the peak pressure graph does not start from zero (Figure 5-26b). Also, the least flexion angle occurs at around 40% of the gait cycle [104], the 800, 1200, and 1600 N were applied at 24%, 34%, and 38% of the gait cycle, respectively, and the equivalent pressures were 3.2, 4.3, and 5.4 MPa, respectively. For the same loads in the present study, measured peak contact pressures were 3.7, 4.6, and 5.5 MPa, respectively, relatively close to what was reported by Wang et al. [104].

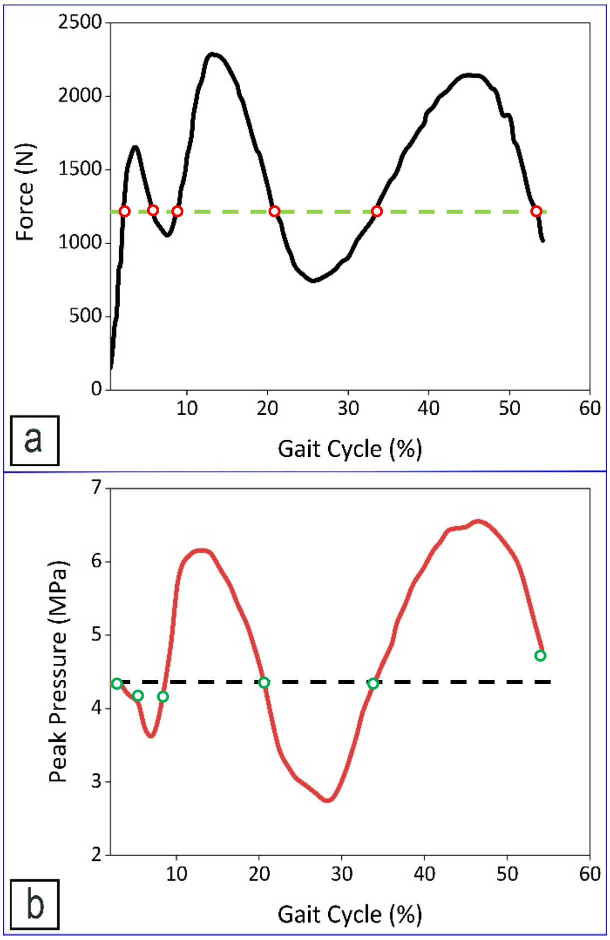

Figure 5-26. a) Input of the knee simulator, b) measured peak contact pressure in the medial side by Tekscan sensor [104].

5.5 Conclusions

A novel extra-articular load-sharing implant for osteoarthritic knees was experimentally investigated in the study reported in this chapter. The implant was initially attached to the medial side of a cadaver knee joint and examined at different flexion angles without modifying the bones or sacrificing and/or damaging the MCL. It was observed that after attachment of the implant, the joint moves smoothly without any resistance caused by the implant. According to AP and lateral X-rays before and after introducing the implant, joint space in the medial compartment increased and both parts of the implant were positioned properly on each other.

Contact pressure in the tibiofemoral joint was also studied under different loading conditions. It was observed that applied forces on both compartments decreased after attaching the implant; however, the force going through the medial side was decreased more than that of the lateral side, because the implant was attached to the medial side. Peak contact pressures were higher in the lateral side, because of the smaller contact area in the lateral compartment as compared to that in the medial side.

It was also observed that, after attachment of the implant and under different loading conditions, the load was reduced by approximately 18% in the medial side. On the other hand, by increasing the applied load on the joint from 800 N to 1600 N, the percentage load reduction decreased from 12% to 4% in the lateral side, due to abduction of the knee joint. Furthermore, the studied implant is minimally invasive and it is not considered to be a permanent implant. Thus, patients would be encouraged to undergo surgery with this implant when the disease is at an early stage.

The results of the study show that this implant can effectively increase the joint space on the medial side and reduce the load going through that side without modifying, sacrificing or damaging any of the hard or soft tissues, indicating the promise of this implant for treatment of knee osteoarthritis.

Chapter 6

Conclusions and Future Work

6.1 Conclusions

A new load-sharing patient-specific implant for knee osteoarthritis was studied in this project using numerical methods as well as experiments. The research aimed to investigate efficacy of this implant using different approaches, and to provide a better understanding for its future development. The particular aspects of the implant which were examined based on the three objectives of the thesis (Chapter 2 section 2.3), including knee and cartilage stress, bone remodelling, surgical procedures and knee contact pressures, and approaches used, were all new to this implant, which had not previously undergone thorough research and investigation. Those objectives were investigated in Chapters 3, 4, and 5, respectively, and the procedure and findings are summarised as follows.

In Chapter 3, Finite Element Analysis (FEA) was performed for an extended knee position, using an anatomically accurate tibiofemoral knee model which included the novel implant. Von Mises stress and contact pressure distributions on the medial and lateral compartments were investigated as well as stress distributions throughout the implant parts. Comparison of FEA results for models without and with the implant showed that the maximum von Mises stress and contact pressure experienced by the femoral cartilage were reduced by 40% and 35%, respectively, after introducing the implant. Despite the use of a different FE model in Chapter 4, the stress reductions in the cartilage after introducing the implant were relatively close to what was observed in Chapter 3. Furthermore, after attaching the implant, the femur was slightly abducted and more stress and pressure were perceived in the lateral compartment as compared to in the model without implant. The maximum von Mises stress in the implant (96 MPa) was far lower than the yield strength of Ti-6Al-4V (~900MPa), the selected material for the implant in the FE model.

The influence of the extra-articular implant on bone remodelling of the knee joint using adaptive bone remodelling was investigated for the first time. Initially, a finite element model of the knee joint was created and a user-defined material subroutine was developed to simulate a heterogeneous Bone Mineral Density (BMD) of the knee joint. The heterogeneous density was then assigned to the knee model with the implant in order to investigate how the implant would affect BMD of the knee joint, in a period of five years postoperatively. It was observed that in the medial compartments of the femur and tibia, bone mineral density increased by approximately 3.4% and 4.1%, respectively, and the density for the fixation holes of both bones increased by around 2.2%. From these results, it is concluded that implanting of this load-sharing device does not result in significantly adverse BMD changes in the femur and tibia.

The effects of these implants on contact mechanics of the joint were evaluated through cadaver experiments. Cadaver knee specimens were used to study the surgical procedure for attachment of the new load-sharing implant, and to determine the contact pressures in the joint without and with the implant. Contact pressure in the tibiofemoral joint was measured using pressure mapping sensors, and radiographs were conducted to investigate the influence of the implant on the joint space. A precise pressure measurement technique and radiographs had not been used before to study this implant. The implant was designed from a 3D model of the specimen reconstructed by segmenting MR images of the knee joint, and it was manufactured by CNC machining. It was observed that attachment of the implant does not affect the anatomy of the knee joint, and the specimen with the implant could move smoothly. Radiographs showed that the implant led to an increase in the joint space on the medial side. According to the contact pressure measurements, the implant reduced the load on the medial side by approximately 18% under all loading conditions.

According to the theoretical and experimental investigations conducted in this research, this load-sharing knee implant shows promise as a treatment for early-onset knee osteoarthritis, through its creation of a conducive loading environment in the knee joint, without sacrificing or damaging any of the hard or soft tissues.

6.2 Future work

In this research, only some specific aspects of this new implant were studied, while many more aspects required for a more complete understanding have yet to be addressed. These should be explored in the future, and include the following:

- The 3D model of the implant used in the current project was designed based on the initial invented concept design [23]. There is scope for more thorough design optimisation, in terms of different features of the implant, such as dimensions, number of holes, lattice structure for bone ingrowth, and detailed geometry.

- Ti-6Al-4V was considered as the implant material for FEA, and stainless steel was used for the prototype used in the experiments. Material selection was not part of this research. Other materials, such as cobalt chrome and ceramics should be investigated numerically and experimentally as possible implant component materials. Also, the combination of different materials, such as metal on metal and metal on polyethylene, particularly for their performance in areas of material contact, requires further study.

- Further Quasi-static analyses, and also dynamic analyses, of the implant can be carried out numerically and experimentally in order to better understand the influence of the implant on the detailed biomechanics of the knee joint at different flexion angles and loading conditions, bone remodelling, longevity, failure modes, and stress distributions in the implant. To do this numerically, development of a more anatomically accurate FE knee model including patellofemoral joint would be required.

- Investigating the influence of quantity, size, and location of the fixation screws on bone mineral density of the femur and tibia postoperatively, and the performance of various fixators in fixing properly the implant for a long period of time, e.g. 1-10 years.

- CNC machining was used to produce a prototype for the experiments in this project; however, other manufacturing techniques, such as additive manufacturing, in particular electron beam melting should be explored in the future.

- Standardising the attachment procedure as well as the development of specialised equipment and tools for precise implant positioning and joint space adjustment intraoperatively are crucial factors in terms of better outcome and reproducibility of the procedure.

- The final stage of investigating the implant involves animal studies, for example with sheep, human trials and clinical studies. Such in vivo studies would allow researchers to perceive how this implant would affect progression of knee OA and cartilage repair. Other aspects of this implant, such as bone ingrowth into implant and porous screws, complications after surgery, implant loosening and bone resorption, longevity of the implant, adverse events after implant removal, cost of the procedure, and patient recovery and satisfaction, could also be studied using human trials.

References

[1] Palmer JS, Monk AP, Hopewell S, Bayliss LE, Jackson W, Beard DJ, Price AJ. Surgical interventions for early structural knee osteoarthritis. The Cochrane library. 2016:1-14.

[2] Wiegant K, van Heerwaarden R, van der Woude J-T, Custers RR, Emans P, Kuchuk N, Mastbergen S, Lafeber FF. Knee joint distraction as an alternative surgical treatment for osteoarthritis: Rationale and design of two randomized controlled trials (vs high tibial osteotomy and total knee prosthesis). International journal of orthopaedics. 2015;2:353-60.

[3] Steadman JR, Briggs KK, Pomeroy SM, Wijdicks CA. Current state of unloading braces for knee osteoarthritis. Knee surgery, sports traumatology, arthroscopy. 2016;24:42-50.

[4] Litwic A, Edwards MH, Dennison EM, Cooper C. Epidemiology and burden of osteoarthritis. British medical bulletin. 2013;105:185-99.

[5] Li CS, Poolman RW, Bhandari M. Treatment preferences of patients with early knee osteoarthritis: a decision board analysis assessing high tibial osteotomy versus the KineSpring® knee implant system. Journal of long-term effects of medical implants. 2013;23:175–88.

[6] Flouzat-Lachaniette C-H, Roubineau F, Heyberger C, Bouthors C. Distraction to treat knee osteoarthritis. Joint bone spine. 2016;84:1-4.

[7] Berend ME, Ritter MA, Meding JB, Faris PM, Keating EM, Redelman R, Faris GW, Davis KE. Tibial component failure mechanisms in total knee arthroplasty. Clinical orthopaedics and related research. 2004;428:26-34.

[8] Bourke A. Kiwis are clueless about healthcare costs Southern Cross Health Society2016.

[9] Graichen H. TKA revision–reasons, challenges and solutions. Journal of orthopaedics. 2014;11:1-4.

[10] Cuckler JM. Removal of the well-fixed total knee. 11th Annual Spring meeting of current concepts in joint replacement. Las Vegas: Elsevier; 2011. p. 189-90.

[11] Ministry of Health. Annual update of key results 2014/15: New Zealand health survey. Wellington: Ministry of Health2015.

[12] Hooper G, Lee AJ, Rothwell A, Frampton C. Current trends and projections in the utilisation rates of hip and knee replacement in New Zealand from 2001 to 2026. The New Zealand medical journal (online). 2014;127:82-93.

[13] Singleton N, Buddicom E, Vane A, Poutawera V. Are there differences between Maori and non-Maori patients undergoing primary total hip and knee arthroplasty surgery in New Zealand? A registry-based cohort study. The New Zealand medical journal (online). 2013;126:1-8.

[14] Slynarski K, Walawski J, Smigielski R, van der Merwe W. Feasibility of the Atlas unicompartmental knee system load absorber in improving pain relief and function in patients needing unloading of the medial compartment of the knee: 1-year follow-up of a prospective, multicenter, single-arm pilot study (PHANTOM high flex trial). Clinical medicine insights: Arthritis and musculoskeletal disorders. 2017;10:1-9.

[15] Parker DA. Management of knee osteoarthritis in the younger, active patient. Heidelberg: Springer; 2016.

[16] Karachalios T. Total knee arthroplasty: Long term outcomes. UK: Springer London; 2015.

[17] Woude J, Wiegant K, Heerwaarden R, Spruijt S, Roermund P, Custers R, Mastbergen S, Lafeber F. Knee joint distraction compared with high tibial osteotomy: A randomized controlled trial. Knee surgery, sports traumatology, arthroscopy. 2016;25:1-11.

[18] Robertsson O, Annette W. The risk of revision after TKA is affected by previous HTO or UKA. Clinical orthopaedics and related research. 2015;473:90-3.

[19] Hayes DA, Waller CS, Li CS, Vannabouathong C, Sprague S, Bhandari M. Safety and feasibility of a KineSpring knee system for the treatment of osteoarthritis: A Case Series. Clinical medicine insights: Arthritis and musculoskeletal disorders. 2015;8:47-54.

[20] Moorman III CT, Kirwan T, Share J, Vannabouathong C. Patient preferences regarding surgical interventions for knee osteoarthritis. Clinical medicine insights: Arthritis and musculoskeletal disorders. 2017;10:1-12.

[21] Slynarski K, Lipinski L. Treating early knee osteoarthritis with the Atlas® unicompartmental knee system in a 26-year-old ex-professional basketball player: A case study. Case reports in orthopedics. 2017;2017:1-5.

[22] Roos EM. Joint injury causes knee osteoarthritis in young adults. Current opinion in rheumatology. 2005;17:195-200.

[23] Kumar P. Knee prosthesis. In: Patent U, editor.: Google Patents; 2010.

[24] Darrow M. The knee sourcebook. United States: McGraw-Hill; 2002.

[25] Blog BW. The planes of motion. Andersonville Physical Therapy Website: http://www.andersonvillept.com/blog/february-2012-body-wellness-planes-motion; 2012.

[26] Quinn M. Defending the deadlift. Full Range CrossFit Website: https://fullrangecrossfit.com/defending-the-deadlift/#.XEQxFrpuJpl; 2015.

[27] Stephen Kishner, Jacques Courseault, Amy Authement, Thomas R Gest. Knee joint anatomy. WebMD LLC Website: http://emedicine.medscape.com/article/1898986-overview#a1; 2015.

[28] POSNA. Patellar dislocation and instability in children American Academy of Orthopaedic Surgeons Website: http://orthoinfo.aaos.org/topic.cfm?topic=A00707; 2014.

[29] OpenStax. Anatomy & physiology. Texas: Rice University; 2013.

[30] Norman H. How can you describe the 3 types of bone cells? Quora Website: https://www.quora.com/How-can-you-describe-the-3-types-of-bone-cells; 2017.

[31] Minas T. A primer in cartilage repair and joint preservation of the knee: Expert consult. Philadelphia: Elsevier Health Sciences; 2011.

[32] Singh AP. Meniscus anatomy, function and significance. BoneAndSpine Website: https://boneandspine.com/meniscus-anatomy-function-and-significance/; 2015.

[33] Clemente CD. Anatomy: A regional atlas of the human body. Los Angeles, California: Wolters Kluwer/Lippincott Williams & Wilkins Health; 2011.

[34] Jakob R, Staubli H. The knee and the cruciate ligaments, anatomy, biomechanics, clinical aspects, reconstruction, complications. Rehabilitation Berlin: Springer. 1992:270-5.

[35] Heidi. Arthrofibrosis. Injured Athlete's Toolbox Website: https://injuredathletestoolbox.com/aboutarthrofibrosis/; 2015.

[36] Hirschmann M, Becker R. The unhappy total knee replacement: A comprehensive review and management guide. London: Springer; 2015.

[37] Miller LE, Sode M, Fuerst T, Block JE. Joint unloading implant modifies subchondral bone trabecular structure in medial knee osteoarthritis: 2-year outcomes of a pilot study using fractal signature analysis. Clinical interventions in aging. 2015;10:351-7.

[38] A.D.A.M. Clinical management of osteoarthritis. Ebix Inc. Website: http://www.anmf.adamondemand.com.au/AODHome/ProductDetails/Clinical-Management-of-Osteoarthritis; 2014.

[39] Arendt EA, Miller LE, Block JE. Early knee osteoarthritis management should first address mechanical joint overload. Orthopedic reviews. 2014;6:21-3.

[40] Gomoll AH, Angele P, Condello V, Madonna V, Madry H, Randelli P, Shabshin N, Verdonk P, Verdonk R. Load distribution in early osteoarthritis. Knee surgery, sports traumatology, arthroscopy. 2016;24:1-11.

[41] Wellsandt E, Gardinier ES, Manal K, Axe MJ, Buchanan TS, Snyder-Mackler L. Decreased knee joint loading associated with early knee osteoarthritis after anterior cruciate ligament injury. The American journal of sports medicine. 2016;44:143-51.

[42] Scuderi GR, Tria AJ. Knee arthroplasty handbook: Techniques in total knee and revision arthroplasty. US: Springer Science & Business Media; 2006.

[43] Toruan IL. Minimally invasive total knee arthroplasty for osteoarthritis. Ivan Lumban Toruan Website: https://ivanlt.wordpress.com/2009/04/25/minimally-invasive-total-knee-arthroplasty-for-osteoarthritis/; 2009.

[44] Foran JRH, Fischer SJ. Unicompartmental knee replacement. American Academy of Orthopaedic Surgeons - Orthoinfo Website: https://orthoinfo.aaos.org/en/treatment/unicompartmental-knee-replacement/; 2016.

[45] Bonnin M, Amendola NA, Bellemans J, MacDonald SJ, Menetrey J. The knee joint: surgical techniques and strategies. France: Springer Science & Business Media; 2013.

[46] Farr J, Gomoll AH. Cartilage restoration: Practical clinical applications. US: Springer New York; 2018.

[47] Manner PA, Foran JRH, Fischer SJ. Osteotomy of the knee. American Academy of Orthopaedic Surgeons - Orthoinfo Website: https://orthoinfo.aaos.org/en/treatment/osteotomy-of-the-knee/; 2017.

[48] van der Woude J, Nair S, Custers R, Van Laar J, Kuchuck N, Lafeber F, Welsing P. Knee joint distraction compared to total knee arthroplasty for treatment of end stage osteoarthritis: simulating long-term outcomes and cost-effectiveness. PloS one. 2016;11:1-13.

[49] Wiegant K. Knee joint distraction: Intrinsic cartilage repair and sustained clinical benefit. Netherlands: Utrecht University; 2015.

[50] Luks HJ. Alternative to knee replacement: Knee joint distraction. Howard Luks MD Website: https://www.howardluksmd.com/orthopedic-social-media/alternative-knee-replacement-knee-distraction/; 2017.

[51] Sun L, Stout DA, Webster TJ. The nano-effect: improving the long-term prognosis for musculoskeletal implants. Journal of long-term effects of medical implants. 2012;22:195-209.

[52] Mcnicholas MJ, Gabriel SM, Clifford AG, Hasler EM. Device length changes and implant function following surgical implantation of the Kinespring in cadaver knees. Medical devices (Auckland, NZ). 2015;8:47-56.

[53] Clifford AG, Gabriel SM, O'Connell M, Lowe D, Miller LE, Block JE. The KineSpring® knee implant system: An implantable joint-unloading prosthesis for treatment of medial knee osteoarthritis. Medical devices: Evidence and research. 2013;6:69-76.

[54] Uboldi FM, Ferrua P, Parente A, Pasqualotto S, Berruto M. Association of a hi-tech with a bio-tech technique in the treatment of early osteoarthritis of the knee: a case report. Joints. 2015;3:221-4.

[55] Gidalevitz Y. KineSpring: Shock absorbing implant reduces joint stress in active patients. Medgadget Website: https://www.medgadget.com/2013/09/kinespring-shock-absorbing-implant-reduces-joint-stress-in-active-patients-video.html; 2013.

[56] Stiebel M, Miller LE, Block JE. Post-traumatic knee osteoarthritis in the young patient: Therapeutic dilemmas and emerging technologies. Open access journal of sports medicine. 2014;5:73-9.

[57] Citak M, Kendoff D, Padhraig F, Klatte TO, Gebauer M, Gehrke T, Haasper C. Failed joint unloading implant system in the treatment of medial knee osteoarthritis. Archives of orthopaedic and trauma surgery. 2013;133:1575-8.

[58] Schüttler KF, Roessler M, Fuchs-Winkelmann S, Efe T, Heyse TJ. Failure of a knee joint load absorber: Pain, metallosis and soft tissue damage. HSS journal®. 2015;11:172-6.

[59] BoneSmart. Knee replacement implant materials. BoneSmart Website: http://bonesmart.org/knee/knee-replacement-implant-materials/; 2011.

[60] McClure G. Different types of knee replacement implants. PeerWell Website: https://www.peerwell.co/blog/2016/10/03/different-types-of-knee-replacement-implants/; 2016.

[61] Crawford M. Layering metal: Additive manufacturing in Medtech. Rodman Media Corp. Website: https://www.mpo-mag.com/issues/2018-11-01/view_features/layering-metal-additive-manufacturing-in-medtech/54306; 2018.

[62] Whittaker P. Innovative medical implant made by additive manufacturing, 5-axis milling and wire EDM. Powder Metallurgy Review Website: https://www.pm-review.com/innovative-medical-implant-made-by-additive-manufacturing-5-axis-milling-and-wire-edm/; 2012.

[63] Centeno C. Hip replacement materials: A complete guide to the best and worst. Regenexx Website: http://www.regenexx.com/hip-replacement-materials-best-worst/; 2015.

[64] Turger A, Köhler J, Denkena B, Correa TA, Becher C, Hurschler C. Manufacturing conditioned roughness and wear of biomedical oxide ceramics for all-ceramic knee implants. Biomedical engineering online. 2013;12:1-17.

[65] Rahaman MN, Yao A, Bal BS, Garino JP, Ries MD. Ceramics for prosthetic hip and knee joint replacement. Journal of the american ceramic society. 2007;90:1965-88.

[66] Ceramtec. BIOLOX®delta for knee replacement surgery: The metal-free knee arthroplasty. Ceramtec Website: https://www.ceramtec.com/biolox/knee-joint-components/; 2017.

[67] Scott M. Mass production to mass customization. Medical Developments Website: http://www.todaysmedicaldevelopments.com/article/tmd0614-knee-implants-innovations-manufacturing/; 2014.

[68] Horáček M, Charvát O, Pavelka T, Sedlák J, Madaj M, Nejedlý J, Dvořáček J. Medical implants by using RP and investment casting technologies. The 69th World foundry congress. Hangzhou, China 2011. p. 107-11.

[69] Lynch R. Orthopaedics manufacturing: It is rocket science. OrthoTec. 2011;3:1-4.

[70] Harish S, Devadath V. Additive manufacturing and analysis of tibial insert in total knee replacement implant. International research journal of engineering and technology. 2015;2:633-8.

[71] Krishnan S, Dawood A, Richards R, Henckel J, Hart A. A review of rapid prototyped surgical guides for patient-specific total knee replacement. Journal of bone and joint surgery: British volume. 2012;94:1457-61.

[72] Zelinski P. Reimagining implants. Gardner Business Media, Inc. Website: http://www.additivemanufacturing.media/articles/reimagining-implants; 2014.

[73] Gong H, Rafi K, Gu H, Ram GJ, Starr T, Stucker B. Influence of defects on mechanical properties of Ti–6Al–4V components produced by selective laser melting and electron beam melting. Materials & design. 2015;86:545-54.

[74] Jin Z. Computational modelling of biomechanics and biotribology in the musculoskeletal system: biomaterials and tissues. United Kingdom: Elsevier; 2014.

[75] Wang Y, Fan Y, Zhang M. Comparison of stress on knee cartilage during kneeling and standing using finite element models. Medical Engineering & Physics. 2014;36:439-47.

[76] Kubíček M, Florian Z. Stress strain analysis of knee joint. Engineering mechanics. 2009;16:315-22.

[77] Li G, Lopez O, Rubash H. Variability of a three-dimensional finite element model constructed using magnetic resonance images of a knee for joint contact stress analysis. Journal of biomechanical engineering. 2001;123:341-6.

[78] Van Jonbergen H-PW, Innocenti B, Gervasi GL, Labey L, Verdonschot N. Differences in the stress distribution in the distal femur between patellofemoral joint replacement and total knee replacement: A finite element study. Journal of orthopaedic surgery and research. 2012;7:1-9.

[79] Carr BC, Goswami T. Knee implants: Review of models and biomechanics. Materials & design. 2009;30:398-413.

[80] Staff B. Bone remodeling process. Bodytomy Staff Website: https://bodytomy.com/bone-remodeling-process; 2018.

[81] Josephine. How does bone grow: Stress sheilding. BoneSmart Website: https://bonesmart.org/forum/threads/how-does-bone-grow-stress-sheilding.46426/; 2018.

[82] Jacobs CR, Levenston ME, Beaupré GS, Simo JC, Carter DR. Numerical instabilities in bone remodeling simulations: the advantages of a node-based finite element approach. Journal of biomechanics. 1995;28:449-51.

[83] Levadnyi I, Awrejcewicz J, Gubaua JE, Pereira JT. Numerical evaluation of bone remodelling and adaptation considering different hip prosthesis designs. Clinical biomechanics. 2017;50:122-9.

[84] Lemaire V, Tobin FL, Greller LD, Cho CR, Suva LJ. Modeling the interactions between osteoblast and osteoclast activities in bone remodeling. Journal of theoretical biology. 2004;229:293-309.

[85] Garcia-Aznar JM, Rüberg T, Doblare M. A bone remodelling model coupling microdamage growth and repair by 3D BMU-activity. Biomechanics and modeling in mechanobiology. 2005;4:147-67.

[86] Pivonka P, Zimak J, Smith DW, Gardiner BS, Dunstan CR, Sims NA, Martin TJ, Mundy GR. Model structure and control of bone remodeling: A theoretical study. Bone. 2008;43:249-63.

[87] Scheiner S, Pivonka P, Hellmich C. Coupling systems biology with multiscale mechanics, for computer simulations of bone remodeling. Computer methods in applied mechanics and engineering. 2013;254:181-96.

[88] Komarova SV, Smith RJ, Dixon SJ, Sims SM, Wahl LM. Mathematical model predicts a critical role for osteoclast autocrine regulation in the control of bone remodeling. Bone. 2003;33:206-15.

[89] Hambli R. Connecting mechanics and bone cell activities in the bone remodeling process: an integrated finite element modeling. Frontiers in bioengineering and biotechnology. 2014;2:1-6.

[90] Huiskes R, Weinans H, Dalstra M. Adaptive bone remodeling and biomechanical design considerations for noncemented total hip arthroplasty. Orthopedics. 1989;12:1255-67.

[91] Kwon JY, Naito H, Matsumoto T, Tanaka M. Estimation of change of bone structures after total hip replacement using bone remodeling simulation. Clinical biomechanics. 2013;28:514-8.

[92] Huiskes R, Weinans H, Van Rietbergen B. The relationship between stress shielding and bone resorption around total hip stems and the effects of flexible materials. Clinical orthopaedics and related research. 1992;274:124-34.

[93] Doblaré M, Garcia J. Anisotropic bone remodelling model based on a continuum damage-repair theory. Journal of biomechanics. 2002;35:1-17.

[94] Quilez MP, Seral B, Pérez MA. Biomechanical evaluation of tibial bone adaptation after revision total knee arthroplasty: A comparison of different implant systems. PloS one. 2017;12:1-14.

[95] Jia Z, Gong H, Hu S, Fang J, Fan R. Influence of design features of tibial stems in total knee arthroplasty on tibial bone remodeling behaviors. Medical Engineering & Physics. 2017;48:103-13.

[96] Robalo T. Analysis of bone remodeling in the tibia after total knee prosthesis (ME thesis). Lisbon, Portugal: Universida de Técnica de Lisboa; 2011.

[97] Georgeanu V, Atasiei T, Gruionu L. Periprosthetic bone remodelling in total knee arthroplasty. Maedica. 2014;9:56-61.

[98] Zdero R. Experimental methods in orthopaedic biomechanics. United Kingdom: Academic Press; 2016.

[99] Cheong K. Design and development of a new knee prosthesis design (ME thesis). Auckland, New Zealand: University of Auckland; 2012.

[100] Wang H, Chen T, Torzilli P, Warren R, Maher S. Dynamic contact stress patterns on the tibial plateaus during simulated gait: A novel application of normalized cross correlation. Journal of biomechanics. 2014;47:568-74.

[101] Elsner JJ, Portnoy S, Zur G, Guilak F, Shterling A, Linder-Ganz E. Design of a free-floating polycarbonate-urethane meniscal implant using finite element modeling and experimental validation. Journal of biomechanical engineering. 2010;132:1-8.

[102] Tekscan I. Pressure mapping sensor 4000. Tekscan Website: https://www.tekscan.com/products-solutions/pressure-mapping-sensors/4000; 2018.

[103] Thambyah A. Contact stresses in both compartments of the tibiofemoral joint are similar even when larger forces are applied to the medial compartment. The knee. 2007;14:336-8.

[104] Wang H, Gee AO, Hutchinson ID, Stoner K, Warren RF, Chen TO, Maher SA. Bone plug versus suture-only fixation of meniscal grafts: Effect on joint contact mechanics during simulated gait. The American journal of sports medicine. 2014;42:1682-9.

[105] Shiramizu K, Vizesi F, Bruce W, Herrmann S, Walsh WR. Tibiofemoral contact areas and pressures in six high flexion knees. International orthopaedics. 2009;33:403-6.

[106] Luyckx T, Didden K, Vandenneucker H, Labey L, Innocenti B, Bellemans J. Is there a biomechanical explanation for anterior knee pain in patients with patella alta? Influence of patellar height on patellofemoral contact force, contact area and contact pressure. Journal of bone and joint surgery. 2009;91:344-50.

[107] Madonna V, Condello V, Piovan G, Screpis D, Zorzi C. Use of the KineSpring system in the treatment of medial knee osteoarthritis: preliminary results. Joints. 2015;3:129-35.

[108] Evans EM, Freeman M, Miller A, Vernon-Roberts B. Metal sensitivity as a cause of bone necrosis and loosening of the prosthesis in total joint replacement. Bone & joint journal. 1974;56:626-42.

[109] Oshkour A, Osman NA, Davoodi M, Bayat M, Yau Y, Abas WW. Knee joint stress analysis in standing. 5th Kuala Lumpur international conference on biomedical engineering. Kuala Lumpur: Springer; 2011. p. 179-81.

[110] Wangerin SD. Development and validation of a human knee joint finite element model for tissue stress and strain predictions during exercise. San Luis Obispo: California Polytechnic State University; 2013.

[111] Erdemir A. Open knee: open source modeling & simulation to enable scientific discovery and clinical care in knee biomechanics. The journal of knee surgery. 2016;29:107-16.

[112] Harrysson OL, Cansizoglu O, Marcellin-Little DJ, Cormier DR, West HA. Direct metal fabrication of titanium implants with tailored materials and mechanical properties using electron beam melting technology. Materials science and engineering: C. 2008;28:366-73.

[113] Thambyah A, Fernandez J. Squatting-related tibiofemoral shear reaction forces and a biomechanical rationale for femoral component loosening. The scientific world journal. 2014;2014:1-7.

[114] Zhang M, Fan Y. Computational biomechanics of the musculoskeletal system. Florida: CRC Press; 2014.

[115] Yao J, Snibbe J, Maloney M, Lerner AL. Stresses and strains in the medial meniscus of an ACL deficient knee under anterior loading: A finite element analysis with image-based experimental validation. Journal of biomechanical engineering. 2006;128:135-41.

[116] Kurzweil PR. Inside-out and outside-in meniscus repair. Musculoskeletal Key Website: https://musculoskeletalkey.com/inside-out-and-outside-in-meniscus-repair/; 2016.

[117] Mesfar W, Shirazi-Adl A. Biomechanics of the knee joint in flexion under various quadriceps forces. The knee. 2005;12:424-34.

[118] Liu X, Zhang M. Redistribution of knee stress using laterally wedged insole intervention: Finite element analysis of knee–ankle–foot complex. Clinical biomechanics. 2013;28:61-7.

[119] Wan C, Hao Z, Wen S. The joint biomechanics change by different anterior cruciate ligament constitutive models under axial torque load. Proceedings of the ASME 2012: International mechanical engineering congress and exposition. USA 2012.

[120] Donahue TLH, Hull M, Rashid MM, Jacobs CR. A finite element model of the human knee joint for the study of tibio-femoral contact. Journal of biomechanical engineering. 2002;124:273-80.

[121] Murr LE, Gaytan SM, Martinez E, Medina F, Wicker RB. Next generation orthopaedic implants by additive manufacturing using electron beam melting. International journal of biomaterials. 2012;2012:1-14.

[122] Tarniţă D, Catana M, Tarnita DN. Modeling and finite element analysis of the human knee joint affected by osteoarthritis. Key engineering materials. 2014;601:147-50.

[123] Long M, Rack HJ. Titanium alloys in total joint replacement: A materials science perspective. Biomaterials. 1998;19:1621-39.

[124] Lerner U. Bone remodeling in post-menopausal osteoporosis. Journal of dental research. 2016;7:584-95.

[125] Behari J. Biophysical bone behaviour: Principles and applications: John Wiley & Sons; 2009.

[126] Martin R. Toward a unifying theory of bone remodeling. Bone. 2000;26:1-6.

[127] Martin RB, Burr DB, Sharkey NA, Fyhrie DP. Skeletal tissue mechanics. New York, USA: Springer; 2015.

[128] Joshi MG, Advani SG, Miller F, Santare MH. Analysis of a femoral hip prosthesis designed to reduce stress shielding. Journal of biomechanics. 2000;33:1655-62.

[129] Bugbee WD, Culpepper WJ, Engh CA, Engh CA. Long-term clinical consequences of stress-shielding after total hip arthroplasty without cement. Journal of bone and joint surgery. 1997;79:1007-12.

[130] Van Lenthe G, Malefijt W, Huiskes R. Stress shielding after total knee replacement may cause bone resorption in the distal femur. Journal of bone and joint surgery. 1997;79B:117-22.

[131] Nagels J, Stokdijk M, Rozing PM. Stress shielding and bone resorption in shoulder arthroplasty. Journal of shoulder and elbow surgery. 2003;12:35-9.

[132] Besier TF, Draper CE, Gold GE, Beaupré GS, Delp SL. Patellofemoral joint contact area increases with knee flexion and weight-bearing. Journal of orthopaedic research. 2005;23:345-50.

[133] Zhang J, Sorby H, Clement J, Thomas CDL, Hunter P, Nielsen P, Lloyd D, Taylor M, Besier T. The MAP client: User-friendly musculoskeletal modelling workflows.

International symposium on biomedical simulation. Strasbourg, France: Springer; 2014. p. 182-92.

[134] Rooks N, Kazemi M, Schneider MTY, Besier T. Validation of five workflows to obtain bone and cartilage meshes for computational human knee modelling. 11th Australasian biomechanics conference. Auckland, New Zealand; 2018.

[135] Kazemi M. A framework to fuse musculoskeletal models into knee finite element analysis (PhD thesis). Auckland, New Zealand: University of Auckland; 2019.

[136] Gubaua JE, Dicati GWO, Pereira JT. Influence of material stiffness of total hip prosthesis in isotropic bone-remodeling process analysis. XXXVIII Iberian latin-american congress on computational methods in engineering. Brazil2017.

[137] Greenwald A, Haynes D. Weight-bearing areas in the human hip joint. Journal of bone and joint surgery: British volume. 1972;54:157-63.

[138] Bagge M. Remodeling of bone structures: PhD Thesis, Technical University of Denmark, Denmark; 1999.

[139] Bagge M. A model of bone adaptation as an optimization process. Journal of biomechanics. 2000;33:1349-57.

[140] Gislason MK, Ingvarsson P, Gargiulo P, Yngvason S, Guðmundsdóttir V, Knútsdóttir S, Helgason Þ. Finite element modelling of the femur bone of a subject suffering from motor neuron lesion subjected to electrical stimulation. European journal of translational myology. 2014;24:187-93.

[141] Pereira AF, Javaheri B, Pitsillides A, Shefelbine S. Predicting cortical bone adaptation to axial loading in the mouse tibia. Journal of the royal society interface. 2015;12:1-14.

[142] Kowalczyk P. Simulation of orthotropic microstructure remodelling of cancellous bone. Journal of biomechanics. 2010;43:563-9.

[143] Soffiatti BB, Gubaua JE, Dicati GWO, Pereira JT. Checkerboard control in 3D analysis of bone remodelling XXXVIII Iberian latin-american congress on computational methods in engineering. Brazil2017.

[144] Chen G, Pettet G, Pearcy M, McElwain D. Comparison of two numerical approaches for bone remodelling. Medical Engineering & Physics. 2007;29:134-9.

[145] Poggie R, Lefebvre L, Grenier S, Chagnon M, Assad M. Efficacy of a new porous titanium compression screw using an ovine osseointegration model. 10th World biomaterials congress. Canada2016.

[146] Miller MD, Wiesel SW. Operative techniques in sports medicine surgery. Philadelphia, US: Lippincott Williams & Wilkins; 2012.

[147] Kelly P. Mechanics lecture notes: An introduction to solid mechanics. Auckland: University of Auckland; 2015.

[148] Martínez-Reina J, Ojeda J, Mayo J. On the use of bone remodelling models to estimate the density distribution of bones: Uniqueness of the solution. PloS one. 2016;11:1-17.

[149] Martin R. Porosity and specific surface of bone. Critical reviews in biomedical engineering. 1984;10:179-222.

[150] Soffiatti BB, Gubaua JE, Dicati GWO, Pereira JT. Analysis of temporal parameter for Stanford isotropic bone remodeling model for improvement of data processing. XXXVIII Iberian latin-american congress on computational methods in engineering. Brazil2017.

[151] Weinans H, Huiskes R, Grootenboer H. The behavior of adaptive bone-remodeling simulation models. Journal of biomechanics. 1992;25:1425-41.

[152] Scannell PT, Prendergast PJ. Cortical and interfacial bone changes around a non-cemented hip implant: Simulations using a combined strain/damage remodelling algorithm. Medical Engineering & Physics. 2009;31:477-88.

[153] Cavalli L, Brandi ML. Periprosthetic bone loss: diagnostic and therapeutic approaches. F1000Research. 2013;2:1-14.

[154] Tuncer M, Patel R, Cobb JP, Hansen UN, Amis AA. Variable bone mineral density reductions post-unicompartmental knee arthroplasty. Knee surgery, sports traumatology, arthroscopy. 2015;23:2230-6.

[155] Wang C-J, Wang J-W, Weng L-H, Hsu C-C, Huang C-C, Chen H-S. The effect of alendronate on bone mineral density in the distal part of the femur and proximal part of the tibia after total knee arthroplasty. Journal of bone and joint surgery. 2003;85:2121-6.

[156] Sievänen H, Oja P, Vuori I. Precision of dual-energy x-ray absorptiometry in determining bone mineral density and content of various skeletal sites. Journal of nuclear medicine: official publication, society of nuclear medicine. 1992;33:1137-42.

[157] Petersen MM, Olsen C, Lauritzen JB, Lund B. Changes in bone mineral density of the distal femur following uncemented total knee arthroplasty. The journal of arthroplasty. 1995;10:7-11.

[158] Wysocki B, Maj P, Sitek R, Buhagiar J, Kurzydłowski K, Święszkowski W. Laser and electron beam additive manufacturing methods of fabricating titanium bone implants. Applied Sciences. 2017;7:1-20.

[159] Strub CG, Frederick LG. The principles and practice of embalming. 4th ed. Dallas: L. G. Frederick; 1967.

[160] Stephan CN, Davidson PL. The placement of the human eyeball and canthi in craniofacial identification. Journal of forensic sciences. 2008;53:612-9.

[161] Lee DC, Byun SJ. High tibial osteotomy. Knee surgery & related research. 2012;24:61-9.

[162] Niinimäki T, Eskelinen A, Mäkelä K, Ohtonen P, Puhto A-P, Remes V. Unicompartmental knee arthroplasty survivorship is lower than TKA survivorship:

A 27-year Finnish registry study. Clinical orthopaedics and related research. 2014;472:1496-501.

[163] Li CS, Karlsson J, Winemaker M, Sancheti P, Bhandari M. Orthopedic surgeons feel that there is a treatment gap in management of early OA: International survey. Knee surgery, sports traumatology, arthroscopy. 2014;22:363-78.

[164] Fojtik E. Finite element analysis of tibiofemoral contact mechanics (MSc thesis). Kalamazoo, US: Western Michigan University; 2017.

Appendix A: Main Parts of the Input File Used in Chapter 3

This appendix includes main part of the input file of the model without implant, which was regenerated based on the Wangerin model.

```
*Heading
** Job name: without-implant-knee-model
** Generated by: Abaqus/CAE 6.14-1
*Preprint, echo=NO, model=NO, history=NO, contact=NO
**
** PARTS
**
*Part, name=LCL
*Nset, nset=Set-3, generate
   1,  34801,      1
*Elset, elset=Set-3, generate
   1,  21094,      1
** Section: Section-4-LCL-1_PM1
*Solid Section, elset=Set-3, material=LIGAMENT
,
*End Part
**
*Part, name=Part-8
*Nset, nset="Femur core G", generate
   1,  93218,      1
*Elset, elset="Femur core G", generate
   1,  63604,      1
*Nset, nset="Femur shell G", generate
   1,  93218,      1
*Elset, elset="Femur shell G", generate
   1,  63604,      1
*Elset, elset="_femoral attach_S2", internal
  383,  1882, 17615, 22623, 25551, 26019, 27204, 29252, 29293, 29459, 29568, 29751, 30386, 30414, 30565, 30809
 30853, 36013, 42639, 47136
*Elset, elset="_femoral attach_S3", internal
 4431,  5364,  5587,  5825,  7348, 14662, 16092, 18396, 18820, 19066, 19103, 19109, 19508, 20202, 20681, 20987
 21058, 21060, 21152, 21247, 22069, 22115, 22473, 22563, 22593, 22656, 22701, 22919, 22941, 23010, 23359, 23415
 23703, 23730, 24046, 24052, 24180, 24230, 24285, 24335, 24353, 24358, 24384, 24407, 24475, 24597, 24636, 24799
 24865, 24933, 25000, 25105, 25141, 25258, 25330, 25385, 25426, 25430, 25484, 25563, 25580, 25703, 25720, 25745
 25747, 25785, 25919, 25952, 26010, 26158, 26201, 26325, 26349, 26380, 26390, 26451, 26465, 26482, 26574, 26688
 26714, 26723, 26725, 26743, 26744, 26751, 26762, 26763, 26770, 26833, 26854, 26860, 26874, 26882, 26889, 26900
 26949, 26975, 27047, 27092, 27093, 27094, 27199, 27212, 27222, 27275, 27277, 27284, 27305, 27334, 27335, 27368
 27415, 27425, 27427, 27466, 27484, 27489, 27496, 27528, 27537, 27539, 27548, 27556, 27590, 27626, 27642, 27645
 27678, 27680, 27688, 27700, 27720, 27736, 27737, 27739, 27783, 27807, 27813, 27848, 27870, 27871, 27873, 27910
 27974, 27995, 28081, 28143, 28190, 28199, 28282, 28295, 28396, 28441, 28445, 28449, 28476, 28482, 28498, 28503
 28574, 28600, 28610, 28662, 28678, 28727, 28740, 28742, 28745, 28780, 28793, 28813, 28855, 28860, 28864, 28893
 28942, 28943, 28951, 28956, 28971, 29034, 29087, 29118, 29161, 29167, 29206, 29223, 29224, 29230, 29246, 29267
 29286, 29342, 29355, 29363, 29379, 29382, 29398, 29412, 29413, 29419, 29470, 29550, 29599, 29653, 29675, 29676
 29745, 29769, 29770, 29773, 29779, 29782, 29793, 29819, 29821, 29839, 29843, 29850, 29857, 29858, 29868, 29886
 29887, 29901, 29904, 29909, 29913, 29916, 29929, 29930, 29942, 29971, 29986, 29987, 29989, 29997, 30009, 30017
 30024, 30025, 30026, 30042, 30045, 30050, 30053, 30056, 30062, 30067, 30073, 30084, 30085, 30089, 30113, 30122
 30130, 30132, 30137, 30163, 30168, 30174, 30179, 30187, 30188, 30190, 30196, 30199, 30202, 30206, 30217, 30225
 30230, 30232, 30233, 30240, 30255, 30261, 30265, 30266, 30268, 30277, 30283, 30289, 30294, 30305, 30307, 30315
 30318, 30320, 30322, 30323, 30324, 30325, 30329, 30334, 30359, 30372, 30391, 30395, 30404, 30416, 30420, 30425
 30435, 30438, 30441, 30446, 30447, 30449, 30456, 30462, 30464, 30470, 30471, 30506, 30515, 30517, 30524, 30528
 30530, 30544, 30547, 30553, 30555, 30560, 30568, 30575, 30583, 30585, 30587, 30593, 30596, 30597, 30598, 30604
 30605, 30670, 30716, 30802, 30816, 30846, 30867, 30870, 30923, 30969, 31080, 31127, 31130, 31371, 31553, 31623
 31637, 31699, 31729, 31808, 31888, 33241, 33918, 33920, 34028, 34035, 34475, 35630, 36008, 36441, 37474, 38143
 40150, 41469, 41719, 43271, 48431, 53134, 54445, 55769, 55780, 62259
*Elset, elset="_femoral attach_S4", internal
 6614,  7666,  7957, 20318, 21299, 24658, 25660, 27353, 27661, 27732, 28411, 28454, 28756, 28928, 29895, 29918
 29984, 30046, 30107, 30189, 30284, 30293, 30358, 30516, 30574, 31807, 31890, 34031, 40012, 40132, 42608, 43923
 45071, 48926, 49037, 49120, 49569, 54497
*Elset, elset="_femoral attach_S1", internal
 7762, 14209, 15953, 17284, 28135, 28240, 29019, 29486, 29915, 30016, 30518, 30566, 31377, 32025, 32077, 32949
 38745, 39051, 40151, 42970, 43179, 47094, 48927, 49567, 53129, 54444, 55198
*Surface, type=ELEMENT, name="femoral attach"
"_femoral attach_S2", S2
"_femoral attach_S3", S3
"_femoral attach_S4", S4
"_femoral attach_S1", S1
*Elset, elset="_Femur surface_S1", internal
  169,   185,   854,  1283,  2452,  4036,  5410,  5489,  5854,  6433,  6692,  6730,  6983,  7056,  7091,  7263
```

```
 7310,  7409,  7713,  8028,  8031,  8085,  8128,  8149,  8291,  8319,  8814,  9029,  9050,  9116,  9139,  9563
 9796, 10119, 10331, 10691, 11022, 11447, 11450, 11702, 12578, 13834, 14604, 14821, 14829, 14914, 14950, 15159
 15252, 15339, 15693, 15883, 15887, 15893, 16027, 16144, 16163, 16406, 16631, 16681, 16705, 16710, 16790, 17043
 17153, 17171, 17181, 17204, 17210, 17347, 17412, 17449, 17517, 17547, 17809, 17948, 18120, 18190, 18257, 18342
 18440, 18631, 18784, 18838, 18870, 18896, 19087, 19376, 19527, 19532, 19571, 19722, 19770, 19806, 19927, 19974
 20523, 20672, 21190, 21401, 21440, 21445, 21456, 21694, 21774, 21796, 21818, 21856, 21890, 22019, 22097, 22223
 22271, 22357, 22401, 22404, 22410, 22499, 22514, 22717, 22901, 22909, 23000, 23011, 23143, 23145, 23175, 23273
 23556, 23641, 23651, 23662, 23764, 23930, 24041, 24049, 24278, 24577, 24601, 24909, 25206, 25276, 25555, 25687
 25820, 26049, 26062, 26083, 26106, 26500, 26645, 26806, 26823, 26827, 26841, 27113, 28988, 29021, 29169, 29309
 30039, 30440, 30630, 30887, 30919, 30922, 30927, 30931, 30961, 31071, 31103, 31125, 31143, 31234, 31293, 31322
 31399, 31477, 31514, 31545, 31617, 31853, 31887, 32057, 32304, 32649, 32775, 32922, 33127, 33150, 33683, 33880
 34089, 34139, 34177, 34252, 34359, 34365, 35294, 35349, 35376, 35724, 36078, 36275, 36388, 36701, 36873, 36912
 37214, 37232, 37317, 37426, 37852, 38386, 38484, 38581, 38701, 38762, 38965, 39245, 39801, 40095, 40527, 40792
 41007, 41382, 41410, 41432, 41450, 41990, 42056, 42399, 42553, 42563, 42616, 42901, 43182, 43234, 43637, 43897
 44071, 44195, 44612, 45191, 45230, 45803, 46187, 46266, 46589, 47550, 48845, 48902, 49075, 49196, 49869, 50172
 50668, 50900, 51072, 51099, 51399, 51907, 51987, 52598, 52603, 53278, 53342, 53346, 53381, 53455, 53470, 53924
 54637, 55948, 55951, 56147, 56716, 56720, 57130, 60400, 60880, 60891, 60897, 60992, 62548, 63544
*Elset, elset="_Femur surface_S4", internal
   252,   857,   902,  2124,  2992,  3225,  5280,  5532,  5757,  5920,  6459,  6466,  6581,  6956,  7061,  7247
  7268,  7462,  7682,  7812,  7856,  7972,  8074,  8197,  8433,  8494,  8526,  8547,  8562,  8596,  8615,  8710
  9000,  9058,  9101,  9115,  9123,  9351,  9388,  9485,  9499,  9747,  9945, 10133, 10288, 10447, 10482, 10524
 10703, 10781, 10961, 11093, 11104, 11184, 11204, 11307, 11322, 11334, 11341, 11390, 11510, 11765, 11968, 12047
 12342, 13011, 14463, 14475, 14677, 14788, 14931, 15140, 15333, 15399, 15466, 15502, 15516, 15579, 15755, 15785
 15788, 15808, 15853, 15879, 15911, 15969, 16138, 16149, 16175, 16353, 16477, 16501, 16624, 16765, 16849, 17084
 17127, 17238, 17393, 17638, 17655, 17687, 17721, 17754, 17796, 17808, 17812, 17817, 17874, 18052, 18165, 18201
 18246, 18395, 18508, 18568, 18576, 18585, 18767, 18839, 19106, 19239, 19269, 19541, 19766, 19880, 19971, 20007
 20361, 20474, 20534, 20549, 20617, 20658, 20928, 21012, 21078, 21103, 21133, 21296, 21390, 21654, 21878, 22006
 22266, 22413, 22506, 22781, 22871, 23057, 23213, 23247, 23253, 23715, 23800, 23805, 23959, 24007, 24032, 24039
 24117, 24280, 24294, 24295, 24570, 24777, 24897, 24927, 25232, 25268, 25300, 25342, 25539, 25683, 25769, 26294
 26412, 26414, 26453, 26608, 26674, 26764, 27382, 27945, 28039, 28422, 28451, 28483, 28797, 29041, 29196, 29235
 29559, 29580, 29787, 29820, 29932, 30010, 30012, 30070, 30379, 30668, 30903, 31030, 31187, 31198, 31442, 31473
 31478, 31533, 31774, 31955, 32048, 32050, 32103, 32264, 32988, 33032, 33152, 33606, 33869, 34047, 34390, 34425
 34491, 34512, 34548, 34818, 35054, 35149, 35187, 35360, 35471, 35646, 35708, 35782, 36162, 36223, 36298, 36696
 36729, 36984, 37139, 37490, 37575, 37682, 38226, 38541, 38604, 39179, 39794, 40048, 40441, 40453, 41044, 41052
 41191, 41289, 41582, 41675, 41816, 41856, 42031, 42082, 42152, 42767, 42816, 43025, 43198, 43297, 43500, 43829
 43830, 44115, 44153, 44343, 44717, 44761, 45140, 45236, 45530, 45754, 45765, 46275, 46538, 47710, 47718, 47974
 48203, 48237, 48300, 48739, 49092, 49347, 49690, 49921, 50390, 50459, 50992, 51444, 51548, 51559, 52117, 52737
 52809, 52881, 53699, 53817, 54579, 54737, 55293, 55567, 55855, 56004, 56628, 56858, 56863, 59065, 59551, 62193
 62539, 62724, 62838
*Elset, elset="_Femur surface_S2", internal
   343,   934,  1187,  1346,  1426,  2918,  3511,  5177,  5184,  5240,  5253,  5403,  5703,  5723,  5930,  5951
  6026,  6452,  6468,  6714,  6755,  6950,  7064,  7087,  7227,  7266,  7353,  7398,  7401,  7443,  7476,  7547
  7689,  7781,  7829,  7863,  7935,  8045,  8082,  8238,  8275,  8735,  8800,  8814,  8896,  8903,  8931,  9520
  9594,  9908, 10019, 10086, 10171, 10292, 10476, 10571, 10807, 10842, 10972, 10987, 11209, 11243, 11818, 13628
 14510, 14659, 14748, 14778, 14782, 14807, 14818, 14892, 14917, 14929, 14951, 14985, 15036, 15071, 15216, 15233
 15325, 15373, 15489, 15794, 15801, 15860, 15885, 16028, 16133, 16171, 16176, 16254, 16409, 16449, 16451, 16580
 16612, 16632, 16635, 16667, 16694, 16704, 16713, 16779, 16794, 16925, 16938, 17017, 17044, 17183, 17190, 17225
 17280, 17336, 17340, 17373, 17443, 17524, 17534, 17546, 17588, 17648, 17652, 17677, 17690, 17704, 17720, 17843
 17924, 17926, 17958, 18217, 18229, 18499, 18572, 18605, 18612, 18635, 18703, 18762, 18780, 18840, 18878, 18880
 19404, 19415, 19442, 19476, 19586, 19753, 20089, 20142, 20368, 20411, 20420, 20459, 20490, 20509, 20560, 20661
 20705, 20730, 20932, 20940, 20970, 21051, 21055, 21059, 21107, 21118, 21206, 21328, 21428, 21482, 21503, 21577
 21615, 21773, 21858, 21878, 21963, 22023, 22127, 22138, 22206, 22389, 22520, 22579, 22604, 22629, 22715, 22854
 23048, 23076, 23133, 23145, 23212, 23411, 23488, 23498, 23525, 23529, 23597, 23663, 23831, 23858, 23889, 23904
 24015, 24378, 24534, 24648, 24656, 24699, 24797, 24908, 24976, 25115, 25510, 25519, 25684, 25847, 25868, 26036
 26535, 26585, 26610, 26611, 26679, 26800, 26805, 26817, 27993, 28129, 28411, 28810, 28934, 29220, 29388, 29418
 29543, 29815, 30808, 30873, 30882, 30892, 30902, 30921, 31010, 31149, 31255, 31363, 31375, 31509, 31522, 31523
 31532, 31544, 31549, 31965, 32025, 32297, 33126, 34490, 34564, 35047, 35406, 35492, 35648, 36088, 40670, 41220
 42031, 42527, 48373, 52247
*Surface, type=ELEMENT, name="Femur surface"
"_Femur surface_S3", S3
"_Femur surface_S1", S1
"_Femur surface_S4", S4
"_Femur surface_S2", S2
** Section: bone core
*Solid Section, elset="femur core", material="BONE trabecular"
,
** Section: bone shell
*Solid Section, elset="femur shell", material="BONE cortical"
,
*End Part
**
*Part, name=Part-9
*Elset, elset="_Tibia surface_S4", internal
   358,   385,   390,   425,   648,  1375,  1630,  1650,  1757,  2013,  2390,  2473,  2544,  3023,  3203,  3280
  3886,  4026,  4124,  4149,  4176,  4234,  4310,  4363,  4439,  4479,  4636,  4663,  4802,  4826,  4828,  4845
  4852,  5062,  5072,  5080,  5106,  5147,  5151,  5339,  5370,  5374,  5375,  5394,  5480,  5525,  5555,  5743
  5752,  5769,  5777,  5828,  6144,  6191,  6317,  6336,  6337,  6342,  6358,  6479,  6522,  6621,  6682,  6722
  6755,  6756,  6783,  6979,  7022,  7206,  7211,  7228,  7234,  7304,  7354,  7376,  7629,  7663,  7665,  7730
```

7852, 8007, 8014, 8055, 8073, 8077, 8110, 8285, 8370, 8412, 8485, 8495, 8512, 8524, 8709, 8828
9040, 9248, 9307, 9496, 9518, 9557, 9673, 9676, 9799, 9863, 9929, 9941, 9949, 9967, 10151, 10258
10309, 10435, 10495, 10603, 10651, 10689, 10709, 10795, 10843, 10873, 11121, 11145, 11167, 11169, 11337, 11368
11400, 11407, 11431, 11442, 11459, 11726, 11743, 11768, 11779, 11898, 11942, 11996, 12251, 12425, 12548, 12649
12716, 12730, 12777, 12883, 12924, 12929, 12952, 13022, 13057, 13128, 13131, 13132, 13152, 13181, 13187, 13230
13292, 13578, 13614, 13735, 13756, 13937, 13938, 14083, 14298, 14302, 14422, 14494, 15043, 15360, 15503, 15622
15770, 15833, 15889, 15901, 15932, 15963, 15977, 16076, 16801, 16817, 16888, 17062, 17327, 17504, 17578, 17645
17687, 17783, 17935, 17997, 18006, 18009, 18024, 18066, 18151, 18200, 18242, 18273, 18304, 18310, 18321, 18481
18514, 18517, 18797, 18819, 18821, 18848, 18984, 19000, 19180, 19181, 19252, 19283, 19304, 19483, 19534, 19541
19577, 19623, 19684, 19737, 19858, 20035, 20175, 20198, 20205, 20299, 20397, 20461, 20488, 20531, 20540, 20599
20676, 20783, 20910, 20915, 21077, 21098, 21220, 21383, 21522, 21657, 21782, 21783, 21984, 22339, 22670, 23040
23140, 23801, 23895, 24426, 24785, 24880, 25079, 25414, 25475, 25520, 25730, 25888, 26156, 26508, 26736, 26753
26861, 26884, 27211, 27232, 27950, 28057, 28230, 28409, 28557, 29024, 29196, 29736, 29826, 30042, 30240, 31142
31597, 31779, 31881, 32025, 32245, 33297, 34007, 34375, 34510, 35089, 35436
*Elset, elset="_Tibia surface_S1", internal
1267, 1441, 1643, 2201, 2444, 2667, 2677, 2877, 3886, 3936, 4000, 4039, 4066, 4176, 4264, 4295
4322, 4361, 4458, 4567, 4598, 4683, 4706, 4752, 4780, 4783, 4839, 4991, 5031, 5040, 5043, 5047
5050, 5086, 5095, 5105, 5124, 5131, 5164, 5325, 5361, 5433, 5438, 5498, 5510, 5673, 5679, 5700
5750, 5751, 5757, 5791, 5803, 5809, 6002, 6070, 6142, 6161, 6229, 6282, 6328, 6388, 6396, 6420
6454, 6458, 6518, 6561, 6619, 6642, 6643, 6649, 6653, 6698, 6728, 6729, 6730, 6747, 6821, 6841
6956, 6959, 6960, 6987, 7005, 7020, 7045, 7079, 7211, 7303, 7346, 7369, 7375, 7383, 7392, 7397
7443, 7457, 7505, 7579, 7609, 7618, 7649, 7723, 7797, 7838, 7896, 7917, 8073, 8078, 8079, 8122
8164, 8202, 8215, 8248, 8283, 8494, 8498, 8579, 8592, 8905, 8937, 8970, 9107, 9147, 9220, 9276
9343, 9502, 9530, 9536, 9555, 9658, 9701, 9732, 9830, 9908, 9914, 10085, 10267, 10321, 10386, 10413
10525, 10530, 10533, 10862, 11055, 11133, 11217, 11229, 11258, 11418, 11488, 11491, 11788, 11827, 11845, 11856
11882, 11885, 11898, 12053, 12218, 12245, 12706, 12906, 13053, 13131, 13151, 13168, 13189, 13229, 13257, 13394
13570, 13776, 13929, 14071, 14077, 14132, 14399, 14621, 14671, 14844, 15081, 15471, 15681, 15825, 15942, 15959
15981, 16006, 16244, 16644, 16749, 17080, 17168, 17252, 17474, 17591, 17668, 17685, 17729, 17815, 17865, 17943
18014, 18070, 18107, 18139, 18170, 18192, 18211, 18388, 18475, 18496, 18545, 18661, 18754, 18762, 18768, 18809
18826, 18866, 18929, 18934, 18979, 18993, 18995, 18999, 19090, 19122, 19142, 19388, 19393, 19410, 19446, 19463
19479, 19613, 19617, 19639, 19640, 19708, 19759, 19818, 19828, 19959, 20052, 20089, 20320, 20322, 20563, 20863
20925, 21070, 21213, 21242, 21293, 21304, 21307, 21407, 21722, 21764, 21886, 22187, 22401, 22407, 22437, 22484
22699, 22713, 22752, 23469, 23544, 23790, 23815, 23899, 23907, 24232, 24665, 24679, 24698, 24858, 25069, 25126
25538, 25565, 25611, 25645, 25702, 25983, 26250, 26294, 26319, 26365, 26377, 26478, 26536, 26537, 26628, 26764
27052, 27074, 27076, 27168, 27299, 27362, 27473, 27500, 27682, 27885, 28180, 28209, 28352, 28354, 28362, 28476
28598, 28647, 28717, 28740, 28898, 28920, 29228, 29230, 29811, 29831, 30123, 30234, 30739, 30826, 30832, 30859
31076, 31691, 31787, 31828, 32556, 32663, 32758, 32821, 32995, 33602, 33888, 33959, 34449, 34808, 34968, 34973
35390, 35403, 36338, 36430, 36541
*Elset, elset="_Tibia surface_S2", internal
149, 710, 735, 1347, 1412, 1566, 1830, 2073, 2780, 2794, 2857, 3166, 3826, 3899, 3907, 3962
3980, 3991, 4175, 4180, 4183, 4204, 4208, 4241, 4250, 4259, 4262, 4308, 4356, 4420, 4425, 4440
4443, 4476, 4502, 4520, 4551, 4651, 4666, 4681, 4737, 4813, 4815, 4888, 4903, 4939, 4966, 4982
5028, 5070, 5072, 5096, 5099, 5137, 5157, 5169, 5179, 5180, 5223, 5322, 5375, 5397, 5468, 5521
5532, 5576, 5579, 5585, 5683, 5699, 5728, 5743, 5760, 5806, 5840, 5869, 5890, 5891, 5902, 5976
6042, 6104, 6123, 6180, 6252, 6314, 6320, 6367, 6404, 6423, 6552, 6600, 6654, 6716, 6740, 6749
6794, 6850, 6876, 6880, 6925, 6931, 6961, 7002, 7069, 7072, 7104, 7107, 7115, 7124, 7153, 7177
7295, 7308, 7316, 7323, 7374, 7386, 7387, 7395, 7431, 7585, 7606, 7607, 7636, 7682, 7742, 7745
7847, 7866, 7871, 7878, 7890, 8069, 8084, 8100, 8231, 8339, 8373, 8396, 8404, 8521, 8575, 8578
8587, 8661, 8666, 8672, 8677, 8794, 8907, 8914, 8916, 9033, 9042, 9054, 9128, 9146, 9208, 9264
9295, 9310, 9313, 9315, 9324, 9347, 9355, 9413, 9537, 9616, 9660, 9663, 9677, 9693, 9699, 9711
9959, 10001, 10076, 10246, 10264, 10291, 10302, 10306, 10504, 10511, 10523, 10525, 10530, 10549, 10620, 10674
10826, 10840, 10852, 10859, 10878, 11116, 11359, 11361, 11372, 11375, 11427, 11434, 11513, 11548, 11573, 11595
11626, 11706, 11768, 11852, 11869, 11873, 11927, 12028, 12040, 12067, 12069, 12486, 12490, 12495, 12539, 12619
12634, 12709, 12711, 12713, 12835, 12925, 12943, 13011, 13036, 13095, 13130, 13140, 13145, 13151, 13160, 13671
13877, 13967, 14016, 14018, 14040, 14085, 14294, 14310, 14317, 14499, 14511, 14514, 14610, 14641, 14727, 15247
15585, 15649, 15741, 15832, 15871, 15900, 15932, 15933, 15946, 15960, 16497, 16650, 16833, 17510, 17566, 17611
17646, 17707, 17741, 17752, 17941, 17945, 17961, 17976, 18025, 18033, 18096, 18127, 18146, 18210, 18278, 18299
18351, 18394, 18414, 18470, 18487, 18493, 18501, 18596, 18619, 18630, 18647, 18707, 18716, 18753, 18769, 18833
18838, 18853, 18950, 18998, 19094, 19130, 19156, 19160, 19193, 19199, 19206, 19207, 19229, 19310, 19434, 19458
19479, 19484, 19532, 19603, 19614, 19618, 19674, 19688, 19727, 19797, 19801, 19829, 19846, 19864, 19948, 19960
19975, 20012, 20193, 20201, 20252, 20280, 20376, 20437, 20503, 20538, 20555, 20626, 20674, 20715, 20725, 20837
21019, 21439, 21554, 23572, 23581, 24849, 25526, 25590, 27283, 27659, 29082
*Surface, type=ELEMENT, name="Tibia surface"
"_Tibia surface_S4", S4
"_Tibia surface_S3", S3
"_Tibia surface_S2", S2
"_Tibia surface_S1", S1
*Elset, elset="_tibial attach_S4", internal
2203, 3135, 4216, 5724, 10564, 11584, 11923, 13652, 13737, 14432, 14472, 15327, 16206, 16336, 16450, 16632
16927, 22719, 23462, 24077, 27193, 27463, 27867, 31283, 31509, 32633
*Elset, elset="_tibial attach_S1", internal
3984, 9420, 11442, 12486, 13392, 14467, 14713, 14724, 14727, 16398, 16579, 16905, 19078, 22663, 29890, 30365
31506, 31523, 32134, 33268, 35988
*Elset, elset="_tibial attach_S3", internal
4217, 4405, 6253, 6867, 6890, 7336, 7417, 7748, 9114, 9127, 9390, 9393, 9492, 9494, 9679, 9708
10319, 10548, 10553, 10588, 10619, 10912, 11183, 11456, 11507, 11574, 11635, 11655, 12064, 12415, 12452, 12519
12687, 12704, 12742, 12787, 13076, 13078, 13167, 13371, 13492, 13535, 13576, 13607, 13639, 13721, 13755, 13829
13853, 13862, 13866, 13895, 14154, 14255, 14323, 14331, 14355, 14357, 14371, 14377, 14398, 14402, 14423, 14429

```
14641, 14715, 14738, 14747, 14768, 14816, 14826, 14834, 14866, 14870, 14875, 14883, 14906, 14917, 14918, 14919
14920, 14925, 14929, 14957, 14975, 14989, 14999, 15019, 15037, 15064, 15092, 15093, 15098, 15112, 15155, 15167
15170, 15189, 15195, 15205, 15218, 15248, 15272, 15305, 15353, 15366, 15373, 15378, 15383, 15389, 15399, 15406
15446, 15448, 15468, 15480, 15507, 15516, 15525, 15530, 15633, 15699, 15702, 15707, 15712, 15714, 15733, 15980
15983, 16042, 16073, 16075, 16077, 16107, 16114, 16123, 16125, 16131, 16136, 16160, 16168, 16172, 16182, 16184
16186, 16192, 16197, 16199, 16210, 16219, 16246, 16250, 16255, 16262, 16265, 16275, 16276, 16282, 16284, 16299
16301, 16302, 16305, 16310, 16311, 16329, 16332, 16334, 16340, 16343, 16349, 16350, 16359, 16363, 16364, 16379
16380, 16387, 16389, 16399, 16403, 16406, 16411, 16412, 16413, 16417, 16418, 16419, 16421, 16432, 16449, 16458
16461, 16468, 16469, 16471, 16477, 16478, 16480, 16492, 16496, 16504, 16517, 16525, 16529, 16530, 16531, 16549
16557, 16563, 16565, 16570, 16578, 16580, 16586, 16597, 16606, 16618, 16620, 16625, 16627, 16630, 16636, 16645
16676, 16699, 16700, 16702, 16716, 16721, 16725, 16735, 16746, 16747, 16750, 16754, 16768, 16783, 16786, 16790
16791, 16793, 16808, 16809, 16814, 16847, 16849, 16856, 16859, 16882, 16891, 16906, 16917, 16925, 16950, 16951
16952, 16962, 16968, 16970, 16976, 16979, 17030, 17037, 17175, 17229, 17483, 18214, 18222, 18387, 18435, 18451
18461, 19151, 21789, 21876, 22092, 22280, 22281, 22351, 22791, 24025, 24174, 24472, 28111, 29553, 34067
*Elset, elset="_tibial attach_S2", internal
12325, 13170, 14560, 15068, 15140, 15244, 15347, 15390, 16109, 16113, 16221, 16272, 16327, 16465, 24182
*Surface, type=ELEMENT, name="tibial attach"
"_tibial attach_S4", S4
"_tibial attach_S1", S1
"_tibial attach_S2", S2
"_tibial attach_S3", S3
** Section: bone core
*Solid Section, elset="tibia core", material="BONE trabecular"
,
** Section: bone shell
*Solid Section, elset="tibia shell", material="BONE cortical"
,
*End Part
**
*Part, name=acl
*Nset, nset=Set-3, generate
    1,  58478,      1
*Elset, elset=Set-3, generate
    1,  38604,      1
** Section: Section-1-ACL-1_PM1
*Solid Section, elset=Set-3, material=LIGAMENT
,
*End Part
**
*Part, name="f cartilage"
*Nset, nset=Set-3, generate
     1,  207223,      1
*Elset, elset=Set-3, generate
     1,  132345,      1
** Section: Section-2-FCART-1_PM1
*Solid Section, elset=Set-3, material="ARTICULAR CARTILAGE"
,
*End Part
**
*Part, name=mcl
*Nset, nset=Set-3, generate
     1,  110269,      1
*Elset, elset=Set-3, generate
    1,  72908,      1
** Section: Section-7-MCL-1_PM1
*Solid Section, elset=Set-3, material=LIGAMENT
,
*End Part
**
*Part, name="meniscus L"
*Nset, nset=Set-3, generate
    1,  24242,      1
*Elset, elset=Set-3, generate
    1,  14754,      1
*Nset, nset="menisci lateral edge"
   36,   56,   76,   96,  116,  136,  156,  175,  194,  213,  234,  252,  273,  293,  312,  331
  349,  359,  379,  410,  430,  450,  476,  496,  516,  536,  556,  559,  581,  603,  624,  645
  659,  678,  688,  707,  727,  741,  761,  780,  800,  890,  925,  964,  1004,  1047,  1086,  1118
 1155,  1197,  1242,  1267,  1294,  1319,  1342,  1366,  1389,  1403,  1423,  1455,  1474,  1494,  1525,  1548
 1570,  1591,  1612,  1618,  1641,  1664,  1689,  1717,  1745,  1791,  1817,  1859,  1904,  1935,  1985,  2032
 2082,  3893,  4795,  6003,  6404,  6805,  7530,  9947, 10497, 10759, 11251, 11372, 12146, 14333, 14722, 14777
15424, 15500, 15504, 15592, 15850, 16193, 16279, 16809, 16973, 17421, 17427, 17485, 18013, 18051, 18080, 18488
18536, 18614, 19122, 19135, 19351, 19486, 19580, 19888, 19942, 20134, 20294, 20296, 20493, 20620, 21129, 21260
21425, 21434, 21717, 21870, 21880, 22027, 22105, 22339, 22518, 22568, 22569, 22714, 22742, 22770, 22893, 22925
22943, 22952, 23102, 23191, 23226, 23322, 23445, 23488, 23562, 23594, 23705, 23717, 23851, 23993, 24134, 24190
24211,
*Elset, elset="menisci lateral edge"
   57,  274,  579,  693,  815,  1045,  1913,  2192,  2285,  2480,  2530,  2575,  2760,  2814,  3570,  3752
```

```
 3758,  3770,  3771,  3976,  4084,  4121,  4122,  4188,  4312,  4494,  4552,  4836,  4937,  5171,  5196,  5201
 5259,  5571,  5588,  5606,  5879,  5909,  5947,  6337,  6351,  6476,  6609,  6718,  6817,  7022,  7091,  7305
 7319,  7496,  7497,  7658,  7671,  7793,  7890,  7910,  7917,  8037,  8042,  8308,  8470,  8643,  8856,  8863
 8887,  8921,  9034,  9170,  9276,  9508,  9519,  9660,  9765, 10111, 10304, 10364, 10365, 10552, 10599, 10655
10818, 10870, 10901, 10926, 10928, 11153, 11210, 11404, 11482, 11685, 11752, 11945, 12047, 12090, 12235, 12324
12349, 12540, 12609, 12612, 12634, 12651, 13008, 13192, 13419, 13608, 13609, 13691, 13736, 13749, 13755, 14033
14326, 14448, 14452, 14671, 14744
*Elset, elset=_Surf-1_S4, internal
   57,   136,   220,   560,   595,   787,   832,  1045,  1110,  1191,  1203,  1844,  2135,  2751,  2782,  2935
 2952,  3096,  3181,  3681,  3746,  4084,  4102,  4188,  4232,  4420,  4454,  4494,  4739,  4754,  4928,  4960
 5574,  5587,  5588,  5616,  6056,  6064,  6374,  6439,  6539,  6609,  6714,  6747,  6817,  6955,  7032,  7305
 7496,  7700,  7721,  7729,  7748,  7813,  7932,  8059,  8229,  8345,  8349,  8368,  8528,  8898,  9065,  9199
 9262,  9598,  9621,  9836,  9985, 10001, 10041, 10069, 10140, 10153, 10241, 10242, 10261, 10263, 10267, 10331
10404, 10438, 10535, 10552, 10563, 10599, 10681, 10684, 10686, 10901, 11036, 11194, 11229, 11231, 11249, 11567
11685, 11945, 11976, 12100, 12235, 12277, 12324, 12385, 12652, 12703, 13039, 13082, 13103, 13419, 13625, 13693
13843, 13992, 14002, 14341, 14540
*Elset, elset=_Surf-1_S1, internal
   23,   598,   815,  1785,  1786,  1877,  2275,  2516,  2811,  2821,  2951,  3092,  3231,  3302,  3350,  3494
 3498,  3570,  3770,  3929,  3934,  4312,  4726,  4937,  4970,  5259,  5617,  5820,  6013,  6151,  6219,  6453
 6659,  6718,  7014,  7443,  7788,  8130,  8155,  8252,  8358,  9142,  9276,  9366,  9387,  9518,  9765,  9868
 9984, 10111, 10187, 10246, 10365, 10411, 10439, 10520, 10525, 11210, 11224, 11418, 11604, 12364, 12609, 12651
13008, 13586, 13881, 14033, 14500, 14547
*Elset, elset=_Surf-1_S2, internal
   54,  1620,  2172,  2748,  3307,  3346,  3452,  3752,  4006,  4014,  4379,  4548,  4552,  4724,  4814,  4836
 4945,  5251,  5608,  5825,  5981,  5987,  6438,  7090,  7268,  7774,  8013,  8159,  8525,  8656,  8672,  8805
 9506,  9508,  9512,  9519,  9526,  9660,  9683,  9880, 10154, 10157, 10184, 10201, 10304, 10364, 10378, 10655
10800, 10818, 10858, 10952, 11008, 11404, 11427, 11514, 11689, 11943, 12269, 13116, 13422, 13454, 13473, 13476
13558, 13838, 14027, 14326, 14355
*Surface, type=ELEMENT, name=Surf-1
_Surf-1_S3, S3
_Surf-1_S4, S4
_Surf-1_S2, S2
_Surf-1_S1, S1
*End Part
**
*Part, name="meniscus m"
*Nset, nset=Set-3, generate
     1,  24780,      1
*Elset, elset=Set-3, generate
     1,  15574,      1
*Nset, nset=Set-4
   37,    52,    72,    92,   104,   125,   144,   169,   192,   225,   252,   277,   298,   319,   342,   352
  373,   400,   421,   442,   462,   482,   502,   522,   542,   562,   581,   601,   620,   641,   662,   682
  701,   721,   741,   761,   784,   806,   826,  1207,  1228,  1249,  1275,  1284,  1307,  1339,  1360,  1382
 1402,  1422,  1443,  1465,  1488,  1515,  1543,  1574,  1607,  1640,  1675,  1707,  1738,  1770,  1802,  1834
 1866,  1893,  1916,  9993, 11434, 12224, 13728, 14557, 15148, 15700, 16190, 16846, 17287, 17666, 17743, 17840
18361, 18424, 18876, 19293, 19504, 19693, 19758, 19907, 20395, 20441, 20904, 20973, 21061, 21218, 21238, 21360
21570, 21585, 21588, 21615, 21796, 21807, 21890, 22048, 22080, 22082, 22105, 22273, 22278, 22336, 22457, 22474
22490, 22557, 22794, 22820, 22894, 22974, 23041, 23168, 23213, 23401, 23735, 23875, 24109, 24190, 24313, 24343
24402, 24405, 24514, 24590, 24778
*Elset, elset=Set-4
 1805,  2342,  2635,  3263,  3784,  4089,  4386,  4617,  4962,  5171,  5172,  5373,  5408,  5480,  5540,  5766
 5815,  6104,  6458,  6650,  6788,  6840,  6954,  7367,  7413,  7420,  7822,  7892,  7954,  8092,  8116,  8238
 8484,  8495,  8496,  8523,  8603,  8759,  8763,  8879,  9043,  9086,  9091,  9101,  9302,  9314,  9397,  9555
 9578,  9586,  9689, 10086, 10178, 10271, 10419, 10538, 10695, 10767, 11012, 11649, 11651, 12009, 12548, 12551
12698, 12711, 13128, 13201, 13352, 13363, 13661, 14000, 14314, 14422, 14424, 14748, 14954, 15442
*Elset, elset=_Surf-1_S2, internal
  259,  1610,  1805,  2440,  2480,  2722,  3103,  3465,  3568,  3644,  3767,  3793,  3864,  3867,  4073,  4238
 4470,  4489,  4501,  4514,  4811,  4849,  4859,  5263,  5373,  5480,  5557,  5612,  5623,  5695,  5815,  5894
 5959,  5986,  6065,  6075,  6128,  6233,  6248,  6290,  6323,  6757,  6788,  6812,  6954,  7065,  7200,  7232
 7449,  7470,  7648,  8080,  8127,  8160,  8484,  8794,  8879,  9110,  9460,  9689,  9815,  9987, 10194, 10330
10550, 10556, 10824, 11238, 11436, 11532, 11677, 12055, 12920, 13054, 13160, 13439, 13585, 13676, 13866, 14090
14125, 14314, 14331, 14422, 14473, 14476, 14702, 14740, 14748, 15313, 15370
*Elset, elset=_Surf-1_S4, internal
  167,   303,   541,   796,  1657,  1865,  1887,  2182,  2578,  2596,  2635,  2828,  3561,  3776,  3968,  3970
 4284,  4378,  5108,  5171,  5408,  5568,  5595,  5948,  6267,  6431,  6582,  6755,  6966,  7018,  7069,  7170
 7183,  7367,  7420,  7484,  7571,  7658,  7727,  7883,  8340,  8437,  8523,  8899,  8952,  9045,  9211,  9388
 9444,  9561,  9586,  9725,  9825,  9946,  9962, 10072, 10271, 10402, 10419, 10438, 10732, 10891, 11759, 11769
11897, 12185, 12494, 12623, 12698, 12852, 13147, 13241, 13292, 13479, 13574, 13661, 13869, 13953, 13998, 14044
14109, 14193, 14227, 14371, 14554, 15026, 15049, 15051, 15127, 15338, 15483, 15501, 15512
*Elset, elset=_Surf-1_S3, internal
   33,   168,   635,   759,  1332,  1895,  2035,  2190,  2399,  2435,  2449,  2450,  2484,  2491,  2493,  2626
 2639,  2645,  2647,  2654,  2664,  2681,  2707,  2713,  2716,  2729,  2790,  2831,  2912,  2914,  3105,  3179
 3189,  3194,  3220,  3263,  3297,  3325,  3328,  3350,  3360,  3445,  3555,  3558,  3566,  3572,  3575,  3578
 3640,  3646,  3716,  3763,  3770,  3784,  3788,  3790,  3841,  3848,  3851,  3853,  3855,  3859,  3870,  3929
 3941,  3971,  3975,  4028,  4078,  4084,  4089,  4154,  4159,  4169,  4173,  4177,  4180,  4183,  4237,  4386
 4389,  4439,  4448,  4479,  4481,  4490,  4521,  4586,  4592,  4600,  4614,  4617,  4643,  4706,  4767,  4774
 4790,  4795,  4816,  4823,  4833,  4838,  4839,  4862,  4864,  4942,  4962,  4963,  5140,  5161,  5175,  5180
```

```
 5189,  5210,  5216,  5234,  5265,  5268,  5273,  5343,  5385,  5545,  5569,  5575,  5578,  5579,  5587,  5592
 5596,  5599,  5601,  5619,  5626,  5631,  5709,  5714,  5766,  5835,  5904,  5923,  5930,  5939,  5947,  5955
 5956,  5957,  5960,  5964,  5969,  5983,  5996,  6003,  6062,  6064,  6082,  6087,  6104,  6108,  6124,  6127
 6156,  6247,  6259,  6262,  6280,  6291,  6306,  6311,  6313,  6321,  6329,  6330,  6370,  6378,  6379,  6383
 6385,  6419,  6439,  6441,  6454,  6458,  6492,  6540,  6562,  6570,  6595,  6601,  6626,  6632,  6639,  6642
 6645,  6668,  6698,  6750,  6751,  6778,  6779,  6791,  6801,  6809,  6840,  6865,  6866,  6879,  6911,  6924
 6931,  6935,  6939,  6945,  6961,  6994,  7034,  7051,  7059,  7072,  7078,  7088,  7120,  7166,  7181,  7189
 7191,  7192,  7221,  7226,  7231,  7235,  7245,  7259,  7268,  7283,  7284,  7317,  7375,  7377,  7406,  7414
 7441,  7446,  7448,  7461,  7462,  7490,  7493,  7500,  7504,  7505,  7520,  7522,  7549,  7560,  7565,  7567
 7576,  7577,  7600,  7605,  7627,  7640,  7650,  7652,  7656,  7659,  7683,  7684,  7692,  7755,  7760,  7761
 7765,  7779,  7792,  7797,  7798,  7799,  7811,  7819,  7822,  7827,  7833,  7837,  7841,  7856,  7859,  7861
 7863,  7866,  7871,  7877,  7881,  7898,  7947,  7949,  7950,  7954,  7959,  7966,  8043,  8045,  8047,  8058
 8074,  8077,  8079,  8081,  8092,  8101,  8110,  8119,  8125,  8151,  8154,  8155,  8159,  8165,  8180,  8197
 8199,  8204,  8236,  8238,  8310,  8323,  8324,  8327,  8329,  8333,  8335,  8337,  8341,  8345,  8348,  8349
 8358,  8368,  8369,  8371,  8375,  8381,  8382,  8387,  8412,  8431,  8451,  8465,  8466,  8476,  8480,  8481
 8495,  8496,  8497,  8498,  8500,  8509,  8520,  8550,  8567,  8587,  8595,  8599,  8604,  8606,  8610,  8613
 8624,  8631,  8637,  8648,  8690,  8692,  8733,  8775,  8782,  8786,  8793,  8802,  8858,  8859,  8860,  8869
 8875,  8887,  8896,  8912,  8918,  8927,  8929,  8947,  8969,  9000,  9035,  9043,  9053,  9054,  9101,  9114
 9115,  9117,  9119,  9123,  9129,  9149,  9164,  9174,  9175,  9179,  9193,  9195,  9209,  9212,  9297,  9302
 9314,  9332,  9342,  9359,  9382,  9385,  9387,  9389,  9390,  9394,  9397,  9399,  9406,  9420,  9425,  9435
 9436,  9439,  9442,  9449,  9455,  9465,  9475,  9523,  9555,  9568,  9584,  9594,  9606,  9651,  9653,  9655
 9656,  9662,  9664,  9672,  9691,  9695,  9705,  9717,  9724,  9727,  9741,  9758,  9847,  9874,  9923,  9925
 9928,  9933,  9934,  9936,  9959,  9971,  9972,  9975,  9980,  9993, 10002, 10005, 10012, 10013, 10017, 10030
10031, 10082, 10086, 10088, 10089, 10110, 10124, 10174, 10178, 10181, 10182, 10198, 10200, 10202, 10203, 10212
10230, 10239, 10251, 10253, 10255, 10264, 10276, 10282, 10284, 10308, 10328, 10373, 10380, 10381, 10385, 10387
10390, 10393, 10397, 10411, 10418, 10430, 10440, 10485, 10487, 10490, 10501, 10521, 10536, 10538, 10540, 10542
10551, 10553, 10557, 10568, 10570, 10576, 10578, 10579, 10582, 10586, 10591, 10610, 10611, 10612, 10618, 10625
10695, 10696, 10697, 10703, 10767, 10768, 10778, 10795, 10805, 10816, 10830, 10835, 10839, 10851, 10854, 10859
10866, 10870, 10872, 10881, 10886, 10902, 10909, 10912, 10915, 10917, 10922, 10923, 10926, 10930, 10975, 10989
11012, 11017, 11018, 11023, 11026, 11078, 11085, 11103, 11105, 11111, 11114, 11155, 11163, 11168, 11197, 11198
11207, 11215, 11222, 11224, 11228, 11231, 11239, 11243, 11253, 11260, 11277, 11286, 11291, 11293, 11400, 11407
11422, 11426, 11430, 11481, 11484, 11490, 11501, 11519, 11521, 11522, 11526, 11531, 11536, 11542, 11544, 11547
11551, 11555, 11567, 11579, 11599, 11603, 11643, 11648, 11649, 11651, 11663, 11673, 11680, 11681, 11709, 11712
11765, 11785, 11788, 11792, 11801, 11804, 11815, 11844, 11852, 11854, 11876, 11916, 11934, 11938, 11943, 11959
12002, 12005, 12009, 12019, 12112, 12137, 12157, 12160, 12204, 12205, 12222, 12259, 12261, 12265, 12267, 12272
12285, 12290, 12315, 12349, 12448, 12457, 12472, 12474, 12477, 12478, 12485, 12497, 12543, 12546, 12547, 12550
12551, 12584, 12586, 12588, 12595, 12596, 12599, 12600, 12603, 12605, 12612, 12629, 12684, 12700, 12708, 12711
12794, 12813, 12815, 12820, 12823, 12827, 12869, 12895, 12921, 12924, 12934, 12936, 12940, 12947, 12951, 13026
13028, 13049, 13056, 13104, 13105, 13109, 13110, 13113, 13131, 13134, 13143, 13198, 13201, 13202, 13210, 13212
13227, 13228, 13254, 13265, 13276, 13281, 13298, 13304, 13315, 13333, 13352, 13359, 13364, 13383, 13446, 13450
13452, 13460, 13465, 13476, 13480, 13484, 13488, 13491, 13492, 13530, 13534, 13564, 13565, 13566, 13571, 13588
13593, 13600, 13616, 13628, 13675, 13682, 13692, 13717, 13779, 13788, 13807, 13815, 13817, 13847, 13871, 13903
13905, 13912, 13927, 13932, 13934, 13937, 14000, 14009, 14016, 14093, 14113, 14120, 14161, 14179, 14222, 14228
14232, 14250, 14264, 14271, 14297, 14324, 14328, 14329, 14334, 14337, 14419, 14424, 14457, 14462, 14544, 14550
14569, 14578, 14589, 14601, 14609, 14614, 14620, 14669, 14678, 14747, 14749, 14765, 14777, 14954, 14975, 15009
15014, 15069, 15079, 15101, 15104, 15105, 15118, 15119, 15165, 15201, 15202, 15228, 15230, 15309, 15319, 15424
15453, 15457, 15500, 15550, 15551
*Elset, elset=_Surf-1_S1, internal
  423,  1496,  1889,  2411,  3454,  3461,  3580,  3680,  3760,  3777,  3792,  3796,  4003,  4017,  4079,  4200
 4299,  4306,  4603,  4640,  4642,  4717,  4861,  4978,  5200,  5207,  5256,  5381,  5544,  5611,  5622,  5934
 5968,  6237,  6286,  6308,  6334,  6604,  6650,  6967,  7056,  7382,  7730,  7890,  8116,  8130,  8192,  8390
 8539,  8540,  8700,  8764,  9095,  9097,  9585,  9686, 10575, 10903, 11156, 11174, 11255, 11911, 11987, 12026
12162, 12479, 12791, 12796, 13128, 13155, 13335, 13363, 13378, 13562, 13845, 14761, 14858, 14956, 15005, 15047
15236, 15419, 15442
*Surface, type=ELEMENT, name=Surf-1
_Surf-1_S2, S2
_Surf-1_S4, S4
_Surf-1_S3, S3
_Surf-1_S1, S1
*End Part
**
*Part, name=pcl
*Nset, nset=Set-3, generate
    1,  74120,      1
*Elset, elset=Set-3, generate
    1,  48794,      1
** Section: Section-12-PCL-1_PM1
*Solid Section, elset=Set-3, material=LIGAMENT
,
*End Part
**
*Part, name="t cartilage-L"
*Nset, nset=Set-3, generate
    1,  33201,      1
*Elset, elset=Set-3, generate
    1,  19852,      1
** Section: Section-6-LTCART-1_PM1
*Solid Section, elset=Set-3, material="ARTICULAR CARTILAGE"
```

```
,
*End Part
**
*Part, name="t cartilage-m"
*Nset, nset=Set-3, generate
    1,  39396,      1
*Elset, elset=Set-3, generate
    1,  24182,      1
** Section: Section-9-MTCART-1_PM1
*Solid Section, elset=Set-3, material="ARTICULAR CARTILAGE"
,
*End Part
**
**
** ASSEMBLY
**
*Assembly, name=Assembly
**
*Instance, name=Part-8-1, part=Part-8
*End Instance
**
*Instance, name=Part-9-1, part=Part-9
*End Instance
**
*Instance, name="f cartilage-1", part="f cartilage"
*End Instance
**
*Instance, name=mcl-1, part=mcl
*End Instance
**
*Instance, name=LCL-1, part=LCL
*End Instance
**
*Instance, name=acl-1, part=acl
*End Instance
**
*Instance, name=mcl-2, part=mcl
*End Instance
**
*Instance, name="meniscus L-1", part="meniscus L"
*End Instance
**
*Instance, name="meniscus m-1", part="meniscus m"
*End Instance
**
*Instance, name=pcl-1, part=pcl
*End Instance
**
*Instance, name="t cartilage-L-1", part="t cartilage-L"
*End Instance
**
*Instance, name="t cartilage-m-1", part="t cartilage-m"
*End Instance
**
*Nset, nset="LCL bottom nodes", instance=LCL-1
    1,    2,    3,    4,    5,    6,    7,    8,    9,   10,   11,   12,   13,   14,   15,   16
   17,   18,   19,   20,   21,   22,   23,   24,   25,   26,   27,   28,   29,   30,   31,   32
   33,   34,   35,   36,   37,   38,   39,   40,   41,   42,   43,   44,   45,   46,   47,   48
   49,   50,   51,   52,   53,   54,   55,   56,   57,   58,   59,   60,   61,   62,   63,   64
   65,   66,   67,   68,   69,   70,   71,   72,   73,   74,   75,   76,   77,   78,   79,   80
   81,   82,   83,   84,   85,   86,   87,   88,   89,   90,   91,   92,   93,   94,   95,   96
   97,   98,   99,  100,  101,  102,  103,  104,  105,  106,  107,  108,  109,  110,  111,  112
  113,  114,  115,  116,  117,  118,  119,  120,  121,  122,  123,  124,  125,  126,  127,  128
  129,  130,  131,  132,  133,  134,  135,  145,  853,  854,  855,  856,  857,  858,  859,  860
  861,  862,  863,  864,  865,  866,  867,  868,  869,  870,  871,  872,  873,  874,  875,  876
  877,  878,  879,  880,  881,  882,  883,  884,  885,  886,  887,  888,  889,  890,  891,  892
  893,  894,  895,  896,  897,  898,  899,  900,  901,  902,  903,  904,  905,  906,  907,  908
  909,  910,  911,  912,  913,  914,  915,  916,  917,  918,  919,  920,  921,  922,  923,  924
  925,  926,  927,  928,  929,  930,  931,  932,  933,  934,  935,  936,  937,  938,  939,  940
  941,  942,  943,  944,  945,  946,  947,  948,  949,  950,  951,  952,  953,  954,  955,  956
  957,  958,  959,  960,  961,  962,  963,  964,  965,  966,  967,  968,  969,  970,  971,  972
  973,  974,  975,  976,  977,  978,  979,  980,  981,  982,  983,  984,  985,  986,  987,  988
  989,  990,  991,  992,  993,  994,  995,  996,  997,  998,  999, 1000, 1001, 1002, 1003, 1004
 1026, 1027, 1028, 1029, 1030, 1031, 1032, 1033, 3328, 3329, 3330, 5341, 5524, 5789, 5791, 5793
 5820, 5849, 5861, 5864, 5883, 6058, 6081, 6086, 6087, 6196, 6199, 6200, 6353, 6895, 6899, 6900
 7384, 8047, 8054, 8084, 8160, 8218, 8283, 8284, 8286, 8289, 8304, 8315, 8322, 8379, 8513, 8515
 8516, 9063, 9161, 9226, 9227, 9242, 9243, 9291, 9410, 9413, 9414, 9432, 9433, 9434, 9685, 9686
 9741, 10264, 10308, 10320, 10321, 11156, 11160, 11161, 11162, 11165, 11166, 11171, 11175, 11176, 11312, 11427
```

11485, 11489, 11490, 11539, 12188, 12197, 12204, 12205, 12206, 12210, 12211, 12213, 12221, 12223, 12224, 12233
12246, 12712, 13880, 13900, 13904, 13905, 13925, 13926, 13981, 13990, 13991, 13992, 13994, 13998, 13999, 14002
14004, 14006, 14008, 14011, 14022, 14027, 14031, 14037, 14042, 14053, 14057, 14111, 14126, 14127, 14128, 14179
14186, 14234, 14239, 14347, 14682, 14684, 14686, 15128, 15130, 15155, 15157, 15159, 15476, 15479, 15480, 15485
15732, 15744, 15757, 15764, 15773, 15782, 15982, 15986, 15997, 16000, 16003, 16010, 16983, 17069, 17237, 17241
17242, 17244, 17250, 17642, 17643, 17647, 18041, 18271, 18745, 18751, 18770, 19169, 19171, 19365, 19375, 19382
19384, 19385, 19387, 19390, 19754, 19757, 19974, 20293, 20978, 20980, 20981, 20983, 20984, 21013, 21016, 21017
21024, 21025, 21027, 21029, 21031, 21033, 21041, 21043, 21044, 21051, 21052, 21054, 21056, 21058, 21062, 21064
21080, 21123, 21124, 21433, 21434, 21436, 21439, 21440, 21457, 21462, 21464, 21466, 21487, 21489, 21494, 21495
21513, 21514, 21535, 21549, 21566, 21569, 21571, 21572, 21573, 21575, 21577, 21578, 21579, 21580, 21584, 21585
21631, 21633, 22544, 22716, 22718, 22724, 22726, 22728, 22730, 22738, 22740, 22741, 22744, 22745, 22753, 22754
22757, 22758, 22765, 22767, 22768, 22792, 22794, 22796, 22797, 22799, 22801, 22813, 22814, 22817, 22818, 22829
22846, 22868, 22870, 22872, 22874, 22876, 22878, 22882, 22883, 22884, 22886, 22891, 22893, 22895, 22901, 22909
22911, 22913, 22919, 22921, 22923, 22925, 22926, 22927, 22939, 22942, 22943, 22945, 22946, 22961, 22962, 22970
22971, 22976, 22978, 22980, 22995, 22996, 22998, 23002, 23007, 23008, 23020, 23022, 23024, 23026, 23028, 23030
23044, 23045, 23047, 23048, 23054, 23056, 23058, 23067, 23072, 23095, 23096, 23097, 23113, 23114, 23118, 23142
23144, 23145, 23149, 23150, 23151, 23152, 23153, 23155, 23161, 23162, 23186, 23191, 23192, 23193, 23195, 23196
23198, 23201, 23210, 23233, 23234, 23235, 23239, 23241, 23255, 23256, 23258, 23260, 23262, 23263, 23270, 23272
23279, 23280, 23281, 23282, 23288, 23289, 23292, 23294, 23300, 23301, 23313, 23314, 23316, 23322, 23323, 23336
23339, 23346, 23348, 23353, 23358, 23361, 23363, 23364, 23365, 23373, 23376, 23378, 23380, 23382, 23397, 23399
23401, 23406, 23407, 23408, 23409, 23410, 23416, 23417, 23423, 23424, 23426, 23427, 23434, 23435, 23436, 23437
23438, 23439, 23444, 23446, 23448, 23455, 23457, 23458, 23460, 23461, 23462, 23463, 23465, 23467, 23471, 23473
23475, 23477, 23478, 23479, 23481, 23484, 23487, 23489, 23491, 23492, 23494, 23495, 23496, 23497, 23498, 23502
23504, 23505, 23520, 23526, 23527, 23528, 23532, 23536, 23538, 23539, 23544, 23546, 23552, 23553, 23565, 23569
23571, 23572, 23579, 23580, 23582, 23586, 23597, 23598, 23607, 23614, 23615, 23617, 23621, 23623, 23625, 23638
23640, 23641, 23649, 23651, 23655, 23665, 23667, 23693, 23695, 23697, 23698, 23700, 23701, 23702, 23720, 23723
23724, 23730, 23731, 23732, 23735, 23746, 23747, 23748, 23750, 23753, 23754, 23771, 23777, 23779, 23789, 23790
23792, 23807, 23815, 23816, 23827, 23829, 23831, 23833, 23834, 23845, 23857, 23859, 23861, 23862, 23868, 23869
23871, 23873, 23874, 23881, 23882, 23888, 23893, 23894, 23895, 23900, 23901, 23902, 23913, 23914, 23915, 23928
23930, 23932, 23941, 23942, 23947, 23948, 23949, 23961, 23962, 23972, 23973, 23975, 23988, 23989, 23991, 23993
23995, 23996, 23998, 23999, 24000, 24006, 24007, 24017, 24018, 24033, 24035, 24037, 24042, 24043, 24044, 24046
24047, 24052, 24054, 24056, 24057, 24059, 24060, 24061, 24077, 24079, 24086, 24087, 24088, 24089, 24091, 24095
24105, 24107, 24111, 24114, 24115, 24116, 24124, 24125, 24127, 24128, 24136, 24138, 24144, 24145, 24146, 24147
24150, 24152, 24162, 24168, 24170, 24179, 24180, 24186, 24188, 24189, 24194, 24196, 24198, 24199, 24201, 24209
24211, 24213, 24214, 24216, 24221, 24223, 24224, 24225, 24227, 24237, 24239, 24246, 24247, 24259, 24260, 24266
24268, 24270, 24284, 24287, 24288, 24289, 24292, 24313, 24317, 24318, 24320, 24322, 24326, 24336, 24337, 24341
24342, 24344, 24345, 24346, 24347, 24352, 24353, 24355, 24357, 24358, 24365, 24373, 24374, 24375, 24377, 24378
24384, 24385, 24408, 24409, 24410, 24412, 24421, 24422, 24423, 24427, 24430, 24434, 24436, 24440, 24442, 24444
24445, 24453, 24455, 24457, 24458, 24467, 24468, 24469, 24470, 24471, 24487, 24491, 24498, 24499, 24507, 24511
24512, 24513, 24514, 24523, 24525, 24527, 24537, 24539, 24541, 24547, 24549, 24552, 24553, 24554, 24556, 24557
24558, 24575, 24593, 24594, 24595, 24597, 24598, 24599, 24600, 24602, 24603, 24605, 24608, 24650, 24651, 24674
24675, 24681, 24683, 24685, 24687, 24690, 24691, 24694, 24695, 24701, 24703, 24709, 24717, 24719, 24720, 24721
24732, 24739, 24751, 24752, 24754, 24764, 24769, 24770, 24771, 24773, 24775, 24776, 24781, 24786, 24830, 24831
24832, 24838, 24841, 24872, 24878, 24880, 24885, 24900, 24904, 24907, 24914, 24922, 24927, 24928, 24929, 24931
24933, 24934, 24943, 24944, 24954, 24955, 24956, 24958, 24974, 24975, 24980, 24984, 24990, 24995, 24997, 25003
25006, 25007, 25012, 25014, 25015, 25037, 25045, 25046, 25053, 25056, 25070, 25071, 25074, 25076, 25077, 25078
25084, 25086, 25129, 25130, 25173, 25197, 25199, 25203, 25204, 25225, 25228, 25265, 25266, 25275, 25277, 25298
25353, 25355, 25356, 25357, 25359, 25375, 25380, 25381, 25432, 25434, 25455, 25461, 25467, 25469, 25485, 25486
25514, 25620, 25639, 25640, 25650, 25658, 25659, 25676, 25678, 25694, 25718, 25750, 25821, 25826, 25900, 25903
27078, 33242, 33520
*Elset, elset=Set-87, instance=Part-8-1
258, 1072, 2829, 2876, 3247, 3259, 5033, 5051, 5337, 5343, 5344, 5375, 5471, 5673, 5680, 5682
5689, 5704, 5716, 5720, 5726, 5734, 5735, 5743, 5744, 5751, 5759, 5766, 5770, 5773, 5776, 5925
6049, 6070, 6179, 6189, 6360, 6414, 6425, 6426, 6431, 6436, 6437, 6732, 6734, 6736, 6739, 6782
6798, 6807, 6813, 6816, 6824, 6833, 6838, 6856, 6875, 6876, 7069, 7105, 7115, 7122, 7124, 7140
7163, 7165, 7166, 7169, 7173, 7174, 7188, 7198, 7208, 7212, 7639, 7693, 7708, 7715, 7725, 7727
7734, 7748, 7751, 7755, 7776, 7814, 7817, 7830, 7843, 7844, 7845, 7852, 7867, 7901, 7908, 7909
8328, 8332, 8344, 8352, 8357, 8361, 8371, 8377, 8381, 8397, 8414, 8416, 8423, 9061, 9072, 9081
9097, 9122, 9160, 9164, 9176, 9202, 9203, 9238, 9239, 9253, 9271, 9282, 9285, 9287, 9289, 9299
9304, 9309, 9311, 9316, 9342, 9373, 9661, 9662, 9678, 9704, 9712, 9715, 9721, 9738, 9750, 9758
9763, 9766, 10091, 10346, 10348, 10350, 10353, 10354, 10384, 10389, 10395, 10409, 10417, 10426, 10429, 10438
10453, 10466, 10470, 10480, 10482, 10501, 10508, 10520, 10556, 10559, 10577, 10585, 10602, 10605, 10612, 10613
10618, 10625, 10639, 10641, 10657, 10658, 10663, 10667, 10717, 10720, 10750, 10752, 10771, 10808, 10815, 10818
10845, 10850, 11252, 11267, 11269, 11270, 11274, 11319, 11321, 11335, 11354, 11361, 11366, 11373, 11392, 11399
11409, 11412, 11421, 11430, 11431, 11434, 11437, 11448, 11453, 11454, 11459, 11467, 11470, 11472, 11475, 11477
11480, 11483, 11486, 11488, 11489, 11494, 11497, 11502, 11506, 11509, 11512, 11521, 11527, 11528, 11532, 11538
11540, 11546, 11549, 11553, 11557, 11561, 11563, 11576, 11579, 11588, 11590, 11593, 11595, 11598, 11603, 11611
11612, 11615, 11617, 11618, 11622, 11624, 11629, 11631, 11632, 11641, 11643, 11645, 11646, 11649, 11650, 11652
11653, 11654, 11657, 11658, 11661, 11671, 11675, 11677, 11681, 11682, 11686, 11687, 11694, 11699, 11708, 11709
11710, 11715, 11716, 11720, 11724, 11725, 11727, 11736, 11740, 11744, 11748, 11756, 11760, 11764, 11777, 11778
11779, 11780, 11782, 11786, 11790, 11800, 11803, 11812, 11816, 11819, 11820, 11830, 11834, 11836, 11841, 11849
11850, 11854, 11860, 11868, 11870, 11871, 11877, 11881, 11884, 11886, 11888, 11890, 11893, 11897, 11898, 11899
11903, 11905, 11909, 11913, 11917, 11918, 11926, 11927, 11929, 11930, 11932, 11934, 11936, 11940, 11945, 11949
11952, 11953, 11958, 11959, 11964, 11965, 11969, 11973, 11977, 11986, 11990, 11991, 11995, 11996, 12000, 12001
12011, 12012, 12018, 12022, 12029, 12030, 12034, 12035, 12039, 12040, 12043, 12048, 12049, 12060, 12061, 12062
12063, 12068, 12070, 12071, 12076, 12079, 12082, 12090, 12092, 12093, 12097, 12098, 12099, 12101, 12106, 12107
12109, 12114, 12118, 12120, 12121, 12129, 12132, 12134, 12135, 12145, 12151, 12153, 12154, 12155, 12156, 12158
12163, 12167, 12170, 12171, 12172, 12180, 12181, 12185, 12186, 12187, 12195, 12200, 12204, 12210, 12213, 12222

12223, 12225, 12229, 12230, 12231, 12232, 12236, 12242, 12245, 12253, 12255, 12262, 12267, 12268, 12278, 12282
12283, 12285, 12293, 12295, 12297, 12302, 12303, 12304, 12312, 12320, 12321, 12323, 12333, 12337, 12340, 12342
12343, 12348, 12349, 12351, 12359, 12361, 12371, 12372, 12377, 12380, 12382, 12384, 12389, 12396, 12403, 12412
12414, 12425, 12427, 12428, 12429, 12438, 12442, 12446, 12451, 12452, 12456, 12458, 12460, 12461, 12463, 12464
12468, 12470, 12472, 12473, 12474, 12478, 12480, 12482, 12483, 12485, 12491, 12493, 12495, 12500, 12508, 12509
12510, 12513, 12514, 12519, 12524, 12526, 12528, 12531, 12538, 12539, 12543, 12545, 12547, 12550, 12552, 12553
12560, 12563, 12565, 12568, 12569, 12570, 12571, 12581, 12587, 12588, 12601, 12605, 12606, 12607, 12610, 12611
12614, 12626, 12628, 12631, 12634, 12636, 12638, 12640, 12653, 12657, 12658, 12661, 12664, 12668, 12669, 12672
12673, 12675, 12676, 12677, 12681, 12684, 12689, 12690, 12691, 12696, 12697, 12702, 12705, 12709, 12711, 12714
12715, 12719, 12723, 12725, 12726, 12731, 12733, 12734, 12735, 12738, 12743, 12744, 12750, 12752, 12755, 12756
12761, 12766, 12767, 12769, 12776, 12778, 12787, 12789, 12790, 12791, 12797, 12799, 12801, 12803, 12809, 12810
12811, 12814, 12815, 12816, 12817, 12818, 12819, 12820, 12824, 12828, 12834, 12839, 12843, 12845, 12847, 12849
12852, 12857, 12859, 12860, 12861, 12865, 12866, 12875, 12876, 12877, 12879, 12880, 12882, 12883, 12884, 12888
12889, 12891, 12897, 12900, 12903, 12905, 12911, 12918, 12925, 12928, 12930, 12940, 12943, 12948, 12949, 12952
12953, 12955, 12962, 12965, 12969, 12974, 12976, 12982, 12988, 12990, 12991, 12996, 12998, 13003, 13010, 13023
13025, 13026, 13031, 13032, 13033, 13036, 13040, 13046, 13047, 13051, 13052, 13054, 13056, 13057, 13063, 13065
13068, 13069, 13070, 13074, 13079, 13080, 13081, 13085, 13087, 13089, 13090, 13091, 13092, 13099, 13100, 13112
13120, 13128, 13131, 13133, 13136, 13137, 13140, 13143, 13147, 13148, 13151, 13154, 13158, 13160, 13161, 13163
13168, 13171, 13173, 13174, 13175, 13186, 13190, 13193, 13194, 13195, 13200, 13201, 13204, 13210, 13211, 13214
13215, 13218, 13219, 13221, 13224, 13227, 13228, 13230, 13243, 13244, 13248, 13249, 13251, 13257, 13262, 13267
13269, 13270, 13272, 13273, 13284, 13292, 13294, 13298, 13299, 13300, 13304, 13308, 13309, 13310, 13312, 13315
13321, 13322, 13324, 13325, 13328, 13334, 13335, 13338, 13341, 13343, 13344, 13351, 13352, 13367, 13372, 13373
13377, 13379, 13382, 13383, 13385, 13388, 13391, 13392, 13395, 13396, 13397, 13401, 13402, 13403, 13405, 13406
13412, 13415, 13419, 13422, 13430, 13431, 13434, 13436, 13439, 13440, 13444, 13445, 13448, 13449, 13452, 13459
13460, 13466, 13467, 13468, 13469, 13470, 13473, 13474, 13475, 13477, 13479, 13482, 13483, 13485, 13486, 13488
13492, 13495, 13497, 13498, 13501, 13502, 13503, 13507, 13508, 13509, 13510, 13511, 13513, 13518, 13522, 13523
13526, 13528, 13534, 13535, 13538, 13541, 13547, 13548, 13549, 13551, 13553, 13556, 13558, 13559, 13561, 13572
13573, 13578, 13583, 13584, 13585, 13586, 13591, 13592, 13594, 13599, 13604, 13605, 13609, 13612, 13616, 13617
13622, 13625, 13626, 13629, 13631, 13633, 13636, 13641, 13643, 13654, 13657, 13661, 13663, 13664, 13673, 13676
13684, 13687, 13688, 13689, 13693, 13694, 13701, 13702, 13704, 13707, 13713, 13719, 13720, 13721, 13724, 13725
13726, 13729, 13732, 13736, 13741, 13748, 13750, 13752, 13754, 13755, 13757, 13760, 13761, 13764, 13766, 13768
13771, 13773, 13776, 13778, 13783, 13784, 13785, 13786, 13787, 13788, 13791, 13794, 13796, 13799, 13801, 13808
13813, 13814, 13816, 13817, 13819, 13822, 13823, 13824, 13825, 13826, 13828, 13829, 13838, 13839, 13843, 13844
13846, 13850, 13855, 13857, 13864, 13866, 13867, 13869, 13872, 13874, 13878, 13887, 13889, 13894, 13895, 13897
13898, 13899, 13902, 13903, 13905, 13921, 13922, 13925, 13928, 13929, 13934, 13936, 13938, 13942, 13944, 13951
13960, 13963, 13964, 13965, 13968, 13969, 13971, 13973, 13974, 13982, 13983, 13987, 13988, 13989, 13995, 13996
14000, 14005, 14006, 14008, 14009, 14011, 14012, 14017, 14018, 14023, 14024, 14025, 14027, 14028, 14030, 14032
14034, 14035, 14037, 14042, 14043, 14048, 14056, 14057, 14061, 14064, 14067, 14071, 14072, 14075, 14076, 14079
14083, 14088, 14091, 14095, 14096, 14100, 14101, 14106, 14107, 14111, 14120, 14123, 14129, 14130, 14134, 14136
14137, 14141, 14142, 14148, 14149, 14153, 14157, 14158, 14159, 14160, 14164, 14167, 14169, 14172, 14177, 14183
14185, 14190, 14200, 14201, 14207, 14208, 14211, 14213, 14217, 14219, 14224, 14225, 14231, 14232, 14234, 14237
14241, 14247, 14248, 14249, 14251, 14256, 14259, 14264, 14268, 14271, 14272, 14274, 14276, 14277, 14278, 14283
14286, 14298, 14302, 14303, 14306, 14307, 14313, 14314, 14316, 14318, 14319, 14321, 14326, 14328, 14329, 14330
14334, 14336, 14337, 14343, 14345, 14351, 14353, 14354, 14358, 14359, 14364, 14366, 14367, 14371, 14372, 14374
14377, 14385, 14387, 14388, 14389, 14391, 14392, 14393, 14401, 14402, 14403, 14412, 14413, 14414, 14436, 14438
14439, 14441, 14448, 14452, 14455, 14461, 14467, 14468, 14469, 14472, 14474, 14484, 14486, 14490, 14491, 14496
14505, 14506, 14507, 14508, 14512, 14518, 14519, 14521, 14526, 14527, 14532, 14536, 14539, 14540, 14541, 14542
14545, 14548, 14553, 14554, 14555, 14556, 14557, 14563, 14564, 14566, 14568, 14573, 14574, 14577, 14578, 14583
14587, 14589, 14591, 14592, 14598, 14599, 14600, 14607, 14610, 14611, 14615, 14616, 14617, 15136, 15145, 15146
15147, 15148, 15149, 15150, 15260, 15521, 15526, 15527, 15529, 15533, 15546, 15549, 15552, 15554, 15556, 15557
15565, 15567, 15574, 15576, 15583, 15587, 15593, 15604, 15614, 15615, 15617, 15618, 15620, 15630, 15640, 15998
16153, 16416, 16431, 16483, 16560, 16767, 19434, 19459, 20992, 22164, 22590, 22736, 29000, 29110, 29207, 29516
29563, 29607, 31316, 31596, 31598, 31599, 31602, 31603, 31605, 31777, 31778, 31779, 31780, 31781, 31782, 31783
31786, 31787, 31789, 31792, 31795, 31798, 31826, 31827, 31834, 31842, 31846, 31848, 31907, 31987, 32195, 32467
32471, 32473, 32909, 32966, 32967, 33256, 33320, 33322, 33323, 33328, 33329, 33330, 33346, 33352, 33484, 33513
33516, 33621, 33622, 33623, 33624, 33625, 33670, 33671, 33672, 34082, 34083, 34084, 34086, 34087, 34088, 34089
34090, 34091, 34093, 34169, 34172, 34173, 34271, 34403, 34704, 34705, 34707, 34708, 34710, 35674, 35677, 36068
36115, 36150, 36153, 36157, 36232, 36466, 36619, 36620, 36630, 36689, 36692, 36694, 36761, 36913, 37061, 37128
37221, 37226, 37802, 37824, 37843, 37846, 37849, 37969, 37994, 38002, 38247, 38287, 38466, 38920, 38925, 38995
39497, 39513, 40045, 40436, 40552, 40907, 41209, 41314, 41447, 42269, 42275, 42828, 42829, 42948, 43133, 43144
43207, 43229, 43251, 43590, 43689, 45494, 48767, 49398, 50507, 51483, 53545, 53878
*Nset, nset=TIBATTACH, instance=acl-1
317, 319, 321, 333, 334, 335, 336, 337, 338, 339, 340, 341, 342, 343, 344, 345
346, 347, 348, 349, 350, 351, 352, 353, 354, 355, 356, 357, 358, 359, 360, 361
362, 363, 364, 365, 366, 367, 368, 369, 370, 371, 372, 373, 374, 375, 376, 377
378, 379, 380, 381, 382, 383, 384, 385, 386, 387, 388, 389, 390, 391, 392, 393
394, 395, 396, 397, 398, 399, 400, 401, 402, 403, 404, 405, 406, 407, 408, 409
410, 411, 412, 413, 414, 415, 416, 417, 418, 2729, 2730, 2912, 2913, 2957, 2958, 2965
2966, 2967, 2968, 3099, 3100, 3101, 3102, 3103, 3104, 3105, 3106, 3107, 3108, 3109, 3110, 3111
3112, 3113, 3114, 3115, 3116, 3117, 3118, 3119, 3120, 3121, 3122, 3123, 3124, 3125, 3126, 3127
3128, 3129, 3130, 3131, 3132, 3133, 3134, 3135, 3136, 3137, 3138, 3139, 3140, 3141, 3142, 3143
3144, 3145, 3146, 3147, 3148, 3149, 3150, 3151, 3152, 3153, 3154, 3155, 3156, 3157, 3158, 3159
3160, 3161, 3162, 3163, 3164, 3165, 3166, 3167, 3168, 3169, 3170, 3171, 3172, 3173, 3174, 3175
3176, 3177, 3178, 3179, 3180, 3181, 3182, 3183, 3184, 3185, 3186, 3187, 3188, 3189, 3190, 3191
3192, 3193, 3194, 3195, 3196, 3197, 3198, 3199, 3200, 3201, 3202, 3203, 3204, 3205, 3206, 3207
3208, 3209, 3210, 3211, 3212, 3213, 3214, 3215, 3216, 3217, 3218, 3219, 3220, 3221, 3222, 3223
3224, 3225, 3226, 3227, 3228, 3229, 3230, 3231, 3232, 3233, 3234, 3235, 3236, 3237, 3238, 3239
3240, 3241, 8313, 8317, 8318, 8388, 8700, 9022, 9068, 9072, 9073, 9497, 9499, 9501, 9532, 9534

```
 9536,  9884,  9886,  9888, 10429, 10431, 10793, 10795, 10797, 10863, 10865, 10867, 11415, 11450, 11466, 11648
11649, 11650, 11759, 11761, 11763, 12102, 12103, 12603, 12606, 12695, 12696, 12697, 12892, 12917, 12918, 12925
12926, 12928, 13326, 13509, 13730, 13765, 13769, 13770, 13779, 13780, 13782, 13796, 13797, 13798, 13885, 13886
13888, 13890, 13937, 13945, 13946, 14142, 14144, 14196, 14258, 14267, 14282, 14331, 14333, 14335, 14359, 14362
14363, 14425, 14721, 14724, 14725, 14998, 14999, 15022, 15023, 15107, 15111, 15112, 15156, 15160, 15161, 15187
15191, 15192, 15220, 15224, 15225, 15256, 15258, 15260, 15302, 15303, 15304, 15356, 15357, 15358, 15359, 15360
15377, 15379, 15380, 15389, 15391, 15471, 15475, 15476, 15508, 15512, 15513, 15615, 15619, 15620, 16011, 16013
16095, 16097, 16099, 16104, 16105, 17808, 17810, 17812, 18432, 18436, 18437, 18438, 20116, 20118, 20120, 20125
20240, 20242, 20244, 20258, 20435, 20436, 20471, 20473, 20475, 20974, 21859, 21881, 21883, 21884, 22060, 22061
22063, 22306, 22307, 22308, 22344, 22379, 22945, 22947, 22962, 23131, 23329, 23836, 23880, 23882, 23884, 23908
23910, 23912, 24019, 24021, 24023, 24083, 24899, 24901, 24902, 25761, 25762, 25763, 25798, 25911, 25913, 25915
26861, 27016, 27198, 28331, 28332, 28768, 28770, 29203, 29205, 29571, 29572, 29647, 29688, 29691, 30007, 30009
30011, 30104, 31688, 31691, 31820, 31894, 31895, 31896, 31910, 32094, 32095, 32097, 32122, 32175, 32177, 32179
33517, 33519, 33646, 33656, 33944, 33946, 33955, 34455, 34456, 34470, 34471, 34790, 34792, 35252, 35439, 35489
35490, 35491, 35896, 35897, 35899, 36014, 36015, 36019, 36022, 36340, 36439, 36440, 36443, 36445, 36446, 36448
36483, 36486, 36487, 36488, 36529, 36702, 36894, 36926, 36928, 36969, 36971, 37021, 37022, 37023, 37187, 37490
37845, 37846, 37878, 37879, 38208, 38209, 38290, 38293, 38329, 38461, 38463, 38465, 38497, 38498, 38500, 38507
38612, 38613, 38614, 38615, 38619, 38620, 39633, 39636, 39706, 40071, 40072, 40076, 40084, 40143, 40195, 40282
40297, 40309, 40339, 40340, 40342, 40346, 40495, 40496, 40550, 40866, 40879, 40894, 40895, 40896, 40897, 41271
41272, 41279, 41280, 41997, 43533, 43535, 43537, 43703, 43964, 43967, 43968, 44197, 44355, 44380, 44381, 44418
44419, 44641, 44681, 44801, 44802, 44803, 45411, 45412, 45480, 45488, 45489, 45529, 45530, 45582, 45758, 45876
45889, 46245, 47226, 47277, 47278, 47280, 47281, 47361, 47362, 47606, 47607, 47609, 48227, 48228, 48557, 48673
48674, 49201, 49202, 49257, 49263, 49264, 49452, 49842, 49844, 49927, 50090, 50092, 50342, 52659, 52660, 52661
52694, 52696, 52698, 52736, 52760, 52770, 52772, 52774, 52788, 52790, 52792, 52861, 52863, 53109, 53110, 53112
53151, 53265, 53267, 53291, 53292, 53369, 54268, 54348, 54349, 54458, 54459, 54461, 54462, 54463, 54467, 54469
54482, 54497, 54498, 54499, 54503, 54505, 54506, 54523, 54524, 54757, 54759, 54761, 54803, 54833, 54837, 54848
54849, 54850, 54859, 54861, 54905, 54907, 55018, 55019, 55020, 55075, 55902, 56172, 56175, 56177, 56178, 56179
56180, 56183, 56184, 56186, 56190, 56191, 56193, 56195, 56197, 56198, 56199, 56200, 56244, 56245, 56291, 56321
56375, 56402, 56403, 56411, 56413, 56414, 56415, 56421, 56676, 56678, 56680, 56688, 56689, 56701, 56703, 56714
56716, 56725, 56726, 56727, 56730, 56736, 56737, 56738, 56739, 56744, 56745, 56747, 56750, 56752, 56753, 56754
56755, 56757, 56758, 56760, 56762, 56763, 56764, 56765, 56766, 56767, 56769, 56770, 56802, 56821, 56826, 56827
56852, 56904, 56905, 56906, 56907, 56909, 56911, 56912, 56971, 56972, 57026, 57116, 57117, 57118, 57163, 57183
57184, 57267, 57292, 57331, 57334, 57335, 57391, 57404, 57406, 57407, 57410, 57424, 57425, 57426, 57428, 57436
57437, 57449, 57450, 57459, 57460, 57461, 57470, 57471, 57472, 57473, 57474, 57477, 57478, 57479, 57480, 57481
57485, 57504, 57508, 57510, 57530, 57531, 57541, 57545, 57547, 57548, 57554, 57556, 57560, 57563, 57564, 57565
57566, 57569, 57578, 57579, 57582, 57583, 57590, 57591, 57592, 57594, 57598, 57604, 57605, 57607, 57608, 57610
57611, 57612, 57613, 57614, 57618, 57619, 57620, 57622, 57625, 57628, 57631, 57633, 57634, 57635, 57637, 57640
57641, 57643, 57646, 57652, 57653, 57654, 57658, 57660, 57661, 57664, 57665, 57666, 57667, 57668, 57670, 57672
57673, 57674, 57676, 57681, 57682, 57688, 57689, 57690, 57692, 57695, 57697, 57700, 57701, 57702, 57703, 57705
57706, 57707, 57708, 57709, 57711, 57712, 57713, 57714, 57715, 57716, 57717, 57719, 57723, 57724, 57729, 57730
57731, 57732, 57736, 57737, 57738, 57739, 57740, 57741, 57742, 57744, 57745, 57746, 57748, 57749, 57750, 57752
57753, 57755, 57756, 57757, 57758, 57759, 57762, 57763, 57767, 57769, 57770, 57771, 57774, 57778, 57788, 57822
57871, 57891, 57990, 58368, 58455
*Elset, elset="_Meniscus M top_S1", internal, instance="meniscus m-1"
  865,   904,   909,  1244,  1387,  1777,  1805,  2282,  2771,  2897,  2984,  3141,  3528,  3531,  3611,  3752
 3824,  3924,  4089,  4349,  4382,  4617,  4962,  5023,  5046,  5080,  5172,  5276,  5415,  5427,  5712,  6135
 6527,  6536,  6788,  6799,  6856,  6954,  7011,  7184,  7400,  7961,  8238,  8495,  8658,  8879,  9302,  9397
 9689,  9820, 10086, 10104, 10149, 10178, 10419, 10502, 10538, 10748, 11062, 11160, 11232, 11386, 11480, 12416
12467, 12579, 12762, 12884, 13317, 13474, 13671, 13739, 14081, 14206, 14391, 14480, 14700, 14703, 14848, 14864
15220,
*Elset, elset="_Meniscus M top_S3", internal, instance="meniscus m-1"
   73,    98,   185,   210,   451,   559,   607,   711,   712,   733,   769,   899,  1064,  1120,  1154,  1247
 1255,  1851,  2342,  2538,  2623,  2677,  2682,  2723,  2731,  2755,  2776,  2786,  2798,  2875,  2905,  2916
 3135,  3140,  3214,  3382,  3401,  3443,  3464,  3495,  3512,  3514,  3610,  3622,  3727,  3731,  3740,  3778
 3779,  3795,  3800,  3805,  3812,  3815,  3817,  3873,  3877,  3884,  3913,  3917,  3921,  3957,  3993,  4008
 4012,  4031,  4039,  4045,  4069,  4080,  4096,  4108,  4121,  4134,  4207,  4226,  4242,  4311,  4334,  4338
 4368,  4404,  4407,  4419,  4421,  4423,  4437,  4512,  4527,  4536,  4552,  4554,  4555,  4558,  4560,  4567
 4583,  4638,  4641,  4663,  4689,  4691,  4713,  4716,  4725,  4730,  4738,  4749,  4754,  4757,  4765,  4778
 4884,  4886,  4898,  4909,  4913,  4920,  4944,  4985,  4988,  4991,  5066,  5071,  5076,  5087,  5088,  5114
 5142,  5236,  5248,  5261,  5279,  5281,  5283,  5290,  5297,  5340,  5364,  5378,  5382,  5396,  5397,  5400
 5422,  5456,  5460,  5464,  5467,  5468,  5542,  5566,  5584,  5610,  5627,  5632,  5666,  5708,  5711,  5713
 5752,  5755,  5760,  5765,  5772,  5823,  5827,  5833,  5840,  5850,  5901,  5917,  5984,  5994,  5998,  6002
 6004,  6007,  6008,  6015,  6016,  6020,  6036,  6050,  6115,  6118,  6125,  6130,  6144,  6148,  6150,  6173
 6177,  6180,  6263,  6297,  6299,  6319,  6481,  6517,  6532,  6537,  6538,  6618,  6620,  6630,  6653,  6655
 6696,  6723,  6794,  6827,  6828,  6829,  6830,  6848,  6858,  6862,  6914,  6921,  6944,  6963,  7003,  7022
 7041,  7074,  7086,  7091,  7098,  7106,  7109,  7110,  7112,  7113,  7114,  7158,  7167,  7203,  7228,  7368
 7370,  7372,  7373,  7374,  7392,  7393,  7399,  7401,  7412,  7413,  7422,  7445,  7447,  7472,  7475,  7480
 7513,  7552,  7568,  7602,  7641,  7660,  7664,  7688,  7705,  7706,  7715,  7720,  7726,  7735,  7749,  7768
 7777,  7782,  7818,  7892,  7893,  7930,  7940,  7970,  7972,  7976,  7985,  7986,  8001,  8020,  8050,  8107
 8193,  8220,  8221,  8228,  8229,  8232,  8234,  8239,  8244,  8246,  8263,  8280,  8286,  8292,  8328,  8417
 8422,  8429,  8491,  8507,  8510,  8542,  8544,  8546,  8554,  8557,  8564,  8571,  8577,  8584,  8603,  8638
 8695,  8755,  8763,  8766,  8770,  8778,  8779,  8788,  8807,  8810,  8816,  8820,  8822,  8832,  8862,  8925
 8988,  9006,  9009,  9022,  9055,  9061,  9077,  9080,  9082,  9086,  9091,  9109,  9122,  9137,  9138,  9153
 9154,  9160,  9172,  9182,  9268,  9306,  9313,  9327,  9330,  9353,  9358,  9360,  9378,  9419,  9429,  9528
 9531,  9535,  9540,  9566,  9572,  9578,  9582,  9589,  9591,  9592,  9593,  9601,  9609,  9629,  9635,  9639
 9706,  9713,  9757,  9778,  9799,  9806,  9818,  9856,  9860,  9865,  9882,  9883,  9888,  9894,  9897,  9915
 9973, 10026, 10097, 10107, 10112, 10114, 10122, 10130, 10137, 10144, 10152, 10159, 10190, 10199, 10227, 10245
10263, 10391, 10395, 10400, 10410, 10413, 10420, 10421, 10426, 10434, 10439, 10448, 10449, 10476, 10480, 10512
```

```
10549, 10558, 10587, 10630, 10633, 10634, 10654, 10676, 10682, 10706, 10715, 10719, 10729, 10731, 10734, 10735
10777, 10833, 10838, 10842, 10845, 10973, 10990, 10993, 10999, 11013, 11024, 11029, 11033, 11043, 11048, 11056
11099, 11106, 11130, 11161, 11165, 11181, 11183, 11189, 11206, 11216, 11227, 11264, 11272, 11306, 11308, 11320
11323, 11338, 11339, 11340, 11342, 11346, 11347, 11362, 11363, 11367, 11368, 11375, 11381, 11382, 11397, 11405
11446, 11469, 11478, 11491, 11511, 11514, 11515, 11524, 11527, 11556, 11580, 11600, 11606, 11630, 11672, 11685
11700, 11702, 11720, 11724, 11725, 11730, 11733, 11738, 11782, 11860, 11865, 11878, 11880, 11881, 11883, 11940
11955, 11960, 11995, 12010, 12016, 12020, 12027, 12029, 12031, 12048, 12072, 12083, 12084, 12100, 12104, 12154
12201, 12206, 12209, 12223, 12227, 12257, 12292, 12340, 12355, 12359, 12368, 12380, 12386, 12388, 12389, 12427
12438, 12440, 12480, 12490, 12491, 12511, 12514, 12538, 12541, 12548, 12559, 12563, 12565, 12569, 12571, 12572
12574, 12580, 12581, 12587, 12593, 12606, 12611, 12633, 12689, 12692, 12698, 12701, 12726, 12727, 12768, 12785
12810, 12818, 12826, 12846, 12876, 12877, 12885, 12894, 12897, 12899, 12900, 12901, 12905, 12909, 12911, 12914
12919, 12984, 12988, 13046, 13047, 13059, 13065, 13075, 13078, 13141, 13170, 13183, 13193, 13199, 13211, 13214
13215, 13222, 13239, 13250, 13283, 13294, 13300, 13318, 13374, 13385, 13386, 13395, 13425, 13482, 13489, 13517
13528, 13531, 13541, 13542, 13547, 13554, 13582, 13598, 13614, 13630, 13654, 13673, 13674, 13693, 13700, 13723
13730, 13748, 13755, 13758, 13773, 13804, 13811, 13812, 13829, 13830, 13832, 13843, 13846, 13858, 13875, 13879
13887, 13894, 13899, 13936, 13961, 13968, 13981, 14015, 14033, 14035, 14039, 14041, 14059, 14064, 14133, 14182
14187, 14189, 14199, 14204, 14211, 14243, 14267, 14279, 14289, 14316, 14326, 14336, 14346, 14350, 14354, 14360
14378, 14472, 14496, 14504, 14539, 14546, 14549, 14553, 14556, 14596, 14616, 14641, 14644, 14672, 14689, 14696
14708, 14719, 14720, 14725, 14802, 14805, 14807, 14817, 14820, 14821, 14824, 14826, 14827, 14845, 14846, 14877
14887, 14906, 14932, 14951, 14959, 14960, 14962, 14963, 14967, 14974, 14989, 14990, 14996, 14999, 15037, 15045
15059, 15066, 15077, 15088, 15107, 15120, 15124, 15138, 15148, 15153, 15158, 15159, 15173, 15174, 15207, 15209
15223, 15227, 15243, 15244, 15251, 15253, 15265, 15277, 15281, 15291, 15296, 15324, 15328, 15333, 15343, 15376
15384, 15415, 15429, 15431, 15437, 15467, 15496, 15557, 15573
*Elset, elset="_Meniscus M top_S4", internal, instance="meniscus m-1"
   90,   896,  1288,  1636,  2194,  2262,  2467,  2698,  2760,  3092,  3094,  3112,  3123,  3131,  3213,  3301
 3521,  3543,  3547,  3708,  3784,  3983,  4028,  4291,  4386,  4452,  4498,  4662,  4734,  4903,  5154,  5480
 5540,  5565,  5635,  5667,  5766,  5815,  6104,  6345,  6348,  6458,  6650,  6840,  7126,  7580,  7846,  7954
 8023,  8116,  8300,  8484,  9101,  9151, 10274, 10675, 10711, 10928, 11012, 11333, 11334, 11336, 11494, 11651
11678, 11693, 11695, 11781, 11895, 11918, 11929, 12175, 12397, 12439, 12573, 12741, 12765, 13069, 13128, 13201
13203, 13232, 13508, 13626, 13736, 13761, 13763, 13803, 13827, 13895, 13924, 13943, 14111, 14389, 14428, 14483
14583, 14702, 14731, 14738, 14812, 15012, 15016, 15075, 15442, 15480, 15503
*Elset, elset="_Meniscus M top_S2", internal, instance="meniscus m-1"
  270,  2072,  2635,  3007,  3029,  3032,  3396,  3671,  3897,  3914,  3916,  3991,  4250,  4302,  4529,  4699
 4709,  4900,  5045,  5284,  5408,  5420,  5452,  5507,  5644,  5671,  5813,  6165,  6381,  6490,  6836,  6842
 7101,  7367,  7411,  7712,  7783,  7822,  8092,  8496,  8503,  8523,  8563,  8600,  8759,  8806,  8827,  9043
 9314,  9555,  9586,  9594,  9690, 10103, 10116, 10119, 10271, 10365, 10496, 10547, 10695, 10701, 10708, 10767
10840, 10885, 10931, 11003, 11058, 11399, 12009, 12202, 12217, 12409, 13077, 13082, 13237, 13352, 13355, 13363
13407, 13444, 13513, 13529, 13661, 13747, 13766, 13991, 14000, 14073, 14109, 14402, 14498, 14568, 14833, 15053
15103, 15569
*Surface, type=ELEMENT, name="Meniscus M top"
"_Meniscus M top_S1", S1
"_Meniscus M top_S3", S3
"_Meniscus M top_S4", S4
"_Meniscus M top_S2", S2
*Elset, elset=_Surf-33_S1, internal, instance=Part-8-1
  258,  7105,  7817,  9081,  9239,  9721, 10384, 10389, 10395, 10429, 10438, 10453, 10577, 10602, 10613, 10639
10641, 10658, 10663, 10815, 11454, 11467, 11480, 11528, 11615, 11709, 11790, 11927, 11930, 11952, 11953, 12068
12163, 12222, 12349, 19434, 29207, 29563, 31792, 31834, 33256, 37802, 37849, 39497, 40907, 42828, 43207, 50507
53545,
*Elset, elset=_Surf-33_S3, internal, instance=Part-8-1
 1072,  2829,  2876,  3247,  3259,  5033,  5051,  5337,  5343,  5344,  5471,  5673,  5680,  5682,  5689,  5704
 5716,  5720,  5726,  5734,  5735,  5743,  5744,  5751,  5770,  5773,  5776,  5925,  6049,  6179,  6189,  6360
 6414,  6426,  6431,  6436,  6437,  6732,  6734,  6736,  6739,  6782,  6798,  6807,  6813,  6816,  6824,  6833
 6856,  6875,  6876,  7069,  7115,  7124,  7140,  7163,  7165,  7166,  7169,  7173,  7174,  7188,  7198,  7208
 7212,  7639,  7693,  7708,  7715,  7725,  7727,  7734,  7748,  7751,  7755,  7776,  7814,  7830,  7844,  7845
 7852,  7867,  7901,  7908,  7909,  8328,  8332,  8344,  8352,  8357,  8361,  8371,  8377,  8381,  8397,  8416
 8423,  9061,  9072,  9122,  9160,  9164,  9176,  9202,  9238,  9253,  9271,  9285,  9287,  9289,  9299,  9309
 9311,  9342,  9373,  9661,  9662,  9678,  9704,  9712,  9715,  9738,  9750,  9758,  9763,  9766, 10091, 10346
10348, 10350, 10353, 10354, 10480, 10501, 10508, 10520, 10556, 10559, 10605, 10612, 10657, 10717, 10720, 10750
10752, 10771, 10808, 10818, 11252, 11267, 11269, 11270, 11274, 11319, 11321, 11335, 11354, 11361, 11366, 11373
11392, 11399, 11409, 11412, 11421, 11430, 11431, 11434, 11437, 11453, 11459, 11470, 11472, 11486, 11488, 11489
11497, 11502, 11521, 11527, 11538, 11540, 11546, 11549, 11553, 11557, 11563, 11588, 11590, 11593, 11603, 11611
11612, 11617, 11618, 11622, 11624, 11629, 11631, 11632, 11641, 11643, 11645, 11646, 11649, 11652, 11653, 11654
11657, 11658, 11661, 11671, 11675, 11677, 11681, 11682, 11686, 11687, 11694, 11699, 11708, 11710, 11715, 11716
11720, 11724, 11725, 11736, 11740, 11744, 11748, 11756, 11760, 11764, 11777, 11778, 11779, 11780, 11782, 11786
11800, 11803, 11812, 11816, 11819, 11820, 11830, 11849, 11850, 11870, 11871, 11877, 11881, 11884, 11888, 11897
11898, 11899, 11903, 11905, 11909, 11929, 11932, 11940, 11945, 11949, 11958, 11965, 11973, 11977, 11986, 11990
11991, 11996, 12011, 12012, 12018, 12022, 12029, 12030, 12040, 12043, 12060, 12062, 12063, 12070, 12071, 12076
12079, 12082, 12090, 12092, 12093, 12097, 12098, 12101, 12106, 12107, 12109, 12114, 12118, 12120, 12121, 12129
12132, 12134, 12135, 12145, 12151, 12153, 12154, 12155, 12156, 12158, 12167, 12170, 12171, 12172, 12180, 12181
12185, 12186, 12187, 12200, 12204, 12210, 12223, 12225, 12229, 12230, 12231, 12232, 12236, 12242, 12245, 12253
12255, 12262, 12267, 12268, 12278, 12282, 12285, 12293, 12295, 12297, 12303, 12304, 12312, 12321, 12323, 12337
12340, 12342, 12348, 12351, 12361, 12371, 12372, 12377, 12380, 12384, 12396, 12403, 12412, 12414, 12425, 12427
12428, 12429, 12438, 12442, 12446, 12451, 12452, 12456, 12458, 12460, 12461, 12463, 12464, 12470, 12472, 12473
12474, 12478, 12480, 12482, 12483, 12485, 12491, 12493, 12495, 12500, 12508, 12509, 12510, 12513, 12514, 12519
12524, 12526, 12528, 12531, 12538, 12539, 12543, 12545, 12550, 12552, 12553, 12560, 12563, 12565, 12568, 12569
12570, 12571, 12587, 12601, 12605, 12606, 12607, 12610, 12611, 12614, 12626, 12628, 12631, 12634, 12636, 12638
12640, 12653, 12658, 12661, 12664, 12668, 12669, 12672, 12673, 12675, 12676, 12677, 12684, 12689, 12690, 12691
```

12696, 12697, 12702, 12705, 12709, 12711, 12715, 12719, 12723, 12725, 12726, 12731, 12733, 12734, 12735, 12743
12744, 12750, 12755, 12756, 12761, 12767, 12769, 12776, 12778, 12787, 12789, 12790, 12791, 12797, 12799, 12801
12809, 12810, 12811, 12814, 12815, 12817, 12818, 12819, 12820, 12824, 12828, 12834, 12839, 12843, 12845, 12847
12849, 12852, 12857, 12859, 12860, 12861, 12865, 12866, 12876, 12877, 12879, 12880, 12882, 12883, 12884, 12888
12889, 12891, 12897, 12900, 12903, 12911, 12918, 12925, 12928, 12930, 12940, 12943, 12948, 12949, 12952, 12953
12955, 12962, 12965, 12969, 12974, 12976, 12982, 12988, 12990, 12991, 12996, 12998, 13003, 13010, 13023, 13025
13026, 13031, 13032, 13036, 13040, 13046, 13047, 13051, 13052, 13054, 13056, 13057, 13063, 13065, 13069, 13070
13074, 13079, 13080, 13081, 13085, 13087, 13090, 13091, 13092, 13099, 13112, 13120, 13128, 13131, 13136, 13137
13140, 13143, 13147, 13148, 13151, 13154, 13158, 13160, 13161, 13168, 13171, 13174, 13175, 13186, 13190, 13193
13194, 13195, 13200, 13201, 13204, 13210, 13211, 13218, 13219, 13221, 13224, 13227, 13228, 13230, 13243, 13244
13248, 13249, 13251, 13257, 13262, 13267, 13269, 13270, 13272, 13273, 13284, 13292, 13294, 13298, 13299, 13300
13304, 13308, 13309, 13310, 13315, 13321, 13322, 13324, 13325, 13328, 13334, 13335, 13338, 13341, 13343, 13344
13351, 13367, 13372, 13373, 13377, 13379, 13382, 13383, 13385, 13388, 13392, 13395, 13396, 13397, 13401, 13402
13403, 13405, 13406, 13412, 13415, 13419, 13422, 13430, 13431, 13434, 13436, 13439, 13444, 13445, 13448, 13449
13452, 13459, 13460, 13466, 13467, 13468, 13469, 13470, 13473, 13474, 13475, 13477, 13479, 13482, 13483, 13485
13486, 13488, 13492, 13495, 13497, 13498, 13501, 13502, 13503, 13507, 13508, 13509, 13510, 13511, 13513, 13518
13522, 13523, 13526, 13528, 13534, 13535, 13538, 13541, 13547, 13548, 13549, 13551, 13553, 13556, 13558, 13559
13561, 13572, 13578, 13583, 13584, 13585, 13586, 13591, 13592, 13594, 13599, 13604, 13605, 13609, 13612, 13616
13617, 13622, 13625, 13626, 13629, 13631, 13633, 13636, 13643, 13654, 13657, 13661, 13663, 13664, 13673, 13684
13687, 13688, 13689, 13693, 13694, 13701, 13702, 13704, 13707, 13713, 13719, 13720, 13721, 13724, 13725, 13726
13729, 13732, 13736, 13741, 13748, 13750, 13752, 13754, 13755, 13757, 13760, 13761, 13764, 13768, 13771, 13773
13776, 13778, 13783, 13784, 13785, 13786, 13787, 13788, 13791, 13794, 13796, 13799, 13801, 13808, 13813, 13814
13816, 13817, 13819, 13822, 13823, 13824, 13825, 13828, 13829, 13838, 13839, 13843, 13846, 13850, 13855, 13857
13864, 13866, 13867, 13869, 13872, 13874, 13878, 13887, 13889, 13894, 13895, 13897, 13898, 13899, 13902, 13903
13905, 13921, 13922, 13925, 13928, 13929, 13934, 13936, 13938, 13942, 13944, 13951, 13960, 13963, 13964, 13965
13968, 13969, 13971, 13973, 13974, 13982, 13983, 13987, 13988, 13989, 13995, 13996, 14000, 14005, 14006, 14008
14009, 14011, 14012, 14017, 14018, 14023, 14024, 14025, 14027, 14028, 14030, 14032, 14034, 14035, 14037, 14042
14043, 14048, 14056, 14057, 14061, 14064, 14067, 14071, 14072, 14075, 14076, 14079, 14083, 14088, 14091, 14095
14096, 14100, 14101, 14106, 14107, 14111, 14120, 14123, 14129, 14130, 14134, 14136, 14137, 14141, 14142, 14148
14153, 14157, 14158, 14159, 14160, 14164, 14167, 14169, 14172, 14177, 14183, 14185, 14190, 14200, 14201, 14207
14208, 14211, 14213, 14217, 14219, 14224, 14225, 14231, 14232, 14234, 14237, 14241, 14247, 14248, 14249, 14251
14256, 14259, 14264, 14268, 14271, 14274, 14276, 14277, 14278, 14283, 14286, 14298, 14302, 14303, 14306, 14307
14313, 14314, 14316, 14318, 14319, 14321, 14326, 14328, 14329, 14330, 14334, 14336, 14337, 14343, 14345, 14351
14353, 14354, 14358, 14359, 14364, 14366, 14367, 14371, 14372, 14374, 14377, 14385, 14387, 14388, 14389, 14391
14392, 14393, 14401, 14402, 14403, 14412, 14413, 14414, 14436, 14438, 14439, 14441, 14448, 14452, 14455, 14461
14467, 14468, 14469, 14472, 14474, 14484, 14486, 14490, 14491, 14496, 14505, 14506, 14507, 14508, 14512, 14518
14519, 14521, 14526, 14527, 14532, 14536, 14539, 14540, 14541, 14542, 14545, 14548, 14553, 14554, 14555, 14556
14557, 14563, 14564, 14566, 14568, 14573, 14574, 14577, 14578, 14583, 14587, 14589, 14591, 14592, 14598, 14599
14600, 14607, 14610, 14611, 14615, 14616, 14617, 15136, 15145, 15146, 15147, 15148, 15149, 15150, 15260, 15521
15526, 15527, 15529, 15533, 15546, 15549, 15552, 15554, 15556, 15557, 15565, 15567, 15574, 15576, 15583, 15587
15593, 15604, 15614, 15615, 15617, 15618, 15620, 15630, 15640, 15998, 16153, 16416, 16431, 16483, 16560, 16767
19459, 20992, 22164, 22590, 22736, 29000, 29110, 29607, 31596, 31598, 31599, 31602, 31605, 31777, 31778, 31779
31780, 31781, 31782, 31783, 31786, 31787, 31789, 31795, 31798, 31826, 31827, 31842, 31846, 31848, 31907, 31987
32195, 32467, 32471, 32473, 32909, 32967, 33320, 33322, 33328, 33329, 33330, 33346, 33352, 33484, 33513, 33621
33622, 33623, 33624, 33625, 33670, 33671, 33672, 34082, 34083, 34086, 34087, 34088, 34090, 34091, 34093, 34169
34172, 34173, 34271, 34708, 34710, 35674, 35677, 36115, 36150, 36153, 36157, 36232, 36466, 36619, 36689, 36692
36694, 36913, 37061, 37128, 37221, 37226, 37843, 37994, 38002, 38247, 38287, 38920, 38925, 40045, 40436, 40552
41209, 41314, 42275, 43144, 43251, 49398, 53878
*Elset, elset=_Surf-33_S4, internal, instance=Part-8-1
5375, 6838, 8414, 9203, 9282, 9304, 11475, 11506, 11512, 11595, 11598, 11836, 11841, 11860, 11890, 11969
11995, 12035, 12061, 12283, 12302, 12320, 12343, 12389, 12581, 12657, 12681, 12714, 12752, 12803, 12905, 13100
13163, 13214, 13352, 13440, 13676, 13844, 14149, 14272, 29516, 31316, 31603, 33323, 33516, 34084, 34089, 34704
34705, 36068, 36630, 36761, 37824, 37846, 37969, 38466, 38995, 39513, 41447, 42269, 42829, 42948, 43133, 43229
43590, 43689, 45494, 48767, 51483
*Elset, elset=_Surf-33_S2, internal, instance=Part-8-1
5759, 5766, 6070, 6425, 7122, 7843, 9097, 9316, 10409, 10417, 10426, 10466, 10470, 10482, 10585, 10618
10625, 10667, 10845, 10850, 11448, 11477, 11483, 11494, 11509, 11532, 11561, 11576, 11579, 11650, 11727, 11834
11854, 11868, 11886, 11893, 11913, 11917, 11918, 11926, 11934, 11936, 11959, 11964, 12000, 12001, 12034, 12039
12048, 12049, 12099, 12195, 12213, 12333, 12359, 12382, 12468, 12547, 12588, 12738, 12766, 12816, 12875, 13033
13068, 13089, 13133, 13173, 13215, 13312, 13391, 13573, 13641, 13766, 13826, 32966, 34403, 34707, 36620
*Surface, type=ELEMENT, name=Surf-33
_Surf-33_S1, S1
_Surf-33_S3, S3
_Surf-33_S4, S4
_Surf-33_S2, S2
*Elset, elset="_f cartilage_S4", internal, instance="f cartilage-1"
231, 370, 453, 647, 655, 695, 807, 823, 932, 1007, 1280, 1593, 2061, 2085, 2092, 2167
2446, 2831, 2870, 3206, 3210, 3430, 3431, 3743, 3791, 3949, 3967, 4034, 4042, 4196, 4216, 4314
4444, 4464, 4481, 4540, 4729, 5181, 5318, 5601, 5861, 5984, 6368, 6506, 6729, 6774, 6913, 6942
6962, 7043, 7071, 7086, 7090, 7127, 7248, 7921, 8142, 8180, 8431, 8806, 8846, 8848, 8903, 9341
9443, 9847, 10216, 10480, 10538, 10555, 10603, 10698, 10729, 10796, 10981, 11142, 11328, 11420, 11668, 12017
12135, 12536, 12544, 12695, 12709, 12822, 12932, 12935, 13123, 13169, 13220, 13255, 13552, 13589, 13631, 13728
13844, 13847, 13888, 13985, 13991, 14259, 14287, 14576, 14647, 14733, 14820, 14926, 14964, 15088, 15416, 15452
15469, 15477, 15643, 15646, 15680, 15799, 16181, 16195, 16693, 16791, 16932, 17299, 17372, 17464, 17575, 17664
17697, 17705, 17708, 17842, 17925, 18172, 18179, 18200, 18390, 18447, 18452, 18643, 18913, 19133, 19349, 19402
19534, 19579, 20098, 20408, 20733, 20737, 20844, 21376, 21464, 21612, 21735, 22109, 22224, 22245, 22369, 22382
22448, 22472, 22519, 22727, 22824, 23058, 23551, 23729, 23879, 23922, 23931, 23993, 24019, 24087, 24117, 24154
24164, 24265, 24436, 24443, 24511, 24522, 24638, 24820, 24829, 24833, 24946, 25004, 25010, 25025, 25167, 25401

25414, 25542, 25560, 25572, 25577, 25602, 26131, 26676, 26741, 26758, 26797, 26978, 26984, 27218, 27226, 27278
27439, 27485, 27494, 27658, 27750, 27803, 27806, 27952, 27983, 28122, 28124, 28198, 28434, 28477, 28557, 28563
28578, 28713, 28730, 28774, 28784, 28802, 28829, 28879, 28896, 28959, 28972, 29024, 29171, 29797, 29913, 30415
30595, 30873, 31072, 31118, 31161, 31175, 31407, 31634, 31653, 31654, 31775, 31869, 32061, 32232, 32397, 32406
32424, 32512, 32533, 32568, 32792, 32878, 33005, 33029, 33117, 33149, 33301, 33416, 33443, 33451, 33503, 33564
33581, 33749, 34404, 34434, 34447, 34537, 34575, 34656, 34735, 34747, 34892, 35122, 35139, 35143, 35268, 35320
35391, 35655, 35740, 35803, 35988, 36198, 36316, 36324, 36355, 36366, 36636, 36727, 36952, 37092, 37228, 37435
37552, 37654, 37753, 37824, 37915, 38040, 38299, 38318, 38400, 38612, 38773, 38833, 39026, 39120, 39135, 39152
39219, 39297, 39464, 39474, 39518, 39561, 39684, 39752, 39800, 40058, 40059, 40088, 40374, 40548, 40619, 40630
40639, 40799, 40831, 40932, 41159, 41320, 41348, 41491, 41538, 41541, 41549, 41564, 41612, 41615, 41794, 42010
42120, 42129, 42148, 42240, 42273, 42305, 42416, 42424, 42665, 43072, 43165, 43183, 43204, 43220, 43386, 43506
43571, 43582, 43675, 44188, 44321, 44323, 44348, 44382, 44390, 44519, 44526, 44539, 44777, 44783, 44867, 44912
45142, 45356, 45431, 45501, 45608, 45613, 45619, 45637, 45918, 45935, 45951, 46194, 46203, 46214, 46381, 46421
46679, 46825, 46914, 46918, 46925, 47011, 47093, 47437, 48320, 48358, 48373, 48386, 48388, 48611, 48711, 48720
48762, 48774, 48777, 48778, 48795, 48799, 48927, 49061, 49230, 49268, 49306, 49401, 49516, 49539, 49630, 49921
49973, 50149, 50629, 50936, 51206, 51327, 51447, 51551, 51658, 51765, 51920, 51933, 51963, 51964, 52237, 52279
52349, 52380, 52587, 52640, 52644, 52694, 52725, 52869, 52950, 53461, 53470, 53501, 53548, 53618, 53660, 53763
53964, 54185, 54382, 54388, 54461, 54540, 54572, 54614, 54992, 55059, 55137, 55169, 55306, 55344, 55350, 55488
55505, 55529, 55794, 55864, 55875, 56281, 56338, 56367, 56373, 56692, 56698, 56776, 56781, 56784, 56813, 56824
56848, 56963, 57009, 57255, 57281, 57283, 57287, 57338, 57374, 57468, 57605, 57616, 57632, 57861, 57956, 57977
58012, 58103, 58347, 58420, 58519, 58530, 58582, 58611, 58793, 58998, 59013, 59073, 59081, 59207, 59220, 59436
59466, 59786, 59803, 59827, 59841, 59915, 60011, 60068, 60069, 60252, 60296, 60402, 60438, 60473, 60641, 60774
60805, 60846, 61020, 61169, 61252, 61286, 61360, 61381, 61614, 61730, 61745, 61757, 61842, 61914, 61922, 62024
62059, 62123, 62375, 62410, 62491, 62583, 62628, 62670, 62822, 62896, 63248, 63379, 63469, 63549, 63884, 64480
64622, 64702, 64731, 64828, 64941, 65233, 65360, 65378, 65398, 65407, 65460, 65616, 65631, 65645, 65716, 65744
65810, 65930, 66012, 66146, 66484, 66505, 66654, 66665, 66860, 67738, 67830, 67956, 68142, 68150, 68349, 68420
68519, 68526, 68528, 68706, 68770, 68842, 68847, 68943, 69013, 69424, 69664, 69739, 69747, 69901, 69903, 69906
69918, 69981, 70341, 70346, 70462, 70487, 70687, 70914, 70945, 70973, 71003, 71010, 71301, 71331, 71347, 71351
71571, 71679, 72067, 72069, 72153, 72174, 72295, 72358, 72532, 72610, 72616, 72633, 72922, 72928, 73028, 73184
73364, 73377, 73529, 73701, 73801, 73893, 73906, 73932, 74267, 74378, 74381, 74528, 74625, 74641, 74671, 74722
74757, 75221, 75349, 75440, 75480, 75527, 75531, 75754, 75805, 75927, 75987, 76195, 76281, 76309, 76621, 76926
76952, 77057, 77094, 77108, 77134, 77284, 77447, 77499, 77825, 77836, 77940, 78355, 78372, 78526, 78565, 78605
78606, 78631, 78687, 78917, 78997, 79333, 79340, 79350, 79444, 79491, 79637, 79775, 79873, 80047, 80063, 80200
80205, 80288, 80297, 80353, 80387, 80391, 80968, 80990, 81026, 81035, 81117, 81179, 81187, 81291, 81310, 81371
81430, 81594, 81664, 81853, 81979, 81987, 81990, 82068, 82681, 82764, 82819, 82851, 82853, 83339, 83392, 83451
83454, 83457, 83497, 83801, 83816, 83880, 83917, 84170, 84387, 84592, 84885, 84899, 84930, 84953, 85126, 85216
85241, 85396, 85516, 85646, 85697, 85737, 85893, 85923, 86007, 86022, 86074, 86148, 86235, 86256, 86326, 86367
86408, 86772, 86811, 86932, 86988, 87535, 87540, 87833, 87903, 88016, 88063, 88369, 88415, 88438, 88662, 88668
88848, 88999, 89275, 89362, 89475, 89890, 89895, 90299, 90367, 90401, 90402, 90414, 90589, 90620, 90814, 91087
91207, 91359, 91528, 91619, 91633, 91749, 91761, 91888, 92164, 92169, 92249, 92313, 92353, 92376, 92536, 92865
93026, 93225, 93384, 93469, 93563, 93807, 93886, 93894, 93930, 94224, 94441, 94456, 94638, 94641, 94795, 94887
95176, 95410, 95798, 95930, 95979, 95983, 96071, 96162, 96426, 96569, 96661, 96825, 96966, 97073, 97154, 97266
97268, 97293, 97387, 97435, 97472, 97623, 97736, 97822, 97889, 98394, 98458, 98710, 98728, 98823, 98959, 99054
99060, 99078, 99120, 99122, 99194, 99198, 99402, 99554, 99581, 99609, 99626, 99639, 99686, 99756, 99757, 99871
99910, 99969, 100002, 100346, 100540, 100592, 100750, 100819, 100945, 100992, 101000, 101027, 101066, 101186, 101403, 101538
101659, 101863, 102085, 102121, 102199, 102211, 102275, 102399, 102505, 102671, 102713, 102816, 102846, 102904, 103265, 103399
103447, 103553, 103635, 103723, 103793, 104138, 104234, 104468, 104555, 104584, 104775, 104935, 104954, 105047, 105106, 105115
105293, 105341, 105364, 105605, 105811, 105844, 105924, 106031, 106069, 106078, 106398, 106459, 106646, 106856, 106880, 106977
107084, 107187, 107259, 107740, 107824, 108076, 108246, 108256, 108359, 108448, 108712, 108715, 108894, 108926, 109289, 109620
109802, 109822, 109993, 110135, 110374, 110524, 110649, 110993, 111149, 111185, 111251, 111573, 111659, 111817, 111866, 111916
111937, 111995, 112249, 112294, 112443, 112487, 112494, 112496, 112509, 112544, 112559, 112666, 112898, 113116, 113175, 113228
113229, 113285, 113413, 113463, 113521, 113606, 113751, 113789, 113822, 113915, 114155, 114398, 114522, 114557, 114633, 114882
114924, 115009, 115026, 115072, 115145, 115226, 115294, 115437, 115450, 115590, 115608, 115609, 115683, 115708, 116056, 116146
116369, 116407, 116462, 116515, 116722, 116935, 117065, 117121, 117467, 117504, 117542, 117724, 118055, 118119, 118352, 118356
118395, 118480, 118508, 118554, 118725, 118874, 119264, 119400, 119431, 120123, 120196, 120369, 120376, 120783, 120927, 121012
121338, 121696, 121700, 121786, 121819, 121998, 122000, 122064, 122161, 122301, 122403, 122633, 122816, 122903, 122994, 123081
123294, 123364, 124278, 124545, 124600, 125091, 125189, 125201, 125284, 125399, 125550, 125760, 125945, 125965, 126024, 126054
126175, 126245, 126372, 126420, 126490, 126514, 126715, 126804, 127053, 127174, 127373, 127488, 127535, 127717, 128015, 128295
128422, 128646, 128757, 129033, 129124, 129638, 129788, 129962, 129987, 130049, 130192, 130379, 130580, 130824, 130850, 130872
131497, 131502, 131503, 131617, 131656, 131674, 131813, 131969, 132126
*Elset, elset="_f cartilage_S1", internal, instance="f cartilage-1"
43, 328, 437, 1315, 2427, 2781, 2996, 3114, 3994, 4053, 4147, 4752, 4973, 5552, 5585, 5748
6108, 6125, 6573, 6619, 6772, 7322, 7508, 7605, 7787, 7827, 7940, 8135, 8162, 8250, 8423, 8576
8723, 9030, 9155, 9544, 9685, 9828, 10692, 10833, 10859, 11254, 11367, 11387, 11598, 11719, 11790, 12161
12272, 12481, 12535, 12643, 12923, 13113, 13247, 13249, 13471, 13843, 14609, 14856, 14921, 14975, 15102, 15253
15730, 15814, 15888, 15895, 15928, 15964, 16159, 16194, 16505, 16765, 16843, 17040, 17312, 17609, 17928, 18263
18280, 18397, 18636, 18641, 19418, 19433, 19571, 19933, 20424, 20648, 20652, 21778, 22006, 22034, 22041, 22388
22411, 22426, 22610, 22772, 23360, 23756, 23801, 23883, 24193, 24784, 24832, 25077, 25186, 25224, 25264, 25328
25530, 25781, 26337, 26370, 26594, 26599, 26793, 27275, 27373, 27417, 27793, 28105, 28160, 28235, 28301, 28349
28405, 28501, 28513, 28749, 28785, 28787, 28817, 28827, 28934, 30450, 31378, 31807, 31897, 31943, 32163, 32531
32662, 32779, 33138, 33910, 34046, 34295, 34488, 34499, 34588, 34878, 35206, 35276, 35284, 35324, 35358, 35373
35419, 35559, 35617, 35726, 35840, 35986, 36200, 36313, 36450, 36517, 37741, 38444, 39178, 39390, 39816, 41092
41383, 41543, 41834, 42046, 42545, 42562, 42805, 42860, 43042, 43424, 43453, 43637, 43873, 44174, 44377, 45041
45551, 45805, 46102, 46184, 46449, 46864, 46881, 47323, 47939, 48378, 48566, 48620, 48831, 48910, 48939, 49085
49109, 49291, 49379, 50185, 50509, 50586, 50849, 51401, 51608, 51787, 51815, 52042, 52443, 52481, 52584, 52811
52840, 53396, 54375, 54712, 54955, 55180, 55187, 55327, 55367, 55393, 56261, 56654, 56728, 56850, 57366, 57376
57563, 58014, 58106, 58146, 58242, 58248, 58648, 58668, 58953, 58957, 59726, 59843, 59904, 59956, 60033, 60066
60343, 60372, 60570, 61223, 61280, 61358, 61374, 61384, 61662, 61905, 62187, 62396, 62462, 62571, 62941, 63069

63087, 63635, 63949, 64076, 64478, 64581, 64776, 64848, 65102, 65358, 65525, 65793, 65814, 66294, 66519, 66593
66599, 66634, 66764, 66789, 66803, 66817, 66934, 66965, 67575, 67710, 67782, 67841, 67872, 67891, 67895, 68098
68444, 69165, 69306, 69389, 69406, 69552, 70009, 70089, 70445, 70458, 70518, 70722, 70792, 70855, 70997, 71470
71544, 71940, 71960, 71992, 72203, 72222, 72280, 72327, 72699, 72712, 72765, 73180, 73387, 73409, 73412, 73487
73761, 74559, 74692, 74938, 75438, 75505, 75650, 76044, 76381, 76434, 76558, 77044, 77247, 77401, 77658, 77682
77900, 77909, 77921, 78608, 78723, 78742, 78930, 79312, 79464, 79507, 79967, 80544, 80618, 80709, 80770, 80969
81255, 81358, 81520, 81691, 82069, 82270, 83315, 83395, 83458, 83510, 83545, 83903, 83946, 83968, 84127, 84433
84521, 84688, 84922, 85075, 85191, 85192, 85734, 85758, 85909, 86400, 86441, 86490, 86768, 86899, 86918, 87023
87200, 87298, 87352, 87421, 87489, 87626, 88006, 88034, 88149, 88287, 88414, 88589, 88824, 88856, 88995, 89243
89516, 89529, 90182, 90842, 90868, 91157, 91233, 91576, 91903, 92115, 92256, 92566, 93297, 93310, 93523, 93572
93941, 94433, 94523, 94545, 94686, 95638, 95772, 95952, 95982, 96130, 96149, 96252, 96577, 96630, 96959, 97059
97446, 97745, 97955, 98333, 98399, 98515, 98617, 98758, 99040, 99384, 99599, 99653, 100052, 100181, 100505, 100584
100647, 101185, 101247, 101437, 102010, 102118, 102157, 102200, 102229, 102442, 102828, 102900, 102902, 103026, 103538, 103539
103556, 103711, 104020, 104162, 104209, 104786, 104988, 105198, 105413, 105415, 105798, 105958, 105983, 106224, 106412, 106432
106620, 106684, 106895, 107037, 107157, 107267, 107523, 107823, 107845, 108452, 108670, 108731, 108754, 108867, 108988, 109111
109209, 109283, 109296, 109521, 109646, 110213, 110286, 110755, 111069, 111322, 111473, 111525, 111645, 111797, 112064, 112257
112297, 113150, 113172, 113279, 113316, 113373, 113464, 113769, 113859, 113999, 114085, 114346, 114703, 114883, 115084, 115091
115108, 115209, 115754, 115832, 116052, 116303, 117404, 117482, 117850, 117887, 117911, 118553, 118809, 119045, 119473, 119658
119722, 119740, 119850, 119873, 119971, 120505, 121166, 121454, 122229, 122505, 122829, 122958, 123176, 124507, 124575, 124714
124830, 124837, 124918, 125002, 125154, 125504, 125653, 125911, 125923, 126487, 126607, 126854, 127093, 127131, 127165, 127684
127942, 128135, 128141, 128680, 128731, 128843, 129459, 130348, 130802, 131797, 131828, 131887, 132259
*Elset, elset="_f cartilage_S2", internal, instance="f cartilage-1"
324, 436, 551, 913, 1050, 1643, 1666, 2078, 2079, 2806, 3628, 7304, 8004, 8961, 9974, 10645
12194, 12409, 13243, 13358, 13463, 13532, 13770, 13809, 14254, 14298, 14318, 14415, 14604, 14736, 15213, 15262
15546, 15606, 16177, 16215, 16445, 16663, 16764, 16859, 17026, 17371, 17404, 18061, 18083, 18366, 18472, 18494
18821, 19342, 19373, 19793, 19803, 19810, 19968, 20034, 20454, 20554, 20666, 20690, 20941, 20965, 21285, 21573
21578, 21608, 21627, 21633, 22578, 22660, 23289, 23406, 23520, 23847, 24001, 25417, 25705, 26160, 26557, 27221
27281, 27352, 27394, 27424, 27462, 27766, 27903, 28703, 28761, 28825, 28895, 29068, 29360, 29393, 29980, 30026
30064, 30169, 30322, 30343, 30867, 31268, 31451, 31835, 31922, 32212, 32264, 32425, 32481, 32541, 32571, 32681
32776, 32788, 32910, 32917, 33088, 33131, 33199, 33361, 33707, 33826, 33876, 33915, 34026, 34568, 35058, 35300
35328, 35340, 35376, 35380, 35388, 35450, 35749, 35825, 35838, 35913, 36205, 36349, 37361, 37756, 37890, 37957
38305, 38421, 38432, 38777, 38965, 38970, 39081, 39109, 39138, 39279, 39406, 39604, 39616, 39627, 39936, 39998
40333, 40349, 40360, 40482, 40614, 40616, 41067, 41272, 41443, 41551, 41738, 42141, 42227, 42286, 42492, 42620
42804, 42853, 42872, 42924, 43178, 43270, 43584, 43614, 43627, 43891, 43925, 44042, 44080, 44201, 44467, 44632
44920, 45118, 45122, 45251, 45546, 45929, 46322, 46730, 47080, 47094, 47148, 47222, 47472, 47549, 47603, 47626
47646, 47796, 47858, 47910, 48202, 48416, 48696, 48990, 49007, 49134, 49207, 49451, 49463, 49612, 49625, 49627
49674, 49675, 49682, 49968, 50214, 50258, 50592, 50598, 50604, 51084, 51194, 51538, 51624, 51998, 52131, 52134
52191, 52504, 52727, 52934, 53172, 53207, 53596, 54076, 54152, 54160, 54751, 55056, 55134, 55161, 55348, 55518
55726, 55786, 55831, 55857, 56020, 56102, 56230, 56368, 56468, 56534, 56610, 56740, 56960, 57024, 57103, 57134
57176, 57248, 57571, 57593, 57603, 57612, 58013, 58600, 58653, 58662, 58689, 58700, 58709, 58729, 58824, 58837
59025, 59103, 59171, 59177, 59217, 59224, 59303, 59307, 59489, 59671, 59730, 59849, 59877, 59882, 59905, 59928
60053, 60105, 60172, 60444, 60462, 60792, 60826, 60858, 60879, 61095, 61108, 61113, 61285, 61372, 61373, 61522
61535, 61797, 61835, 61854, 61866, 61892, 62023, 62143, 62639, 62843, 62964, 63072, 63160, 63284, 63328, 63329
63831, 63842, 63880, 63945, 64029, 64051, 64127, 64341, 64854, 65273, 65300, 65362, 65469, 65715, 65741, 65786
65813, 65892, 66123, 66205, 66395, 66512, 66530, 66554, 66576, 66592, 66637, 66647, 66650, 66653, 66658, 66925
67057, 67095, 67393, 67408, 67434, 67881, 67890, 67982, 68577, 68639, 68667, 68761, 68954, 69468, 69518, 69643
69872, 69873, 69988, 70010, 70397, 71050, 71392, 71589, 71967, 71973, 72130, 72221, 72223, 72292, 72347, 72354
72476, 72530, 72571, 72691, 73175, 73289, 73383, 73416, 73552, 73592, 73618, 73805, 74195, 74482, 74636, 75281
75316, 75324, 75393, 75407, 75428, 75477, 75682, 75845, 75858, 75936, 76271, 76286, 76294, 76335, 76403, 76412
76539, 76789, 76838, 76848, 76920, 76983, 77059, 77142, 77818, 77929, 78016, 78169, 78241, 78584, 78673, 78810
78836, 78992, 79235, 79298, 79303, 79354, 79407, 79456, 79474, 79584, 79685, 80073, 80111, 80137, 80512, 80942
81049, 81109, 81195, 81216, 81535, 81671, 81858, 82030, 82548, 82615, 82616, 82642, 82692, 82710, 82733, 82767
82867, 82896, 83216, 83314, 83698, 83724, 83858, 83945, 84026, 84164, 84388, 84431, 84777, 84805, 84902, 84962
85154, 85293, 85354, 85370, 85673, 85813, 85878, 86047, 86194, 86281, 86361, 86448, 86457, 86777, 86803, 87092
87106, 87187, 87196, 87293, 87791, 87999, 88031, 88095, 88105, 88141, 88230, 88307, 88335, 88372, 88380, 88694
88984, 89112, 89232, 89399, 89594, 89631, 89672, 89677, 90101, 90274, 90387, 90671, 91180, 91386, 91540, 91942
91990, 92075, 92302, 92344, 92348, 92363, 92383, 92414, 92480, 92592, 92820, 93036, 93182, 93420, 93652, 93680
93726, 93740, 94216, 94298, 94700, 94979, 95036, 95313, 95562, 95751, 96207, 96216, 96294, 96564, 96669, 96926
97133, 97308, 97342, 97351, 97358, 97389, 97405, 97609, 97856, 97998, 98106, 98192, 98339, 98353, 98366, 98381
98383, 98461, 98480, 98502, 99110, 99614, 99727, 99817, 99900, 100015, 100069, 100250, 100512, 100934, 101049, 101087
101255, 101610, 101623, 102047, 102069, 102101, 102198, 102425, 102467, 102491, 102517, 102529, 102654, 102674, 102679, 102815
102830, 103027, 103386, 103562, 103565, 103864, 103922, 104015, 104077, 104106, 104261, 104605, 104639, 104666, 104754, 104806
104819, 104915, 105013, 105105, 105180, 105473, 105805, 105819, 105835, 105893, 105914, 106207, 106225, 106499, 106522, 106847
106934, 107103, 107104, 107150, 107468, 107898, 108008, 108248, 108685, 108793, 108830, 108876, 109060, 109456, 109628, 109690
109747, 110234, 110323, 110347, 110445, 110507, 110735, 110778, 110992, 111310, 111635, 111819, 111825, 112069, 112361, 112529
112578, 112743, 112917, 112967, 113171, 113299, 113361, 113548, 113916, 113961, 113972, 114022, 114140, 114327, 114378, 114454
114466, 114645, 114739, 114956, 114988, 115138, 115232, 115335, 115347, 115475, 115729, 115772, 116061, 116510, 116564, 116786
117736, 117880, 117882, 118186, 118363, 118766, 119138, 119868, 120368, 120405, 120533, 121060, 121558, 122588, 122993, 123134
123415, 123925, 124011, 124047, 124568, 125448, 126709, 127010, 127243, 127429, 128494, 128811, 129217, 130555, 131009, 131486
131892,
*Surface, type=ELEMENT, name="f cartilage"
"_f cartilage_S3", S3
"_f cartilage_S4", S4
"_f cartilage_S2", S2
"_f cartilage_S1", S1
*Elset, elset="_meniscus L bottom_S3", internal, instance="meniscus L-1"
554, 693, 785, 869, 1020, 1025, 1091, 1100, 1241, 1332, 1415, 1705, 1958, 2007, 2210, 2232
2285, 2302, 2332, 2347, 2351, 2475, 2480, 2530, 2547, 2562, 2567, 2573, 2590, 2616, 2636, 2642

```
 2665,  2676,  2679,  2693,  2722,  2779,  2788,  2791,  2801,  2814,  2832,  2838,  2849,  2872,  2880,  2899
 2918,  2984,  2997,  3046,  3048,  3050,  3064,  3115,  3125,  3137,  3142,  3154,  3178,  3207,  3225,  3301
 3329,  3334,  3358,  3377,  3378,  3386,  3401,  3403,  3404,  3413,  3467,  3468,  3472,  3473,  3478,  3480
 3501,  3508,  3512,  3552,  3577,  3618,  3649,  3651,  3694,  3696,  3698,  3708,  3714,  3719,  3728,  3730
 3733,  3740,  3756,  3758,  3771,  3772,  3798,  3805,  3819,  3828,  3833,  3834,  3835,  3837,  3840,  3846
 3851,  3864,  3877,  3887,  3904,  3906,  3923,  3924,  3953,  3976,  3988,  4041,  4046,  4053,  4067,  4075
 4096,  4098,  4106,  4108,  4114,  4116,  4119,  4121,  4122,  4128,  4133,  4138,  4153,  4159,  4164,  4168
 4170,  4171,  4191,  4201,  4215,  4216,  4239,  4280,  4290,  4294,  4329,  4332,  4350,  4363,  4371,  4374
 4376,  4401,  4406,  4407,  4408,  4410,  4412,  4414,  4416,  4427,  4434,  4448,  4450,  4457,  4458,  4462
 4475,  4484,  4485,  4500,  4501,  4509,  4511,  4528,  4531,  4534,  4544,  4546,  4553,  4569,  4574,  4603
 4614,  4622,  4631,  4644,  4645,  4675,  4681,  4707,  4709,  4794,  4802,  4803,  4821,  4828,  4829,  4846
 4861,  4872,  4879,  4885,  4896,  4907,  4938,  4944,  4966,  4984,  4993,  4994,  5003,  5005,  5050,  5051
 5068,  5073,  5075,  5086,  5094,  5142,  5171,  5183,  5187,  5188,  5195,  5200,  5212,  5244,  5248,  5256
 5274,  5277,  5291,  5325,  5365,  5382,  5416,  5448,  5456,  5476,  5502,  5509,  5513,  5515,  5532,  5534
 5535,  5536,  5539,  5551,  5559,  5567,  5571,  5572,  5575,  5579,  5582,  5591,  5627,  5647,  5648,  5655
 5665,  5672,  5689,  5693,  5750,  5793,  5834,  5840,  5842,  5843,  5872,  5874,  5875,  5876,  5878,  5898
 5919,  5923,  5956,  5991,  6007,  6055,  6062,  6073,  6080,  6091,  6097,  6098,  6254,  6260,  6262,  6265
 6284,  6296,  6312,  6317,  6322,  6342,  6344,  6347,  6394,  6450,  6460,  6469,  6476,  6513,  6529,  6548
 6569,  6593,  6599,  6603,  6635,  6640,  6644,  6652,  6658,  6677,  6704,  6705,  6736,  6737,  6741,  6765
 6802,  6835,  6842,  6843,  6853,  6860,  6873,  6886,  6909,  6922,  6980,  6990,  6993,  6997,  6998,  7024
 7025,  7052,  7149,  7157,  7254,  7288,  7336,  7338,  7342,  7376,  7386,  7427,  7449,  7573,  7605,  7608
 7625,  7635,  7636,  7658,  7659,  7666,  7669,  7670,  7676,  7683,  7690,  7731,  7753,  7794,  7800,  7817
 7829,  7865,  7867,  7873,  7892,  7912,  7917,  7923,  7930,  7939,  7945,  7979,  7980,  7981,  7989,  8040
 8054,  8087,  8092,  8093,  8117,  8123,  8173,  8176,  8223,  8241,  8253,  8258,  8305,  8315,  8321,  8398
 8399,  8409,  8427,  8459,  8471,  8483,  8494,  8505,  8510,  8537,  8547,  8549,  8572,  8593,  8600,  8602
 8611,  8705,  8711,  8717,  8762,  8792,  8793,  8794,  8795,  8796,  8823,  8837,  8849,  8865,  8884,  8887
 8892,  8921,  8943,  8949,  8953,  9004,  9034,  9049,  9053,  9074,  9077,  9085,  9100,  9163,  9170,  9188
 9201,  9208,  9233,  9243,  9277,  9295,  9320,  9331,  9345,  9378,  9380,  9382,  9385,  9451,  9547,  9552
 9594,  9617,  9618,  9624,  9651,  9655,  9698,  9711,  9790,  9812,  9813,  9882,  9890,  9891,  9936,  9961
 10066, 10075, 10180, 10268, 10307, 10355, 10368, 10400, 10475, 10492, 10516, 10527, 10545, 10559, 10606, 10694
 10801, 10819, 10824, 10870, 10909, 10928, 10944, 11017, 11047, 11056, 11072, 11078, 11081, 11084, 11088, 11096
 11127, 11147, 11158, 11171, 11174, 11181, 11195, 11203, 11210, 11213, 11230, 11238, 11252, 11275, 11276, 11318
 11333, 11355, 11356, 11384, 11390, 11396, 11451, 11452, 11464, 11471, 11476, 11477, 11478, 11482, 11487, 11547
 11551, 11582, 11589, 11594, 11595, 11607, 11609, 11626, 11627, 11637, 11647, 11649, 11669, 11687, 11709, 11711
 11728, 11730, 11743, 11752, 11780, 11781, 11791, 11792, 11799, 11829, 11831, 11839, 11848, 11855, 11866, 11896
 11899, 11901, 11912, 11915, 11916, 11924, 11930, 11931, 11953, 11960, 11961, 11965, 11991, 12017, 12036, 12044
 12046, 12047, 12057, 12062, 12090, 12105, 12108, 12120, 12127, 12129, 12133, 12147, 12154, 12206, 12207, 12219
 12250, 12262, 12268, 12304, 12307, 12316, 12325, 12335, 12349, 12352, 12355, 12401, 12412, 12413, 12428, 12440
 12445, 12452, 12455, 12462, 12463, 12486, 12540, 12555, 12563, 12574, 12576, 12583, 12603, 12607, 12609, 12620
 12625, 12626, 12628, 12636, 12637, 12646, 12661, 12731, 12740, 12753, 12762, 12771, 12788, 12794, 12806, 12811
 12816, 12832, 12848, 12849, 12872, 12873, 12940, 12955, 12967, 12976, 12982, 12983, 13005, 13008, 13010, 13037
 13049, 13066, 13069, 13120, 13121, 13128, 13133, 13149, 13152, 13155, 13174, 13181, 13192, 13199, 13201, 13202
 13206, 13226, 13251, 13254, 13257, 13274, 13277, 13278, 13285, 13317, 13346, 13350, 13360, 13370, 13371, 13383
 13385, 13411, 13418, 13419, 13424, 13426, 13478, 13483, 13510, 13515, 13540, 13544, 13546, 13561, 13575, 13580
 13589, 13608, 13610, 13611, 13620, 13621, 13624, 13643, 13650, 13697, 13704, 13736, 13749, 13768, 13813, 13815
 13826, 13833, 13837, 13865, 13928, 13954, 13980, 13988, 14007, 14012, 14014, 14029, 14032, 14033, 14095, 14098
 14100, 14109, 14113, 14128, 14132, 14166, 14174, 14201, 14210, 14217, 14286, 14287, 14297, 14313, 14314, 14324
 14325, 14329, 14364, 14385, 14387, 14392, 14393, 14394, 14397, 14399, 14424, 14430, 14431, 14437, 14441, 14473
 14484, 14486, 14498, 14519, 14536, 14548, 14551, 14552, 14573, 14574, 14604, 14668, 14671, 14698, 14705, 14708
 14719, 14724, 14727, 14733, 14744, 14748, 14750
*Elset, elset="_meniscus L bottom_S1", internal, instance="meniscus L-1"
    57,  2262,  2380,  2389,  2390,  2702,  2888,  3333,  3974,  4084,  4188,  4292,  4494,  4933,  4953,  5143
 5192,  5273,  5566,  5675,  5696,  5792,  5847,  5984,  6371,  6604,  6707,  6915,  6921,  7084,  7241,  7305
 7312,  7496,  8190,  8194,  8476,  8589,  8720,  8788,  8857,  8952,  9038,  9121,  9310,  9519,  9523,  9567
 9568,  9578,  9610,  9714,  9726,  9766,  9783,  9822,  9835,  9853,  9943,  9981, 10015, 10035, 10049, 10084
 10107, 10207, 10212, 10239, 10308, 10323, 10490, 10552, 10581, 10585, 10599, 10604, 10609, 10635, 10706, 10729
 10762, 10780, 10781, 10901, 10998, 11569, 11685, 11936, 11945, 12022, 12143, 12192, 12235, 12319, 12450, 12812
 12867, 13287, 13303, 13723, 14148
*Elset, elset="_meniscus L bottom_S4", internal, instance="meniscus L-1"
   297,   482,   801,  1105,  1562,  1913,  2297,  2392,  2537,  2723,  2794,  3146,  3352,  3526,  3613,  3636
 3836,  3879,  3915,  3951,  3997,  4031,  4312,  4436,  4518,  4552,  4684,  4836,  4954,  4989,  5259,  5270
 5279,  5715,  5832,  5841,  5924,  6247,  6353,  6718,  6940,  7046,  7207,  7242,  7283,  7369,  7403,  7409
 7782,  7804,  7815,  7927,  8217,  8617,  8659,  8769,  9410,  9508,  9538,  9660,  9669,  9724,  9782,  9786
 9897,  9909, 10047, 10079, 10111, 10175, 10304, 10326, 10335, 10345, 10361, 10364, 10388, 10402, 10441, 10573
 10589, 10655, 10818, 10833, 11062, 11108, 11145, 11363, 11404, 11450, 11495, 11552, 12028, 12224, 12236, 12283
 12302, 12454, 12599, 12757, 13158, 13388, 13832, 13922, 14194, 14195, 14326, 14616, 14710
*Elset, elset="_meniscus L bottom_S2", internal, instance="meniscus L-1"
   671,   815,  2587,  2719,  3165,  3233,  3279,  3315,  3465,  3570,  3857,  3981,  4038,  4196,  4311,  4368
 4549,  4718,  4911,  4937,  4951,  5167,  5357,  5428,  5588,  6313,  6609,  6647,  6937,  7022,  7070,  7086
 7158,  7280,  7309,  7497,  7682,  7703,  7944,  8226,  8261,  8308,  8480,  8710,  8722,  8765,  9003,  9046
 9128,  9276,  9301,  9316,  9396,  9505,  9558,  9576,  9750,  9765,  9795,  9847,  9856, 10057, 10082, 10104
 10217, 10299, 10338, 10341, 10342, 10348, 10356, 10365, 10369, 10488, 10546, 10570, 10612, 10615, 10624, 10640
 10687, 10753, 10853, 10867, 10879, 10893, 11085, 11498, 12023, 12119, 12324, 12408, 12470, 12548, 12575, 12651
 12756, 12963, 13229, 13387, 13609, 13645, 14028, 14138, 14427, 14575, 14654, 14731
*Surface, type=ELEMENT, name="meniscus L bottom"
"_meniscus L bottom_S3", S3
"_meniscus L bottom_S1", S1
"_meniscus L bottom_S4", S4
```

"_meniscus L bottom_S2", S2
*Elset, elset="_meniscus L top_S1", internal, instance="meniscus L-1"
235, 358, 593, 2225, 2338, 2681, 3054, 3111, 3227, 3269, 3289, 3298, 3338, 3455, 3759, 3869
3962, 4014, 4282, 4301, 4945, 5038, 5327, 5391, 5487, 5758, 5968, 5981, 6032, 6430, 6501, 6748
6776, 6808, 6945, 8007, 8032, 8071, 8089, 8247, 8672, 8747, 8907, 8919, 9002, 9204, 9258, 9535
9707, 9796, 9846, 9939, 9942, 10034, 10046, 10281, 10294, 10309, 10452, 10453, 10507, 10590, 10669, 10723
10763, 10787, 10790, 10805, 10841, 10864, 11102, 11317, 11574, 11934, 12126, 12656, 12710, 12991, 13102, 13143
13188, 13337, 13573, 13925, 14018, 14079, 14245, 14413, 14421, 14702
*Elset, elset="_meniscus L top_S3", internal, instance="meniscus L-1"
185, 357, 397, 400, 580, 750, 974, 980, 1048, 1064, 1114, 1151, 1171, 1179, 1183, 1335
1337, 1372, 1777, 1811, 1859, 2282, 2379, 2487, 2531, 2552, 2580, 2619, 2620, 2639, 2640, 2648
2658, 2686, 2725, 2733, 2736, 2738, 2770, 2784, 2795, 2803, 2843, 2864, 2875, 2902, 2920, 2923
3033, 3039, 3067, 3075, 3124, 3150, 3204, 3238, 3239, 3246, 3247, 3260, 3264, 3274, 3276, 3277
3278, 3317, 3347, 3359, 3368, 3451, 3511, 3518, 3523, 3527, 3528, 3533, 3554, 3557, 3566, 3572
3573, 3594, 3606, 3608, 3640, 3657, 3660, 3666, 3687, 3697, 3701, 3707, 3762, 3764, 3838, 3843
3845, 3859, 3882, 3890, 3891, 3893, 3903, 3917, 3920, 3921, 3927, 3930, 3931, 3935, 3954, 3960
3996, 4020, 4030, 4040, 4044, 4071, 4088, 4089, 4093, 4131, 4134, 4158, 4209, 4218, 4221, 4230
4247, 4249, 4255, 4264, 4268, 4269, 4271, 4273, 4275, 4277, 4284, 4285, 4369, 4375, 4395, 4423
4433, 4445, 4451, 4503, 4507, 4517, 4533, 4559, 4567, 4576, 4589, 4593, 4605, 4606, 4629, 4633
4636, 4638, 4668, 4686, 4688, 4730, 4753, 4763, 4771, 4784, 4791, 4822, 4869, 4876, 4886, 4887
4890, 4895, 4898, 4906, 4919, 4922, 4929, 4946, 4957, 4961, 4969, 4983, 4985, 4996, 5000, 5001
5002, 5018, 5021, 5022, 5025, 5089, 5116, 5121, 5126, 5136, 5138, 5145, 5157, 5158, 5161, 5168
5175, 5215, 5218, 5234, 5272, 5285, 5313, 5318, 5324, 5331, 5336, 5340, 5367, 5369, 5387, 5389
5437, 5447, 5469, 5471, 5477, 5488, 5494, 5510, 5512, 5533, 5548, 5565, 5576, 5581, 5597, 5599
5619, 5624, 5642, 5646, 5652, 5656, 5663, 5671, 5685, 5699, 5731, 5733, 5741, 5794, 5844, 5845
5855, 5871, 5880, 5883, 5887, 5899, 5918, 5949, 5961, 5963, 5976, 5986, 5992, 5993, 6000, 6004
6009, 6028, 6035, 6040, 6041, 6057, 6060, 6065, 6075, 6077, 6087, 6099, 6138, 6197, 6199, 6205
6206, 6227, 6236, 6258, 6272, 6274, 6277, 6286, 6299, 6307, 6311, 6314, 6332, 6336, 6349, 6360
6384, 6387, 6411, 6416, 6420, 6443, 6446, 6454, 6455, 6457, 6459, 6465, 6475, 6478, 6485, 6486
6494, 6503, 6507, 6510, 6545, 6567, 6576, 6578, 6580, 6595, 6634, 6638, 6639, 6643, 6648, 6682
6697, 6699, 6713, 6730, 6752, 6756, 6758, 6772, 6818, 6826, 6833, 6837, 6864, 6881, 6894, 6936
6947, 6965, 6967, 6969, 6971, 7019, 7020, 7023, 7040, 7053, 7072, 7081, 7098, 7103, 7105, 7135
7160, 7199, 7201, 7222, 7230, 7237, 7239, 7245, 7257, 7284, 7285, 7322, 7337, 7340, 7347, 7350
7351, 7355, 7387, 7430, 7453, 7475, 7480, 7512, 7513, 7534, 7553, 7565, 7572, 7588, 7594, 7598
7603, 7629, 7630, 7631, 7638, 7641, 7652, 7654, 7663, 7681, 7688, 7715, 7716, 7719, 7735, 7740
7743, 7769, 7791, 7799, 7812, 7818, 7823, 7824, 7859, 7871, 7897, 7901, 7919, 7943, 7966, 7971
7973, 7996, 8015, 8025, 8036, 8052, 8055, 8086, 8102, 8110, 8111, 8132, 8167, 8170, 8179, 8277
8284, 8289, 8290, 8294, 8304, 8338, 8341, 8361, 8395, 8420, 8426, 8474, 8475, 8478, 8482, 8506
8508, 8550, 8554, 8577, 8606, 8630, 8655, 8682, 8691, 8708, 8712, 8715, 8716, 8728, 8734, 8751
8774, 8778, 8784, 8790, 8824, 8842, 8843, 8853, 8880, 8959, 8960, 8975, 8976, 9032, 9091, 9108
9114, 9116, 9125, 9126, 9137, 9187, 9203, 9206, 9218, 9223, 9228, 9248, 9250, 9298, 9302, 9323
9332, 9336, 9341, 9343, 9364, 9375, 9384, 9395, 9411, 9414, 9429, 9446, 9485, 9492, 9497, 9531
9549, 9556, 9566, 9569, 9573, 9575, 9614, 9630, 9652, 9661, 9664, 9742, 9779, 9781, 9793, 9794
9803, 9804, 9806, 9807, 9845, 9855, 9903, 9929, 9940, 9953, 9973, 10036, 10040, 10060, 10062, 10074
10081, 10095, 10143, 10161, 10162, 10186, 10193, 10200, 10216, 10221, 10252, 10285, 10286, 10290, 10292, 10328
10330, 10332, 10333, 10343, 10412, 10418, 10449, 10450, 10483, 10502, 10505, 10512, 10542, 10558, 10571, 10588
10688, 10700, 10755, 10765, 10776, 10782, 10788, 10791, 10795, 10799, 10804, 10807, 10827, 10828, 10839, 10845
10984, 11007, 11023, 11031, 11045, 11049, 11057, 11071, 11076, 11077, 11079, 11103, 11114, 11176, 11183, 11196
11212, 11248, 11256, 11273, 11308, 11313, 11326, 11329, 11367, 11373, 11380, 11383, 11459, 11462, 11463, 11470
11481, 11484, 11503, 11550, 11566, 11570, 11591, 11600, 11603, 11610, 11612, 11657, 11664, 11694, 11744, 11801
11830, 11837, 11842, 11844, 11849, 11867, 11868, 11871, 11877, 11898, 11900, 12008, 12016, 12024, 12042, 12052
12061, 12081, 12088, 12091, 12110, 12111, 12116, 12117, 12123, 12128, 12137, 12149, 12155, 12156, 12160, 12167
12203, 12204, 12212, 12281, 12297, 12320, 12321, 12331, 12373, 12385, 12392, 12397, 12407, 12420, 12429, 12431
12443, 12447, 12457, 12483, 12500, 12511, 12536, 12537, 12570, 12584, 12665, 12671, 12678, 12680, 12695, 12700
12708, 12712, 12719, 12730, 12733, 12734, 12737, 12739, 12742, 12748, 12749, 12752, 12755, 12765, 12777, 12782
12802, 12805, 12807, 12813, 12814, 12818, 12820, 12823, 12824, 12833, 12834, 12838, 12862, 12874, 12896, 12908
12935, 12936, 12942, 12943, 12965, 12966, 12974, 12981, 13038, 13067, 13080, 13089, 13090, 13105, 13108, 13109
13124, 13127, 13141, 13148, 13156, 13183, 13205, 13208, 13224, 13235, 13247, 13250, 13270, 13275, 13314, 13324
13384, 13413, 13432, 13453, 13465, 13466, 13506, 13521, 13548, 13549, 13555, 13572, 13578, 13582, 13583, 13601
13653, 13659, 13664, 13666, 13669, 13671, 13673, 13782, 13796, 13812, 13866, 13882, 13883, 13890, 13900, 13904
13914, 13921, 13924, 13933, 13946, 13947, 13948, 13953, 13955, 13971, 13996, 14023, 14031, 14034, 14082, 14083
14085, 14102, 14104, 14110, 14112, 14141, 14149, 14151, 14186, 14224, 14256, 14316, 14337, 14338, 14346, 14356
14373, 14375, 14380, 14384, 14386, 14391, 14405, 14435, 14439, 14440, 14442, 14443, 14456, 14461, 14469, 14497
14508, 14511, 14526, 14535, 14542, 14544, 14553, 14564, 14566, 14568, 14570, 14585, 14586, 14590, 14593, 14605
14617, 14620, 14634, 14670, 14693, 14711, 14723, 14737
*Elset, elset="_meniscus L top_S4", internal, instance="meniscus L-1"
120, 599, 602, 656, 770, 1475, 1771, 2030, 2516, 2637, 2884, 2957, 2958, 3038, 3041, 3053
3162, 3210, 3262, 3452, 3703, 3902, 4097, 4227, 4658, 4666, 4721, 4764, 4810, 4894, 4968, 4976
4980, 5219, 5278, 5480, 5583, 5617, 5660, 5723, 6005, 6125, 6148, 6164, 6196, 6215, 6376, 6419
6453, 6561, 6723, 6810, 6865, 7097, 7144, 7169, 7368, 7443, 7527, 7788, 7810, 7878, 7946, 8383
8444, 8689, 8725, 9225, 9526, 9623, 9659, 9681, 9682, 9800, 9857, 9871, 9894, 9924, 9962, 9964
10067, 10090, 10131, 10210, 10215, 10253, 10275, 10310, 10621, 10770, 10814, 10858, 10891, 11051, 11173, 11348
11377, 11445, 11461, 11835, 11863, 11948, 11995, 12025, 12087, 12134, 12197, 12282, 12364, 12437, 12522, 12657
12743, 12776, 13034, 13064, 13083, 13099, 13427, 13522, 13524, 13930, 14066, 14094, 14500, 14534, 14672, 14706
*Elset, elset="_meniscus L top_S2", internal, instance="meniscus L-1"
65, 418, 1924, 2633, 2820, 3002, 3043, 3080, 3214, 3223, 3267, 3302, 3345, 4094, 4203, 4232
4355, 4556, 4571, 4726, 4739, 5032, 5077, 5096, 5334, 5337, 5616, 5625, 5634, 5668, 5833, 5866
5922, 6261, 6870, 6905, 7051, 7151, 7413, 7434, 7706, 7766, 7828, 8091, 8229, 8551, 8569, 8594

```
 8701,  8845,  9109,  9391,  9466,  9490,  9613,  9858,  9888,  9926,  9977, 10197, 10242, 10446, 10447, 10482
 10484, 10536, 10721, 10764, 10777, 10960, 11220, 11249, 11289, 11531, 11537, 11554, 11606, 11819, 11892, 12124
 12142, 12374, 12513, 12613, 12723, 12882, 13111, 13184, 13209, 13263, 13635, 13662, 13726, 13843, 14139, 14144
 14241, 14341, 14545
*Surface, type=ELEMENT, name="meniscus L top"
"_meniscus L top_S1", S1
"_meniscus L top_S3", S3
"_meniscus L top_S4", S4
"_meniscus L top_S2", S2
*Elset, elset="_meniscus M bottom_S3", internal, instance="meniscus m-1"
   50,  375,  377,  666,  772,  1055,  1437,  1475,  1480,  1497,  1896,  2074,  2440,  2476,  2512,  2518
 2533,  2545,  2548,  2558,  2566,  2567,  2581,  2589,  2594,  2596,  2714,  2893,  3043,  3052,  3063,  3099
 3210,  3311,  3376,  3417,  3422,  3460,  3544,  3576,  3599,  3645,  3672,  3675,  3692,  3693,  3697,  3712
 3735,  3738,  3739,  3741,  3755,  3762,  3768,  3803,  3809,  3847,  3857,  3878,  3901,  3923,  3934,  4014
 4058,  4061,  4071,  4104,  4109,  4111,  4125,  4130,  4158,  4172,  4176,  4187,  4196,  4198,  4209,  4210
 4213,  4222,  4252,  4264,  4265,  4276,  4277,  4278,  4287,  4288,  4289,  4322,  4332,  4351,  4385,  4387
 4393,  4408,  4428,  4447,  4461,  4462,  4469,  4482,  4500,  4509,  4543,  4553,  4557,  4559,  4578,  4612
 4645,  4667,  4700,  4707,  4708,  4710,  4711,  4723,  4737,  4741,  4742,  4746,  4747,  4753,  4770,  4804
 4815,  4822,  4832,  4870,  4875,  4880,  4901,  4910,  4918,  4921,  4922,  4934,  4935,  4936,  4938,  4939
 4940,  4946,  4948,  4950,  4955,  4957,  4986,  4989,  4994,  5017,  5050,  5052,  5056,  5057,  5060,  5072
 5077,  5086,  5090,  5099,  5111,  5116,  5118,  5126,  5143,  5159,  5164,  5190,  5200,  5207,  5226,  5228
 5244,  5275,  5291,  5292,  5302,  5308,  5309,  5347,  5355,  5363,  5371,  5390,  5391,  5398,  5425,  5457
 5466,  5492,  5498,  5518,  5521,  5544,  5567,  5568,  5604,  5617,  5629,  5652,  5658,  5678,  5691,  5715
 5716,  5717,  5719,  5720,  5723,  5724,  5726,  5729,  5753,  5776,  5828,  5841,  5862,  5868,  5879,  5885
 5892,  5895,  5900,  5908,  5934,  5940,  6000,  6031,  6032,  6051,  6055,  6058,  6065,  6070,  6073,  6077
 6079,  6099,  6193,  6203,  6230,  6233,  6236,  6237,  6242,  6243,  6254,  6257,  6266,  6277,  6282,  6283
 6407,  6410,  6431,  6434,  6448,  6467,  6489,  6512,  6545,  6572,  6579,  6580,  6591,  6603,  6604,  6629
 6654,  6670,  6673,  6683,  6692,  6702,  6710,  6728,  6729,  6732,  6740,  6741,  6743,  6755,  6800,  6818
 6841,  6870,  6890,  6910,  6917,  6933,  6952,  6966,  6967,  6969,  6970,  6972,  6998,  7000,  7001,  7015
 7045,  7049,  7055,  7090,  7103,  7159,  7227,  7237,  7241,  7244,  7248,  7286,  7289,  7293,  7299,  7301
 7313,  7319,  7362,  7383,  7453,  7454,  7455,  7464,  7531,  7537,  7564,  7583,  7598,  7609,  7622,  7623
 7647,  7661,  7691,  7747,  7769,  7867,  7868,  7888,  7894,  7897,  7899,  7901,  7908,  7925,  7932,  7937
 7979,  8029,  8041,  8066,  8099,  8118,  8128,  8147,  8177,  8179,  8181,  8184,  8194,  8205,  8219,  8276
 8338,  8399,  8405,  8459,  8460,  8464,  8467,  8493,  8521,  8576,  8602,  8640,  8657,  8688,  8709,  8712
 8724,  8726,  8734,  8739,  8744,  8748,  8751,  8861,  8867,  8886,  8933,  8936,  8945,  8956,  8968,  8970
 8979,  8985,  8991,  9001,  9003,  9014,  9017,  9065,  9067,  9075,  9076,  9078,  9106,  9127,  9171,  9177
 9206,  9213,  9214,  9224,  9225,  9231,  9237,  9244,  9245,  9257,  9267,  9337,  9352,  9395,  9471,  9474
 9477,  9479,  9486,  9496,  9500,  9501,  9560,  9579,  9588,  9603,  9744,  9759,  9770,  9771,  9773,  9781
 9790,  9794,  9796,  9800,  9802,  9803,  9808,  9810,  9839,  9863,  9867,  9940,  9955,  9963,  9966,  9995
 9996, 10020, 10027, 10029, 10047, 10055, 10069, 10076, 10111, 10154, 10169, 10205, 10210, 10249, 10268, 10270
 10292, 10313, 10326, 10327, 10478, 10493, 10499, 10500, 10508, 10510, 10511, 10517, 10520, 10529, 10577, 10589
 10606, 10621, 10623, 10643, 10648, 10650, 10685, 10702, 10710, 10717, 10779, 10783, 10787, 10790, 10799, 10810
 10812, 10813, 10862, 10863, 10865, 10913, 10914, 10935, 10936, 10939, 10941, 10949, 10950, 10960, 10962, 10963
 10980, 11001, 11028, 11042, 11044, 11047, 11108, 11109, 11110, 11112, 11120, 11135, 11145, 11178, 11196, 11201
 11210, 11213, 11223, 11230, 11249, 11259, 11266, 11287, 11315, 11324, 11344, 11357, 11377, 11420, 11433, 11451
 11452, 11463, 11465, 11467, 11545, 11559, 11561, 11575, 11577, 11582, 11589, 11601, 11605, 11610, 11614, 11615
 11625, 11641, 11659, 11660, 11674, 11675, 11707, 11711, 11737, 11740, 11752, 11766, 11771, 11793, 11797, 11800
 11802, 11820, 11858, 11910, 11936, 11939, 11941, 11947, 11951, 11954, 11964, 11968, 11971, 11976, 11979, 11990
 12022, 12023, 12034, 12037, 12043, 12082, 12120, 12134, 12138, 12169, 12173, 12181, 12186, 12240, 12264, 12270
 12275, 12279, 12286, 12298, 12306, 12327, 12329, 12334, 12339, 12378, 12379, 12391, 12395, 12406, 12426, 12456
 12466, 12475, 12482, 12483, 12501, 12505, 12506, 12512, 12589, 12590, 12607, 12616, 12620, 12623, 12627, 12631
 12638, 12649, 12651, 12652, 12659, 12680, 12681, 12738, 12751, 12764, 12788, 12809, 12814, 12816, 12843, 12903
 12908, 12952, 12965, 12970, 12972, 12976, 12979, 12986, 12995, 13003, 13006, 13008, 13018, 13025, 13041, 13045
 13048, 13051, 13103, 13116, 13148, 13156, 13161, 13185, 13224, 13226, 13238, 13249, 13258, 13259, 13261, 13285
 13289, 13308, 13325, 13328, 13371, 13375, 13397, 13408, 13437, 13455, 13494, 13506, 13522, 13536, 13576, 13595
 13596, 13597, 13601, 13605, 13608, 13612, 13632, 13687, 13689, 13728, 13731, 13757, 13760, 13783, 13792, 13801
 13831, 13853, 13855, 13891, 13920, 13933, 13938, 13947, 13949, 13952, 13953, 13972, 13980, 13988, 14019, 14032
 14046, 14050, 14054, 14095, 14096, 14127, 14151, 14171, 14201, 14229, 14259, 14261, 14269, 14273, 14277, 14296
 14298, 14305, 14362, 14367, 14376, 14379, 14393, 14399, 14404, 14432, 14441, 14489, 14493, 14506, 14512, 14516
 14526, 14528, 14632, 14724, 14732, 14799, 14852, 14905, 14923, 14929, 14930, 15048, 15054, 15142, 15143, 15176
 15178, 15293, 15298, 15323, 15360, 15463, 15519, 15522
*Elset, elset="_meniscus M bottom_S2", internal, instance="meniscus m-1"
  303,  468,  511,  1496,  2520,  2665,  2688,  3079,  3350,  3386,  3403,  3404,  3721,  3838,  3860,  4299
 4602,  4607,  4646,  4978,  5037,  5128,  5135,  5153,  5217,  5232,  5326,  5356,  5399,  5403,  5419,  5483
 5583,  5674,  6117,  6648,  7297,  7303,  7498,  7549,  7863,  8192,  8381,  8419,  8604,  9484,  9654,  9741
 10062, 10352, 10492, 10522, 10575, 10670, 11115, 11127, 11156, 11162, 11623, 11627, 11872, 12026, 12122, 12137
 12187, 12293, 12478, 12510, 12771, 12789, 12924, 13022, 13038, 13070, 13158, 13316, 13334, 13376, 13418, 13512
 13571, 13615, 13704, 13750, 13845, 14048, 14154, 14164, 14175, 14377, 14490, 14510, 15483, 15501
*Elset, elset="_meniscus M bottom_S4", internal, instance="meniscus m-1"
  621,  842,  1256,  1266,  1360,  1705,  2563,  2675,  2823,  3183,  3390,  3446,  3574,  3804,  3845,  4001
 4103,  4178,  4219,  4320,  4470,  4601,  4671,  4925,  4984,  4995,  5129,  5145,  5365,  5449,  5463,  5577
 5792,  6059,  6114,  6371,  6443,  6475,  7616,  7812,  7875,  8114,  8125,  8540,  8583,  8692,  8720,  8938
 8997,  9050,  9412,  9519, 10014, 10033, 10170, 10631, 10942, 10974, 11629, 11677, 11885, 11911, 11983, 12188
 12303, 12337, 12515, 12669, 12722, 13786, 13856, 13859, 13974, 14145, 14244, 14684, 14986, 15122, 15313, 15408
 15465, 15481
*Elset, elset="_meniscus M bottom_S1", internal, instance="meniscus m-1"
  443,  477,  761,  1001,  1002,  1658,  2182,  2557,  2651,  2680,  2827,  2829,  2833,  2835,  3203,  3317
 3322,  3328,  3418,  3561,  3667,  3698,  3842,  3861,  3928,  3968,  4037,  4042,  4044,  4224,  4348,  4400
```

```
 4463,  4632,  4775,  4776,  4973,  5034,  5277,  5307,  5402,  5651,  5750,  5778,  5783,  5911,  5971,  6326
 6396,  6569,  6931,  7004,  7014,  7170,  7259,  7448,  7801,  7861,  8264,  9385,  9460,  9675,  9705,  9837
 9980, 10063, 10214, 10339, 10342, 10408, 10425, 10507, 10823, 11188, 11624, 12384, 12626, 12661, 12805, 12985
 13235, 13324, 13523, 13965, 14485, 14757, 15426
*Surface, type=ELEMENT, name="meniscus M bottom"
"_meniscus M bottom_S3", S3
"_meniscus M bottom_S2", S2
"_meniscus M bottom_S4", S4
"_meniscus M bottom_S1", S1
*Elset, elset="_tibia cartilage L_S4", internal, instance="t cartilage-L-1"
   215,   230,   352,   548,   662,   806,   896,   970,   973,  1308,  1411,  1423,  1549,  1705,  1739,  1759
  1783,  1808,  2059,  2149,  2295,  2342,  2383,  2783,  3205,  4017,  4044,  4099,  4273,  4383,  4384,  4387
  4720,  4750,  4781,  4798,  4871,  4980,  5261,  5290,  5302,  5335,  5452,  5604,  5747,  5752,  5918,  5952
  5965,  5979,  6013,  6126,  6279,  6341,  6405,  6410,  6556,  6558,  6561,  6744,  6787,  6892,  7109,  7286
  7289,  7533,  7579,  7675,  7692,  7720,  7817,  7896,  7990,  8177,  8288,  8407,  8464,  8574,  8580,  8615
  8798,  8839,  8871,  9068,  9098,  9113,  9141,  9278,  9437,  9641,  9786,  9912,  9971, 10050, 10311, 10603
 10639, 10649, 10748, 10903, 10913, 10918, 11012, 11104, 11157, 11191, 11222, 11551, 11651, 11707, 11791, 11923
 12047, 12173, 12175, 12399, 12431, 12613, 12670, 12691, 12729, 12770, 12871, 13005, 13013, 13057, 13092, 13155
 13364, 13524, 13526, 13680, 13823, 13866, 13902, 13926, 14000, 14039, 14045, 14184, 14214, 14222, 14275, 14307
 14390, 14455, 14521, 14534, 14571, 14590, 14694, 14745, 14750, 14805, 14814, 14858, 14950, 14984, 15092, 15145
 15238, 15273, 15355, 15385, 15409, 15452, 15583, 15650, 15705, 15749, 15817, 15934, 16079, 16090, 16099, 16312
 16313, 16323, 16342, 16352, 16497, 16531, 16568, 16591, 16598, 16650, 16651, 16657, 16663, 16703, 16724, 16725
 16738, 16746, 16759, 16780, 16869, 16887, 16974, 16982, 16993, 17022, 17038, 17089, 17144, 17214, 17245, 17334
 17448, 17826, 17858, 17860, 17875, 17893, 17935, 18076, 18077, 18190, 18206, 18220, 18329, 18389, 18412, 18641
 18662, 18693, 18697, 18711, 18792, 18822, 18842, 18877, 18917, 18933, 19189, 19231, 19346, 19439, 19509, 19522
 19534, 19544, 19617, 19626, 19744, 19756, 19763, 19817
*Elset, elset="_tibia cartilage L_S1", internal, instance="t cartilage-L-1"
    69,    73,   168,   410,   427,   537,   893,  1067,  1104,  1378,  2119,  2151,  2389,  2780,  3252,  3586
  3792,  3969,  4239,  4329,  4374,  4385,  4897,  5169,  5363,  5597,  5699,  5961,  6037,  6158,  6183,  6185
  6207,  6254,  6335,  6342,  6392,  6464,  6474,  6580,  6617,  6728,  6776,  6833,  6839,  6846,  6893,  6910
  7008,  7096,  7208,  7222,  7264,  7308,  7401,  7461,  7731,  7803,  7897,  8042,  8213,  8317,  8330,  8623
  8661,  8711,  8717,  8835,  8964,  9100,  9236,  9417,  9493,  9834,  9879, 10055, 10064, 10241, 10259, 10784
 10857, 11046, 11184, 11223, 11769, 12317, 12400, 12445, 12569, 12661, 12910, 13008, 13031, 13234, 13268, 13292
 13298, 13314, 13433, 13470, 13553, 13555, 13634, 13754, 13813, 13860, 13937, 14174, 14175, 14197, 14211, 14251
 14333, 14375, 14437, 14473, 14503, 14677, 14789, 14852, 14868, 14882, 14986, 15114, 15147, 15356, 15414, 15698
 16019, 16092, 16121, 16127, 16293, 16668, 16673, 16674, 16675, 16753, 16847, 16911, 16985, 16999, 17008, 17039
 17098, 17130, 17247, 17463, 17512, 17561, 17590, 17628, 17701, 17714, 17786, 17794, 17796, 17835, 17837, 17846
 17855, 17873, 17892, 17976, 18131, 18214, 18363, 18366, 18423, 18431, 18484, 18655, 18698, 18722, 18747, 18966
 19172, 19257, 19425, 19478, 19510, 19514, 19575, 19619, 19794, 19811
*Elset, elset="_tibia cartilage L_S2", internal, instance="t cartilage-L-1"
    39,    70,    83,   217,   273,   876,  1103,  1426,  2495,  2514,  2908,  3392,  3774,  3828,  3947,  4287
  4870,  4956,  5027,  5092,  5128,  5255,  5271,  5279,  5509,  5757,  5875,  5929,  5976,  6018,  6148,  6167
  6181,  6262,  6269,  6327,  6364,  6447,  6739,  6773,  6808,  6852,  6971,  7006,  7022,  7068,  7219,  7256
  7262,  7265,  7276,  7283,  7305,  7309,  7378,  7501,  7809,  7975,  7988,  8145,  8451,  8517,  8657,  8820
  9240,  9289,  9539,  9644,  9659,  9859, 10248, 10389, 10605, 10658, 10773, 10797, 10872, 11288, 11455, 11636
 11813, 11944, 11981, 12061, 12062, 12125, 12268, 12322, 12324, 12325, 12333, 12344, 12460, 12594, 12615, 12689
 12799, 12866, 12906, 12919, 13002, 13099, 13253, 13269, 13282, 13290, 13291, 13300, 13336, 13357, 13376, 13440
 13441, 13512, 13736, 13870, 13928, 14008, 14047, 14167, 14190, 14191, 14193, 14219, 14230, 14233, 14236, 14242
 14385, 14433, 14506, 14513, 14601, 14629, 14655, 14752, 14769, 14774, 14784, 14793, 14799, 14865, 15037, 15038
 15115, 15124, 15129, 15133, 15140, 15150, 15158, 15162, 15435, 15536, 15568, 15605, 15638, 15640, 15697, 15709
 15716, 15752, 15822, 15828, 16064, 16072, 16083, 16098, 16107, 16108, 16112, 16117, 16194, 16330, 16341, 16347
 16403, 16462, 16512, 16556, 16561, 16564, 16653, 16654, 16659, 16662, 16664, 16666, 16788, 16797, 16810, 16894
 16924, 16991, 16996, 17021, 17033, 17061, 17067, 17102, 17110, 17162, 17326, 17449, 17475, 17508, 17514, 17522
 17552, 17573, 17634, 17649, 17653, 17845, 17848, 17854, 17856, 17865, 17870, 17872, 17877, 17888, 17897, 17905
 17915, 17989, 18039, 18055, 18102, 18259, 18271, 18384, 18463, 18488, 18573, 18575, 18592, 18609, 18624, 18657
 18683, 18703, 18727, 18825, 18873, 18891, 19014, 19031, 19049, 19145, 19148, 19169, 19174, 19181, 19188, 19291
 19305, 19309, 19336, 19337, 19479, 19498, 19503, 19529, 19540, 19609, 19612, 19656, 19687, 19721
*Surface, type=ELEMENT, name="tibia cartilage L"
"_tibia cartilage L_S3", S3
"_tibia cartilage L_S4", S4
"_tibia cartilage L_S2", S2
"_tibia cartilage L_S1", S1
*Elset, elset="_tibia cartilage m_S2", internal, instance="t cartilage-m-1"
   644,  1099,  1509,  1687,  1886,  2071,  2316,  2471,  2552,  2655,  2689,  2795,  3115,  3410,  3521,  3594
  4742,  4935,  5100,  5118,  5443,  5598,  5754,  6137,  6408,  6876,  6948,  7371,  7469,  7491,  7552,  7558
  7652,  7694,  7864,  7950,  8064,  8070,  8079,  8126,  8198,  8450,  8695,  8855,  8875,  8891,  8980,  9158
  9388,  9603,  9613,  9658,  9839,  9891,  9906, 10019, 10034, 10328, 10397, 10406, 10470, 10759, 10842, 10851
 10862, 10894, 11292, 11301, 11302, 11428, 11455, 11504, 11617, 11635, 11811, 11903, 12305, 12331, 12509, 12511
 12563, 12600, 12644, 12737, 12768, 12871, 13008, 13025, 13099, 13100, 13440, 13490, 13600, 13606, 13839, 13860
 13972, 14012, 14228, 14356, 14452, 14501, 14538, 14600, 14992, 15008, 15009, 15170, 16195, 16304, 16332, 16355
 16886, 17165, 17229, 17246, 17283, 17319, 17541, 17659, 17683, 17897, 17908, 18103, 18129, 18413, 18717, 18837
 19164, 19430, 19533, 19720, 19830, 19876, 20050, 20268, 20464, 20522, 20556, 20600, 20657, 20674, 20826, 21121
 21410, 21475, 21675, 21739, 21762, 21777, 21792, 21839, 21848, 22199, 22226, 22242, 22388, 22409, 22517, 22588
 22644, 22711, 22751, 22886, 23200, 23205, 23222, 23247, 23328, 23347, 23374, 23403, 23429, 23599, 23626, 23673
 23679, 23737, 23807, 23981, 24016, 24018, 24036, 24078, 24093, 24123, 24153, 24164, 24178
*Elset, elset="_tibia cartilage m_S4", internal, instance="t cartilage-m-1"
    28,   493,   571,   614,   679,   720,   758,   780,   871,  1315,  1480,  1569,  1645,  2050,  2118,  2277
  2286,  2301,  2523,  2713,  2740,  2785,  3161,  3650,  3851,  4119,  4167,  4175,  4271,  4476,  4536,  4601
```

```
 4640,  5168,  5368,  5388,  5646,  5820,  5899,  6294,  6675,  6734,  6812,  6824,  6916,  7282,  7332,  7533
 7699,  7723,  7844,  8003,  8053,  8122,  8181,  8272,  8393,  8403,  8492,  8659,  8742,  8947,  8955,  8977
 9109,  9144,  9250,  9336,  9457,  9657,  9696,  9804,  9897,  9916, 10045, 10061, 10204, 10228, 10385, 10517
10592, 10602, 10672, 10681, 10882, 11145, 11166, 11304, 11426, 11519, 11591, 11906, 12026, 12196, 12303, 12320
12325, 12326, 12460, 12583, 12884, 12950, 13366, 13369, 13488, 13504, 13544, 13647, 13770, 13809, 13893, 13904
13982, 13988, 13992, 14043, 14057, 14064, 14163, 14333, 14479, 14509, 14579, 14597, 14624, 14655, 14773, 14780
14921, 14991, 15003, 15143, 15157, 15396, 15404, 16226, 16348, 16490, 16733, 17181, 17360, 17505, 17545, 17674
17785, 18015, 18243, 18449, 18458, 18693, 18695, 18813, 18855, 18995, 18998, 19001, 19027, 19189, 19249, 19346
19398, 19496, 19955, 20046, 20131, 20228, 20349, 20532, 20552, 20679, 20682, 20738, 20825, 20836, 20995, 20999
21039, 21552, 21556, 21587, 21617, 21646, 21652, 21854, 21905, 22034, 22069, 22227, 22332, 22386, 22417, 22485
22486, 22537, 22552, 22564, 22609, 22681, 22767, 22839, 22928, 22947, 22952, 22974, 23018, 23102, 23261, 23290
23808, 23957, 24045, 24065, 24075, 24108
*Elset, elset="_tibia cartilage m_S1", internal, instance="t cartilage-m-1"
   16,   387,   392,   465,  1297,  1501,  1761,  1849,  2176,  2179,  2249,  2253,  2280,  2283,  2446,  2510
 2677,  2835,  2948,  3668,  4071,  4163,  4183,  4734,  5023,  5121,  5606,  5883,  5911,  6110,  6415,  7344
 7362,  7516,  7777,  7826,  8000,  8041,  8067,  8069,  8132,  8231,  8573,  8577,  8666,  8832,  8844,  8864
 8898,  9147,  9187,  9223,  9269,  9358,  9393,  9404,  9609,  9659,  9795,  9840,  9888, 10183, 10638, 10834
10843, 10881, 10940, 10968, 11339, 11654, 11705, 11893, 12011, 12115, 12232, 12641, 13035, 13296, 13636, 14051
14166, 14372, 14384, 14687, 14689, 14801, 14919, 15053, 15439, 15445, 15524, 15778, 16274, 16350, 16864, 16898
16944, 17052, 17209, 17323, 17490, 17568, 17706, 17831, 18802, 18986, 19107, 19120, 19214, 19290, 19433, 19438
19840, 19947, 20394, 20551, 20957, 21102, 21224, 22217, 22719, 22919, 22959, 22978, 23381, 23837, 23907
*Surface, type=ELEMENT, name="tibia cartilage m"
"_tibia cartilage m_S3", S3
"_tibia cartilage m_S2", S2
"_tibia cartilage m_S4", S4
"_tibia cartilage m_S1", S1
*Surface, type=NODE, name=FEMATTACH_CNS_, internal
FEMATTACH, 1.
*Surface, type=NODE, name=TIBATTACH_CNS_, internal
TIBATTACH, 1.
** Constraint: Constraint-4
*Tie, name=Constraint-4, adjust=no, position tolerance=1., type=NODE TO SURFACE
FEMATTACH_CNS_, Part-8-1."Femur surface"
** Constraint: Constraint-7
*Tie, name=Constraint-7, adjust=no, position tolerance=1., type=NODE TO SURFACE
TIBATTACH_CNS_, Part-9-1."Tibia surface"
*End Assembly
*Distribution Table, name=Ori-1-DiscOrient_Table
coord3D, coord3D
*Distribution Table, name=Ori-1-DiscOrient-1_Table
coord3D, coord3D
**
** MATERIALS
**
*Material, name="ARTICULAR CARTILAGE"
*Elastic
10., 0.45
*Material, name="BONE cortical"
*Density
 1.5e-09,
*Elastic
17000., 0.33
*Material, name="BONE trabecular"
*Density
 1.5e-09,
*Elastic
400., 0.33
*Material, name=LIGAMENT
*Hyperelastic, mooney-rivlin, test data input
*Uniaxial Test Data
 0.122187, 0.207152
 0.122187, 0.700771
 0.461638,  1.21907
 0.885952,  1.66333
   1.3633,  2.13227
   2.0316,   2.4778
  2.34983,  2.77397
  2.82082,  3.04546
  3.49548,  3.41568
   4.0683,  3.68717
  4.78964,  4.00802
  5.74434,  4.40292
  6.26413,  4.67441
  6.99607,  4.99526
  9.54195,  5.72746
  12.9789,  6.69825
  13.9972,   7.0191
  17.1796,   7.9652
```

```
 18.1979,  8.25315
 21.7622,  9.24039
 22.7805,  9.53656
 24.4778,  10.0713
 25.7083,  10.4498
 26.6842,  10.7295
 28.8907,  11.3383
 31.0334,  11.9553
 31.9457,  12.2761
 32.4549,   12.523
 33.6217,  12.9425
 34.2052,  13.2387
 34.9583,  13.5349
 35.3572,  13.9248
 35.5948,  14.1025
 36.3586,  14.4728
 36.4965,  14.7689
 36.5707,  15.0651
 36.5707,    15.46
 36.5283,  15.6328
*Material, name=MENISCUS
*Elastic, type=ENGINEERING CONSTANTS
125.,  27.5,  27.5,   0.1,   0.1,  0.33,    2.,    2.
 10.33,
**
** INTERACTION PROPERTIES
**
*Surface Interaction, name=FRICTIONLESS
1.,
*Friction, slip tolerance=0.005
0.,
*Surface Behavior, pressure-overclosure=HARD
**
** CONTACT INITIALIZATION DATA
**
*Contact Initialization Data, name="Contact Initialization"
**
** BOUNDARY CONDITIONS
**
** Name: BC-3 Type: Symmetry/Antisymmetry/Encastre
*Boundary
Part-9-1."tibia bottom nodes new", ENCASTRE
** Name: BC-6 Type: Displacement/Rotation
*Boundary
Set-87, 3, 3
**
** INTERACTIONS
**
** Interaction: FRICTIONLESS-1
*Contact Pair, interaction=FRICTIONLESS, type=SURFACE TO SURFACE
"meniscus L top", "f cartilage"
** Interaction: FRICTIONLESS-2
*Contact Pair, interaction=FRICTIONLESS, type=SURFACE TO SURFACE
"tibia cartilage L", "f cartilage"
** Interaction: FRICTIONLESS-3
*Contact Pair, interaction=FRICTIONLESS, type=SURFACE TO SURFACE
"Meniscus M top", "f cartilage"
** Interaction: FRICTIONLESS-4
*Contact Pair, interaction=FRICTIONLESS, type=SURFACE TO SURFACE
"tibia cartilage m", "f cartilage"
** Interaction: FRICTIONLESS-5
*Contact Pair, interaction=FRICTIONLESS, type=SURFACE TO SURFACE
"meniscus L bottom", "tibia cartilage L"
** Interaction: FRICTIONLESS-6
*Contact Pair, interaction=FRICTIONLESS, type=SURFACE TO SURFACE
"meniscus M bottom", "tibia cartilage m"
** ----------------------------------------------------------------
**
** STEP: ApplyFemRotation
**
*Step, name=ApplyFemRotation, nlgeom=YES, inc=1000
Apply rotation to femur about joint center.
*Static, stabilize, factor=0.0002, allsdtol=0., continue=NO
0.01, 0.1, 1e-15, 0.1
**
** INTERACTIONS
**
** Contact Controls for Interaction: FRICTIONLESS-1
```

```
*Contact Controls, master="f cartilage", slave="meniscus L top", reset
** Interaction: FRICTIONLESS-2
*Model Change, type=CONTACT PAIR, remove
"tibia cartilage L", "f cartilage"
** Contact Controls for Interaction: FRICTIONLESS-3
*Contact Controls, master="f cartilage", slave="Meniscus M top", reset
** Interaction: FRICTIONLESS-4
*Model Change, type=CONTACT PAIR, remove
"tibia cartilage m", "f cartilage"
** Contact Controls for Interaction: FRICTIONLESS-5
*Contact Controls, master="tibia cartilage L", slave="meniscus L bottom", reset
** Contact Controls for Interaction: FRICTIONLESS-6
*Contact Controls, master="tibia cartilage m", slave="meniscus M bottom", reset
**
** OUTPUT REQUESTS
**
*Restart, write, frequency=0
**
** FIELD OUTPUT: F-Output-3
**
*Output, field, frequency=99999
*Contact Output
CDISP, CSTRESS
**
** FIELD OUTPUT: F-Output-1
**
*Node Output
CF, RF, U
**
** FIELD OUTPUT: F-Output-2
**
*Element Output, directions=YES
E, S
**
** HISTORY OUTPUT: H-Output-1
**
*Output, history, variable=PRESELECT, frequency=99999
*End Step
** ----------------------------------------------------------------
**
** STEP: ApplyLoads
**
*Step, name=ApplyLoads, nlgeom=YES, inc=1000
Apply standing compressive load to joint
*Static, stabilize, factor=0.0002, allsdtol=0., continue=NO
0.01, 0.1, 1e-15, 0.1
**
** LOADS
**
** Name: Load-8   Type: Pressure
*Dsload
Surf-33, P, 0.6
**
** INTERACTIONS
**
** Interaction: FRICTIONLESS-2
*Model Change, type=CONTACT PAIR, add
"tibia cartilage L", "f cartilage"
** Interaction: FRICTIONLESS-4
*Model Change, type=CONTACT PAIR, add
"tibia cartilage m", "f cartilage"
**
** OUTPUT REQUESTS
**
*Restart, write, frequency=0
**
** FIELD OUTPUT: F-Output-6
**
*Output, field, frequency=99999
*Contact Output
CDISP, CSTRESS
**
** FIELD OUTPUT: F-Output-4
**
*Node Output
CF, RF, U
**
** FIELD OUTPUT: F-Output-5
```

```
**
*Element Output, directions=YES
E, S
**
** HISTORY OUTPUT: H-Output-2
**
*Output, history, variable=PRESELECT, frequency=99999
*End Step
```

Appendix B: Dissection Steps of the Specimen for the Experiments

In this appendix, dissection procedure of a knee specimen is shown step by step using photos. It starts from a fully embalmed leg and ends with the final specimen ready for the experiments.

Warning: Some of the photos include graphic content and may disturb some people.

Figure B 1. Embalmed left leg before dissection.

Figure B 2. Dissected proximal femur.

Figure B 3. Removing the tissue surrounding the femur diaphysis.

Figure B 4. Dissected distal tibia.

Figure B 5. Removing the tissue surrounding the tibia diaphysis.

Figure B 6. Intact dissected knee joint.

Figure B 7. The knee specimen after removing the skin and its fat layer.

Figure B 8. Final dissected specimen used for the experiments.